UNIVERSIDADE DE LISBOA
FACULDADE DE CIÊNCIAS

UNIVERSITÉ CLERMONT AUVERGNE
ÉCOLE DOCTORALE DES SCIENCES FONDAMENTALES

Solid-liquid interactions in ionanofluids. Experiments and molecular simulation

Doutoramento em Química
Especialidade em Química Física

João Manuel Pedro Moisão França

Tese orientada por:
Prof. Dr. Carlos Alberto Nieto de Castro (Universidade de Lisboa)
Prof. Dr. Agílio A. H. Pádua (Université Clermont Auvergne)

Documento especialmente elaborado para a obtenção do grau de doutor em cotutela entre a Universidade de Lisboa e Université Clermont Auvergne

2017

UNIVERSIDADE DE LISBOA
FACULDADE DE CIÊNCIAS

UNIVERSITÉ CLERMONT AUVERGNE
ÉCOLE DOCTORALE DES SCIENCES FONDAMENTALES

Solid-liquid interactions in ionanofluids. Experiments and molecular simulation

Doutoramento em Química
Especialidade em Química Física

João Manuel Pedro Moisão França

Tese orientada por:
Prof. Dr. Carlos Alberto Nieto de Castro (Universidade de Lisboa)
Prof. Dr. Agílio A. H. Pádua (Université Clermont Auvergne)

Júri:
Presidente:

- Doutora Ana Maria Jara Ponces da Costa Freire, Professora Catedrática, Faculdade de Ciências da Universidade de Lisboa

Vogais:

- Doutor Agílio Alexandre Henriques Pádua, Professor Catedrático, *Institute de Chimie de Clermont-Ferrand* da *Université Clermont Auvergne* & *CNRS*, França - Orientador
- Doutor João Paulo Serejo Goulão Crespo, Professor Catedrático, Faculdade de Ciências e Tecnologia da Universidade Nova de Lisboa
- Doutor José Manuel da Silva Simões Esperança, Investigador Principal, Faculdade de Ciências e Tecnologia da Universidade Nova de Lisboa
- Doutor José Nuno Aguiar Canongia Lopes, Professor Associado com Agregação, Instituto Superior Técnico da Universidade de Lisboa
- Doutor Carlos Alberto Nieto de Castro, Professor Catedátrico, Faculdade de Ciências da Universidade de Lisboa - Orientador
- Doutora Maria José Vitoriano Lourenço, Professora Auxiliar, Faculdade de Ciências da Universidade de Lisboa

Documento especialmente elaborado para a obtenção do grau de doutor em cotutela entre a Universidade de Lisboa e Université Clermont Auvergne

Financiado pela Fundação para a Ciência e Tecnologia (FCT) através da bolsa SFRH/BD/79378/2011

2017

Acknowledgments

No matter how hard you try, nobody achieves their goals alone. There is always somebody who motivates and/or encourages you, whether it's in the most direct and comforting way or even if you aren't aware of it in the moment. Being no exception to this, many people were essential to conclude this stage in my life. As such, I would like to express my appreciation.

To my supervisors, Professor Carlos Nieto de Castro and Professor Agílio Pádua, for their guidance, wisdom and support throughout the course of the project. After working with Professor Carlos for nearly a decade now, it is remarkable how he was able to motivate me every time we talked about this topic. Always open for debate, he taught me more than I can measure. Professor Agílio introduced me to an area on which I had little knowledge of and always challenged me to leave my "comfort zone". His vision and *modus operandi* are inspiring and will guide me in my career. I am also grateful for the way he welcomed me in Clermont-Ferrand and for providing the opportunity to work at MIT.

To Professor Daniel Blankschtein at MIT, for having me as a Visiting PhD student and creating an excellent ambience for research and learning.

To the members of MTFT, TIM and DB research groups, for all the support and companionship. Particularly to Professor Fernando Santos, Professor Manuel Matos Lopes, S. M. S. Murshed, Filipe Reis, Ana Catarina Mendonça, Gaëlle Filippini, Gaëtan Maurel and Julien Devémy. I would to like to express a special acknowledgment to Margarida Costa Gomes, a great person and researcher with whom one can always count on, Leila Moura, a friend and colleague that is an example to anyone around her, and Émilie Bordes, always available to lend a friendly and helping hand.

To all my friends who, in a way, shared this experience with me. Their caring and friendship made a world of difference, whether I was in

Portugal, France or the USA. To Tiago Silva, Ricardo Hipólito, João Silva, Ievgeniia Topolniak, Ali Amanat, Jonathan Correia, Catarina Santos, Andreia Araújo, Anabela Reis, Maria João Figueiredo, Ana Paula Ribeiro, Verónica Felício, José Múrias, Verônica Brito, Abi, Antoine Delbegue, Emilien Mallet, Ewa Czajkowska, Marco Domingues, Professor Isabel Pereira and Dr. Isabel Santos. To the Ferreira, Vieira and Calçada *clans*. To Carina Torcato and Etienne Lopes. To Aida Torcato and António Torcato. To everyone who cared, I would like to express my deepest gratitude.

To my parents and brother, whose unconditional support and motivation was a constant. Their love and understanding were essential in achieving this goal.

Last but not least, to my girlfriend Inês Torcato, for all the love, patience, caring and friendship. Once again, her fundamental support is a clear representation of the pillar that she is in my life, without whom everything would be infinitely harder.

To all, thank you!

"*Everybody has a plan until they get punched in the mouth.*"
Mike Tyson

"*Best of you", 2:26 – 5:13"* – Live at *Cheese and Grain*,
Frome, UK, 2017
Foo Fighters

Abstract

One of the main areas of research in chemistry and chemical engineering involves the use of ionic liquids and nanomaterials as alternatives to many chemical products and chemical processes, as the latter are currently considered to be environmentally non-friendly. Their possible use as new heat transfer fluids and heat storage materials, which can obey to most principles of green chemistry or green processing, requires the experimental and theoretical study of the heat transfer mechanisms in complex fluids, like the ionanofluids. It was the purpose of this dissertation to study ionanofluids, which consist on the dispersion of nanomaterials in an ionic liquid.

The first objective of this work was to measure thermophysical properties of ionic liquids and ionanofluids, namely thermal conductivity, viscosity, density and heat capacity in a temperature range between -10 e 150 ºC and at atmospherical pressure. In this sense, the thermophysical properties of a considerable set of ionic liquids and ionanofluids were measured, with particular emphasis on the thermal conductivity of the fluids. The ionic liquids studied were $[C_2mim][EtSO_4]$, $[C_4mim][(CF_3SO_2)_2N]$, $[C_2mim][N(CN)_2]$, $[C_4mim][N(CN)_2]$, $[C_4mpyr][N(CN)_2]$, $[C_2mim][SCN]$, $[C_4mim][SCN]$, $[C_2mim][C(CN)_3]$, $[C_4mim][C(CN)_3]$, $[P_{66614}][N(CN)_2]$, $[P_{66614}][Br]$ and their suspensions with 0.5% and 1% w/w of multi-walled carbon nanotubes (MWCNTs).

The results obtained show that there is a substantial enhancement of the thermal conductivity of the base fluid due to the suspension of the nanomaterial, considering both mass fractions. However, the enhancement varies significantly when considering different base ionic liquids, with a range between 2 to 30%, with increasing temperature. This fact makes it more difficult to unify the obtained information in order to obtain a model that allows predicting the enhancement of the thermal conductivity. Current models used to calculate the thermal conductivity of nanofluids present values that are considerably

underestimated when compared to the experimental ones, somewhat due to the considerations on the role of the solid-liquid interface on heat transport.

Considering density, the impact from the addition of MWCNTs on the base fluid's density is very low, ranging between 0.25% and 0.5% for 0.5% w/w and 1% w/w MWCNTs, respectively. This was fairly expected and is due to the considerable difference in density between both types of materials. However, viscosity was the property for which the highest values of enhancement were verified, ranging between 28 and 245% in both mass fractions of MWCNTs. The heat capacity was the only of the four properties mentioned above not to be studied in this work due to technical issues with the calorimeter to be used. Nevertheless, the amount of data collected on the remainder thermophysical properties was extensive. It is believed that the latter contributes meaningfully to a growing database of ionic liquids and ionanofluids' properties, while providing insight on the variation of said properties obtained from the suspension of MWCNTs in ionic liquids.

The second objective of this work consisted on the development of molecular interaction models between ionic liquids and highly conductive nanomaterials, such as carbon nanotubes and graphene sheets. These models were constructed based on quantum calculations of the interaction energy between the ions and a cluster, providing interaction potentials. Once these models were obtained, a second stage on this computational approach entailed to simulate, by Molecular Dynamics methods, the interface nanomaterial/ionic liquid, in order to understand the specific interparticle/molecular interactions and their contribution to the heat transfer. This would allow to study both structural properties, such as the ordering of the ionic fluid at the interface, and dynamic ones, such as residence times and diffusion.

The first stage consisted on adjusting a site-site interaction potential model between each atom of the ionic liquid and graphene, in order to reproduce the calculated energy values using quantum chemistry

methods. This step had an exploratory feature, since no similar work was available at the time in the literature. The choice of potential function that better described the energy values lead to a *n-m* potential, with *n* and *m* exponents different from the typically used for simple organic molecules (12-6). The transferability of the adjusted parameters to interaction energy values between ionic liquids and graphene was also evaluated. This was performed through the calculation of interaction energy values between an ionic liquid and a nanotube, without further adjustment. A more modest set of calculations were also performed to evaluate the charge distribution in graphene sheets and nanotubes, considering both *zig-zag* and *arm-chair* structures. As such, a model that correctly represents the interactions of several ionic liquids with carbon nanomaterials with different structures was obtained.

These models were subsequently used in molecular dynamics simulations, considering two types of carbon nanomaterial (a single-walled carbon nanotube, SWCNT, and a stack of graphene sheets) solvated by an ionic liquid ($[C_4mim][N(CN)_2]$, $[C_4mim][SCN]$, $[C_4mim][C(CN)_3]$ e $[C_4mim][tf_2N]$). The structural information obtained, i.e., the organization of the ions at the solid-liquid interface, demonstrated a greater proximity of the anion to the carbon surface. By studying two different SWCNTs (with different chirality indexes, namely (7,7) and (10,10), entailing distinct diameter values), it was possible to observe that the cations of ionic liquid are organized differently inside and outside of nanotube relatively to their position and orientation. In the widest nanotube, the alkyl chains are directed towards the center of the tube, creating a non-polar domain.

Using this structural information, NEMD (non-equilibrium molecular dynamics) simulations were performed with the aim of calculating the thermal conductivity of each system at different temperatures. The results obtained agree reasonably with the experimental results, with a good prediction of the relative order between ionic liquids. The thermal conductivity was calculated in the composite systems considering different directions of the heat flow. In the case of the system composed by ionic liquids and a SWCNT, the thermal

conductivity was calculated along the direction of the axis of the nanotube. The enhancement verified in this case is due to the conduction of heat trough the nanomaterial and is system-dependent, as seen in the experimental results. Regarding the systems composed by a stack of graphene sheets and ionic liquid, the thermal conductivity was calculated considering a heat flux perpendicular to the nanomaterial. As such, the global values of thermal conductivity of these composite systems were lower than the ones containing solely ionic liquid. However, this configuration allowed the study of the thermal conductivity of the interfacial region, where a significant enhancement was observed when compared to the bulk liquid in the same simulation box. In addition, no significant discontinuity was verified in the temperature profile at the solid-liquid interface, which represents a useful contribution for future predictive models for heat transport and properties.

Lastly, the final segment of this dissertation consisted on using the information obtained both from experiment and from simulation. In this sense, the feasibility of the studied substances as heat transfer fluids was evaluated. This was attained through the calculation of heat transfer areas (the main design parameter in heat exchangers) considering a specific process and using the values of thermophysical properties obtained. The results were compared with heat transfer areas calculated for currently used heat transfer fluids. It was verified that some of the studied ionanofluids could compete with the commercial heat transfer fluids in terms of area necessary to transfer the same amount of heat. This fact supports further research on considering ionanofluids as heat transfer fluids.

Keywords: ionic liquids, carbon nanotubes, ionanofluids, thermophysical properties, thermal conductivity, interaction potential, molecular dynamics, heat transfer area.

Resumo

Uma das principais áreas de investigação em química e engenharia química está relacionada com o uso de líquidos iónicos e nanomateriais como alternativas a vários produtos e processos químicos, visto que os últimos são actualmente considerados como ambientalmente prejudiciais. O potencial dos líquidos iónicos como fluidos de transferência de calor e de materiais de armazenamento de calor, aliado ao facto de serem concordantes com a maioria dos princípios da química verde, requer o estudo experimental e teórico dos mecanismos de transferência de calor em fluidos complexos, como os ionanofluidos. Estes últimos, que consistem na dispersão de nanomateriais num liquido iónico, foram o principal objecto de estudo da presente dissertação.

O primeiro objectivo deste trabalho consistiu na medição de propriedades termofísicas de líquidos iónicos e ionanofluidos, nomeadamente a condutibilidade térmica, viscosidade, densidade e capacidade calorífica entre -10 e 150 ºC e à pressão atmosférica. Para o efeito, foram medidas as referidas propriedades de um vasto conjunto de líquidos iónicos e ionanofluidos, com ênfase particular na condutibilidade térmica. Os líquidos iónicos estudados foram $[C_2mim][EtSO_4]$, $[C_4mim][(CF_3SO_2)_2N]$, $[C_2mim][N(CN)_2]$, $[C_4mim][N(CN)_2]$, $[C_4mpyr][N(CN)_2]$, $[C_2mim][SCN]$, $[C_4mim][SCN]$, $[C_2mim][C(CN)_3]$, $[C_4mim][C(CN)_3]$, $[P_{66614}][N(CN)_2]$, $[P_{66614}][Br]$ e as suas suspensões compostas por 0.5% e 1% w/w de nanotubos de carbono de parede múltipla (MWCNTs – do inglês *multi-walled carbon nanotubes*).

Os resultados obtidos ilustram um aumento considerável da condutibilidade térmica devido à suspensão do nanomaterial, em ambas as fracções mássicas. No entanto, o aumento da condutibilidade térmica varia significativamente entre líquidos iónicos (entre 2 a 30%, em função da temperatura). Este facto dificulta a uniformização da informação obtida com vista à obtenção de um modelo que permita prever o mencionado aumento da condutibilidade térmica. Os modelos actuais prevêm uma condutibilidade térmica

muito abaixo da experimentalmente observada, em parte devido ao papel atribuído à interface sólido-líquido no transporte de calor nesses modelos.
Por outro lado, o impacto na densidade no líquido é muito baixa (0.25 e 0.5% para 0.5% w/w e 1% w/w MWCNTs, respectivamente), devido à diferença considerável entre os valores da mesma propriedade para líquidos iónicos e MWCNTs. No entanto, a viscosidade é a propriedade entre as estudadas com aumentos mais elevados, variando entre 28 e 245% em ambas as fracções mássicas de MWCNTs estudadas. A capacidade calorífica foi a única propriedade a não ser medida devido a problemas técnicos com o calorímetro a ser usado. No entanto, foram obtidos dados relevantes (no caso dos ionanofluidos, inéditos) das restantes propriedades termofísicas. Esta componente do trabalho gerou um volume considerável de dados experimentais que contribuem não só para o aumento de uma base de dados em crescimento, mas também para o conhecimento da variação das propriedades termofísicas dos líquidos iónicos proveniente da suspensão de MWCNTs em líquidos iónicos.

O segundo objectivo do presente trabalho consistiu esenvolvimento de modelos de interacção molecular entre líquidos iónicos e nanomateriais altamente condutores, tais como nanotubos de carbono e folhas de grafeno. Estes modelos foram construídos com base em calculos quânticos da energia de interacção entre os iões e um material, dando origem a potenciais de interacção . Uma vez obtidos, a etapa seguinte desta abordagem computacional envolveu o uso destes modelos, usando métodos de dinâmica molecular, para simular a interface nanomaterial/líquido iónico com vista a perceber as interacções moleculares específicas e a sua contribuição para a transferência de calor. Esta abordagem permitiu estudar propriedades estruturais (organização do líquido na zona interfacial) e propriedades dinâmicas (tempos de residência e difusão).
A primeira fase contemplou o ajuste dum modelo de potencial de interação de tipo *site-site*, entre cada átomo dos líquidos iónicos e de grafeno, de modo a reproduzir as energias calculadas através de

métodos de química teórica. Esta etapa teve um carácter exploratório, dado que nenhum trabalho deste tipo foi encontrado na literatura. A escolha do tipo de função de potencial que melhor reproduz os resultados de energia conduziu a um potencial de tipo *n-m*, com expoentes *n* e *m* diferentes dos habitualmente utilizados para moléculas orgânicas simples (12-6). A transferabilidade dos parâmetros ajustados a pontos de energia de interação entre o líquido iónico e uma folha de grafeno foi avaliada calculando a energia de interação entre o líquido e nanotubos, sem ajustes adicionais ao modelo. Foi também efectuado um conjunto mais modesto de cálculos para produzir uma distribuição de cargas electrostáticas em folhas de grafeno e nanotubos, tanto de estrutura "*zig-zag*" como "*arm-chair*". Desta forma, foi desenvolvido um modelo que representa corretamente as interações de vários líquidos iónicos com nanocarbonos de estruturas diversas.

Estes modelos foram subsequentemente utilizados em simulações de dinâmica molecular de dois tipos de nanomateriais de carbono (um SWCNT (do inglês *single-walled carbon nanotube*) e um conjunto de folhas de grafeno) solvatados por líquido iónico ($[C_4mim][N(CN)_2]$, $[C_4mim][SCN]$, $[C_4mim][C(CN)_3]$ e $[C_4mim][tf_2N]$). Foram obtidas informações estruturais relativamente à organização dos iões na interface sólido-líquido que demonstraram a maior proximidade do anião da superfície em ambos os casos. Ao estudar sistemas com dois SWCNTs diferentes (diferentes índices de quiralidade, nomeadamente (7,7) e (10,10), implicando diferentes diâmetros), foi observado que os catiões do líquido iónico se organizam de forma distinta no interior do nanotubo relativamente à sua posição e orientação. No tubo de diâmetro maior, as cadeias alquílicas estão direccionadas para o centro do tubo, formando um domínio apolar.

Usando as informações estruturais acima descritas, foram realizados estudos de NEMD (do inglês *non-equilibrium molecular dynamics*) com o intuito de calcular a condutibilidade térmica de cada sistema a diferentes temperaturas. Os resultados obtidos estão razoavelmente concordantes com os resultados experimentais e com uma boa previsão no que diz respeito à ordem relativa entre diferentes líquidos

iónicos. A condutibilidade térmica foi calculada nos sistemas compostos usando diferentes direcções do fluxo de calor, nomeadamente ao longo do nanotubo e através das folhas de grafeno. O aumento da condutibilidade térmica global (do sistema) no primeiro caso é devido à condução de calor através do material, como seria de esperar. O referido aumento é dependente do sistema em questão, tal como verificado nos dados experimentais. No entanto, um fluxo de calor perpendicular ao material, como no caso do grafeno, gera valores de condutibilidade térmica global inferiores quando comparados com os sistemas compostos por apenas líquido iónico. Esta configuração permitiu que fosse estudada simultaneamente a condutibilidade térmica da zona interfacial entre nanomaterial e líquido, onde foi verificado um aumento significativo da condutibilidade térmica comparativamente ao valor calculado para o líquido iónico puro na mesma caixa. Adicionalmente, foi também verificado que o gradiente de temperatura nas caixas com grafeno e líquido iónico não apresenta descontinuidades significativas na interface em todos os sistemas estudados, o que representa um contributo considerável para futuros modelos de previsão de propriedades e de transporte de calor.

Por fim, a parte final desta dissertação consisitiu em usar a informação obtida pelas vertentes experimental e de dinâmica molecular. Neste sentido, foram cálculadas as áreas de transferência de calor (parâmetro principal para a projecção de permutadores de calor) para um processo particular, usando para o efeito as propriedades termofísicas dos fluidos estudados. Os resultados obtidos foram comparados com valores de área de transferência de calor de fluidos actualmente usados e comercializados. Desta forma, foi possível concluir que algumas das suspensões de líquidos iónicos com nanotubos de carbono podem competir com os fluidos comerciais em termos de área necessária para transferir a mesma quantidade de calor. Este facto apoia a investigação futura de ionanofluidos como fluidos de transferência de calor.

Palavras-chave: líquidos iónicos, nanotubos de carbono, ionanofluidos, propriedades termofísicas, condutibilidade térmica, potencial de interacção, dinâmica molecular, área de transferência de calor.

Resumée

L'un des principaux domaines de recherche en chimie et en ingénierie chimique implique l'utilisation de liquides ioniques et de nanomatériaux comme alternatives à de nombreux produits chimiques et processus chimiques, comme ce dernier étant actuellement considérés comme non respectueux de l'environnement. Leur utilisation potentiel comme nouveaux fluides de transfert de chaleur et matériaux de stockage de chaleur, qui peuvent obéir à la plupart des principes de la chimie verte, nécessite l'étude expérimentale et théorique des mécanismes de transfert de chaleur dans les fluides complexes comme les ionanofluides. Le but de cette thèse était d'étudier les ionanofluides, qui consistent en la dispersion de nanomatériaux dans un liquide ionique.

Le premier objectif de ce travail était de mesurer les propriétés thermophysiques des liquides ioniques et ionanofluides, à savoir la conductivité thermique, la viscosité, la densité et la capacité thermique dans une gamme de température comprise entre -10 et 150 ºC et à pression atmosphérique. Dans ce sens, les propriétés thermophysiques d'un ensemble considérable de liquides ioniques et d'ionanofluides ont été mesurées, avec un accent particulier sur la conductivité thermique des fluides. Les liquides ioniques étudiés étaient $[C_2mim][EtSO_4]$, $[C_4mim][(CF_3SO_2)_2N]$, $[C_2mim][N(CN)_2]$, $[C_4mim][N(CN)_2]$, $[C_4mpyr][N(CN)_2]$, $[C_2mim][SCN]$, $[C_4mim][SCN]$, $[C_2mim][C(CN)_3]$, $[C_4mim][C(CN)_3]$, $[P_{66614}][N(CN)_2]$, $[P_{66614}][Br]$ et leurs suspensions avec 0.5% et 1% w/w de nanotubes de carbone multi-parois (MWCNTs - de l'anglais *multi-walled carbon nanotubes*).
Les résultats obtenus montrent qu'il y a une augmentation substantielle de la conductivité thermique du fluide de base due à la suspension du nanomatériau, en considérant les deux fractions massiques. Cependant, l'amélioration varie de manière significative lorsqu'on considère différents liquides ioniques de base, avec une gamme comprise entre 2 et 30%, avec une température croissante. Ce fait rend plus difficile l'unification des informations obtenues afin d'obtenir un modèle permettant de prédire l'amélioration de la

conductivité thermique. Les modèles actuellement utilisé pour calculer la conductivité thermique des nanofluides présentent des valeurs considérablement sous-estimées par rapport aux valeurs expérimentales, en partie à cause des considérations sur le rôle de l'interface solide-liquide sur le transport de la chaleur.
En ce qui concerne la densité, l'impact de l'ajout de MWCNTs sur la densité du fluide de base est très faible, variant entre 0.25% et 0.5% pour 0.5% w/w et 1% w/w MWCNTs, respectivement. Cela était assez attendu et est dû à la différence considérable de densité entre les deux types de matériaux. Cependant, la viscosité était la propriété pour laquelle les valeurs les plus élevées d' augmentation ont été vérifiées, allant de 28 à 245% pour les deux fractions massiques de MWCNT. La capacité calorifique était la seule des quatre propriétés mentionnées ci-dessus à ne pas être étudiée dans ce travail en raison de problèmes techniques avec le calorimètre à utiliser. Néanmoins, la quantité de données recueillies sur les propriétés thermophysiques restantes était extensif. On pense que ce dernier contribue de manière significative à une base de données croissante des propriétés des liquides ioniques et des ionanofluides, tandis que en fournissant un aperçu de la variation des propriétés obtenues à partir de la suspension de MWCNTs dans des liquides ioniques.

Le deuxième objectif de ce travail consistait à développer des modèles d'interactions moléculaires entre les liquides ioniques et les nanomatériaux hautement conducteurs, tels que les nanotubes de carbone et les feuilles de graphène. Ces modèles ont été construits sur la base de calculs quantiques de l'énergie d'interaction entre les ions et un *cluster*, fournissant des potentiels d'interaction. Une fois ces modèles obtenus, une seconde étape de cette approche computationnelle a consisté à simuler, par des méthodes de Dynamique Moléculaire, l'interface nanomatériau/liquide ionique, afin de comprendre les interactions interparticulaires/moléculaires spécifiques et leur contribution au transfert de chaleur. Cela permettrait d'étudier les propriétés structurelles, telles que l'ordre du

fluide ionique à l'interface, et propriétés dynamiques, telles que les temps de résidence et la diffusion.

La première étape a consisté à ajuster un modèle de potentiel d'interaction site-site entre chaque atome du liquide ionique et le graphène, afin de reproduire les valeurs d'énergie calculées en utilisant des méthodes de chimie quantique. Cette étape avait un caractère exploratoire, car aucun travail similaire n'était disponible à l'époque dans la littérature. Le choix de la fonction potentielle qui décrit le mieux les valeurs énergétiques conduit à un potentiel *n-m*, avec des exposants *n* et *m* différents de ceux habituellement utilisés pour les molécules organiques simples (12-6). La transférabilité des paramètres ajustés aux valeurs d'énergie d'interaction entre les liquides ioniques et le graphène a également été évaluée. Cela a été effectué par le calcul des valeurs d'énergie d'interaction entre un liquide ionique et un nanotube, sans autre ajustement. Un ensemble plus modeste de calculs a également été effectué pour évaluer la distribution des charges dans les feuilles de graphène et les nanotubes, en tenant compte à la fois des structures en *zigzag* et en *armchair*. En tant que tel, un modèle qui représente correctement les interactions de plusieurs liquides ioniques avec des nanomatériaux de carbone avec des structures différentes a été obtenu.

Ces modèles ont ensuite été utilisés dans des simulations de dynamique moléculaire, en considérant deux types de nanomatériaux de carbone (un nanotube de carbone à paroi unique, SWCNT (de l'anglais *single-walled carbon nanotube*), et une pile de feuilles de graphène) solvatés par un liquide ionique ($[C_4mim][N(CN)_2]$, $[C_4mim][SCN]$, $[C_4mim][C(CN)_3]$ e $[C_4mim][tf_2N]$). L'information structurelle obtenue, c'est-à-dire l'organisation des ions à l'interface solide-liquide, a démontré une plus grande proximité de l'anion à la surface du carbone. En étudiant deux SWCNTs différents (avec différents indices de chiralité, à savoir (7,7) et (10,10), impliquant des valeurs de diamètres distincts), il a été possible d'observer que les cations de liquide ionique sont organisés différemment à l'intérieur et à l'extérieur des nanotubes à leur position et leur orientation. Dans le

nanotube le plus large, les chaînes alkyles sont dirigées vers le centre du tube, créant un domaine non polaire.
En utilisant cette information structurelle, NEMD (de l'anglais *non-equilibrium molecular dynamics*) simulations ont été effectuées dans le but de calculer la conductivité thermique de chaque système à différentes températures. Les résultats obtenus concordent raisonnablement avec les résultats expérimentaux, avec une bonne prédiction de l'ordre relatif entre les liquides ioniques. La conductivité thermique a été calculée dans les systèmes composites en considérant différentes directions du flux de chaleur. Dans le cas du système composé de liquides ioniques et d'un SWCNT, la conductivité thermique a été calculée dans la direction de l'axe du nanotube. L'amélioration vérifiée dans ce cas est due à la conduction de la chaleur dans le nanomatériau et dépend du système, comme le montrent les résultats expérimentaux. En ce qui concerne les systèmes composés d'un empilement de feuilles de graphène et de liquide ionique, la conductivité thermique a été calculée en considérant un flux de chaleur perpendiculaire au nanomatériau. En tant que telles, les valeurs globales de conductivité thermique de ces systèmes composites étaient inférieures à celles contenant uniquement un liquide ionique. Cependant, cette configuration a permis l'étude de la conductivité thermique de la région interfaciale, où une amélioration significative a été observée par rapport au liquide pur dans la même boîte de simulation. De plus, aucune discontinuité significative n'a été vérifiée dans le profil de température à l'interface solide-liquide, ce qui représente une contribution utile pour de futurs modèles prédictifs de transport thermique et de propriétés.

Enfin, le dernier segment de cette thèse a consisté à utiliser les informations obtenues expérimentalement et par simulation. Particulièrement, la faisabilité des substances étudiées comme fluides de transfert de chaleur a été évaluée. Ceci a été atteint par le calcul des aires de transfert de chaleur (le paramètre de conception principal dans les échangeurs de chaleur) en considérant un processus spécifique et en utilisant les valeurs des propriétés thermophysiques

obtenues. Les résultats ont été comparés aux aires de transfert de chaleur calculées pour les fluides de transfert de chaleur actuellement utilisés. Il a été vérifié que certains des ionanofluides étudiés pouvaient rivaliser avec les fluides de transfert de chaleur commerciaux en termes de aire nécessaire pour transférer la même quantité de chaleur. Ce fait appuie d'autres recherches sur la considération des ionanofluides comme fluides de transfert de chaleur.

Mots clés: liquides ioniques, nanotubes de carbone, ionanofluides, propriétés thermophysiques, conductivité thermique, potentiel d 'interaction, dynamique moléculaire, aire de transfert de chaleur.

Notes from the author

The work presented is a result of co-tutelage PhD project between the University of Lisbon and Université Clermont Auvergne (resultant of the merger in January 2017 between Université Blaise Pascal, whom with the co-tutelage agreement was signed, and Université d'Auvergne). The work was mainly developed in two groups: Molecular Thermophysics and Fluid Technology (MTFT) at Centro de Química Estrutural (CQE) in Lisbon, Portugal and Molecular Thermodynamics of Ionic Liquids (TIM) at Institute of Chemistry of Clermont-Ferrand (ICCF), in Clermont-Ferrand, France. Additionally, for the period of four months in 2015, the work was developed at Daniel Blankschtein's (DB) Group, at the Department of Chemical Engineering at the Massachusetts Institute of Technology (MIT), in Cambridge, USA.

This work was funded by Fundação para a Ciência e Tecnologia (FCT) through a PhD grant with reference SFRH/BD/79378/2011.

Chapters 2 - 5 consist of published and peer-reviewed scientific papers, with the exception of the chapter 5, which has been submitted for review at the time this dissertation has been delivered for appraisal. The remainder scientific papers were published throughout the duration of the PhD project. The methodologies used are described at length in each Chapter, which are presented chronologically.

Contents

Acknowlegments iv

Abstract viii

Resumo xii

Resumée xvii

Notes from the author xxii

List of acronyms xxiv

Chapter 1 — Introduction 1

Chapter 2 - Thermal Conductivity of $[C_4mim][(CF_3SO_2)_2N]$ and $[C_2mim][EtSO_4]$ and Their IoNanofluids with Carbon Nanotubes: Experiment and Theory. *J. Chem Eng. Data, 2013, 58, 467 — 476.* . . 8

Chapter 3 - Thermophysical properties of ionic liquid dicyanamide (DCA) nanosystems. *J. Chem. Thermodynamics, 2014, 79, 248 — 257.* 20

Chapter 4 - Molecular interactions and thermal transport in ionic liquids with carbon nanomaterials. *Phys. Chem. Chem. Phys., 2017, 19, 17075.* 33

Chapter 5 - Thermal Conductivity of Ionic Liquids and IoNanofluids and their Feasibility as Heat Transfer Fluids. *Submitted to I&EC Research (ACS).* . 51

Chapter 6 - Conclusions and future perspectives . . 70

References 76

Annex 1 — Supporting Information to Chapter 4 . . . 83

Annex 2 — Supporting Information to Chapter 5 . . . 116

List of Acronyms

IL – Ionic Liquid
MWCNT – Multi-Walled Carbon Nanotube
SWCNT – Single-Walled Carbon Nanotube
dca – dicyanamide
THW – Transient Hot-Wire
TEM – Transmission Electron Microscopy
SEM – Scanning Electron Microscopy
DFT – Density Functional Theory
OPLS-AA – Optimized Potentials for Liquid Simulations-All Atom
vdW – van der Waals
MSD – Mean-Squared Displacement
LJ – Lennard-Jones
GK – Green-Kubo
(R)NEMD – (Reverse) Non-Equilibrium Molecular Dynamics
MP – Müller-Plathe
IUPAC - International Union of Pure and Applied Chemistry

Chapter 1

Introduction

Throughout history, society has been constantly evolving and searching for new options to improve and/or replace its ways in every field. The search for new and more efficient ways to carry out our daily routines, both professionally and in our private lifes, is constant and at a frantic pace.
The same can be said for scientific advancements. Each year there are revolutionizing discoveries in almost every field that occasionally lead to questioning the discoveries made in previous years. The technological progress allows us to acquire knowledge faster than ever and with higher accuracy. The paradigms have also shifted in the past few decades. There is an increasing awareness that the preservation of environment and energy saving have to be priorities, particularly when performing research on an area such as chemistry and chemical processes. If we consider the latter on an industrial scale, there is one particular process that is transversal on this activity: heat transfer.

Currently used heat transfer units and heat transfer fluids were developed in a time where fewer environmental or global economic restrictions were existent. There is a need for new and efficient heat transfer liquids that can meet the cooling challenges for advanced devices as well as energy conversion for domestic and industrial applications. Simplifying: everyone wants to use the smallest equipment possible, with the highest efficiency attainable and with the least maintenance possible. In addition, the contemporary heat transfer fluids consist of non-degradable chemical compounds, such as silicon-based fluids, which present a problem from an environmental point of view.

It has been proved in the past, with common and ionic liquids, that the values of their thermophysical properties have a significant effect on the design of physicochemical processing and reaction units [1-5], influencing directly the design parameters and performance of equipment like heat exchangers, distillation columns, and reactors. When evaluating a potential heat transfer fluid and/or dimensioning heat transfer equipment, the heat transfer area (*i.e.*, the area necessary to transfer a determined amount of heat) is one of the main design parameters of heat exchangers, which can be estimated from the thermophysical properties of the heat transfer fluid. These thermophysical properties consist of the thermal conductivity, heat capacity, density and viscosity. As such, accurate data on these properties is crucial. Results obtained [5, 6] show that the influence of actual errors in the thermophysical properties of ionic liquids can render any future design of a heat transfer unit as not working or excessively costing. For instance, the simultaneous overestimation of thermal conductivity by 10% and the underestimation of viscosity by 20% (explained by the presence of water, for example), the heat transfer area necessary for a given process is underestimated by 15%, with the resulting ill-functioning of the heat exchanger [5].

Over the past few years, ionic liquids have been suggested as potential heat transfer fluids. Several of these ionic substances have proven to be safe and sustainable alternatives for many purposes in industry and chemical manufacturing, as they can be tailored for a given application from a vast number of possible combinations of ions. These applications can be very diverse, such as solvents in catalysis and in great variety of organic synthesis [7], as an extraction medium in liquid-gas mixtures [8], as electrolytes in batteries and fuel cells [9, 10], for antimicrobial usages [11] or nuclear waste treatment [12].
The optimal technological design of green processes requires the characterization of the ionic liquids used, namely their thermodynamic, transport, dielectric properties and their

environmental impact. Concerning heat transfer and the abovementioned thermophysical properties, the latter have been characterized at great extent in the past two decades, among others when considering different applications. However, the enormous variety of possible ionic fluids and their complexity poses challenges to establish structure-property relations that can simplify the choice of an ionic liquid for a given process. This is also true concerning the environmental impact of ionic liquids. More time is necessary to evaluate the long-term effect of ionic liquids in the environment, although recent studies have been positively promising [13].

In 2009, a study published on the influence of thermophysical properties of ionic liquids on chemical process design [5] showed that some ionic liquids could be approximately as efficient as current heat transfer fluids, in terms of heat transfer area. Given the versatility of these ionic fluids, it was a matter of obtaining the right combination of cation and anion in order to attain the values of the thermophysical properties to match or (possibly) surpass the efficiency of the commercial heat transfer fluids. Or, there could be an alternative route: what if the thermophysical properties of a seemingly appropriate ionic liquid could be enhanced? This could be accomplished by uniformly dispersing small amounts of nanoparticles in an ionic liquid, as it was shown in 2010 by Nieto de Castro *el al.* [14], where the term *ionanofluid* was first used.

Nanofluids are manufactured through the dispersion of particles with an average size below of 100 nm on a given fluid. The term *ionanofluid* consists on using an ionic liquid as a base fluid. Since the conception of the term “nanofluid” in 1993 by S. Choi, the scientific community has been performing groundbreaking research on the surprising enhancement of the thermal properties of fluids when nanomaterials are added. For example, the enhancement of the thermal conductivity of EG by 11.9% when adding 0.2 % volume fraction of graphene [15], the enhancement of thermal conductivity of water by 32% when

adding 4.3% volume fraction of Al_2O_3 [16], or the increase of the heat capacity of [C_4mim][PF_6] up to 8% due to the addition of 0.015 mass fraction MWCNTs [14]. One of the main reason for this amplified interest lies on the possibility of developing highly efficient heat transfer fluids with significantly different thermal properties when compared with conventional heat transfer fluids [17]. Considering the thermal conductivity, it is expected that this property will play a vital role when considering a given fluid for heat transfer. However, traditional heat transfer fluids are usually characterized by a low thermal conductivity. Which leads to the question: how to enhance the thermal conductivity of a fluid?

Since the pioneer work of Maxwell in 1873 [18] regarding the enhancement of the thermal conductivity of liquids by the addition of solid particles, considerable research has been accomplished in order to enhance the generally low thermal conductivity of liquids, particularly when compared to the one of the solids. However, a considerable amount of research on this field was done considering particles on the *mili* or *micro* scale, which tend to quickly form deposits at the bottom of the vessel containing them. Additionally, the use of particles on these scales would not be compatible with the emerging miniaturized devices, as they would tend to clog the pipelines of said devices.

Several types of nanomaterials have been object of study over time, including metals, metal oxides, ceramics, polymers, among many others. However, the main focus appears to be on synthetic amorphous silica and nanocarbons [19].

Considering the latter, the dispersion of nanomaterials based on carbon such as carbon nanotubes or graphene in ionic liquids have been an active research topic since the discovery of “bucky gels” in 2003 by Fukushima *et al.* [20, 21], being described then as gelatinous, soft composite materials. These and related systems have a number of applications including in new materials, processes, and electronic or electrochemical devices. Ionic liquids supported in gels are relevant as

membranes for separations [22], and ionic liquids can be designed as solvents for exfoliation [23, 24] of carbon nanomaterials, leading to stable suspensions and new ways to functionalize or manipulate these nanomaterials, or new composite phases. The interface between ionic liquids and carbon nanomaterials is relevant in other contexts, for example in the development of better electrolytic supercapacitors [25], either by the design of organic electrolytes or of electrode materials, usually a nanoporous carbon [26], the use of carbon nanofibers in IL-based catalytic beds to improve the specific surface area [27] or the performance enhancement of dye-sensitized solar cells with IL electrolytes using carbon dots [28]. The work performed by Nieto de Castro *et al.* [14] showed enhancement of the thermal conductivity and heat capacity of ionic liquids through the addition of small amounts of multi-walled carbon nanotubes. But why did this enhancement occur? How does the heat transport take place in these systems? Can the interaction between these two types of materials explain the increase in the thermal conductivity, creating favorable paths for heat conduction? Can the extent of the enhancement be predicted? The answer to these questions required approaches in two fronts.

In addition to an expansion in the database of ionanofluids' properties, through the experimental analysis of different amounts of nanomaterial with various ionic liquids, a fundamental understanding at the level of molecular interactions, structure and dynamics of the liquid phase is essential to explain this enhancement. Little is known about the influence of the thermal conductivity at the interface between ionic liquids and nanomaterials, as well as on the structure and extent of the interface, leading to a lack of understanding about the reasons for the observed enhancement and preventing the development of models [14, 29, 30] that can accurately predict the thermal conductivity of nanofluids. The use of current theories for

heat transfer in nanofluids raises several important questions namely that of the role of the interfacial (solid-liquid) properties.

Molecular simulation can provide insights into the conduction of heat in composite systems, while considering that a detailed description of the interactions at the ionic liquid/nanocarbon material interface is important to obtain a realistic description of both the ordering of ions at the interface and heat transfer. In spite of several studies in theoretical physical chemistry [23, 27, 31], using electronic structure calculations and molecular simulation while aiming to understand the interactions between ionic liquids and carbon nanomaterials, the present knowledge is still not sufficient to establish structure–property relations that can guide the choice of the best fluids and materials in view of applications. Therefore, it is necessary to improve the understanding of systems composed of ionic liquids and carbon nanomaterials, such as graphene sheets and nanotubes, through a detailed modeling of the interactions at the interface and a study of the resulting structural, energetic and transport properties, using molecular simulation.

Ultimately, the articulation of experimental and theoretical studies is the main objective of the work here presented: the measurement of thermophysical properties of ionanofluids and the modeling of the interactions between ionic liquids and nanomaterials, with a particular emphasis on the solid-liquid interface. A brief contextualization of the work performed is at the beginning of each upcoming chapter in this dissertation. Chapter 2 and 3 consist essentially of experimental data on ionanofluids. Chapter 4 presents the results obtained through molecular dynamics studies, regarding structural information and heat transport on composite systems with ionic liquids and a single-walled carbon nanotube or a stack of graphene sheets. Chapter 5 presents the final set of experimental results on ionanofluids and comparison of the performance between

conventional heat transfer fluids and ionanofluids for a given process, regarding the heat transfer area. Finally, the conclusions and future perspectives are presented on Chapter 6.

The author of the present dissertation is responsible for the majority of the production and analysis of the results obtained in the following chapters, properly supported by the supervisors and with the collaboration of the remaining authors of the articles.

Chapter 2

Thermal Conductivity of $[C_4mim][(CF_3SO_2)_2N]$ and $[C_2mim][EtSO_4]$ and Their IoNanofluids with Carbon Nanotubes: Experiment and Theory

The first results regarding the measurement of thermal conductivity of ionanofluids are presented in this chapter, considering a different method than the one used by Nieto de Castro *et al.* [14]. The difference between the present and the latter consists on obtaining a stable suspension with some fluidity, instead of a "bucky gel". The ability for the ionanofluid to flow is vital when considering an application such as heat transfer since a gel would be too thick to flow in the tubes of a heat exchanger. At the time, thermal conductivity data of ionic liquids was scarce and of ionanofluids even scarcer.

The main goals of this work were to understand the effect of adding multiwalled carbon nanotubes (MWCNTs) to an ionic liquid matrix and quantify the enhancement on its thermal conductivity. To that effect, three different values of mass fraction of nanomaterial were suspended in the ionic liquids to allow an analysis of the quantity of MWCNTs in two ways: 1) confirm that the enhancement of the thermal property is proportional to the quantity of nanomaterial; 2) at what point the fluidity of the suspension is compromised by the amount of nanomaterial suspended. The present chapter presents data on the thermal conductivity of 1-*n*-butyl-3-methylimidazolium bis(trifluoromethanesulfonylimide) ($[C_4mim][(CF_3SO_2)_2N]$) and 1-ethyl-3-methylimidazolium ethylsulfate ($[C_2mim][EtSO_4]$) at temperatures between 293 and 343 K and ionanofluids with MWCNTs based on the mentioned liquids.

It is worth mentioning that no surfactants were used in this work, or in the coming chapters. While the use of surfactants would most likely facilitate the suspension and, to some extension, remove the stability issue from the "equation", it would also affect the value of thermal conductivity of the suspensions. Therefore, the enhancement data obtained would be ambiguous concerning its source, *i.e.*, it would not be possible to ascertain which material was responsible for the thermal conductivity's enhancement and in what proportion.

Additionally, a test of the effect of water on the thermal conductivity of $[C_4mim][(CF_3SO_2)_2N]$ was also performed and the results showed that, at any given temperature, the thermal conductivity decreases with the amount of water added and that the effect increases with increasing temperature. This portion of the work was important to establish a relation between the presence of water in the ionic liquids and its influence on the thermal conductivity.

Finally, a theoretical interpretation of the thermal conductivity's enhancement was attempted using a model developed at the time for suspensions containing cylindrical particles [14]. The disparity between experimental and calculated values called out to the fact that the model was not able to distinguish different base fluids and greatly overestimated the enhancement of the thermal conductivity. These conclusions lead to consider and re-evaluate the role of the solid-liquid interface.

In the coming article, the author of the present dissertation designed and assembled the apparatus used for sustaining the vial containing the fluids to be measured, assisted on preparing the suspensions, performed the measurements, processed and applied the model to the experimental data, and wrote the manuscript draft.

Journal of chemical & engineering data

Article

pubs.acs.org/jced

Thermal Conductivity of $[C_4mim][(CF_3SO_2)_2N]$ and $[C_2mim][EtSO_4]$ and Their IoNanofluids with Carbon Nanotubes: Experiment and Theory

J. M. P. França, S. I. C. Vieira, M. J. V. Lourenço, S. M. S. Murshed, and C. A. Nieto de Castro*

Departamento de Química e Bioquímica and Centro de Ciências Moleculares e Materiais, Faculdade de Ciências, Universidade de Lisboa, 1749-016 Lisboa, Portugal

ABSTRACT: Measurements of the thermal conductivity of ionic liquids are extremely important for current chemical plant design of new environmentally safe processes. Existing data are very scarce and inaccurate. IoNanofluids have emerged as a possible alternative to current engineering fluids for heat transfer applications, namely in small volume heat exchangers. In the present paper we report new data on the thermal conductivity of of 1-*n*-butyl-3-methylimidazolium bis(trifluoromethanesulfonylimide ($[C_4mim][(CF_3SO_2)_2N]$) and 1-ethyl-3-methylimidazolium ethylsulfate ($[C_2mim][EtSO_4]$) at temperatures between (293 and 343) K and IoNanofluids with multiwalled carbon nanotubes based on them, to understand the effect of adding nanomaterials to a ionic liquid matrix and its effect on the mentioned thermal property. The application of existing models to predict the behavior of the IoNanofluids, namely, the enhancement in the thermal conductivity, showed that it is fundamental to understand better the mechanism of heat transfer in these systems, namely, the role played by the interface ionic liquid (cation and anion)−nanoparticle, whatever molecular shape they have. A test of the effect of water on the purity of $[C_4mim][(CF_3SO_2)_2N]$ was also performed, and results showed that at any given temperature the thermal conductivity decreases with the amount of water added and that the effect increases with increasing temperature.

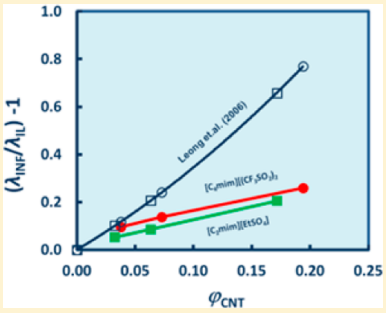

INTRODUCTION

In a time where the environmental awareness and the optimization of current energy technologies are so evidently emphasized, the unique characteristics of ionic liquids have drawn the attention of chemical companies and of the researching community over the last years. In fact, the potential displayed by these fluids reveals applicability in several areas of modern chemistry, from analytical chemistry to catalysis and from petrochemical industry to nuclear industry. Furthermore, these substances promise some benefits regarding the preservation of the environment, stimulating the practice of the philosophy of green chemistry.[1,2]

Nanomaterials and nanotechnology are a considerable part of the daily discussions on our society, revealing an ability to revolutionize modern life on various fields, from engineering to medicine. The main objective of current research is to minimize the volume of any material used, maintaining or upgrading the efficiency of the latter and to support a healthy economy. Modern nanotechnology can generate metallic or nonmetallic particles with distinct mechanical, optical, magnetic, electrical, and thermal properties.[3] When stably suspended in a fluid, these particles can greatly enhance the properties of the host fluid, becoming a nanofluid.[4]

Ionic liquids have been studied as possible heat transfer fluids due to their high volumetric heat capacity and good thermal conductivity,[5] and the combination of nanomaterials with these fluids creates great expectation considering the enhancement of the thermal properties. Recent work on this area has been accomplished by Nieto de Castro et al.,[6−9] successfully measuring the thermal conductivity of mainly imidazolium based ionic liquids with suspended multiwalled carbon nanotubes (MWCNTs) as a function of temperature, giving rise to the term IoNanofluids. The use of nanoparticles as enhancing agents of the fluid properties enables the association of little quantities of different nanoparticles with different ionic liquids, thus obtaining flexible and designable (on a molecular level) substances that can be conceived according to the properties needed for a certain application.

This work reports thermal conductivity measurements of 1-*n*-butyl-3-methylimidazolium bis(trifluoromethanesulfonylimide ($[C_4mim][(CF_3SO_2)_2N]$) and 1-ethyl-3-methylimidazolium ethylsulfate ($[C_2mim][EtSO_4]$) at temperatures between (293 and 343) K and IoNanofluids based on them, to understand the effect of adding nanomaterials to a ionic liquid matrix and its effect on the mentioned thermal property. This is justified by the fact that results previously obtained for the thermal conductivity enhancement for $[C_4mim][(CF_3SO_2)_2N]$[7] were much higher than the corresponding values for the other members of the 1-alkyl-3-methylimidazolium and for the need to assess the exact uncertainty of the data

Received: November 5, 2012
Accepted: January 15, 2013
Published: January 30, 2013

obtained with commercial equipment, increasing the performance of the measuring device used. Therefore, a calibration with the use of reference substances such as water and toluene and other liquids with thermal conductivities within the values of these fluids was carried out to account for the deviation of the device.

Finally, the enhancement on the thermal conductivity was evaluated and analyzed by comparison with a recently conceived theoretical model[10] developed to estimate the thermal conductivity of nanofluids with cylindrical nanoparticles. However, some limitations were found, as described below. This problem was discussed in detail in our recent publications.[11,12]The application of existing models to predict the behavior of IoNanofluids, namely, the enhancement in the thermal conductivity, showed that it is fundamental to understand better the mechanism of heat transfer in these systems, namely, the role played by the interface ionic liquid (cation and anion)−nanoparticle, whatever shape they have. Such understanding requires theoretical developments and molecular simulation studies that will give the insight for developing new heat transfer models.

EXPERIMENTAL SECTION

Materials. Both ionic liquids were purchased from IoLiTec, Ionic Liquids Technologies, Germany, and the product specifications of the certificate analysis can be found in Table 1. The estimated mass purity is 99 % or better. The unusual color of the liquids is due to a vestigial presence (below 1 part in 10 000) of the corresponding bromide precursor, since it is common for these liquids to be synthetized with a chloride precursor and therefore, usually, remain colorless. The water content was confirmed using Coulometric Karl Fischer titration (Metrohm 831). No further purification was performed, especially drying, as the influence of water in the thermal conductivity only becomes significant for concentrations bigger than 1000 ppm at the higher temperatures, as described below. Therefore, even for a liquid like $[C_2mim][EtSO_4]$, completely miscible with water, the water control and its influence on the thermal conductivity can be easily controlled.

Table 1. Ionic Liquid Specifications

property	$[C_4mim][NTf_2]$	$[C_2mim][EtSO_4]$
identity (NMR, IR)	pass	pass
assay (NMR)	> 99 %	99 %
cation (IC)	99.8 %	> 99 %
anion (IC)	99.9 %	> 99 %
halides (IC)	< 100 ppm	< 100 ppm
water (KF)	70 ppm	360 ppm
appearance	yellow liquid	orange liquid
date	Jan 29, 2010	Jan 29, 2010

The carbon nanotubes used were multiwalled carbon nanotubes, Baytubes C150 HP (MWCNTs) from Bayer Material Science, a development product that has been previously used by our group; detailed specifications can be found in Table 2.[6]

Table 2. Baytubes C150 HP Product Specification[a]

property	value	unit	method
C-purity	> 99	%	elementary analysis
free amorphous carbon	not detectable	%	TEM
number of walls	3−15		TEM
outer mean diameter	13−16	nm	TEM
outer diameter distribution	5−20	nm	TEM
inner mean diameter	4	nm	TEM
inner diameter distribution	2−6	nm	TEM
length	1−10	μm	SEM
bulk density	140−230	$kg \cdot m^{-3}$	EN ISO 60

[a]http://www.baytubes.com/product_production/baytubes_data.html.

Equipment and Methodology. Thermal conductivity was measured using KD2 Pro Thermal Properties Analyzer (Decagon Devices, Inc.). The principle of measurement is based on the transient hot-wire method (THW) using a single-needle sensor (1.3 mm diameter and 60 mm long). This sensor contains a heating element and a thermal resistor which should be inserted vertically in the sample to ensure that free convection is minimized. The measurement is accomplished through the heating of the sensor (inserted in the sample) at a certain rate while simultaneously monitoring the temperature variation. All this is controlled by a microprocessor connected to the sensor that also calculates the thermal conductivity of the sample based on a parameter-based corrected version of the temperature model given by Carslaw and Jaeger for an infinite line heat source with constant heat output and zero mass in an infinite medium.[13] Further information on these calculations can be found elsewhere.[6,14] Each measured sample had an approximate volume of 85 cm^3 to ensure that the dimensional requirements of the sensor were matched, since it was specified in the device's manual that a minimum amount of material should be present in all directions. With the sensor inserted vertically, the glass vial was then suspended (not inserted, to avoid that the vibrations of the bath could induce convection) in a temperature-controlled oil bath (Haake C25; oil − Galp Electric 2) and allowed to stabilize the temperature for each sample measured. The time to reach the desired temperature fluctuated with the sample being measured since in the case of the IoNanofluids it took longer as these fluids are more viscous and thick, therefore with smaller thermal diffusivity. Once the desired temperature was attained, 8 to 10 measurements were taken with an interval of 15 min between each one to ensure reproducibility. Temperature was measured by a platinum resistance probe, part of the thermal conductivity probe, with an uncertainty of 0.1 K.

Calibration is an important part of any analytical procedure in the sense that it allows determining the extension of the deviation of the measured property of the substance being studied through the comparison/correspondence with the value of the same property of a known and rigorously studied standard. Regarding thermal conductivity of liquid substances, water and toluene are two substances considered as standards by IUPAC, as their thermal conductivity was determined by the use of the most accurate measuring method, the transient hot-wire (THW).[15,16] As such, the thermal conductivity of water and toluene were measured. Since the gap between the values of thermal conductivity of these two substances is substantial (λ_{water} = 0.6065 $W \cdot m^{-1} \cdot K^{-1}$ and $\lambda_{toluene}$ = 0.13088 $W \cdot m^{-1} \cdot K^{-1}$ at 298.15 K and 0.1 MPa), it was completed with the measurements of three other fluids that had also been measured with the THW method, obtaining a significant range of thermal conductivities in which the device's deviation was accounted for, as shown in Table 3, namely, glycerin and a 50/50 (w/w) mixture of glycerin and water.[17] The aqueous solution of NaCl had the additional purpose of confirming that the sensor was electrically insulated, since the ionic liquid is electrically

Table 3. Thermal Conductivities of the Calibrating Liquids between (293 and 298) K

substance	T/K	λ/W·m^{-1}·K^{-1}
water[16]	298.15	0.6065
toluene[15]	298.15	0.13088
glycerin[17]	293.15	0.2850
glicerine + water (50:50 w/w)[17]	293.15	0.4198
$NaCl_{(aq)}$ (m = 2.7015 mol·kg^{-1})[18]	297.39	0.5891

conducting.[18] If the sensor had any flaw in its insulation then, at least partially, the electrical current that passes through the sensor to generate heat would be transferred to the sample (ions in the ionic liquid). Hence, the current would cause an increase in the ions movement, leading to convection and, finally, to a misleading increase in the thermal conductivity, which was never observed.

Once all of the calibrants were measured, the calibration constant was determined using eq 1:

$$K = \frac{\lambda_{meas}}{\lambda_{ref}} \quad (1)$$

where λ_{meas} represents the measured thermal conductivity of the fluid (average result of several measurements) and λ_{ref} represents the thermal conductivity of the reference fluid, at the same temperature and pressure.

Based on previous work[6,7] and on the suggestions of Fukushima and co-workers,[19,20] the IoNanofluids were prepared using a sonication probe (Sonicator Sonics & Materials, VC50) to disperse 0.5 %, 1 %, and 3 % mass fraction of MWCTN's in both ionic liquids. Contrary to the above-mentioned work,[6,7] the present goal was to obtain a fluid and not a gel to acknowledge the possible use of these IoNanofluids as a heat transfer fluids.[21,22] In that sense, these substances had to possess fluidity and, therefore, were prepared in different conditions. It is worth mentioning that no surfactants were added to the emulsion since any thermal conductivity values would be masked due to the presence of such substances and it was our intention to acquire the most truthful data possible. In fact, in a recent paper,[23] Murshed et al. demonstrated that all surfactant-added nanofluids have a larger enhancement of thermal conductivity compared to the same nanofluids without any surfactant, for nanofluids based in water. Moreover, while the addition of surfactant contributes in enhancing the effective thermal conductivity, the nanoparticle clustering showed negative impact on both the stability and the effective thermal conductivity of nanofluids.

Lastly, the uncertainty of the thermal conductivity was estimated from the standard deviations of the calibration and experimental measurements, considering a 95 % confidence level and a coverage factor k = 2.

RESULTS AND DISCUSSION

Calibration. The set of calibrants was measured at different temperatures as presented in Table 4. To obtain K, it was needed to consider the average value of the measurements of thermal conductivity at each temperature. Therefore, eq 1 was used to obtain K_i at each temperature. Performing the arithmetic mean of the values of K_i we obtained the value of K. Thus, the calibration constant has a value of 1.206 with a standard deviation of ± 0.034. This value of K illustrates that the thermal conductivities measured with the device have a deviation of +2.1 % relatively to the reference values. To correct this deviation, all of the values of the studied substances in this work were divided by K, and the intrinsic deviation of KD2 Pro was accounted for.

The variation of the calibration constant with the thermal conductivity of the calibrants and with temperature is shown in Figures 1 and 2. It can be seen on these figures that most of the values fall within the statistical interval $K \pm \sigma$. The value found for the NaCl aqueous solution is slightly smaller, but only one temperature was measured. However it is within the statistical interval of 95 % confidence ($K \pm 2\sigma$), so we cannot conclude that this is cause by an electric leakage in the thermal probe.

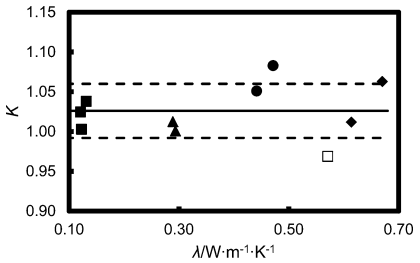

Figure 1. Calibration constant K as a function of the thermal conductivity of the calibrating liquids. ---, K = 1.026 ± 0.034; ♦, water; ■, toluene; ▲, glycerine; ●, glycerine + water (50 % w/w); □, NaCl (aq).

From the results obtained we can conclude that K is liquid-independent according to Figure 1 and also temperature-independent, according to Figure 2, as expected.

Table 4. Mean and Reference Values of Thermal Conductivity To Estimate the Calibration Constant K

substance	T/K	λ_{meas}/W·m^{-1}·K^{-1}	λ_{ref}/W·m^{-1}·K^{-1}	K_i	K	σ_K
water	298.3	0.6138	0.6066	1.0118	1.026	0.034
	313.7	0.6701	0.6305	1.0629		
toluene	313.9	0.1311	0.1263	1.0382		
	328.1	0.1224	0.1221	1.0029		
	343.7	0.1205	0.1176	1.0247		
glycerine	293.8	0.2888	0.2852	1.0125		
	321.5	0.2933	0.2931	1.0008		
glycerine + water	293.3	0.4412	0.4198	1.0511		
	312.7	0.4711	0.4350	1.0830		
$NaCl_{(aq)}$	298.1	0.5707	0.5891	0.9688		

dx.doi.org/10.1021/je301183r | J. Chem. Eng. Data 2013, 58, 467−476

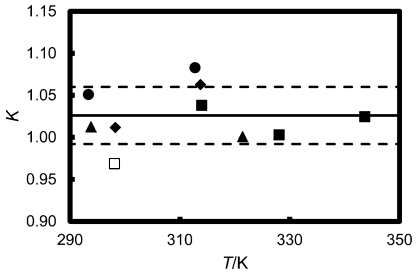

Figure 2. Calibration constant K as a function of temperature. ---, K = 1.026 ± 0.034; ♦, water; ■, toluene; ▲, glycerin; ●, glycerin + water (50 % w/w); □, NaCl (aq).

As a final note on this subsection, from this point onward all experimental values of thermal conductivity are referred to average values, in agreement with the mentioned 8 to 10 measurements for each temperature in the Experimental Section.

Pure Ionic Liquids. The thermal conductivities of $[C_4mim][(CF_3SO_2)_2N]$ and $[C_2mim][EtSO_4]$ were measured between (293 and 343) K at 0.1 MPa. Table 5 shows the results obtained. Based on previous work,[5−7] the ILThermo[24] database was consulted to obtain reference values to compare our results with, but no such references were found for $[C_4mim][(CF_3SO_2)_2N]$. Therefore, our reference thermal conductivity value was found in Ribeiro et al.[7] work. Concerning $[C_2mim][EtSO_4]$, such reference was found the work of Ge et al.[25] Analyzing the results, a small scatter can be seen with increasing temperature for both liquids, but it was more noticeable in the case of $[C_4mim][(CF_3SO_2)_2N]$, while in the case of $[C_2mim][EtSO_4]$ it tends to softly decrease with temperature. As it will be seen further in this paper, the standard deviations of the thermal conductivities of the latter were greater than the ones for $[C_2mim][EtSO_4]$. Such facts can be accounted for by the difference in viscosity between them. According to the values found in the literature, $[C_2mim][EtSO_4]$ has a higher viscosity at room temperatures (0.05001 Pa·s)[26] than $[C_4mim][(CF_3SO_2)_2N]$ (0.0285 Pa·s).[27] KD2 Pro is a device that greatly depends on the viscosity of the fluids being measured,[28] meaning that the greater the viscosity of the fluid, the more accurate will the measurements be. Considering that for both liquids viscosity decreases with temperature, this would explain the dissimilarity in standard deviation values and, consequently, the uncertainty of each value. The results obtained for each liquid were fitted to a straight line, according to eq 2, and Table 6 shows the coefficients obtained, as well as the root-mean-square deviations of the fits.

$$\lambda(\mathrm{W{\cdot}m^{-1}{\cdot}K^{-1}}) = a_1 + a_2(T/\mathrm{K}) \quad (2)$$

It can be seen that the variation is linear for both liquids. For $[C_4mim][(CF_3SO_2)_2N]$ no data point departs from linearity by more than ± 1.1 %, with an almost independent temperature variation. The root-mean-square deviation of the fits did not exceed 1.14 $\mathrm{mW{\cdot}m^{-1}{\cdot}K^{-1}}$, about 1 %. For $[C_2mim][EtSO_4]$ no data point departs from linearity by more than ± 1.1 %, with an almost independent temperature variation. The root-mean-square deviation of the fits did not exceed 1.22 $\mathrm{mW{\cdot}m^{-1}{\cdot}K^{-1}}$, about 0.7 %.

The uncertainties of the experimental data were estimated to obtain the expanded uncertainty, U_G, using the normal procedure. This parameter is obtained multiplying the combined standard uncertainty, u_G, by an expansion factor k, that depends of the confidence limit of the interval, usually 95 %, and therefore k = 2. The expression to calculate the standard uncertainty is the following:

$$u_G^2 = u_{cal}^2 + u_{exp}^2 \quad (3)$$

where u_{cal} represents the uncertainty of the calibration (the standard deviation of the calibration constant, 0.034) and u_{exp} the uncertainty of the each experimental measurement, (the standard deviation of the average thermal conductivity at each temperature, taken from 8 to 10 measurements). The value of U_G is therefore given by:

$$U_G = k{\cdot}u_G \quad (4)$$

The major contribution for the uncertainty results from the calibration constant. The uncertainty obtained is about 0.008 $\mathrm{W{\cdot}m^{-1}{\cdot}K^{-1}}$ or 7.1 %, for $[C_4mim][(CF_3SO_2)_2N]$, and 0.011

Table 5. Experimental Thermal Conductivities of Pure Ionic Liquids as a Function of Temperature

ionic liquid	T/K	λ/$\mathrm{W{\cdot}m^{-1}{\cdot}K^{-1}}$
$[C_4mim][(CF_3SO_2)_2N]$	293.42	0.1114
	302.84	0.1133
	313.61	0.1135
	323.25	0.1111
	333.30	0.1123
	343.39	0.1111
$[C_2mim][EtSO_4]$	293.42	0.1706
	302.86	0.1708
	313.61	0.1707
	323.67	0.1667
	333.55	0.1653
	343.91	0.1648

Table 6. Coefficients of eq 2 for Pure Ionic Liquids and IoNanofluids

ionic liquid	$a_1 \pm \sigma_{a1}$ $\mathrm{W{\cdot}m^{-1}{\cdot}K^{-1}}$	10^5 $(a_2 \pm \sigma_{a2})$ $\mathrm{W{\cdot}m^{-1}{\cdot}K^{-2}}$	10^5 σ $\mathrm{W{\cdot}m^{-1}{\cdot}K^{-1}}$
$[C_4mim][(CF_3SO_2)_2N]$	0.11799 ± 0.00870	−1.846 ± 2.728	114
$[C_2mim][EtSO_4]$	0.21230 ± 0.00918	−13.86 ± 2.878	122
$[C_4mim][(CF_3SO_2)_2N]$ + 0.5 % MWCNT	0.13673 ± 0.00630	−5.071 ± 1.961	76
$[C_4mim][(CF_3SO_2)_2N]$ + 1 % MWCNT	0.13836 ± 0.00145	−4.021 ± 0.450	17
$[C_4mim][(CF_3SO_2)_2N]$ + 3 % MWCNT	0.15352 ± 0.00085	−4.536 ± 0.265	10
$[C_2mim][EtSO_4]$ + 0.5 % MWCNT	0.19459 ± 0.00307	−5.238 ± 0.957	37
$[C_2mim][EtSO_4]$ + 1 % MWCNT	0.19731 ± 0.00190	−4.157 ± 0.590	23
$[C_2mim][EtSO_4]$ + 3 % MWCNT	0.20558 ± 0.00141	−0.179 ± 0.437	17

$W \cdot m^{-1} \cdot K^{-1}$ or 6.4 % for $[C_2mim][EtSO_4]$, very similar values. We can therefore conclude that the instrument used, the KD2Pro, con only give, even after careful calibration with reference liquids, data not better than 6 % to 7 % uncertainty, at a 95 % confidence level. This is very high for accurate thermophysical data research, but reasonable when exploring new complex fluids, as the IoNanofluids. Current research in our laboratory aims to develop an accurate system, based on the transient hot-strip technique with metal-film sensors, especially designed for ionic liquids.[29,30]

A comparison of this data with existing data is presented in Figure 3. Only two sets of data, both taken at QUILL, one

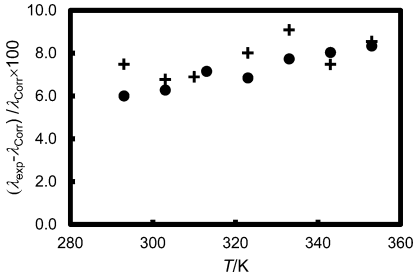

Figure 3. Comparison between the data obtained and those existing in the literature. +, $[C_4mim][(CF_3SO_2)_2N]$, Ribeiro et al.;[7] ●, $[C_2mim][EtSO_4]$, Ge et al.[25]

involving our group.[7,25] Both sets of data, as found in previous publications, are systematically higher by 6 % to 9 %. One possible explanation for such difference may reside in the dissimilarity in the precursors used in the synthesis of the ionic liquids in each case. Ge et al.[25] showed that the presence of the chloride anion increases the thermal conductivity of the ionic liquid. In the present case, the precursor used was a bromide anion, having a light color as presented in Table 1, which can be considered as an explanation to the difference in the thermal conductivity between the values presented in this work and the references. However, the deviations are within the mutual uncertainty of the data, though showing a slightly different trend with the variation with temperature.

IoNanofluids. The thermal conductivities of the IoNanofluids based on $[C_4mim][(CF_3SO_2)_2N]$ and $[C_2mim][EtSO_4]$, with 0.5 %, 1 %, and 3 % mass fraction were measured between (293 and 343) K at 0.1 MPa. Tables 7 and 8 show the results obtained as well as the percentage of enhancement of the thermal conductivity. This enhancement is estimated based on the thermal conductivity at the correspondent temperature of the base fluid for each case. Figures 4 and 5 show a plot of the thermal conductivity as a function of temperature, including the thermal conductivities of the corresponding ionic liquid shown in the previous section to allow a visual perception of the enhancement attained. The increase in the thermal conductivity of the base liquid is easily seen as well as the small temperature coefficient of the thermal conductivity of the IoNanofluids, as reported before for other systems. When placing the IoNanofluids in the measuring cell, it was noted that the time needed to stabilize the temperature was greater that with all of the fluids measured up to this point. As a result of the addition of nanomaterials the fluid's viscosity increased but not to a point that it did not flow (as that would be a factor to exclude these suspensions from the use as heat transfer fluids). As in

Table 7. Experimental Thermal Conductivities of IoNanofluids Based on $[C_4mim][(CF_3SO_2)_2N]$ as a Function of Temperature

substance	T/K	λ_{INF}/W·m^{-1}·K^{-1}	enhancement/%
$[C_4mim][(CF_3SO_2)_2N]$ + 0.5 % (w/w) MWCNTs	293.68	0.1220	9.52
	313.15	0.1209	6.52
	332.78	0.1190	5.97
	344.84	0.1199	7.92
$[C_4mim][(CF_3SO_2)_2N]$ + 1 % (w/w) MWCNTs	293.75	0.1266	13.65
	313.59	0.1257	10.75
	333.68	0.1248	11.13
	344.31	0.1247	12.24
$[C_4mim][(CF_3SO_2)_2N]$ + 3 % (w/w) MWCNTs	293.67	0.1402	25.85
	313.27	0.1394	22.82
	333.26	0.1383	23.15
	344.33	0.1380	24.21

Table 8. Experimental Thermal Conductivities of IoNanofluids Based on $[C_2mim][EtSO_4]$ as a Function of Temperature

substance	T/K	λ_{INF}/W·m^{-1}·K^{-1}	enhancement/%
$[C_2mim][EtSO_4]$ + 0.5 % (w/w) MWCNTs	293.69	0.1794	5.16
	313.49	0.1778	4.16
	333.67	0.1770	7.08
	343.71	0.1768	7.28
$[C_2mim][EtSO_4]$ + 1 % (w/w) MWCNTs	293.79	0.1852	8.56
	313.32	0.1842	7.91
	333.33	0.1832	10.83
	343.40	0.1832	11.17
$[C_2mim][EtSO_4]$ + 3 % (w/w) MWCNTs	293.77	0.2055	20.46
	313.36	0.2055	20.39
	333.41	0.2053	24.20
	343.42	0.2057	24.82

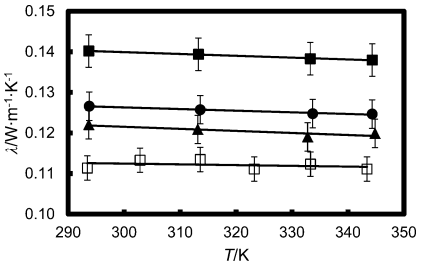

Figure 4. Thermal conductivity of pure $[C_4mim][(CF_3SO_2)_2N]$ and its IoNanofluids as a function of temperature. □, pure $[C_4mim][(CF_3SO_2)_2N]$; ▲, INF 0.5 % (w/w) MWCNTs; ●, INF 1 % (w/w) MWCNTs; ■, INF 3 % (w/w) MWCNTs. Error bars corresponding to ± u_G were inserted.

any suspension, obtained using sonication or mechanical grinding, time must be allowed for the suspension to stabilize to confirm that separation does not occur. Fukushima et al.[19,20] mentioned that the highest stable mass fraction that could be attained should be 1 % mass fraction, but we could achieve stable suspensions up to 3 % mass fraction of MWCNTs, still possessing fluidity. In their works, they introduced the concept of "bucky gels", being described as gelatinous, soft composite materials. There, a schematic structure was proposed by the authors suggesting a columnar arrangement between the ionic liquids and MWCNTs, a fact that has not yet been proved.

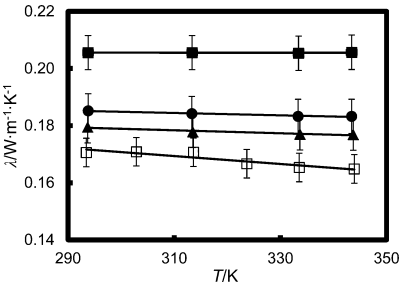

Figure 5. Thermal conductivity of pure $[C_2mim][EtSO_4]$ and its IoNanofluids as a function of temperature. □, pure $[C_2mim][EtSO_4]$; ▲, INF 0.5 % (w/w) MWCNTs; ●, INF 1 % (w/w) MWCNTs; ■, INF 3 % (w/w) MWCNTs. Error bars corresponding to ± u_G were inserted.

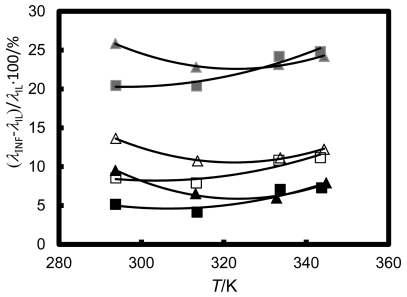

Figure 6. Thermal conductivity enhancement of IoNanofluids as a function of temperature. $[C_4mim][(CF_3SO_2)_2N]$, squares; $[C_2mim][EtSO_4]$, triangles; ▲, ■, 0.5 % (w/w) MWCNTs; △, □, 1 % (w/w) MWCNTs; gray ▲, ■, 3 % (w/w) MWCNTs.

Assuming that an identical arrangement occurred when preparing the IoNanofluids, a more organized structure appeared within the fluid. On the other hand, the organized structure of solids is one defining feature for better thermal conduction than liquids. Hence, it is safe to assume that the suspension of MWCNTs in the ionic liquid not only forces the ions to arrange in a more organized way, but they also take on an active role in heat conduction, justifying the enhancement of the thermal conductivity of these fluids. Measurements of the viscosity of these IoNanofluids and their Newtonian behavior are under progress and will be reported soon, a fact that will help to characterize better these systems, and their behavior as true suspensions or gels. A possible influence of the interfacial layer structure is advanced below.

Analyzing the experimental results, a clear inference can be made in addition to the thermal enhancement. As the mass fraction of nanomaterial increased, the experimental measurements of the thermal conductivity of the fluid were less scattered. From an application point of view, this feature can be quite relevant if the process in question needs a heat transfer fluid that can be used in a range of temperatures without compromising the efficiency of the fluid. From previous works[5,31] it was shown that the volumetric heat capacity of several ionic liquids is substantially greater than several commercial heat transfer fluids. Although further study is needed on this subject, if the thermal conductivity can be enhanced up to near 26 % and that the heat capacity also increases with the addition of nanomaterials,[6] an independence of the thermal conductivity relatively to temperature (at least in the studied range) is one more point in favor considering these suspensions as heat transfer fluids.

When comparing the enhancement obtained between ionic liquids, a slight difference was acknowledged. To support such observation, the enhancement percentages were plotted as shown in Figure 6. In the case of IoNanofluids based on $[C_4mim][(CF_3SO_2)_2N]$, a soft curve is noticeable with the increase of temperature, while in the case of the other set of IoNanofluids there is an increase at higher temperatures, surpassing the initial value of enhancement. While it is safe to say that the results corresponded when comparing the three mass fractions, further work on this topic may have interesting results to ascertain the progress of the enhancement at higher temperatures; that is, whether the enhancement of the first mentioned IoNanofluids would continue to increase or if the enhancement of the second group would stabilize.

Keeping in mind that all suspensions were prepared in the same way, the IoNanofluids based on $[C_2mim][EtSO_4]$ present a slightly higher enhancement at high temperatures, whereas the enhancement differs by 4 % to 5 % at the lowest temperature. On the other hand, $[C_4mim][(CF_3SO_2)_2N]$ has the lowest thermal conductivity of the two ionic liquids. Considering the two lowest temperatures, the benefit of the adding MWCNTs was greater in the case of $[C_4mim][(CF_3SO_2)_2N]$ following the argument on inducing order in the fluid mentioned before. The ions of $[C_2mim][EtSO_4]$ are significantly smaller when compared with the ions of $[C_4mim][(CF_3SO_2)_2N]$, and as such the packing and organization of the ions (limited to the characteristics of the fluid) are easier than with a superiorly bulky ion as $[(CF_3SO_2)_2N]^-$. Consequently, when adding the MWCNTs to prompt the appearance of the before mentioned columnar structure, the extension of the induced order is superior in the case of $[C_4mim][(CF_3SO_2)_2N]$ since the $[C_2mim][EtSO_4]$ ions are already more efficiently packed among them.

To support the findings related to the enhancement of the thermal conductivity, Lopes and Pádua[32] reported that $[C_nmim][(CF_3SO_2)_2N]$ and $[C_nmim][PF_6]$ ionic liquids are characterized by nanostructures. If the alkyl chains were $n \geq 4$, aggregation of the alkyl chains of the cation occurred, establishing nonpolar domains. This leads to the formation of a 3D network of ionic channels made by the anions and by the cations' imidazolium rings, allowing a microphase separation in polar in nonpolar zones in the ionic liquid structure. When MWCNTs are dispersed in the ionic liquid, these will rather interact with nonpolar zones associated to the alkyl chains, generating microaggregates that will enhance heat transfer. Further investigations in this subject are under progress, and we hope to report them soon.

The values reported here for the enhancement of the thermal conductivity of the IoNanofluid based on $[C_4mim][(CF_3SO_2)_2N]$ (≈ 12 %) are smaller than those obtained by Ribeiro et al.[9] (32 %), for 1 % (w/w) of MWCNTs. Also, the temperature dependence is different, facts that can in principle be explained by different manufacturing steps of the suspensions, and/or different lots of carbon nanotubes, although with the same manufacturer specifications. This results support the conclusion that the behavior of these IoNanofluids are strongly dependent on the procedure used in the manufacturing, and therefore it must be well-characterized, namely, the stability of the suspension/emulsion.

Table 9. Water Content of the Pure Ionic Liquids, Before and After the Measurements

ionic liquid	stated manuf. purity/%	manuf. H_2O/ppm	before measurements H_2O/ppm	after measurements H_2O/ppm
$[C_4mim][(CF_3SO_2)_2N]$	> 99 %	70	104.2 ± 19	239.2 ± 8
$[C_2mim][EtSO_4]$	> 99 %	360	486.1 ± 31	653.7 ± 11

Effect of Small Amounts of Water in the Thermal Conductivity of Ionic Liquids. As explained before, ionic liquids can absorb water from the atmosphere, and that effect on the measured values of the properties depends on these, being more significant for viscosity.[33,34] To access the influence of the water content in the thermal conductivity we have performed two independent essays. First, the water content of the samples was determined by Karl Fischer coulometry, just after the arrival from the manufacturer, and after the measurements (in the case of pure ionic liquids). The results are shown in Table 9. When the flasks were open, the water content was already 35 % to 50 % higher than the manufacturer statement. After the manipulation, filling the thermal conductivity cell and changing the temperature up to 343 K, the water content increased from (104.2 to 239.2) ppm for $[C_4mim][(CF_3SO_2)_2N]$, and from (486.1 to 653.7) ppm for $[C_2mim][EtSO_4]$. Although this variation is smaller than 1000 ppm or 0.1 %, it has to be known and monitored.

We were faced with the need to understand the effect of such quantities of water in the thermal conductivity of the measured samples, which lead us to the second test. Quantities of water to make mixtures with 0.5 % and 1 % (w/w) were added to $[C_4mim][(CF_3SO_2)_2N]$, and the solution was homogenized. Determinations at the same temperature were made for the pure fluid, and the "doped" solutions, for temperatures between (293.15 and 343.15) K. The results obtained are displayed in Table 10 and in Figure 7. It can be seen that adding water

Table 10. Values of the Thermal Conductivity of $[C_4mim][(CF_3SO_2)_2N]$ Water "Doped" Mixtures

ionic liquid mixture	T/K	λ/W·m^{-1}·K^{-1}
$[C_4mim][(CF_3SO_2)_2N]$ + 0.5 % (w/w) water	293.86	0.1140
	313.19	0.1141
	343.53	0.0991
$[C_4mim][(CF_3SO_2)_2N]$ + 1 % (w/w) water	293.82	0.1142
	303.74	0.1075
	313.40	0.1064
	323.07	0.1054
	333.24	0.0992
	343.34	0.0955

decrease the thermal conductivity of the ionic liquid, and that the effect increases with increasing temperature, except around room temperatures. Also, increasing the amount of water added, the thermal conductivity decreases more. This variation, at a given temperature can be estimated with eq 5:

$$\frac{\partial \lambda}{\partial x} \approx -b/\mathrm{W{\cdot}m^{-1}{\cdot}K^{-1}} \quad (5)$$

where we used molar fraction as the composition variable. The values obtained for b where $b = 0$ at 293 K, $b = 0.05$ at 313 K, and $b = 0.09$ at 343 K. The dependence of the molar fraction of water can be visualized in Figure 8, where the measuring uncertainty bars were included. These numbers show that the effect is significant and larger than the measurement uncertainty. This is indeed relevant to all experimental

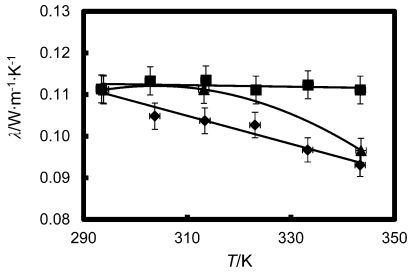

Figure 7. Thermal conductivity of water "doped" $[C_4mim][(CF_3SO_2)_2N]$ as a function of temperature. ■, pure ionic liquid; ▲, 0.5 % water; ♦, 1 % water. Error bars corresponding to ± u_G were inserted.

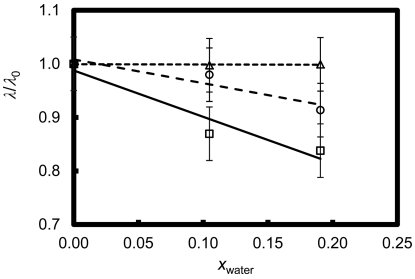

Figure 8. The ratio between the thermal conductivity of "doped" to that of "nondoped" ionic liquid, λ_0, as a function of the amount of water added, for $[C_4mim][(CF_3SO_2)_2N]$ at different temperatures. △, 293 K; ○, 313 K; □, 343 K. Error bars corresponding to ± u_G were inserted.

measurements concerning ionic liquids that are carried out on a global level, since the ill-handling of these substances can lead to erroneous results.

This fact is very surprising as the standard thermal conductivity of water[15] at 298.15 K and 0.1 MPa is 0.6065 W·m^{-1}·K^{-1}, about 6 times greater than that of the pure ionic liquid. Therefore an increase in the thermal conductivity of the mixture would be expected. The fact that water molecules "break" the structure of the ionic liquid, reducing the paths for heat conduction, at least at very low concentrations, has to be understood, and maybe molecular simulations, in addition to further experimental measurements of more concentrated mixtures IL + water, can help.

Theoretical Interpretation of the Results. Over the past few years, many publications have addressed to the clarification on why such enhancement occurs to the thermal conductivity of nanofluids through models other than the classical such as Maxwell's[35] since these fail to predict accurately the thermal conductivity of nanofluids considering that they were confined to suspensions with milli or microparticles.[3] Wang et al.[36] and Keblinski et al.[37] suggested possible mechanisms to explain the thermal conductivity enhancement, followed by other authors.[6,35,38] However, one generally accepted concept is the one

of the nanolayer interface, as liquid molecules can form a layer surrounding the nanoparticles and, consequently, increase the local order of the atomic structure at the interface region.[36] Such fact would implicate an order considerably greater than the one of the pure liquid since the order in solids is much greater as has been mentioned before. In this way, the nanolayer may be considered as an important factor relatively to enhancement of the thermal conductivity of nanofluids.

To clarify this situation Ribeiro et al. obtained TEM images of a sample of the IoNanofluid $[C_4mim][BF_4]$ + 1 % MWCNT.[7] These images show clearly the existence of a structured interface, the MWCNTs with the random coil 3D structure, but involved by a very clear white aureole, possible reproducing the interfacial layer with $[C_4mim][BF_4]$ molecules (average size of each unit (100 to 120) nm, with an interface layer around (50 to 70) nm thick), with a long-range attraction by the nanotubes. The aggregation of the different coils is clear, confirming the existence of microclusters that will enhance the heat transfer paths.

The model developed by Leong et al.[10,39] used for carbon nanotube IoNanofluids by Nieto de Castro et al.,[6] for infinitely long cylinders, takes into account a difference between the thermophysical properties between three distinct entities: the pure liquid, the nanoparticles, and the interface. The following equations were obtained for the thermal conductivity of a nanofluid containing cylindrical particles such as carbon nanotubes:

$$\lambda_{NF} = \{(\lambda_{CNT} - \lambda_{Int})\phi_{CNT}\lambda_{Int}[2\gamma_1^2 - \gamma^2 + 1] + (\lambda_{CNT} + 2\lambda_{Int})\gamma_1^2[\phi_{CNT}\gamma^2(\lambda_{Int} - \lambda_{IL}) + \lambda_{IL}]\} / \{\gamma_1^2(\lambda_{CNT} + 2\lambda_{Int}) - (\lambda_{CNT} - \lambda_{Int})\phi_{CNT}[\gamma_1^2 + \gamma^2 - 1]\} \quad (6)$$

where

$$\gamma = 1 + \frac{h}{a}$$

$$\gamma_1 = 1 + \frac{h}{2a} \quad (7)$$

In these equations, λ_{Int} represents the thermal conductivity of the interphase (interfacial layer), a the radius of the cylinder and h the thickness of the interfacial layer (nanolayer at the interface MWCNT-IL). As mentioned in Nieto de Castro's work, there is no actual value for λ_{Int} for such systems; hence this parameter is assumed as adjustable, with a value between those of the two components of the suspension, that is, $\lambda_{IL} < \lambda_{Int} \ll \lambda_{MWCNT}$. Similarly, we also considered the h with the value of 2 nm, since there is no theoretical model currently that allows the estimate of this parameter, according to Murshed et al.[10] Furthermore, in the same work it was considered that h is not critical to perform these calculations.

According to the Baytubes product certificate, a = 7.5 nm and the density (ρ) of the MWCNTs is 185 kg·m^{-3}. The values of density of the $[C_4mim][(CF_3SO_2)_2N]$ and $[C_2mim][EtSO_4]$ were taken from refs 40 and 41, respectively. Since there was no pre-established value for λ_{Int}, the following condition was applied: $\lambda_{Int} = \lambda_{IL}$. This condition is located at the lowest extreme of the interval mentioned above, and the thermal conductivity of the ionic liquid was experimentally measured in this work. The calculations were performed at 293 K and 0.1 MPa.

The results are shown in Figure 9, where the thermal conductivity enhancement is plotted as a function of the volume fraction of the IoNanofluid. It is clear that the theoretical values are remarkably different from the experimental ones, all being higher, except for the lowest volume fraction. In addition the model does not distinguish between the two ionic liquids, as shown by the line that fits the six theoretical points, three compositions for each fluid. Therefore, the model, at least with the parameters chosen, is not adequate for volume fractions higher than 4 %.

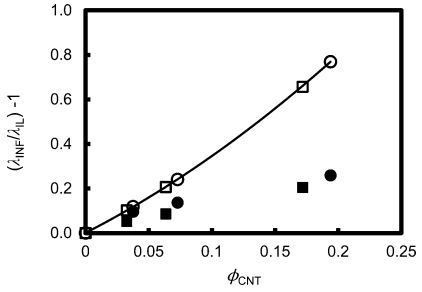

Figure 9. Thermal conductivity enhancement, $(\lambda_{INF}/\lambda_{LI})^{-1}$, as a function of the volumetric fraction of MWCNT, ϕ_{CNT}, for the IoNanofluids, at 293 K and 0.1 MPa. ●, $[C_4mim][(CF_3SO_2)_2N]$ INF, experimental; ■, $[C_2mim][EtSO_4]$, experimental; ○, $[C_4mim][(CF_3SO_2)_2N]$ INF, theory; □, $[C_2mim][EtSO_4]$ INF, theory.

As a simple exercise, it can be shown[42] that, by varying the thermal conductivity of the interphase, we can only obtain smaller calculated values if the thermal conductivity of the interface is below that range of values, basis of the model, i.e. $\lambda_{IL} < \lambda_{Int} \ll \lambda_{MWCNT}$. Also, the value of λ_{Int} needed to attain the value of λ_{meas} is inversely proportional to the mass fraction of nanomaterial. This reveals that the more MWCNTs are in suspension, the less relevant the thermal conductivity of the interface of IoNanofluid is.

This result, however, is not supported by the SEM images reported before, which lead us to a deeper analysis of the models for the heat transfer in nanofluids. On important result is that the interface seems much thicker than what was supposed by the model theories application ((50 to 70) nm thick, compared with h = 2 nm used). Recently Murshed and Nieto de Castro[12,43] have applied the concept of heat transfer by Brownian motion to the prediction of the thermal conductivity of nanofluids, with better results. We hope to report soon on this application to IoNanofluids.

■ CONCLUSIONS

This paper presents thermal conductivity values for $[C_4mim][(CF_3SO_2)_2N]$ and $[C_2mim][EtSO_4]$ and for IoNanofluids with MWCNTs. The measurements were performed with the KD2 Pro analyzer, which was demonstrated to be a suitable device for the measurement of thermal conductivity, with moderate uncertainty (6 % to 7 %, at a 95 % confidence level), provided that the instrument is carefully calibrated. A temperature and thermal conductivity calibration constant was obtained.

The thermal conductivity values of the pure ionic liquids are in agreement with the data published by other authors, within

their mutual uncertainty. Comparing the two IoNanofluids systems presented, $[C_4mim][(CF_3SO_2)_2N]$ based fluids have a greater enhancement of the thermal conductivity at lower temperatures, therefore benefiting more from the addition of MWCNTs as thermal enhancing agents. Enhancement percentages between 4 % and 26 % show that the thermal conductivity of potential heat transfer fluids such as ionic liquids is significant, which supports its use as new heat transfer fluids. It was possible to obtain highly stable suspensions with an elevated mass fraction of nanomaterial and still possess fluidity to be efficiently used as heat transfer fluids. Although the actual cost of ionic liquids is higher than conventional heat transfer fluids like water, ethylene and silicon oils, the future production of higher quantities can make their use competitive, especially if a target price of 25 US$/kg is achieved.[7,11]

The presence of water in the ionic liquids and its effect on the thermal conductivity showed that small amounts of water decrease it, a result contrary to what could be predicted in advance.

Finally the application of heat transfer models to IoNanofluids show an overestimation of the effects found, a fact that justifies further investigation.

AUTHOR INFORMATION

Corresponding Author

*E-mail: cacastro@fc.ul.pt.

Funding

The authors would like to thank FCT—Fundação para a Ciência e Tecnologia, Portugal, for funding projects PTDC/EQU-FTT/104614/2008 and PEst-OE/QUI/UI0536/2011 to C.C.M.M. and to BAYER Materials Science for supplying the MWCNTs (Baytubes).

Notes

The authors declare no competing financial interest.

REFERENCES

(1) *Ionic Liquids in Synthesis*; Wasserscheid, P., Welton, T., Eds.; Wiley-VCH: Weinheim, 2007.

(2) Pârvulescu, V.; Hardacre, C. Catalysis in Ionic Liquids. *Chem. Rev.* **2007**, *107*, 2615−2665.

(3) *Nanofluids: Science and Technology*; Das, S. K., Choi, S. U. S., Yu, W., Pradeep, T., Eds.; John Wiley & Sons, Inc.: New York, 2008; Chaps. 1−3.

(4) Choi, S. U. S.; Zhang, Z. G.; Yu, W.; Lockwood, F. E.; Grulke, E. A. Anomalous thermal conductivity enhancement in nanotube suspensions. *Appl. Phys. Lett.* **2001**, *79*, 2252−2254.

(5) França, J. M. P.; Nieto de Castro, C. A.; Lopes, M. M.; Nunes, V. M. B. The Influence of Thermophysical Properties of Ionic Liquids in Chemical Process Design. *J. Chem. Eng. Data* **2009**, *54*, 2569−2575.

(6) Nieto de Castro, C. A.; Lourenço, M. J. V.; Ribeiro, A. P. C.; Langa, E.; Vieira, S. I. C. Thermal Properties of Ionic Liquids and IoNanofluids of Imidazolinium and Pyrrolinium Liquids. *J. Chem. Eng. Data* **2010**, *55*, 653−661.

(7) Ribeiro, A. P. C.; Vieira, S. I. C.; Goodrich, P.; Hardacre, C.; Lourenço, M. J. V.; Nieto de Castro, C. A. Thermal conductivity of $[C_nmim][(CF_3SO_2)_2N]$ and $[C_4mim][BF_4]$ IoNanofluids with carbon nanotubes—Measurement, theory and structural characterization. *J. Nanofluids* **2013**, *2*, in press.

(8) Nieto de Castro, C. A.; Murshed, S. M. S.; Lourenço, M. J. V.; Santos, F. J. V.; Matos Lopes, M. L.; França, J. M. P. Ionanofluids—new heat transfer fluids for green process development, Chapter 8; In *Green Solvents I: Properties and Applications in Chemistry*; Mohammad, A., Inamuddin, Eds.; Springer Science and Business Media: Dordrecht, 2012.

(9) Nieto de Castro, C. A.; Murshed, S. M. S.; Lourenço, M. J. V.; Santos, F. J. V.; Matos Lopes, M. L.; França, J. M. P. Enhanced thermal conductivity and specific heat capacity of carbon nanotubes ionanofluids. *Int. J. Therm. Sci.* **2012**, *62*, 34−39.

(10) Murshed, S. M. S.; Leong, J. K.; Yang, C. Investigations of thermal conductivity and viscosity of nanofluids. *Int. J. Therm. Sci.* **2008**, *47*, 560−568.

(11) Nieto de Castro, C.; Ribeiro, A. P. C.; Vieira, S. I. C.; França, J. P. M.; Lourenço, M. J. V.; Santos, F. V.; Murshed, S. S. M.; Goodrich, P.; Hardacre, C. Synthesis, Properties and Physical Applications of IoNanofluids, Chapter 7. In *Ionic Liquids - New Aspects for the Future*; Kadokawa, J., Ed.; Intech: New York, 2013; pp 165−193.

(12) Murshed, S. M. S.; Nieto de Castro, C. A. Predicting the Thermal Conductivity of Nanofluids− Effect of Brownian Motion of Nanoparticles. *J. Nanofluids* **2012**, *1*, 180−185.

(13) *Conduction of Heat in Solids*; Carslaw, H. S., Jaeger, J. C.; Oxford University Press: London, 1959; p 256.

(14) Kluitenberg, G. J.; Ham, J. M.; Bristow, K. L. Error Analysis of the Heat Pulse Method for Measuring Soil Volumetric Heat Capacity. *Soil Sci. Soc. Am. J.* **1993**, *57*, 1444−1451.

(15) Ramires, M. L. V.; Nieto de Castro, C. A.; Nagasaka, Y.; Nagashima, A.; Assael, M. J.; Wakeham, W. A. Standard Reference Data for the Thermal Conductivity of Water. *J. Phys. Chem. Ref. Data* **1995**, *24*, 1377−1381.

(16) Ramires, M. L. V.; Nieto de Castro, C. A.; Perkins, R. A.; Nagasaka, Y.; Nagashima, A.; Assael, M. J.; Wakeham, W. A. Standard Reference Data for the Thermal Conductivity of Toluene over a Wide Range of Temperature. *J. Phys. Chem. Ref. Data* **2000**, *29*, 133−139.

(17) *Liquid Thermal Conductivity: A Data Survey to 1973*; Jamieson, D. T., Irving, J. B., Tudhope, J. S.; National Engineering Laboratory, HMSO: Edinburgh, 1975.

(18) Ramires, M. L. V.; Nieto de Castro, C. A.; Fareleira, J. M. N. A.; Wakeham, W. A. The Thermal Conductivity of Aqueous Sodium Chloride Solutions. *J. Chem. Eng. Data* **1994**, *39*, 186−190.

(19) Fukushima, T.; Kosaka, A.; Ishimura, Y.; Yamamoto, T.; Takigawa, T.; Ishii, N.; Aida, T. Molecular Ordering of Organic Molten Salts Triggered by Single-Walled Carbon Nanotubes. *Science* **2003**, *300*, 2072−2075.

(20) Fukushima, T.; Aida, T. Ionic Liquids for Soft Functional Materials with Carbon Nanotubes. *Chem.—Eur. J.* **2007**, *13*, 5048−5058.

(21) França, J. M. P.; Vieira, S. I. C.; Murshed, S. M. S.; Lourenço, M. J. V.; Nieto de Castro, C. A. Thermal conductivity of [C2mim][dca], [C4mim][dca] and [C4mpyr][dca] and their IoNanofluids with Nanosystems. To be submitted to *Fluid Phase Equilib.*

(22) França, J. M. P.; Reis, F.; Nieto de Castro, C. A.; Lopes, M. L. M. Importance of accurate data on the thermal conductivity, viscosity, density and heat capacity of ionic liquids and IoNanofluids: Heat exchanger design. To be submitted to *J. Chem. Eng. Data.*

(23) Murshed, S. M. S.; Nieto de Castro, C. A.; Lourenço, M. J. V. Effect of surfactant and nanoparticle clustering on thermal conductivity of aqueous nanofluids. *J. Nanofluids* **2012**, *1*, 175−179.

(24) *Ionic Liquids Database - (IL Thermo)*; NIST Standard Reference Database No. 147; NIST: Gaithersburg, MD, 2009.

(25) Ge, R.; Hardacre, C.; Nancarrow, P.; Rooney, D. W. Thermal Conductivities of Ionic Liquids over the Temperature Range from 293 to 353 K. *J. Chem. Eng. Data* **2007**, *52*, 1819−1823.

(26) Gomez, E.; Gonzalez, B.; Calvar, N.; Tojo, E.; Dominguez, A. Physical Properties of Pure 1-Ethyl-3-methylimidazolium Ethylsulfate and Its Binary Mixtures with Ethanol and Water at Several Temperatures. *J. Chem. Eng. Data* **2006**, *51*, 2096−2102.

(27) Harris, K. R.; Kanakubo, M.; Woolf, L. A. Temperature and Pressure Dependence of the Viscosity of the Ionic Liquids 1-Hexyl-3-methylimidazolium Hexafluorophosphate and 1-Butyl-3-methylimidazolium Bis(trifluoromethylsulfonyl)imide. *J. Chem. Eng. Data* **2007**, *52*, 1080−1085.

(28) *KD2 Pro Thermal Properties Analyzer Operator's Manual (version 7)*; Decagon Devices Inc.: Pullman, WA, 2008−2009.

(29) Ribeiro, A. P. C.; Lourenço, M. J. V.; Santos, F. J. V.; Serra, J. M.; Nieto de Castro, C. A. Design of new hot-strip sensors to measure thermal conductivity of ionic liquid systems. Paper presented at *WILS2012 - International Workshop on Ionic Liquids - Seeds for New Engineering Applications* FCUL Campus, Lisbon, Portugal, February 2−3, 2012.
(30) Ribeiro, A. P. C.; Lourenço, M. J. V.; Santos, F. J. V.; Serra, J. M.; Nieto de Castro, C. A. Thermal Conductivity of Ionic Liquids − New Hot-Strip Sensors and Measurements. Paper presented at the *18th Symposium on Thermophysical Properties*, Boulder, Colorado, June 24−29, 2012.
(31) Holbrey, J. Heat capacities of common ionic liquids—Potential applications as thermal fluids? *Suppl. Chim. Oggi/Chem. Today* **2007**, *25* (6), 24−26.
(32) Canongia Lopes, J. N. A.; Pádua, A. A. H. Nanostructural organization in ionic liquids. *J. Phys. Chem. B* **2006**, *110*, 3330−3335.
(33) Widegren, J. A.; Laesecke, A.; Magee, J. W. The effect of dissolved water on the viscosities of hydrophobic room-temperature ionic liquids. *Chem. Commun.* **2005**, *12*, 1610−1612.
(34) Widegren, J. A.; Magee, J. W. Density, viscosity, speed of sound, and electrolytic conductivity for the ionic liquid 1-hexyl-3-ethylimidazolium bis(trifluoromethylsulfonyl)imide and its mixtures with water. *J. Chem. Eng. Data* **2007**, *52*, 2331−2338.
(35) *A Treatise on Electricity and Magnetism*, 3rd ed.; Maxwell, J. C.; Clarendon Press: Oxford, U.K., 1891.
(36) Wang, X.; Xu, X.; Choi, S. U. S. Thermal conductivity of nanoparticle-fluid mixture. *J. Thermophys. Heat Transfer* **1999**, *13*, 474−480.
(37) Keblinski, P.; Phillpot, S. R.; Choi, S. U. S. Mechanisms of heat flow in suspensions of nano-sized particles (nanofluids). *Int. J. Heat. Mass. Transfer* **2002**, *45*, 855−863.
(38) Murshed, S. M. S.; Leong, K. C.; Yang, C. Thermophysical and electrokinetic properties of nanofluids - A critical review. *Appl. Therm. Eng.* **2008**, *28*, 2109−2125.
(39) Leong, K.; Yang, C.; Murshed, S. A model for the thermal conductivity of nanofluids - the effect of interfacial layer. *J. Nanopart. Res.* **2006**, *8*, 245−254.
(40) Troncoso, J.; Cerdeirina, C. A.; Sanmamed, Y. A.; Romani, L.; Rebelo, L. P. N. Thermodynamic Properties of Imidazolium-Based Ionic Liquids: Densities, Heat Capacities and Enthalpies of Fusion of [BMIM][PF_6] and [BMIM][NTF_2]. *J. Chem. Eng. Data* **2006**, *51*, 1856−1859.
(41) Garcia-Miaja, G.; Troncoso, J.; Romani, L. Excess enthalpy, density, and heat capacity for binary systems of alkylimidazolium-based ionic liquids + water. *J. Chem. Thermodyn.* **2009**, *41*, 161−166.
(42) França, J. M. P. Thermal Properties of IoNanofluids. MSc Thesis, Química Tecnológica, Faculdade de Ciências, Universidade de Lisboa, Lisboa, Portugal, 2010.
(43) Murshed, S. M. S.; Nieto de Castro, C. A. Contribution of Brownian Motion in Thermal Conductivity of Nanofluids. *Proc. World Congress Eng.*, July 6−8, 2011, London, U.K.; pp 1905−1909.

Chapter 3

Thermophysical properties of ionic liquid dicyanamide (DCA) nanosystems

The present chapter consists on a direct follow-up to the previous work in what concerns the measurement of thermophysical properties of ionic liquids and ionanofluids.

The results obtained with the previous work showed that the thermal conductivity of the base fluid was greatly enhanced by the addition of MWCNTs, supporting the consideration of ionic liquids and ionanofluids as heat transfer fluids. However, after considering the effects of adding MWCNTs on the viscosity and while the ionanofluids were still able to flow, the addition of mass fraction of nanomaterial up to 1% would undoubtedly increase the viscosity of the base fluid (as it will be discussed in the last chapter of this dissertation). This fact could represent a major set back in using these substances in a heat transfer application. As such, it was opted to proceed with similar work but with "low viscosity" ionic liquids. If the starting point of the suspension were to be an ionic liquid with lower viscosity, the end result should be a fluid with a more adequate viscosity and, consequently, a more suitable performance on the aforementioned application. At the time, dicyanamide ($N(CN)_2^-$) based ionic liquids showed great potential as they were considered to be part of the class of ionic liquids with lower viscosity.

As it was expected, a considerable enhancement of the thermal conductivity was observed in the ionic liquids studied here, specifically 1-*n*-butyl-3-methyl-imidazolium dicyanamide ($[C_4mim][N(CN)_2]$), 1-ethyl-3-methyl-imidazolium dicyanamide ($[C_2mim][N(CN)_2]$) and 1-butyl-1-methyl-pyrrolidinium dicyanamide ($[C_4mpyr][N(CN)_2]$), and ionanofluids with 0.5% and 1% w/w MWCNTs based on them. Thermal conductivity was measured at temperatures between 293 and 343 K at 0.1 MPa. The enhancement suggested an increase

in the organization of the fluid when carbon nanotubes are added to it. Though it was not entirely clear at the time what organized structure exists in these suspensions, a more organized structure is in agreement with a higher thermal conductivity.

However, the results also showed that the enhancement differs greatly from fluid to fluid, whether considering similar anions or cations. At this time, those involved in this work became aware that the idea of a unified model to estimate the enhancement of the thermal conductivity was becoming difficult to attain. Molecular dynamics studies on this topic would, to some extent, support this interpretation, as it can be seen in the Chapter 4. Nevertheless, the database on this topic was growing and conclusions could be drafted regarding the effect of the side alkyl chain, the planarity of the cation's head group and the anion identity in the thermal conductivity of the ionic liquids and also in the respective ionanofluids.

In addition to the thermal conductivity, the first data on density of ionanofluids was also presented. The samples and temperature range were the same as for the thermal conductivity. As expected, the variation of density from the addition of MWCNTs was very small due to extremely high difference in densities between the ionic liquids and the MWCNTs. From an application standpoint as heat transfer fluids, such low change in the density values by the addition of the MWCNTs can represent a positive outcome. Considering the four thermophysical properties of a heat transfer fluid necessary to design a heat transfer unit (thermal conductivity, heat capacity, viscosity and density), an increase in density represents a decrease in the principal design parameter, the heat transfer area, which in turn leads to an decrease in capital and operational costs. Therefore, a proper balance between these properties must be accomplished. Although a greater increase in the density would be preferable, this very low variation in density by the addition of MWCNTs indicates that there is one less variable that can influence the heat transfer area and the mentioned

balance will be more dependent on the variation of the remainder properties. The last chapter will provide more detail on this matter.
In the coming article, the author of the present dissertation prepared the suspensions, performed the thermal conductivity measurements, assisted on the density measurements, processed and applied the model to the experimental data and wrote the manuscript draft.

J. Chem. Thermodynamics 79 (2014) 248–257

Contents lists available at ScienceDirect

J. Chem. Thermodynamics

journal homepage: www.elsevier.com/locate/jct

Thermophysical properties of ionic liquid dicyanamide (DCA) nanosystems

J.M.P. França [a], F. Reis [a], S.I.C. Vieira [a], M.J.V. Lourenço [a], F.J.V. Santos [a], C.A. Nieto de Castro [a,*], A.A.H. Pádua [b]

[a] Centro de Ciências Moleculares e Materiais, Faculdade de Ciências, Universidade de Lisboa, 1749-016 Lisboa, Portugal
[b] Institut de Chimie de Clermont-Ferrand, Université Blaise Pascal and CNRS, BP 80026, 63171 Aubière, France

ARTICLE INFO

Article history:
Received 19 November 2013
Received in revised form 29 April 2014
Accepted 6 May 2014
Available online 22 May 2014

Dedicated to the memory of the late Professor Manuel Ribeiro da Silva.

Keywords:
Ionic liquids
IoNanofluids
Nanosystems
1-Ethyl-3-methyl-imidazolium dicyanamide
1-*n*-Butyl-3-methyl-imidazolium dicyanamide
1-Butyl-1-methyl-pyrrolidinium dicyanamide

ABSTRACT

IoNanofluids have emerged as a possible alternative to current engineering fluids for heat transfer applications, namely in small volume heat exchangers and micro-channels. Thermal conductivity and density play a crucial role for the chemical plant design of green processes. Existing data are very scarce and inaccurate, mostly affected by impurities and the presence of water in the ionic liquids.

In the present paper, we report new data on the thermal conductivity and density of 1-*n*-butyl-3-methyl-imidazolium dicyanamide ([C_4mim][dca]), 1-ethyl-3-methyl-imidazolium dicyanamide ([C_2mim][dca]) and 1-butyl-1-methyl-pyrrolidinium dicyanamide ([C_4mpyr][dca]) at temperatures between (293 and 343) K at $p = 0.1$ MPa and IoNanofluids based on them with MWCNTs (multi-walled carbon nanotubes), in order to understand the effect of adding nanomaterials to a ionic liquid matrix and its modification of the heat transfer mechanism. Discussion about the effect of the cation, its side alkyl chain, head group and anion structure in the properties studied concluded that it is essential to understand better the mechanism of heat transfer in these systems, namely the role played by the interface ionic liquid (cation and anion)-nanoparticle, whatever molecular shape they have. Current theories used to calculate the thermal conductivity enhancement are insufficient to predict its value and variation with volume fraction of the nanomaterial.

1. Introduction

In a time where the environmental awareness and the optimization of current energy technologies are so evidently emphasized, the unique characteristics of ionic liquids have drawn the attention of chemical companies and scientific community over recent years. The potential displayed by these fluids reveals applicability in several areas of modern chemistry, from analytical chemistry to catalysis and from petrochemical industry to nuclear industry. Furthermore, these substances promise some benefits regarding the preservation of the environment, stimulating the practice of the philosophy of green chemistry [1,2]. In the field of heat transfer, there is a need for new heat transfer fluids, capable of replacing environmentally harmful existing ones with properties that can result in maximum possible energy efficiency, in order to support healthy and sustainable applications, either domestic and/or industrial.

Nanomaterials and nanotechnology are a considerable part of the daily discussions on our society, revealing an ability to revolutionize modern life within various fields from engineering to medicine. The main objective of current research is to minimize the volume of any material used, maintaining or upgrading the efficiency of the latter and to support a healthy economy. Modern nanotechnology can generate metallic or non-metallic particles and structures with distinct mechanical, optical, magnetic, electrical, chemical and thermal properties [3]. Once stably suspended in a fluid, these particles can greatly enhance the properties of the host fluid, becoming a nanofluid [4].

Ionic liquids have been studied as possible heat transfer fluids due to their high volumetric heat capacity and good thermal conductivity [5] and the combination of nanomaterials with these fluids creates great expectation considering the enhancement of their thermophysical properties. Recent work on this area has been accomplished by Nieto de Castro *et al.* [6–10] successfully measuring the thermal conductivity and heat capacity of mainly imidazolium based ionic liquids with suspended multi-walled carbon nanotubes (MWCNTs) as a function of temperature, giving rise to

* Corresponding author. Tel.: +351 217 500 918; fax: +351 963 665 672.
E-mail address: cacastro@fc.ul.pt (C.A. Nieto de Castro).

http://dx.doi.org/10.1016/j.jct.2014.05.008
0021-9614/

the term IoNanofluids. The use of nanoparticles as enhancing agents of the fluids properties enables the association of little quantities of different nanoparticles with different ionic liquids, thus obtaining flexible and designable (on a molecular level) substances that can be conceived according to the properties needed for a certain application. In what concerns heat transfer, the fluid chosen for such a task should possess fluidity in order to be able to flow through the tubes of, for example, a shell and tube heat exchanger, or any other heat transfer unit. On the other hand, the fluidity of the suspension of nanoparticles will depend on the method used to attain the suspension itself. Considering the work of Aida and Fukushima [11,12], the use of "bucky gels" (there described as gelatinous, soft composite materials) in such an application would be somewhat limited, due to the lack of fluidity on part of these suspensions. In our latest work [10], the IoNanofluids based on $[C_4mim][(CF_3SO_2)_2N]$ and $[C_2mim][EtSO_4]$ could be described as slightly-to-moderate viscous fluids, *i.e.*, possessing considerable fluidity. As should be expected, the addition of nanomaterials to an ionic liquid should lead to an increase of the viscosity of the resulting IoNanofluid. Hence, if the starting point of the IoNanofluid were to be an ionic liquid with lower viscosity, the end result should be a fluid with a more adequate viscosity and, consequently, a more suitable performance on the aforementioned application. When comparing the viscosity values of the ionic liquids studied in reference [10,13,14] with the imidazolium dicyanamide ionic liquids here presented [15,16] at $T = 298.15$ K and 0.1 MPa, one can assess that the dicyanamide ionic liquids can have lower viscosity values that can range from (0.02 to 0.074) Pa · s. Thus, these ionic liquids may well be an optimum starting point considering the use of IoNanofluids as heat transfer fluids [5,8,10].

This work reports thermal conductivity and density measurements of 1-*n*-butyl-3-methyl-imidazolium dicyanamide ([C_4mim][dca]), 1-ethyl-3-methyl-imidazolium dicyanamide ([C_2mim][dca]) and 1-butyl-1-methyl-pyrrolidinium dicyanamide ([C_4mpyr][dca]) at temperatures between (293 and 343) K at 0.1 MPa and IoNanofluids based on them with MWCNTs. It also compares the obtained results with current theories of thermal conductivity enhancement in nanofluids.

2. Materials and methods

2.1. Materials

All three ionic liquids were purchased from IoLiTec, Ionic Liquids Technologies, Germany, and the product specifications of the certificate analysis can be found in table 1. The estimated mass fraction purity is 0.98 or better. As usual in the ionic liquids supplied by this company, the unusual colour of the liquids is due to the presence (below 2%) of the corresponding bromide precursor since it is common for these liquids to be synthesized with a chloride precursor and therefore, usually, remain colourless. The water content was confirmed using Coulometric Karl Fischer titration (Metrohm 831) and, being considerable to create an effect on the thermal conductivity [10], further purification was performed through drying the ionic liquids around $T = 333$ K, under vacuum, for a minimum period of 48 h. As the presence of water changes considerably the properties of the ionic liquids, its content was analyzed before and after the experimental measurements. Measurements were made at atmospheric pressure. Taking into account its variation in the laboratory during the measurement period, the values are reported to 0.1 MPa ± 1 kPa, the uncertainty being estimated by the maximum daily variation in the barometric pressure in the laboratory.

TABLE 1
Ionic liquids product specifications, purity as mass fraction.

Property	[C_2mim][dca]	[C_4mim][dca]	[C_4mpyr][dca]
Identity (NMR. IR)	Pass	Pass	Pass
Assay (NMR)	>0.98	>0.98	>0.98
Cation (IC)	0.987	0.992	0.999
Anion (IC)	0.989	0.985	0.995
Halides (IC)	<0.02	<0.02	<0.02
Water (KF)	$1850 \cdot 10^{-6}$	$1480 \cdot 10^{-6}$	$1710 \cdot 10^{-6}$
Appearance	Yellow liquid	Yellow liquid	Orange liquid
Date	02.02.2010	02.02.2011	02.02.2011

The carbon nanotubes used were multi-walled carbon nanotubes Baytubes C150 HP (MWCNTs) form Bayer Material Science, a development product that has been previously used by our group [6], and whose characteristics are displayed in table 2.

2.2. Equipment and methodology

2.2.1. Thermal conductivity

Thermal conductivity was measured using the KD2 Pro™ Thermal Properties Analyzer (Decagon Devices, Inc.). The principle of measurement is based on the transient hot-wire method (THW) using a single-needle sensor (1.3 mm diameter and 60 mm long). This sensor contains a heating element and a thermal resistor, which should be inserted vertically in the sample to assure that free convection, is minimized. The measurement is accomplished through the heating of the sensor (inserted in the sample) at a certain rate while simultaneously monitoring the temperature variation. All this is controlled by a microprocessor connected to the sensor that also calculates the thermal conductivity of the sample based on a parameter-based corrected version of the temperature model given by Carslaw and Jaeger for an infinite line heat source with constant heat output and zero mass in an infinite medium [17]. Further information on these calculations can be found elsewhere [6,18]. Each measured sample had an approximate volume of 85 cm^3 to ensure that the dimensional requirements of the sensor were matched, since it was specified in the device's manual that a minimum amount of material should be present in all directions. With the sensor inserted vertically, the glass vial was then suspended (not inserted, in order to avoid the vibrations of the bath that could induce convection) in a temperature-controlled oil bath (Haake C25; oil – Galp Electric 2) and allowed to stabilize the temperature for each sample measured. The time to reach the desired temperature fluctuated with the sample being measured, as for the IoNanofluids it took longer because these fluids are more viscous and thick, therefore with smaller thermal diffusivity. Once attained the desired temperature, 8 to 10 measurements were taken with an interval of 15 min between each one to ensure reproducibility. Temperature was measured by a platinum resistance probe, part of the thermal conductivity probe, with an uncertainty $u(T) = 0.1$ K.

Calibration is an important part of any analytical procedure in the sense that it allows determining the extension of the deviation of the measured property of the substance being studied through the comparison/correspondence with the value of the same property of a known and rigorously studied standard. The procedure of the calibration for the thermal conductivity measurements presented on this work has been extensively described elsewhere [10]. In summary, the experimental thermal conductivity of substances such as water, toluene, glycerin, a mixture of glycerin and water (50/50 w/w) and an aqueous solution of NaCl was used to obtain a calibration constant, K, given by equation (1):

$$K = \frac{\lambda_{meas}}{\lambda_{ref}}, \quad (1)$$

based on the ratio between the experimental thermal conductivity (λ_{meas}) and a bibliographic reference (λ_{ref}) of the same property at

TABLE 2
Baytubes® C150 HP product specification.[a]

Property	Value	Unit	Method
C-purity	>0.99	Mass fraction	Elementary analysis
Free amorphous carbon	Not detectable	Mass fraction	TEM
Number of walls	3 to 15		TEM
Outer mean diameter	13 to 16	nm	TEM
Outer diameter distribution	5 to 20	nm	TEM
Inner mean diameter	4	nm	TEM
Inner diameter distribution	2 to 6	nm	TEM
Length	1 to 10	μm	SEM
Bulk density	140 to 230	$kg \cdot m^{-3}$	EN ISO 60

[a] http://www.baytubes.com/product_production/baytubes_data.html.

the same temperature and pressure. This constant, liquid and temperature-independent, was found to have the value of (1.026 ± 0.034), illustrating an overestimate (+2.6% relatively to the reference values) by the device, and leading to the correction of the experimental data. The values for the reference values of the calibrating fluids can be found in reference [10].

2.2.2. Density

Density measurements were carried out in a vibrating tube densimeter Anton Paar DMA 512P, at atmospheric pressure. The range of temperature was obtained with the aid of the above mentioned temperature-controlled oil bath and monitored with a calibrated platinum thermometer with an expanded uncertainty of T = 0.05 K, placed at the entrance of the measuring cell.

Actions were taken to ensure that all of the material and adjacent parts of the densimeter were well cleaned and dry before measuring the density of each sample. After cautiously injecting the sample in the cell (in order to avoid the formation of bubbles), the liquid was allowed to stabilize at the current temperature for at least 15 min. Once the thermal equilibrium was attained, the vibrating period was registered (at least 10 records) given that the variation of the value was negligible.

The calibration for the density measurements of the present work was accomplished using a one-fluid calibration method based on the work of Lampreia and Nieto de Castro [19]. Although the theory of the instrument is well known, its use is still object of less accurate applications. Therefore we describe briefly its application here.

The density ρ of a given sample depends on the period of vibration τ of the mechanical oscillator through equation (2):

$$\rho = A\tau^2 - B, \tag{2}$$

where A and B are instrument characteristics which are determined through the use of calibrating fluids of known density. The measurement principle of the instrument is based on the change of natural frequency of a hollow oscillator when filled with different fluids. Equation (2) can be derived considering a system represented by a hollow body of mass M_0 under vacuum and volume $V(P,T)$ filled with a sample of density $\rho(P,T)$. This body would be suspended on a spring with a stiffness $K(P,T)$. The expressions for coefficients A and B are:

$$A = \frac{K}{4\pi^2 V}, \tag{3}$$

$$B = \frac{M_0}{V}. \tag{4}$$

Although A and B in equation (2) are physically meaningful parameters of the oscillating tube, they are usually evaluated by calibration with at least two fluids of known density. If the aim of the work is to measure density as a function of temperature and pressure, one should have accurate data for the two or more calibration fluids for the entire range of T and P, since they are temperature and pressure dependent. The work of Lagourette *et al.* [20] and Sousa *et al.* [21] visualized an alternative calibration method based on the experimental determination of the vibrating period of the evacuated tube, $\tau_0(T)$, assuming that the stiffness parameter K does not depend on P. As a consequence of this assumption, $A(T,P)$ and $B(T,P)$ would vary with P in the same way and A/B would be independent of P. The resulting working equation in this case is represented by equation (5):

$$\rho = \frac{M_0}{V}\left(\frac{\tau^2}{\tau_0^2} - 1\right) = B\left(\frac{\tau^2}{\tau_0^2} - 1\right). \tag{5}$$

This equation would thus correspond to a one fluid calibration method, provided that $\tau_0(T)$ is known. The most difficult part of this method consists on obtaining the latter experimentally, since perfect vacuum can never be attained. Consequently, the uncertainty of the measurements would be considerably affected. In this sense, the period of four certified density calibrants, water, toluene, glycerin and tetrachloroethylene, was measured and then, through simple mathematical manipulations of the equations, it is possible to obtain suitable values of $\tau_0(T)$ in order to use equation (5). Further information on the derivation of this method can be found in references [19,21].

2.2.3. Manufacture of IoNanofluids

Based on previous work [6,7,10] and on the suggestions of Fukushima and co-workers [11,12], the IoNanofluids were prepared using a sonication probe (Sonicator Sonics & Materials, VC50) to disperse (0.5 and 1)% mass fraction of MWCTNs in all three ionic liquids. Contrary to the above-cited work [6,7], the present goal was to obtain a fluid and not a gel in order to acknowledge the possible use of these IoNanofluids as a heat transfer fluids. In that sense, these substances had to possess some fluidity and, therefore, were synthesized under different conditions. It is worth mentioning that no surfactant was added to the emulsion since any thermal conductivity values would be masked due to the presence of such substances and it was our intention to acquire the most truthful data possible. In fact, Murshed *et al.* demonstrated in a recent publication [22] that all surfactant-added nanofluids have a larger enhancement of the thermal conductivity compared to the same nanofluids without any surfactant, for nanofluids based in water. Moreover, while addition of surfactant contributes in enhancing the effective thermal conductivity, the nanoparticle clustering showed negative impact on both the stability and the effective thermal conductivity of nanofluids. The uncertainty in the IoNanofluids mass fraction was found to be $u(w)$ = 0.0004.

The demonstration that aggregates are not present in the IoNanofluids can only be made by dynamical light scattering studies, a procedure used for nanofluids before. However, in the case of black nanofluids, these studies are more difficult to achieve and were not performed in the current study. However, our previous experience with other IoNanofluids, suggest that no aggregation is present at a microscopic scale, as the suspension could sediment with the presence of surfactants, which was not observed for several months.

3. Results and discussion

3.1. Thermal conductivity

3.1.1. Pure ionic liquids

The thermal conductivity of the three pure ionic liquids and several IoNanofluids was measured at temperatures between

(293 and 343) K at 0.1 MPa. In the case of the pure ionic liquids, the water content was confirmed using Coulometric Karl Fischer titration after the thermal conductivity (and density) measurements, values that are presented in table 3. Some increase in the water content was to be expected but, particularly in the case of the thermal conductivity, the increase was minor.

Table 4 displays the values obtained for the pure ionic liquids, which generally tend to softly decrease with temperature. The exception to this tendency is the thermal conductivity of [C_2mim][dca] at $T = 323$ K, where a considerable oscillation can be observed. Such a fact can be attributed to the sensitivity of the KD2 Pro to the variation of viscosity of the fluid being measured [10,23], given that the viscosity of ionic liquids decreases with the increase of temperature.

The results obtained for each liquid were fitted to a straight line, according to equation (6), and table 5 shows the coefficients obtained, as well as the root mean square deviations of the fits.

$$\lambda(\mathrm{W\cdot m^{-1}\cdot K^{-1}}) = \alpha_1 + \alpha_2(\mathrm{T/K}). \quad (6)$$

Figure 1 shows the variation of the thermal conductivity of the pure ionic liquids with temperature, for the range between (293 and 343) K at 0.1 MPa. It can be seen that the variation is linear for all three ionic liquids. For [C_2mim][(dca] no data point departs from linearity by more than ±1.06% (except for the value at $T = 323$ K, which undoubtedly differs from the rest of the data). The root mean square deviation of the fits did not exceed 3.83 mW · m^{-1} · K^{-1}, about 2%. For [C_4mim][dca], no data point departs from linearity by more than ±1.4% (except for the value at $T = 323$ K, which departs from linearity by +2.5%). The root mean square deviation of the fits did not exceed 2.73 mW · m^{-1} · K^{-1}, about 1.6%. Finally, for [C_4mpyr][dca], no data point departs from linearity by more than ±1.3%. The root mean square deviation of the fits did not exceed 1.74 mW · m^{-1} · K^{-1}, about 1.1%. For all three pure ionic liquids, the variation of the values is almost independent with the variation of temperature.

The uncertainties of the experimental data were estimated to obtain the expanded uncertainty, U_G, using the normal procedure. This parameter is obtained multiplying the combined standard uncertainty, u_G, by an expansion factor, k, that depends of the confidence limit of the interval, usually 95%, and therefore $k = 2$. The expression to calculate the standard uncertainty is the following:

$$U_G^2 = u_{\mathrm{cal}}^2 + u_{\mathrm{exp}}^2, \quad (7)$$

where u_{cal} represents the uncertainty of the calibration (the standard deviation of the calibration constant, 0.034) and u_{exp} the uncertainty of the each experimental measurement, (the standard deviation of the average thermal conductivity at each temperature, taken from 8 to 10 measurements). The value of U_G is therefore given by:

$$U_G = k \times u_G. \quad (8)$$

The major contribution for the uncertainty results from the uncertainty of each experimental measurement. The uncertainty obtained fluctuated between (0.012 and 0.021) W · m^{-1} · K^{-1}(6.7 to 12.5)% for [C_2mim][dca], between (0.010 and 0.014) W · m^{-1} · K^{-1} (6.6 to 9.2)% for [C_4mim][dca] and between (0.010 and 0.017) W · m^{-1} · K^{-1} (6.6 to 11.8)% for [C_4mpyr][dca]. The poorest case is represented by [C_2mim][dca], which exhibits only two values of thermal conductivity below 10% uncertainty. The low viscosity and the continued decrease of the latter with the increase of temperature of these ionic liquids had a greater influence on the results that would be desired. In this particular case, more than 10 measurements were acquired in order to minimize the fluctuation of the value obtained, specifically at the temperatures were this oscillation was observed. However, the results kept on fluctuating in the same fashion. In previously measured pure ionic liquids, the uncertainty of the thermal conductivity fluctuated between (6 and 7)% at a 95% confidence level, greatly influenced by the value of the calibration.

TABLE 3
Water content of the pure ionic liquids (Karl–Fischer coulometer).

Ionic liquid	[C_2mim][dca]	[C_4mim][dca]	[C_4mpyr][dca]
After drying $H_2O/10^{-6}$	234.7 ± 48.6	324.9 ± 86.4	349.6 ± 47.9
After measuring λ $H_2O/10^{-6}$	488.9 ± 58.6	683.6 ± 41.7	637.0 ± 57.0
After measuring ρ $H_2O/10^{-6}$	1007.4 ± 55.4	741.2 ± 20.3	1601.3 ± 84.5

TABLE 4
Thermal conductivities of pure ionic liquids as a function of temperature, at $p = 0.1$ MPa.[a]

Ionic liquid	T/K	λ/W · m^{-1} · K^{-1}
[C_2mim][dca]	293.4	0.183 ± 0.01
	303.3	0.179 ± 0.01
	313.1	0.178 ± 0.02
	323.0	0.181 ± 0.02
	333.2	0.170 ± 0.02
	343.4	0.165 ± 0.02
[C_4mim][dca]	293.6	0.167 ± 0.01
	303.3	0.166 ± 0.01
	313.4	0.163 ± 0.01
	323.5	0.163 ± 0.01
	333.7	0.153 ± 0.01
	344.2	0.150 ± 0.01
[C_4mpyr][dca]	293.5	0.155 ± 0.01
	303.2	0.155 ± 0.01
	313.3	0.153 ± 0.01
	323.3	0.151 ± 0.01
	333.2	0.147 ± 0.01
	343.4	0.142 ± 0.02

[a] Standard uncertainties are $u(T) = 0.1$ K, $u(p) = 1$ kPa and the experimental expanded uncertainty, $U_c = U_c$ (λ) = 0.01 to 0.02 W · m^{-1} · K^{-1}, with 0.95 level of confidence ($k = 2$).

Fröba *et al.* [24] measured the thermal conductivity of [C_2mim][dca] with a stationary guarded parallel-plate instrument, with an estimated expanded uncertainty of 3%. However, these values deviate from our values between (10 and 15)%, as the temperature increases (smaller temperature slope), a value greater than the mutual uncertainty of the data. The same type of deviation occurs for [C_2mim][$EtSO_4$] [7], but the comparison for [C_2mim][$(CF_3SO_2)_2$N] and [C_6mim][$(CF_3SO_2)_2$N] show deviations smaller than 2%, an excellent result. No explanation was found for these discrepancies, depending on the ionic liquid studies, and the fact needs further investigation.

3.1.2. IoNanofluids

The thermal conductivities of the IoNanofluids based on [C_2mim][dca], [C_4mim][dca] and [C_4mpyr][dca], with (0.5 and 1)% mass fraction were measured at temperatures between (293 and 343) K at 0.1 MPa. Tables 6–8 show the results obtained as well as the percentage of enhancement of the thermal conductivity. This enhancement is estimated based on the thermal conductivity at the correspondent temperature of the base fluid for each case. Figures 2–4 show a plot of the thermal conductivity of the IoNanofluids as a function of temperature, for the same temperature range than the pure fluids. These figures also display the thermal conductivity of the base ionic liquid. The uncertainty of the values of thermal conductivity of the IoNanofluids fluctuated between (6.6 and 6.7)%. The situation of these suspensions is clearly

TABLE 5
Coefficients of equation (6) for pure ionic liquids and IoNanofluids.[a]

Substance	$a_1 \pm s_{a1}$ /W · m^{-1} · K^{-1}	10^5 ($a_2 \pm s_{a2}$) /W · m^{-1} · K^{-2}	$10^5 s$ /W · m^{-1} · K^{-1}
[C_2mim][dca]	0.28027 ± 0.029	−32.873 ± 9.2	383
[C_4mim][dca]	0.27205 ± 0.021	−35.136 ± 6. 5	273
[C_4mpyr][dca]	0.23328 ± 0.013	−25.989 ± 4.2	174
[C_2mim][dca] 0.5% w/w MWCNTs	0.22242 ± 0.0055	−12.753 ± 1.7	65
[C_2mim][dca] 1% w/w MWCNTs	0.23141 ± 0.0041	−13.128 ± 1.3	50
[C_4mim][dca] 0.5% w/w MWCNTs	0.20176 ± 0.00038	−9.959 ± 0.12	4.5
[C_4mim][dca] 1% w/w MWCNTs	0.21211 ± 0.0047	−11.124 ± 1.5	56
[C_4mpyr][dca] 0.5% w/w MWCNTs	0.18059 ± 0.00065	−6.760 ± 0.20	7.9
[C_4mpyr][dca] 1% w/w MWCNTs	0.21204 ± 0.0082	−14.775 ± 2.6	98

[a] With expanded uncertainty at 0.95 level of confidence (k = 2).

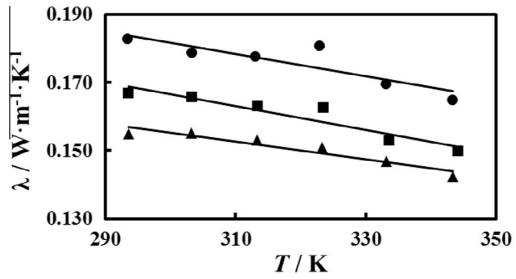

FIGURE 1. Plot of thermal conductivity of pure ionic liquids as a function of temperature. ● – [C_2mim][dca]; ■ – [C_4mim][dca]; ▲ – [C_4mpyr][dca]. Lines are given by equation (10) with coefficients shown in table 10.

different than the one stated for the pure ionic liquids because the viscosity is considerably greater due to the addition of MWCNTs. As expected, the dispersion of data obtained at each temperature was almost negligible and the uncertainty values are almost entirely dictated by the calibration.

The increase in the thermal conductivity of the base ionic liquid is easily observed, as is the stabilization of the thermal property, *i.e.*, the decrease in thermal conductivity as a function of temperature is smaller due to the addition of MWCNTs. From an application perspective, such feature could be significant if the process in question would require a heat transfer fluid that can be used in a range of temperature without compromising its efficiency. Additionally, and as expected, the enhancement of the thermal conductivity is directly proportional to the mass fraction of the nanomaterial. The fact that the enhancement can go up to 16.5% with a 1% mass fraction of MWCNTs and its dependence of temperature in the studied range supports the prospect of using these suspensions as heat transfer fluids.

TABLE 6
Thermal conductivities of Ionanofluids based on [C_2mim][dca] as a function of temperature, at p = 0.1 MPa.[a]

Substance	T/K	λ/W · m^{-1} · K^{-1}	Enhancement/%
[C_2mim][dca]	293.6	0.185	1.33
0.5% w/w MWCNTs	312.6	0.183	2.74
	332.5	0.179	5.82
	343.1	0.179	8.82
[C_2mim][dca]	293.5	0.193	5.49
1% w/w MWCNTs	313.1	0.191	7.35
	333.2	0.187	10.42
	343.9	0.187	13.25

[a] Standard uncertainties are $u(T)$ = 0.1 K, $u(p)$ = 1 kPa and the experimental expanded uncertainty, $U_c = U_c(\lambda)$ = 0.01 W · m^{-1} · K^{-1}, with 0.95 level of confidence (k = 2).

TABLE 7
Thermal conductivities of Ionanofluids based on [C_4mim][dca] as a function of temperature, at p = 0.1 MPa.[a]

Substance	T/K	λ/W · m^{-1} · K^{-1}	Enhancement/%
[C_4mim][dca]	293.7	0.173	3.51
0.5% w/w MWCNTs	313.0	0.171	4.60
	333.3	0.169	10.37
	343.3	0.168	11.95
[C_4mim][dca]	293.7	0.180	7.72
1% w/w MWCNTs	312.8	0.177	8.79
	332.8	0.175	14.19
	343.5	0.174	16.51

[a] Standard uncertainties are $u(T)$ = 0.1 K, $u(p)$ = 1 kPa, $u(w)$ = 0.0004 and the experimental expanded uncertainty, $U_c = U_c(\lambda)$ = 0.01 W · m^{-1} · K^{-1}, with 0.95 level of confidence (k = 2).

TABLE 8
Thermal conductivities of Ionanofluids based on [C_4mpyr][dca] as a function of temperature, at p = 0.1 MPa.[a]

Substance	T/K	λ/W · m^{-1} · K^{-1}	Enhancement/%
[C_4mpyr][dca]	293.1	0.161	3.71
0.5% w/w MWCNTs	312.4	0.160	4.20
	333.4	0.158	7.70
	343.7	0.157	10.55
[C_4mpyr][dca]	293.7	0.168	8.68
1% w/w MWCNTs	312.6	0.167	8.78
	333.0	0.162	10.23
	343.7	0.162	13.70

[a] Standard uncertainties are $u(T)$ = 0.1 K, $u(p)$ = 1 kPa, $u(w)$ = 0.0004 and the experimental expanded uncertainty, $U_c = U_c(\lambda)$ = 0.01 W · m^{-1} · K^{-1}, with 0.95 level of confidence (k = 2).

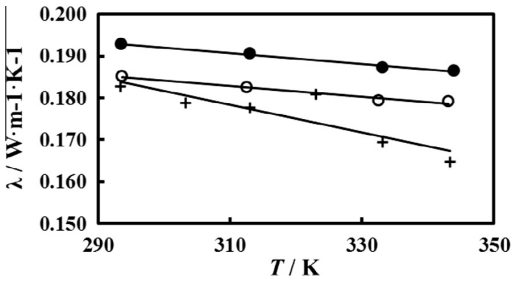

FIGURE 2. Plot of thermal conductivity of pure [C_2mim][dca] and its IoNanofluids as a function of temperature. ● – [C_2mim][dca] pure; ○ – INF 0.5% w/w MWCNTs; + – INF 1% w/w MWCNTs. Lines are given by equation (10) with coefficients shown in table 10.

Figures 5 and 6 show the plot of the enhancement, ($\lambda_{INF}/\lambda_{IL} - 1$), where λ_{INF} is the thermal conductivity of the IoNanofluid and λ_{IL} the thermal conductivity of the base ionic liquid, as a function of

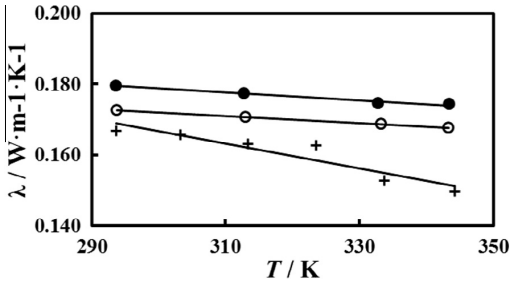

FIGURE 3. Plot of thermal conductivity of pure [C_4mim][dca] and its IoNanofluids as a function of temperature. ● – [C_4mim][dca] pure; ○ – INF 0.5% w/w MWCNTs; + – INF 1% w/w MWCNTs. Lines are given by equation (10) with coefficients shown in table 10.

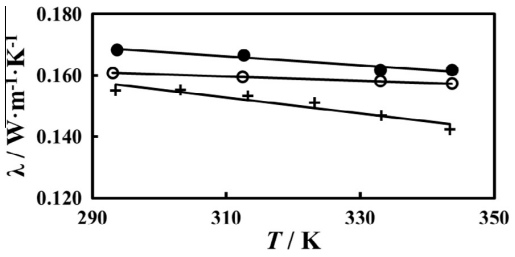

FIGURE 4. Plot of thermal conductivity of pure [C_4mpyr][dca] and its IoNanofluids as a function of temperature. ● – [C_4mpyr][dca] pure; ○ – INF 0.5% w/w MWCNTs; + – INF 1% w/w MWCNTs. Lines are given by equation (10) with coefficients shown in table 10.

temperature, and volume fraction, respectively. The work of Fukushima *et al.* [12,13] suggested an increase in the organization of the fluid when carbon nanotubes are added to it. Though it is not entirely clear at this time what organized structure exists in these suspensions, such fact is in agreement with an increase in thermal conductivity since it is well known that solids conduct heat much more effectively than liquids. Based on this idea, when comparing the results between different base ionic liquids, it is possible to state that [C_4mim][dca] is the one that benefits more from the addition of MWCNTs.

The enhancement of the thermal conductivity of this ionic liquid is higher in either mass fraction in the majority of the temperature values studied, which could support the idea of a greater increase in the organization of the liquid nanostructure, favouring a higher transfer of heat. Since the anion is the same for all three ionic liquids and if we take into account the idea of the increase of organization when adding MWCNTs, we could infer that the cation is the controlling factor for the differences in structure of the pure ionic liquids, and also for the IoNanofluids.

The compounds studied can be separated into head group (imidazolium or pyrrolidinium with methyl substitution), an aliphatic side chain and an anion (the same). The data obtained justifies that by changing the side chain length, the enhancement in the thermal conductivity increases, possibly due to a better interaction between this chain and the carbon nanotube surface (non-polar entities) that facilitates heat transfer. The same effect was found for the [$C_n$mim][$(CF_3SO_2)_2$N] family [7], ranging from $n = 2$ to $n = 8$.

The change of the head group does not seem to affect the enhancement, except for volume fraction of the nanotube greater than 0.04, where the methylimidazolium seems to win.

Finally, we can compare data for liquids that have the same cation, [C_2mim], and different anions, [$N(CN)_2$], [$C_2H_5OSO_3$] [10] and [$(CF_3SO_2)_2$N] [7]. The anion structure affects the enhancement, with the [$(CF_3SO_2)_2$N] salt having the smallest and the [$C_2H_5OSO_3$] the highest. The same result is obtained when we compare the liquids based on the [C_4mim] cation, with the [$(CF_3SO_2)_2$N] salt having smaller enhancement than the [$N(CN)_2$] one.

Depending on the ionic liquid and the quantity of MWCNTs, the variation of the thermal conductivity can be seemingly linear or described by a power function. Such dissimilarity increases the difficulty of establishing a model that allows the accurate prediction of the enhancement of the thermal conductivity of this sort of suspensions. Recent experimental results attested that one of the models conceived for suspensions of cylindrical particles in ionic liquids display a great lack of agreement between experience and theory [10]. For the systems studied here the results obtained are displayed in figure 7, where the thermal conductivity enhancement at $T = 293$ K and 0.1 MPa is plotted as a function of the volume fraction of the carbon nanotubes in the IoNanofluid. It is very clear that the theoretical values are much less than the experimental ones, that the theory is not sensitive to the base ionic liquid and that the volume fraction dependence is weaker.

One of the variables of this model that significantly influences the outcome is the thermal conductivity of the ionic liquid–MWCNTs interface, to which no specific values exist to date. Consequently, further understanding on the interactions that take place at this interface is required in order to envisage an accurate model for the prediction of the abovementioned effect [7,10]. Studies using molecular simulation are under way to study structure and dynamics of ionic liquids in contact with carbon nanomaterials, such as graphene sheets and nanotubes, and results will be presented soon [25].

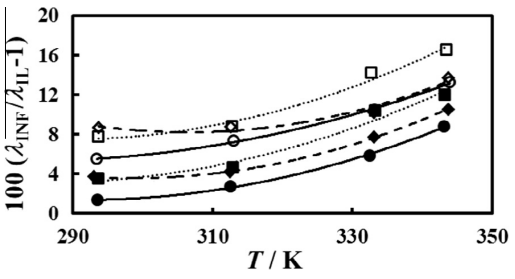

FIGURE 5. Plot of thermal conductivity enhancement of INFs as a function of temperature. Full symbols – INF 0.5% w/w MWCNTs; open symbols – IL 1% w/w MWCNTs. —, ●, ○ – [C_2mim][dca]; ····, ■, □ – [C_4mim][dca]; - - -, ♦, ◇ – [C_4mpyr][dca].

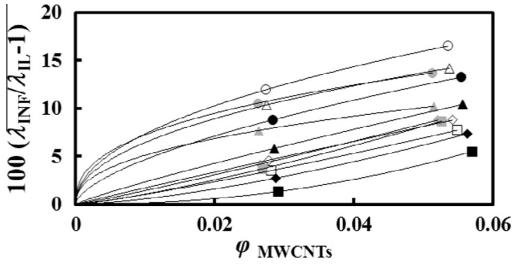

FIGURE 6. Plot of thermal conductivity enhancement of the IoNanofluids as a function of the volume fraction of MWCNTs. ■, □, ■ – $T = 293$ K; ♦, ◇, ◆ – $T = 313$ K; ▲, △, ▲ – $T = 333$ K; ●, ○, ● – $T = 343$ K; full symbols: – IoNanofluids based on [C_2mim][dca]; empty symbols: – ionanofluids based on [C_4mim][dca]; grey symbols: – IoNanofluids based on [C_4mpyr][dca]. Lines are just drawn for clarity, having no special meaning.

3.2. Density

As mentioned above, the method used to calibrate the densimeter relies on the contribution of the parameter τ_0. According to reference [19], by applying equation (5) to two calibrating fluids, whose density values $\rho_{1,\mathrm{ref}}$ and $\rho_{2,\mathrm{ref}}$, are accurately known as a function of temperature and pressure, and dividing the two equations in order to eliminate the B parameter, we obtain a new equation having τ_0 as a single unknown variable. Solving this last equation for τ_0 we obtain equation (9):

$$\tau_{0,\mathrm{calc}} = \left(\frac{\rho_{1,\mathrm{ref}}\tau_2^2 - \rho_{2,\mathrm{ref}}\tau_1^2}{\rho_{1,\mathrm{ref}} - \rho_{2,\mathrm{ref}}} \right)^{1/2}, \quad (9)$$

where τ_1 and τ_2 are experimentally obtained vibrating periods for the respective reference liquids at each fixed temperature. The set of calibrants aforementioned cover the range of densities of interest and, following the procedure on reference [19], we obtain an associated standard uncertainty of $u(\rho) = 0.22\ \mathrm{kg \cdot m^{-3}}$ for both pure ionic liquids and IoNanofluids.

3.2.1. Pure Ionic Liquids

The density of the three pure ionic liquids and several IoNanofluids was measured at temperatures between (293 and 343) K at 0.1 MPa. The results for the pure liquids can be found in table 9, which shows a steady decrease on the value of the property as a function of temperature. The results obtained for each liquid were fitted to a function, according to equation (10), and table 10 shows the coefficients obtained, as well as the root mean square deviations of the fits.

$$\rho(\mathrm{kg \cdot m^{-3}}) = a_1 + a_2 T(\mathrm{K}) + a_3 T^2(\mathrm{K}). \quad (10)$$

It was first attempted to fit the results to a straight line but fitting the latter equation provided significantly lower values of standard error. From the table, it can be acknowledged that the root mean square deviation of the fits did not exceed $0.285\ \mathrm{kg \cdot m^{-3}}$ for any of the fluids in question. Also, no data departs from the fit by more than ±0.05% for the pure ionic liquids and ±0.03% for the suspensions.

Contrary to the case of the thermal conductivity, there are numerous data of ionic liquid densities to which is possible to compare our results with. Figure 8 shows the existing data for the density of [C_2mim][dca], compared with the present results. The comparison shows that there are two distinctive trends, which do not agree within their mutual uncertainty, apart from a very different value (single point) obtained by Yoshida *et al.* [26], well apart from the others (~2.1%). The upper results were obtained by Fröba *et al.* [27], Wong *et al.* [28], Soriano *et al.* [29] and Klomfar *et al.* [30], while the lower end results show the values obtained by Schreiner *et al.* [31], Freire *at al.* [16] and Quijada-Maldonado *et al.* [32]. Both sets of results differ by more than 0.7%. This result is more expressed in the insertion, were the deviations from equation (10) are displayed as a function of temperature. Our results agree with the lower data set, within ±0.2%, or within the mutual uncertainty of the data. In order to check the results in our laboratory, different measurements were performed by Molias *et al.* [33], with a smaller uncertainty (DSA 5000 M, 0.05%). These results confirm the lower rim tendency of the data, agreeing with the present data within their mutual uncertainty.

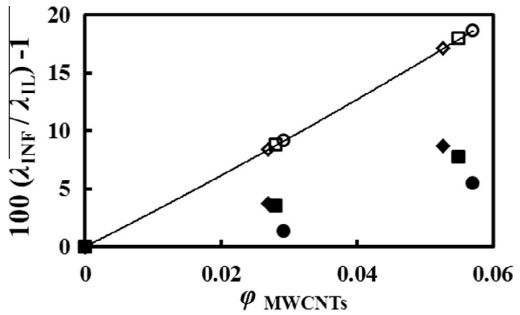

FIGURE 7. Plot of thermal conductivity enhancement of the IoNanofluids, as a function of the volumetric fraction of MWCNTs, at $T = 293$ K and 0.1 MPa. Open symbols, experiment. Closed symbols theory. ●, ○ – [C_2mim][dca]; ■, □ – [C_4mim][dca]; ♦, ◇ – [C_4mpyr][dca].

TABLE 9
Densities of the pure ionic liquids as a function of temperature, at $p = 0.1$ MPa.[a]

T/K	ρ/kg · m^{-3}		
	[C_2mim][dca]	[C_4mim][dca]	[C_4mpyr][dca]
293.2	1107.5	1064.5	1018.3
303.2	1100.4	1057.5	1011.8
313.2	1093.5	1051.0	1006.1
323.2	1087.0	1045.1	1000.6
333.2	1081.0	1040.6	995.6
343.2	1076.1	1035.7	991.3

[a] Standard uncertainties are $u(T) = 0.1$ K, $u(p) = 1$ kPa and the experimental expanded uncertainty, $U_c = U_c\ (\rho) = 0.2\ \mathrm{kg \cdot m^{-3}}$, with 0.95 level of confidence ($k = 2$).

With respect to [C_4mim][dca], the results nearest to ours are the ones of Seoane *et al.* [15], while the remainders [34,35] deviate from the ones obtained in the present work around (−0.2 to 0.4)%, especially at the higher temperatures. Our previously reported data [36], measured with a different densimeter, agrees with the present one within 0.05% up to $T = 323.15$ K and −0.25% at 243.15 K. For [C_4mpyr][dca], there are three sets of data. One published by Sanchez *et al.* [34], which differ approximately 9% from our data for each temperature. Results presented by Blahut and Dohna [37] agree with our data to within −0.2%. Recently, González and Corderí [38] presented one single point, at $T = 298.15$ K, that deviates from our correlated data by −0.15%.

The difference between the data herein presented and other published sets of data by more than their mutual uncertainty (0.2 to 0.5)% might be due to dissimilarities in the techniques used to handle and/or to dry the ionic liquids or to the purity of samples.

3.2.2. IoNanofluids

The densities of the IoNanofluids based on [C_2mim][dca], [C_4mim][dca] and [C_4mpyr][dca], with (0.5 and 1)% mass fraction were measured at temperatures between (293 and 343) K at 0.1 MPa. Tables 11–13 show the results obtained as well as the percentage of enhancement of the density. As expected, the enhancement is very small due to extremely high difference in densities between the ionic liquids and the MWCNTs, reaching its peak at 0.65% for the case of the IoNanofluid [C_4mim][dca] 1% w/w at $T = 313$ K. Again, from an application standpoint as heat transfer fluids, such low change in the density values by the addition of the MWCNTs can represent a positive outcome. Considering the four thermophysical properties of a heat transfer fluid necessary to design a heat transfer unit (thermal conductivity, heat capacity, viscosity and density), an increase in density represents a decrease in the principal design parameter, the heat transfer area, which in turn leads to an decrease in capital and operational costs [5]. Therefore, a proper balance between these properties must be accomplished. Although a greater increase in the density would be preferable, this very low variation in density by the addition of MWCNTs indicates that there is one property less that can

TABLE 10
Coefficients of equation (10) for pure ionic liquids and IoNanofluids.[a]

Fluid	$a_1 \pm s_{a1}$/kg · m^{-3}	$(a_2 \pm s_{a2})$/kg · K^{-1} · m^{-3}	10^5 $(a_3 \pm s_{a3})$/kg · K^{-2} · m^{-3}	s/kg · m^{-3}
[C_2mim][dca]	1555.81 ± 34	−2.294 ± 0.20	260.892 ± 33	0.204
[C_4mim][dca]	1564.43 ± 47	−2.672 ± 0.30	329.757 ± 47	0.285
[C_4mpyr][dca]	1423.55 ± 11	−2.102 ± 0.072	245.525 ± 11	0.069
[C_2mim][dca] 0.5% w/w MWCNTs	1588.89 ± 2.1	−2.472 ± 0.013	287.159 ± 2.0	0.012
[C_2mim][dca] 1% w/w MWCNTs	1556.03 ± 39	−2.258 ± 0.25	254.011 ± 39	0.236
[C_4mim][dca] 0.5% w/w MWCNTs	1496.25 ± 14	−2.189 ± 0.086	248.680 ± 14	0.083
[C_4mim][dca] 1% w/w MWCNTs	1331.62 ± 42	−1.113 ± 0.27	75.948 ± 42	0.255
[C_4mpyr][dca] 0.5% w/w MWCNTs	1428.40 ± 19	−2.117 ± 0.12	247.461 ± 19	0.113
[C_4mpyr][dca] 1% w/w MWCNTs	1400.33 ± 34	−1.927 ± 0.21	219.137 ± 33	0.204

[a] With expanded uncertainty at 0.95 level of confidence (k = 2).

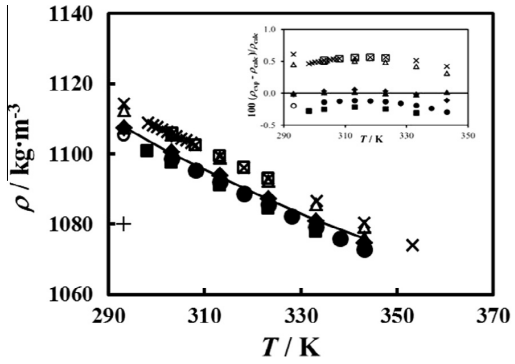

FIGURE 8. Plot of density of [C_2mim][dca] as a function of temperature. + Yoshida *et al.* [25]; △ Froba *et al.* [26]; □ Wong *et al.* [27]; × Soriano *et al.* [28]; ■ Schreiner *et al.* [29]; ● Quijada-Maldonado *et al.* [30]; ○ Nieto de Castro *et al.* [31]; ▲ present work. In the insert the relative deviations (%) between the density measurements obtained in this work (ρ_{exp}), and those reported in literature (ρ_{lit}) as function of temperature, using equation (10) as the reference.

influence the heat transfer area and the mentioned balance will be more dependent on the variation of the remainder properties.

Figures 9–11 contain a plot of the density of the IoNanofluids as a function of temperature, including the densities of the corresponding base ionic liquid presented in the previous section in order to allow a better visual perception of the enhancement due to the addition of MWCNTs. The small increase on the density of the base ionic liquid is easily observed, as the values are very close between them for each temperature. As it was stated for the thermal conductivity, the enhancement of the density is directly proportional to the mass fraction of the nanomaterial.

TABLE 11
Densities of IoNanofluids based on [C_2mim][dca] as a function of temperature, at p = 0.1 MPa.[a]

Substance	T/K	ρ/kg · m^{-3}	Enhancement/%
[C_2mim][dca] 0.5% w/w MWCNTs	293.2	1110.9	0.30
	303.2	1103.3	0.27
	313.2	1096.3	0.25
	323.2	1089.8	0.26
	333.2	1083.9	0.27
	343.2	1078.6	0.24
[C_2mim][dca] 1% w/w MWCNTs	293.2	1112.4	0.44
	303.2	1104.8	0.41
	313.2	1098.4	0.44
	323.2	1091.5	0.42
	333.2	1085.6	0.43
	343.2	1080.4	0.40

[a] Standard uncertainties are $u(T)$ = 0.1 K, $u(p)$ = 1 kPa, $u(w)$ = 0.0004 and the experimental expanded uncertainty, $U_c = U_c$ (ρ) = 0.2 kg · m^{-3}, with 0.95 level of confidence (k = 2).

TABLE 12
Densities of Ionanofluids based on [C_4mim][dca] as a function of temperature, at p = 0.1 MPa.[a]

Substance	T/K	ρ/kg · m^{-3}	Enhancement/%
[C_4mim][dca] 0.5% w/w MWCNTs	293.2	1068.1	0.34
	303.2	1061.1	0.35
	313.2	1054.4	0.32
	323.2	1048.5	0.32
	333.2	1042.9	0.22
	343.2	1037.8	0.20
[C_4mim][dca] 1% w/w MWCNTs	293.2	1070.5	0.56
	303.2	1063.9	0.61
	313.2	1057.8	0.65
	323.2	1050.9	0.56
	333.2	1045.0	0.42
	343.2	1039.1	0.33

[a] Standard uncertainties are $u(T)$ = 0.1 K, $u(p)$ = 1 kPa, $u(w)$ = 0.0004 and the experimental expanded uncertainty, $U_c = U_c$ (ρ) = 0.2 kg · m^{-3}, with 0.95 level of confidence (k = 2).

TABLE 13
Densities of Ionanofluids based on [C_4mpyr][dca] as a function of temperature, at p = 0.1 MPa.[a]

Substance	T/K	ρ/kg · m^{-3}	Enhancement/%
[C_4mpyr][dca] 0.5% w/w MWCNTs	293.2	1020.6	0.22
	303.2	1014.2	0.23
	313.2	1008.4	0.23
	323.2	1002.9	0.23
	333.2	997.8	0.22
	343.2	993.6	0.23
[C_4mpyr][dca] 1% w/w MWCNTs	293.2	1023.9	0.55
	303.2	1017.5	0.56
	313.2	1012.1	0.60
	323.2	1006.6	0.60
	333.2	1001.5	0.59
	343.2	997.3	0.61

[a] Standard uncertainties are $u(T)$ = 0.1 K, $u(p)$ = 1 kPa, $u(w)$ = 0.0004 and the experimental expanded uncertainty, $U_c = U_c$ (ρ) = 0.2 kg · m^{-3}, with 0.95 level of confidence (k = 2).

Shown in figure 12 is the plot of the enhancement as a function of volume fraction, in a similar way that was presented for the thermal conductivity. Once again, it is illustrated that the variation of a property can depend on the ionic liquid, quantity of nanomaterial and temperature. Such dependence complicates the determination of a model that can predict the enhancement of the density of an ionic liquid with suspended nanoparticles. While the range of enhancement for density is low, rigorous and reliable data are needed in order to plan the use of these substances in applications.

As done with thermal conductivity data in previous work [10], we propose a comparison between experimental data and calculated values of densities using a model. In order to calculate the value of the density of the liquids with suspended particles, the work of Pak and Cho [39] was modified by Ribeiro [40] to obtain equation (11):

$$\rho = (1 - \varphi_p)\rho_{IL} + \varphi_p \rho_p, \tag{11}$$

where ρ_{IL} and ρ_p are the densities of the ionic liquid and particles, respectively, and φ_p represents the volume fraction of the suspended particles. Figure 13 shows a plot of the density as a function of the volume fraction of MWCNTs for the experimental data and the calculated data using equation (11). Density of the MWCNT's used was taken from table 2 (average value of 185 $g \cdot cm^{-3}$). Although it may seem that the data are considerably apart and the slope is noticeably different, the experimental values do not differ by more than (−2.43 for 0.5)% w/w mass fraction IoNanofluids and −4.74% for the 1% w/w mass fraction IoNanofluids. Such a divergence may be due to the fact that the equation fails to take in to account for, as an example, specific interaction forces between the two kinds of material. As it was said for the case of thermal conductivity, further understanding on the interactions that take place at the solid-liquid interface is required.

Regarding structural interpretations, it can be seen that the liquid that has the highest density is [C_2mim][dca], and the lowest density is [C_4mpyr][dca], probably because the increase in the alkyl side chain makes the structure of the liquid less packed, and that planar head groups pack much better than non-planar. In the IoNanofluids the enhancement is so small that no discernible difference in the enhancements is found, the packaging trend being similar to the pure ionic liquids. This fact can have two possible interpretations. Either the ions enter the carbon nanotubes (2 to 6) nm diameter, as shown in the molecular simulation studies

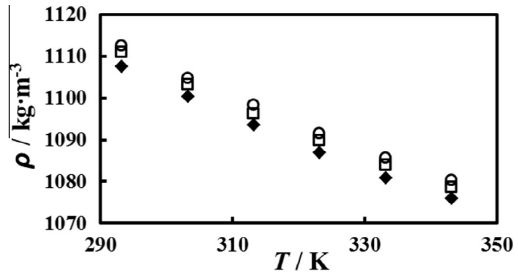

FIGURE 9. Plot of density of IoNanofluids based on [C_2mim][dca] and of the pure ionic liquid as a function of temperature. ♦ – [C_2mim][dca] pure; □ – [C_2mim][dca] INF 0.5% w/w MWCNTs; ○ – [C_2mim][dca] INF 1% w/w MWCNTs.

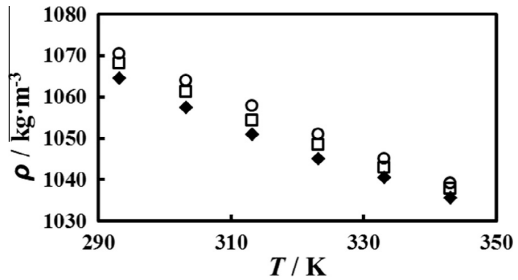

FIGURE 10. Plot of density of IoNanofluids based on [C_4mim][dca] and of the pure ionic liquid as a function of temperature. ♦ – [C_4mim][dca] pure; □ – [C_4mim][dca] 0.5% w/w MWCNTs; ○ – [C_4mim][dca] 1% w/w MWCNTs.

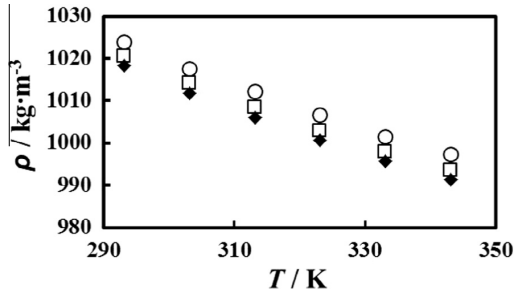

FIGURE 11. Plot of density of IoNanofluids based on [C_4mpyr][dca] and of the pure ionic liquid as a function of temperature. ♦ – [C_4mpyr][dca] pure; □ – [C_4mpyr][dca] 0.5% w/w MWCNTs; ○ – [C_4mpyr][dca] 1% w/w MWCNTs.

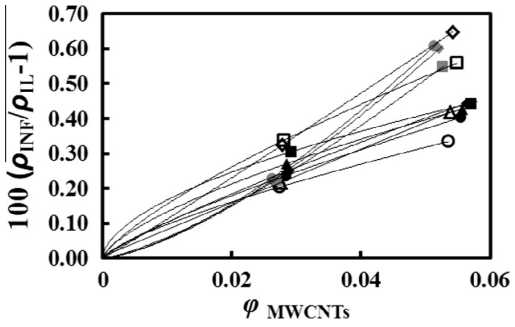

FIGURE 12. Plot of density enhancement of the IoNanofluids as a function of the volume fraction of MWCNTs. ■, □, ■ – T = 293 K; ♦, ◇, ◆ – T = 313 K; ▲, △, ▲ – T = 333 K; ●, ○, ● – T = 343 K; Full symbols: – Ionanofluids based on [C_2mim][dca]; empty symbols: – Ionanofluids based on [C_4mim][dca]; grey symbols: – Ionanofluids based on [C_4mpyr][dca].

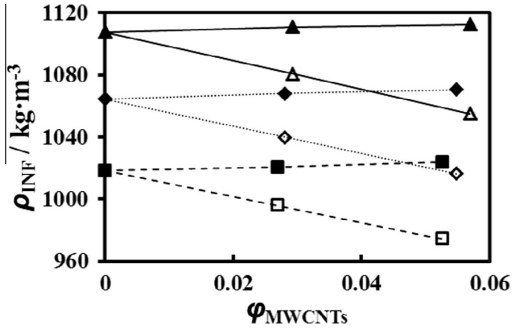

FIGURE 13. Plot of density of the IoNanofluids as a function of volume fraction. ▲, △ – IoNanofluids based on [C_2mim][dca]; ♦, ◇ – IoNanofluids based on [C_4mim][dca]; ■, □ – IoNanofluids based on [C_4mpyr][dca], full symbols: experimental values; empty symbols: calculated values from equation (12).

[41], or if the CNT's are "empty" and therefore contribute with their intrinsic density according to the volume fraction in the fluid. In the first case the enhancement will be more discernible. More studies about the density of IoNanofluids are needed to clarify this point.

4. Conclusions

The thermophysical properties (thermal conductivity and density) of ionic liquids with a common anion, dicyanamide, and their IoNanofluids with multi-walled carbon nanotubes, were studied at temperatures between (293 and 343) K, at 0.1 MPa. The results obtained show that there are significant enhancements of the thermal conductivity caused by the suspension of this nanomaterial in the base liquid, which cannot be explained by current theories that do not consider the importance of the process of heat transfer in the interface ionic liquid - nanomaterial. On the other hand the enhancements in the density, to our knowledge the first results for IoNanofluids, are very small and not very dependent of the structure of the cation.

The results obtained help to understand the effect of the side alkyl chain, the planarity of the head group and the anion identity in the thermal conductivity of the ionic liquids and also in the respective IoNanofluids. Dicyanamide ionic liquids can be a good alternative for new heat transfer fluids, due to their low viscosity and to the enhancement in the thermal conductivity. Studies of the heat capacity and viscosity, the other two important thermophysical properties for heat transfer design are under way.

Molecular dynamics studies with real interaction potentials of interaction between the ionic liquid moieties and the carbon nanostructures will help to understand the true mechanism for thermal conductivity in ionic liquids and IoNanofluids, which we hope to report about soon.

Acknowledgments

The authors would like to thank FCT- Fundação para a Ciência e Tecnologia, Portugal, for funding projects PTDC/EQU-FTT/104614/2008 and PEst-OE/QUI/UI0536/2011 to Centro de Ciências Moleculares e Materiais and to BAYER Materials Science for supplying the MWCNTs (Baytubes). JMP França and SIC Vieira want to thank FCT for the PhD Grants SFRH/BD/79378/2011 and SFRH/BD/64974/2009, respectively.

References

[1] P. Wasserscheid, T. Welton (Eds.), Ionic Liquids in Synthesis, Wiley-VCH, Weinheim, 2007.
[2] V. Pârvulescu, C. Hardacre, Chem. Rev. 107 (2007) 2615–2665.
[3] S.K. Das, S.U.S. Choi, W. Yu, T. Pradeep, Nanofluids: Science and Technology, John Wiley & Sons Inc, New Jersey, 2008. Chaps. 1–3.
[4] S.U.S. Choi, Z.G. Zhang, W. Yu, F.E. Lockwood, E.A. Grulke, Appl. Phys. Lett. 79 (2001) 2252–2254.
[5] J.M.P. Franca, C.A. Nieto de Castro, M.L.M. Lopes, V.M.B.J. Nunes, J. Chem. Eng. Data 54 (2009) 2569–2575.
[6] C.A. Nieto de Castro, M.J.V. Lourenço, A.P.C. Ribeiro, E. Langa, S.I.C. Vieira, P. Goodrich, C. Hardacre, J. Chem. Eng. Data 55 (2010) 653–661.
[7] A.P.C. Ribeiro, S.I.C. Vieira, P. Goodrich, C. Hardacre, M.J.V. Lourenco, C.A. Nieto de Castro, J. Nanofluids 2 (2013) 55–62.
[8] C.A. Nieto de Castro, S.M. Sohel Murshed, M.J.V. Lourenço, F.J.V. Santos, M.L. Matos Lopes, J.M.P. França, Ionanofluids – new heat transfer fluids for green process development, in: A. Mohammad, Inamuddin (Eds.), Chapter 8 in Green Solvents I: Properties and Applications in Chemistry, Springer Science+Business Media Dordrecht, 2012.
[9] C.A. Nieto de Castro, S.M. Sohel Murshed, M.J.V. Lourenço, F.J.V. Santos, M.L.M. Lopes, J.M.P. França, Int. J. Therm. Sci. 62 (2012) 34–39.
[10] J.M.P. França, S.I.C. Vieira, M.J.V. Lourenço, S.M.S. Murshed, C.A. Nieto de Castro, J. Chem. Eng. Data 58 (2013) 467–476.
[11] T. Fukushima, T. Aida, Chem. Eur. J. 13 (2007) 5048–5058.
[12] T. Fukushima, A. Kosaka, Y. Ishimura, T. Yamamoto, T. Takigawa, N. Ishii, T. Aida, Science 300 (2003) 2072–2075.
[13] E. Gomez, B. Gonzalez, N. Calvar, E. Tojo, A. Dominguez, J. Chem. Eng. Data 51 (2006) 2096–2102.
[14] K.R. Harris, M. Kanakubo, L.A. Woolf, J. Chem. Eng. Data 52 (2007) 1080–1085.
[15] R.G. Soane, S. Corderí, E. Gómez, N. Calvar, E.J. González, E.A. Macedo, Á. Domínguez, Ind. Eng. Chem. Res. 51 (2012). 2942-2504.
[16] M.G. Freire, A.R.R. Teles, M.A.A. Rocha, B. Schröder, C.M.S.S. Neves, P.J. Carvalho, D.V. Evtuguin, L.M.N.B.F. Santos, J.A.P. Coutinho, J. Chem. Eng. Data 56 (2011) 4813–4822.
[17] H.S. Carslaw, J.C. Jaeger, Conduction of Heat in Solids, Oxford University Press, London, 1959. p. 256.
[18] G.J. Kluitenberg, J.M. Ham, K.L. Bristow, Soil Sci. Soc. Am. J. 57 (1993) 1444–1451.
[19] I.M.S. Lampreia, C.A. Nieto de Castro, J. Chem. Thermodyn. 43 (2011) 537–545.
[20] B. Lagourette, C. Boned, H. Saint-Guirons, P. Xans, H. Zout, Meas. Sci. Technol. 3 (1992) 699–703.
[21] A.T. Sousa, P.S. Fialho, C.A. Nieto de Castro, R. Tufeu, B. LeNeindre, Fluid Phase Equilib. 80 (1992) 213–225.
[22] S.M.S. Murshed, C.A. Nieto de Castro, M.J.V Lourenço, J. Nanofluids 1 (2012) 175–179.
[23] KD2 Pro Thermal Properties Analyzer Operator's Manual (version 7); Decagon Devices Inc.: Pullman, WA, 2008–2009.
[24] A.P. Fröba, M.H. Rausch, K. Krzeminski, D. Assenbaum, P. Wasserscheid, A. Leipertz, Int. J. Thermophys. 31 (2010) 2059–2077.
[25] J.M.P. França, C.A. Nieto de Castro, A.A.H. Pádua, Interactions of imidazolium dicyanamide ionic liquids with carbon nanomaterials, in: presented at COIL-5/3IMIL, Congress on Ionic Liquids, Vilamoura, Algarve, April 21–25, 2013.
[26] Y. Yoshida, K. Muroi, A. Otsuka, G. Saito, M. Takahashi, T. Yoko, Inorg. Chem. 43 (4) (2004) 1458–1462.
[27] A. Fröba, H. Kremer, A. Leipertz, J. Phys. Chem. B 112 (2008) 12420–12430.
[28] C.-L. Wong, A.N. Soriano, M.-H. Li, Fluid Phase Equilib. 271 (2008) 43–52.
[29] A.N. Soriano, B.T. Doma Jr., M.-H. Li, J. Taiwan Inst. Chem. Eng. 41 (2010) 115–121.
[30] J. Klomfar, M. Souckova, J. Patek, J. Chem. Eng. Data 57 (2012) 1213–1221.
[31] C. Schreiner, S. Zugmann, R. Hartl, H.J. Gores, J. Chem. Eng. Data 55 (5) (2010) 1784–1788.
[32] E. Quijada-Maldonado, S. van der Boogaart, J.H. Lijbers, G.W. Meindersma, A.B. de Haan, J. Chem. Thermodyn. 51 (2012) 51–58.
[33] C.A. Nieto de Castro, S. Molías, F.J.V. Santos, M.J.V. Lourenço, S.M.S. Murshed, B. Waghmode, K.S. Patil, D. Salavera, A. Coronas, Thermophysical properties of IL+H2O mixtures for absorption refrigeration, in: invited lecture presented at International Workshop on New Working Fluids for Absorption Heat Pumps and Refrigeration Systems, Eurotherm Seminar no 100, Tarragona, Spain, 22–23 July (2013), to be published in Workshop Procs., in press.
[34] L.G. Sánchez, J.R. Espel, F. Onink, G.W. Meindersma, A.B. de Haan, J. Chem. Eng. Data 54 (2009) 2803–2812.
[35] P.J. Carvalho, T. Regueira, L.M.N.B.F. Santos, J. Fernandez, J.A.P. Coutinho, J. Chem. Eng. Data 55 (2010) 645–652.
[36] C.A. Nieto de Castro, E. Langa, A.L. Morais, M.L. Matos Lopes, M.J.V. Lourenço, F.J.V. Santosa, M.S.C.S. Santos, J.N. Canongia Lopes, H.I.M. Veiga, M. Macatrão, J.M.S.S. Esperança, C.S. Marques, L.P.N. Rebelo, C.A.M. Afonso, Fluid Phase Equilib. 294 (2010) 157–179.
[37] A. Blahut, V. Dohna, J. Chem. Eng. Data 56 (2011) 4909–4918.
[38] B. González, S. Corderí, Fluid Phase Equilib. 354 (2013) 89–94.
[39] B.C. Pak, Y.I. Cho, Exp Heat Transfer 11 (1998) 151–170.
[40] A.P.C. Ribeiro, Structure and electrical and thermal properties of carbon nanotubes and nanofluids with ionic liquids (Ph.D. thesis in Chemistry (Physical Chemistry)), Faculdade de Ciências, Universidade de Lisboa, 2012.
[41] Y. Shim, H.J. Kim, ACS Nano 3 (2009) 1693–1702.

JCT 13-688

Chapter 4

Molecular interactions and thermal transport in ionic liquids with carbon nanomaterials

This chapter consists on the work done using molecular dynamics simulation, which was used to study the effect of suspended carbon nanomaterials, nanotubes and graphene sheets, on the thermal conductivity of ionic liquids, an issue related to understanding the properties of nanofluids studied experimentally in the two previous chapters.

One of the main objectives of this work consisted on developing an atomistc interaction model that described realistically both the ordering of ions at the interface and heat transfer phenomena in that region. This model was intended to be relatively transferable between families of ionic liquids and also able to represent graphene planes and nanotubes. In order to do so, the potential energy of interaction between the ions of the ionic liquids and a small model structure representing a graphene flake or a nanotube was calculated using quantum mechanics (DFT – density functional theory), at various distances and mutual orientations. The objects of study were ionic liquids composed of alkylimidazolium cations, $C_nC_1im^+$, with three different anions: dicyanamide, $N(CN)_2^-$, thiocyanate, SCN^-, tricyanomethanide, $C(CN)_3^-$, and bis(trifluoromethanesulfonyl)imide, $(CF_3SO_2)_2N^-$ or tf_2N^-. Concerning the carbon nanomaterials, the structures considered were two armchair single-walled carbon nanotubes with chirality indices (7,7) and (10,10) and a stack of graphene sheets. The latter can also represent a multi-walled carbon nanotube.

It was not presumed that the Lennard-Jones (LJ) potential would represent correctly the interactions of ions with the nanomaterial, based on previous work. Therefore, more elaborate functional forms

were considered. As will be seen in this chapter, the structure (or ordering of ions) obtained using the potential here developed and LJ are significantly different. The present model provides a better distinction on the location of the ions regarding the carbon surface and a more pronounced interfacial ordering.

The development of the potential was the portion of the work where a bigger effort was required. From choosing the appropriate method and a suitable charge scheme, to the actual fit of a function to the potential energy values calculated required the development of several scripts to process the data and the adaptation of existing ones already created by the group in Clermont-Ferrand. The fitting of a function to the data has more to it than simply letting the computer "run the numbers", since the values of the function have to be physically meaningful and the relation between several parameters must be respected.

Several conclusions can be drawn from the work presented in this chapter. Structural information concerning the ordering of ions in the interfacial layer showed similarities in the cyano-ILs, with the anion often found close to the carbon surface, which was unexpected given the relative intensity of attraction of isolated ions in the interaction model. With $[C_4mim][tf_2N]$, the non-polar alkyl side chains of the cation are found closer to the carbon surface than with the other ionic liquids. In the (7,7) and (10,10) nanotubes, cations are found most likely near the centre of the nanotubes, with their positions and orientations depending on the diameter of the tube. The alkyl side chains of the cations aggregate in the centre of the (10,10) nanotube creating a non-polar domain.

The thermal conductivity of pure ionic liquids and of the composite systems containing a SWCNT or a stack of graphene sheets was calculated using the reverse non-equilibrium (RNEMD) scheme of Müller-Plathe (MP) [32] to relate a temperature gradient to the heat flux across the simulation box. The idea of the MP method is to drive a heat flux through the simulated system. In order to attain a steady

state with a constant temperature gradient, energy is transferred continuously from one region of the system, denoted as the 'cold' region, to another one, the 'hot' region. The two regions are spatially separated, for example, in the z direction of the simulation box. The cold and the hot region of the system are created by interchanging the velocity of the hottest atom in the cold region with the velocity of the coldest atom in the hot region. This implies that a known amount of heat is transferred between the two regions. By repeating the transfer periodically, an artificial heat flux j_z is created from the cold to the hot region, summed over the exchange events. When the steady state has been reached, the same amount of energy per time and area (j_z) flows from the hot to the cold region by heat conduction. This equality of the two fluxes follows from energy conservation. As a result, a temperature gradient $\langle \mathrm{d}T/\mathrm{d}z \rangle$ is formed in the system. From the known imposed j_z and the calculated $\langle \mathrm{d}T/\mathrm{d}z \rangle$, the thermal conductivity λ is calculated as $\lambda = -j_z/\langle \mathrm{d}T/\mathrm{d}_z \rangle$, assuming the validity of a linear response (Fourier's law) [32, 33].

The first approach to the calculation of the thermal conductivity was made using the Green-Kubo expression (GK). Originally, the idea was to obtain values from both GK and Müller-Plathe (MP) and compare the results obtained with each approach. However, after several attempts (different cut-off values, ensembles) the simulations performed with GK did not yield a converged system energy when testing it with pure ionic liquids. According to Liu and Maginn [34], the thermal conductivity may also be computed using the GK expression involving the heat flux although, in systems with long range electrostatic interactions, the heat flux is not rigorously defined since many-body interactions exist. Therefore, the RNEMD is more appropriate to calculate the thermal conductivity in systems with ionic liquids, keeping in mind that a nominal T has to be assumed since a ΔT is created.

Regarding the results on heat transport, reasonable agreement was found between the experimental data and the NEMD values of thermal

conductivity of the pure ionic liquids, with a good prediction of the relative order between the different ILs. However, the NEMD values of thermal conductivity of pure ionic liquids are overestimated by a factor of 1.5 and by a factor of 1.7 in the case of the composite systems with a SWCNT. The thermal conductivity of the composite systems was calculated along the direction of the axis of the nanotube, and across the graphene planes. In the former, the thermal conductivity is enhanced due to conduction through the material. In the latter, a perpendicular orientation to heat flow reduces the thermal conductivity. The enhancement was found to be system-dependent, with different rates obtained for different ILs with a SWCNT in the IL phase, as verified by the experimental data.

An enhancement of thermal conductivity was observed in the interfacial layers of the ionic liquid near a graphene stack, of the order of 15 - 30% with respect to the value in the bulk fluid. This conclusion was made possible by the structural information obtained, where it is shown that the interfacial region has different widths depending on the liquid, being around 1 nm in $[C_4C_1im][tf_2N]$ and between 0.84 and 0.89 nm in cyano ILs. The temperature gradients are continuous from the bulk ionic liquid to the interface in all the systems we studied, showing no remarkable interfacial discontinuity (Kapitza length) [35]. This result regarding the interfacial thermal conductivity is useful for establishing predictive models for heat transport.

The supporting information for the work presented in this chapter can be found in Annex 1.

In the coming article, the author of the present dissertation performed the quantum mechanical calculations, assisted on the development of scripts to process the DFT data and used adapted scripts developed by the Clermont-Ferrand group to fit the DFT data. Regarding the molecular dynamics simulations, the author was responsible for preparing and launching the simulations, processed the structural data with the aid of scripts developed by the Clermont-Ferrand group,

developed scripts to process the heat transport data and wrote the manuscript draft.

PCCP

PAPER

View Article Online
View Journal | View Issue

Cite this: *Phys. Chem. Chem. Phys.*, 2017, **19**, 17075

Molecular interactions and thermal transport in ionic liquids with carbon nanomaterials†

João M. P. França, [ab] Carlos A. Nieto de Castro [b] and Agílio A. H. Pádua *[a]

We used molecular dynamics simulation to study the effect of suspended carbon nanomaterials, nanotubes and graphene sheets, on the thermal conductivity of ionic liquids, an issue related to understanding the properties of nanofluids. One important aspect that we developed is an atomistic model of the interactions between the organic ions and carbon nanomaterials, so we did not rely on existing force fields for small organic molecules or assume simple combining rules to describe the interactions at the liquid/material interface. Instead, we used quantum calculations with a density functional suitable for non-covalent interactions to parameterize an interaction model, including van der Waals terms and also atomic partial charges on the materials. We fitted a *n*–*m* interaction potential function with *n* values of 9 or 10 and *m* values between 5 and 8, so a 12-6 Lennard-Jones function would not fit the quantum calculations. For the atoms of ionic liquids and carbon nanomaterials interacting among themselves, we adopted existing models from the literature. We studied the imidazolium ionic liquids $[C_4C_1im][SCN]$, $[C_4C_1im][N(CN)_2]$, $[C_4C_1im][C(CN)_3]$ and $[C_4C_1im][(CF_3SO_2)_2N]$. Attraction is stronger for cations (than for anions) above and below the π-system of the nanomaterials, whereas anions show stronger attraction for the hydrogenated edges. The ordering of ions around and inside (7,7) and (10,10) single-walled nanotubes, and near a stack of graphene sheets, was analysed in terms of density distribution functions. We verified that anions are found, as well as cations, in the first interfacial layer interacting with the materials, which is surprising given the interaction potential surfaces. The thermal conductivity of the ionic liquids and of composite systems containing one nanotube or one graphene stack in suspension was calculated using non-equilibrium molecular dynamics. Thermal conductivity was calculated along the axis of the nanotube and across the planes of graphene, in order to see the anisotropy. In the composite systems containing the nanotube, there is an enhancement of the overall thermal conductivity, with calculated values comparing well with experiments on nanotube suspensions, namely in terms of the order of the different ionic liquids. In the systems containing the graphene stack, the interfacial region of the ionic liquid near the surface of the material has an enhanced thermal conductivity with respect to the bulk liquid, but no significant discontinuity in the temperature profiles were observed. This is important information for models of thermal conduction in nanofluids.

Received 27th March 2017,
Accepted 31st May 2017

DOI: 10.1039/c7cp01952a

rsc.li/pccp

Introduction

Composites of carbon nanomaterials with ionic liquids have raised interest since the discovery of "bucky-gels"[1] formed by carbon nanotubes and ionic liquids. These and related systems have a number of applications including in new materials, processes, and electronic or electrochemical devices. Ionic liquids supported in gels are relevant as membranes for separations,[2] and ionic liquids can be designed as solvents for exfoliation[3,4] of carbon nanomaterials, leading to stable suspensions and new ways to functionalize or manipulate these nanomaterials, or new composite phases. The interface between ionic liquids and carbon nanomaterials is relevant in other contexts, for example in the development of better electrolytic supercapacitors,[5] either by the design of organic electrolytes or of electrode materials, usually a nanoporous carbon,[6] the use of carbon nanofibers in IL-based catalytic beds to improve the specific surface area[7] or the performance enhancement of dye-sensitized solar cells with IL electrolytes using carbon dots.[8]

Among the interesting properties of composite systems formed by carbon nanomaterials and ionic liquids is the enhancement in

[a] *Institut de Chimie de Clermont-Ferrand, Université Clermont Auvergne & CNRS, 63178 Aubière, France. E-mail: agilio.padua@uca.fr*
[b] *Centro de Química Estrutural, Faculdade de Ciências, Universidade de Lisboa, Campo Grande, 1749-016, Lisboa, Portugal*

† Electronic supplementary information (ESI) available: Additional figures and tables concerning the development of the interaction potential and the simulation results. See DOI: 10.1039/c7cp01952a

transport properties, namely thermal conductivity, possibly leading to efficient, non-volatile and safe heat transfer fluids. Several recent studies[9–11] have shown that the suspension of small amounts of multi-walled carbon nanotubes in ionic liquids can enhance the thermal conductivity of the base fluid up to 30% and lead to a smaller decrease of the thermal conductivity with temperature, which is an important feature when considering several ranges of temperature in heat transfer.[12] However, little is known about the influence of the thermal conductivity at the interface between ionic liquids and nanomaterials, as well as about the structure and extent of the interface, leading to a lack of understanding about the reasons for the observed enhancement and preventing the development of models[13–15] that can accurately predict the thermal conductivity of nanofluids.

Molecular simulation can provide insights into the conduction of heat in the composite systems, but we believe that a detailed description of the interactions at the IL/nanocarbon material interface is important to obtain a realistic description of both the ordering of ions at the interface and heat transfer.

In spite of several studies in theoretical physical chemistry,[3,7,16] using electronic structure calculations and molecular simulation while aiming to understand the interactions between ionic liquids and carbon nanomaterials, the present knowledge is still not sufficient to establish structure–property relations that can guide the choice of the best fluids and materials in view of applications. Ionic liquids[17] are organic salts composed of large, flexible and asymmetric ions, with complex interaction resulting from the distribution of the electrostatic charge over many atoms, delocalized and highly polarizable π electrons, hydrogen bonds, and the presence of various chemical functional groups. The interactions of these large, complex ions with the extended π systems of graphene and other sp^2 carbon nanomaterials, including their edges, are also difficult to describe.

The aim of this work is to improve our understanding of systems composed of ionic liquids and carbon nanomaterials, such as graphene sheets and nanotubes, through a detailed modeling of the interactions at the interface and a study of the resulting structural, energetic and transport properties using molecular simulation. We start by constructing a specific molecular interaction model (atomistic force field) based on electronic structure calculations of the interaction energy between the ions and sp^2-carbon nanomaterials. We base our force-field development on calculations of the potential energy of interaction between organic ions and model compounds that are extended polycyclic molecules, such as larger versions of coronene representing graphene basal planes and their hydrogenated edges, and also small nanotubes. This same strategy has been used in various studies of the interactions between carbon nanomaterials and water.[18–21]

This force field is then used in molecular simulations of systems composed of ionic liquids and graphene flakes or nanotubes. This study is focused on ionic liquids with (relatively) low viscosity, whose suspensions of carbon nanotubes have been characterized recently.[10] The ordering of the ions in the interfacial layers is analyzed both near graphene planes and solvating nanotubes.

Then, the thermal transport in the composite systems is studied using non-equilibrium molecular dynamics. Generally, phonon conduction (vibrational modes) is assumed to be the main factor responsible for thermal transport in carbon nanotubes,[22] but factors such as chirality, diameter and/or length may contribute to the increase of the thermal transport through electronic modes. As the electronic band gap decreases, as for armchair nanotubes (where it approximates zero), the electronic contribution for the thermal conductivity increases. On the other hand, the electronic band gap increases when nanotubes have small diameters and small values of chirality indexes n and m, approaching semiconductor values.[23] The length of the tube and the temperature of the system also influence the value of the thermal conductivity, considering an adequate size for the phonon mean-free path and/or the dependency on low frequency (acoustic) phonons at low temperatures.[23–25] Considering the former, the occurrence of Umklapp scattering (phonon–phonon or electron–phonon scattering process) above 400 K leads to lower values of thermal conductivity. With regard to graphene, the thermal conductivity similarly depends greatly on the vibrational modes (zero electronic band gap), although the heat conduction decreases exponentially as the number of parallel sheets increase due to the rise in phonon scattering channels.[26] Furthermore, the thermal conductivity anisotropy can be of the order of 10^3 W m^{-1} K^{-1} depending on whether heat is conducted in-plane or cross-plane considering a stack of graphene sheets and graphite, with a similar dependence being seen on perfect,[27] defective[28] or composite systems.[29] We will be focusing on the latter.

Development of the interaction model

Choice of methods

The two main issues concerning the choice of methods are the representation of a graphene flake by a relatively small model structure and the choice of density functional for the electronic structure calculations of the interaction energy. The main computational task when developing a force field for ionic liquids with carbon nanomaterials is calculating using quantum mechanics (DFT – density functional theory), at various distances and mutual orientations, the potential energy of interaction between the ions of the ionic liquids and a small model structure representing a graphene flake or a nanotube.

We intend to build an atomistic interaction model that is relatively transferable between families of ionic liquids and also able to represent graphene planes and nanotubes. The interactions between ions in the ionic liquid phase are described by the CL&P atomistic force field[30,31] which is compatible with the OPLS-AA force field for organic compounds.[32] This class of force fields is fully flexible in terms of the internal molecular degrees of freedom (bond stretching, angle bending, and conformational torsions) and all atoms are represented by Lennard-Jones (LJ) sites with partial electrostatic charges. OPLS-AA can also be used to represent aromatic compounds, graphene or nanotubes.[20]

Because our liquids are ionic, we consider it perilous to assume that the interactions of the ions with graphene materials can be well described by simple combining rules between the parameters of the pure materials, mainly because of the distinct forces between ions and extended delocalized π-systems, which are highly polarizable. The present study concerns interactions of nano-scale objects, which are known to be non-additive in various contexts.[33] Thus, we opted here to develop specific parameters for the cross-interactions. In order to attain a level of transferability, we followed a strategy of dividing the ionic liquid into three kinds of fragments: the cation head-group containing most of the positive charge, the alkyl side-chain (which can be of various lengths or contain chemical functional groups), and the anion. In certain ionic liquids, the anions can possess non-polar alkyl chains (*e.g.* alkylsulfonate anions) and some of the parameters developed here can eventually be used to represent these ionic liquids. However, in the present work, only side chains on cations are considered.

In this work, we studied ionic liquids composed of alkylimidazolium cations, $C_nC_1im^+$, with three different anions: dicyanamide, $N(CN)_2^-$, thiocyanate, SCN^-, tricyanomethanide, $C(CN)_3^-$, and bis(trifluoromethanesulfonyl)imide, $(CF_3SO_2)_2N$ or tf_2N^-. In the calculations of the interaction energy with graphene, the fragment chosen to represent the head-group of the cation is a dimethylimidazolium, so that the methyl groups attached to the imidazolium rings are parameterized taking into account the effect of the positive charge. To parameterize the alkyl side chain, we considered a butane molecule, because it contains sufficient methyl and methylene groups, allowing the construction of side chains with different lengths by appropriate combination of sites. The anions were considered in their entireties. In order to limit the number of adjustable parameters in the ionic liquid–material interactions, hydrogen atoms of the ions were not attributed to specific Lennard-Jones sites, but only electrostatic partial charges. The pertinence of this simplification will be subject to validation by comparing the potential energy surfaces obtained from DFT with those generated by the atomistic potential.

With regard to the choice of model structures for the carbon nanomaterials, we wish to represent the basal plane of graphene, or the mid-section of a nanotube, as well as their edges. Explicit edges are relevant because they allow the simulation of flakes of arbitrary shape and of nanotubes with different chiralities (armchair, zig-zag). Electrostatic charge distributions in edges are specific and affect the interactions of carbon nano-objects with liquid solvents. Therefore, our model structures should not be too small, underrepresenting the basal plane, nor too large, underrepresenting edges. In this work, the edges of graphene flakes or carbon nanotubes are considered to be hydrogenated.

Electronic structure calculations were carried out using the Gaussian 09 software[34] using the M06-2X density functional, which performs well for non-covalent interactions involving nonmetals.[35] We used the cc-pVTZ basis set, and for larger systems removed the higher angular momentum f functions in the interest of speed, while retaining good performance in the calculation of quantities relevant to force field development.[36] The counterpoise method was used to correct for basis set superposition.

The influence of the size of the graphene flake was assessed by test calculations between the ionic liquid $[C_4C_1im][N(CN)_2]$, divided into fragments in the manner described above, with planar structures with different numbers of carbon atoms, starting with 6 (benzene), 24 (coronene), 54, 96 and 148 carbon atoms. Details are given in the ESI,† Fig. S1. The potential energy of interaction was not convergent with respect to the size of the graphene flake, but this aspect is not essential for our application since we will be fitting the individual interatomic potential between each site on the ionic liquid fragments and each atom of the nanomaterial. For the subsequent calculations, we chose the flake with 96 C atoms, which we think has a balanced representation of both the basal plane and the edges.

Electrostatic charge distributions

Electrostatic charge distributions were calculated on planar graphenic flakes of different sizes and also on zig-zag and armchair nanotubes. Our main purpose is to describe the charge distributions on atoms at or near the edges, as illustrated in Fig. 1.

When defining a set of partial charges for the graphenic materials, a compromise has to be found between the level of detail and the transferability between structures of different sizes or curvatures, namely between planar flakes and nanotubes. The method to fit the electrostatic potential surface (CHELPG)[37] produces small variations in charges, which can be averaged out for equivalent atoms leading to a simpler and transferable scheme. We started by considering a relatively detailed set of charges in which five different atom types at or near the edge had different charge values (Fig. S2 and Table S1, ESI†). The atoms of the basal plane or tube far from the edges have zero charge. However, when fitting the interaction energies of ionic liquids with the material (discussed below) good results were obtained when adopting an even simpler charge scheme in which hydrogen atoms have a partial charge of $+0.115e$ and the edge carbon atoms $-0.115e$, with all other

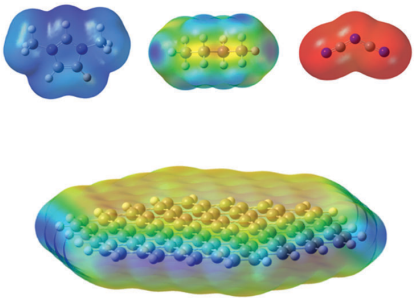

Fig. 1 Electrostatic surface potential (ESP) plot of the charge density on the fragments of the ionic liquids (dimethylimidazolium, butane and dicyanamide) and on a graphene flake composed of 96 carbon atoms, calculated at the M06-2X/cc-pVTZ(-f) level. The edge of the flake is saturated with hydrogen atoms. Red is more negative, blue more positive.

carbon atoms having charge zero. This corresponds to the OPLS-AA scheme for aromatic molecules[21] and proved to be a transferable, simple and robust scheme for graphenic materials.[20,38]

van der Waals interaction parameters

The van der Waals (vdW) energies of interaction between the different fragments of the ionic liquids and the carbon nanomaterials were evaluated by a series of calculations performed for each fragment at several orientations with respect to the nanocarbon structure, and for each orientation at a series of separations. No geometry optimizations were performed at each point, since our purpose was to reproduce the quantum mechanical energies obtained using the classical force field. Because the quantity of interest is the difference between the total potential energy of the ionic liquid fragment and nanocarbon at a given separation, and their energy at a very large separation (with no interaction), it is sufficient that the quantum calculation and the calculation using classical force field be performed at the same atomic coordinates. The basis set superposition error was corrected using the counterpoise technique.

In order to limit the number of adjustable parameters in the vdW potential, hydrogen atoms in the IL fragments and in the nanocarbon materials are lumped into the heavier atoms (so that only electrostatic charges are maintained in the positions of the H atoms). A similar strategy is also followed in widely used classical force fields. For example, in the OPLS-AA[32] force field for alcohols or amines, or in many models of water,[39] the H atoms are present as point charges but only the O or N atoms have Lennard-Jones sites.

The repulsive and attractive exponents of the Lennard-Jones potential, fixed at 12 and 6, respectively, do not necessarily yield a good fit to quantum energies, especially the repulsive exponent which does not have a theoretical justification. One alternative is to use an exponential-6 potential, or else to allow different values for the exponents in an n–m potential, given by eqn (1), but the increased flexibility of these functions comes at the cost of additional parameters to adjust.

$$u_{\mathrm{vdW}}(r) = \frac{E_0}{(n-m)}\left[m\left(\frac{r_0}{r}\right)^n - n\left(\frac{r_0}{r}\right)^m\right] \qquad (1)$$

When determining the van der Waals parameters, two types of sites were considered in the carbon materials: the ones on the rim of the flake with lumped H atoms (CR) and the C atoms of the plane (CG). In the butane fragment, only one type of site was considered, the carbon atom (C). For dimethylimidazolium, three vdW site types were defined: the carbon atoms in the aromatic ring (CA), the nitrogen atoms in the same ring (N) and the methyl groups on the edges (CM). In the dicyanamide fragment, the central nitrogen atom (NA) and the terminal ones (NZ) were differentiated, and the carbon atoms (CZ) also had specific parameters. For both thiocyanate and bis(trifluoromethylsulfonyl)imide, all the atoms of each fragment were defined as vdW interaction sites. Finally, for tricyanomethanide, three sites were considered: the central carbon atom (C3), the nitrogen atoms (N) and the remainder carbon atoms (C).

Table 1 Parameters of the van der Waals interaction potential between atomic sites of the carbon nanomaterial and atomic sites of the ionic liquids. The overall standard deviation of the fit to the quantum mechanical energies is given for each fragment

Graphene site	Fragment site	E_0	r_0	n	m
Butane (σ = 0.31 kJ mol^{-1})					
CG	C	0.449	3.85	11	10
CR		0.464	4.16	11	10
$C_1C_1im^+$ (σ = 0.78 kJ mol^{-1})					
CG	CA	0.995	3.80	10	9
	N	0.303	1.17	10	9
CR	CA	2.47	3.80	10	5
	N	1.26	4.16	10	5
CG & CR	CM	0.834	3.61	10	9
$N(CN)_2^-$ (σ = 0.57 kJ mol^{-1})					
CG	NA	1.13	3.43	9	6
	NZ	1.69	3.43	9	6
	C	0.396	1.60	9	6
CR	N	2.88	2.76	9	5
	C	3.35	4.25	9	5
SCN^- (σ = 0.59 kJ mol^{-1})					
CG	S	2.24	3.59	9	6
	C	0.188	4.42	9	6
	N	2.37	3.28	9	6
CR	S	5.09	3.89	9	5
	C	1.11	2.97	9	5
	N	5.94	3.94	9	5
$C(CN)_3^-$ (σ = 0.33 kJ mol^{-1})					
CG	C3	0.409	4.02	9	8
	C	0.409	1.38	9	6
	N	1.46	3.38	9	6
CR	C3	0.589	3.60	9	5
	C	1.29	4.12	9	5
	N	1.52	4.17	9	5
tf_2N^- (σ = 0.25 kJ mol^{-1})					
CG	C	0.193	3.84	10	6
	F	0.123	3.77	10	6
	S	0.227	4.51	10	6
	N	0.553	2.60	10	6
	O	0.800	3.35	10	6
CR	C	0.507	3.51	10	5
	F	0.560	3.39	10	5
	S	0.955	3.70	10	5
	N	0.612	3.40	10	5
	O	2.90	3.65	10	5

The parameters corresponding to the best fit to the DFT potential energy curves are listed in Table 1 and, as illustrative example, the plot of the interaction between the dicyanamide fragment and the graphene flake is shown in Fig. 2. The plots of the remaining fragments can be found in the ESI,† Fig. S3–S7.

Considering the plots for the butane and dimethylimidazolium fragments, the most attractive orientation is the one with the fragments parallel with respect to the graphene sheet.

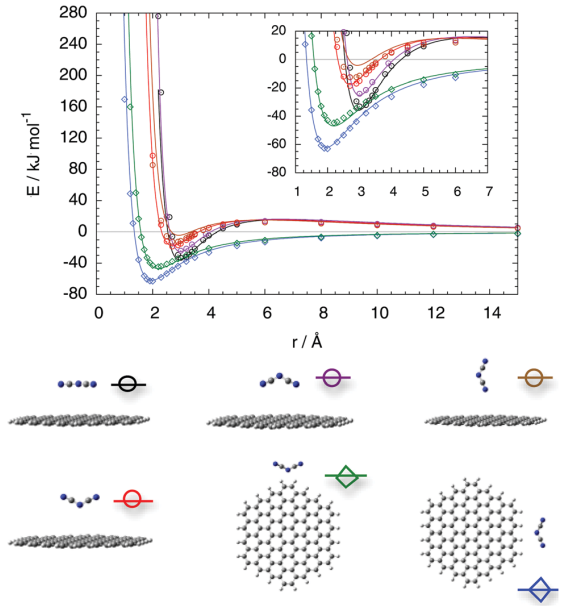

Fig. 2 Potential energy of interaction between the dicyanamide fragment and a 96 C atom flake. Symbols are quantum calculations of the interaction energy at the M06-2X/cc-pVTZ level. Lines result from fitting using the *n*–*m* potential function. The color and the symbol below the plot indicate the mutual orientation of the ionic liquid fragment and the graphene flake.

The interaction between butane and the graphene flake is considerably weaker than with the cation fragment, as expected due to the absence of major electrostatic and polarization components in the DFT energies. The potential energy surfaces of butane and the dimethylimidazolium cation look fairly typical, being always attractive. The stronger attraction of cations happens when they approach the graphenic plane from above, an indication of the favorable cation–π interactions. The interactions of cations approaching from the (positively charged) edge are much less attractive. The plots of the anions also have notable features: first, the strongest interaction for anions lies with the fragments approaching the graphene flake from the edge rather than from above, which is due to the positive charged edges; second, in the orientations where the fragment approaches the plane from above, there is a repulsive maximum beyond the attractive energy minimum (for tf_2N^- there is one orientation which is almost fully non-binding). The significant repulsion of the anions when placed above the graphene plane at intermediate distances is related to the interactions between anions and the π-electron cloud of the material. The same phenomenon was reported[40] relative to the interaction between benzene and hydride.

The overall standard deviations of the fit of the *n*–*m* functions to the DFT energies obtained for each fragment depend on the number of site types used and the flexibility of the potential function. We did not treat the *n* and *m* exponents as true free parameters of the fits. Instead, we tested several combinations, such as 9–5 or 10–6, which are reasonable values, and aimed for a good overall fit by optimizing E_0 and r_0 only. In all cases, it was concluded that a repulsive exponent of 12 was too steep, which is something we had already observed in previous studies.[41,42]

In order to show the importance of parameterizing specifically the ionic liquid–material interactions, we compare in Fig. S8 (ESI†) the DFT energies with calculations using a 12-6 Lennard-Jones potential with parameters taken from the literature, obtained based on combining rules between LJ parameters of the dicyanamide anion[43] and the force field for graphene.[20] The conclusion is that the traditional 12-6 potential for unlike interactions based on combining rules of pure-compound parameters is not adequate to describe the interaction of the ionic solvent and the nanomaterial.

Once the interaction parameters were obtained for the ionic liquids with a graphene flake, we needed to test if they were transferable to other carbon nanomaterials, such as a single-walled carbon nanotube (SWCNT). Using the same DFT methods and basis set described above, potential energy points were obtained for a SWCNT composed of 168 C atoms, with the edges saturated with H atoms in a zig-zag conformation. The ionic liquid fragments considered were butane, dimethylimidazolium and dicyanamide. The potential energies calculated using the present force field agree with the DFT calculations with an overall standard deviation of σ = 1.6 kJ mol^{-1} for an attractive well of the order of *ca.* −80 kJ mol^{-1}, as can be seen in Fig. 3.

Further plots for the other fragments are presented in the ESI,† in Fig. S9 and S10. For the dimethylimidazolium cation, a somewhat larger discrepancy is observed, corresponding to an overall standard deviation of σ = 6.7 kJ mol^{-1} for the set of orientations and distances considered, and an interaction potential energy minimum of −90 kJ mol^{-1}. For the butane fragment, the transferability of parameters is excellent leading in the former to σ = 0.6 kJ mol^{-1} for a potential minimum of −20 kJ mol^{-1}.

System setup

The study of the structural and transport properties of the composite systems containing ionic liquids and carbon nanomaterials was performed on two model setups: (1) single-walled carbon nanotubes in ionic liquids, which solvate the curved interface and can enter the pore of the nanotube and (2) a stack of several graphene sheets and the corresponding interfaces with ionic liquids. The latter can also represent a multi-walled carbon nanotube (MWCNT). Computational costs pose constraints to the maximum length of the SWCNT and the number of graphene sheets that can be studied using a fully atomistic model, mainly because the surrounding ionic liquid has to be simulated as well and that the periodic images of the carbon nanomaterial must not affect each other. Two armchair SWCNTs were built using the VMD software with indices (7,7) and (10,10). The (10,10) nanotube has a length of 81.7 Å and a diameter of 13.8 Å, while the (7,7) nanotube has a length of 81.6 Å and a diameter of 9.5 Å. The graphite unit cell was used to build

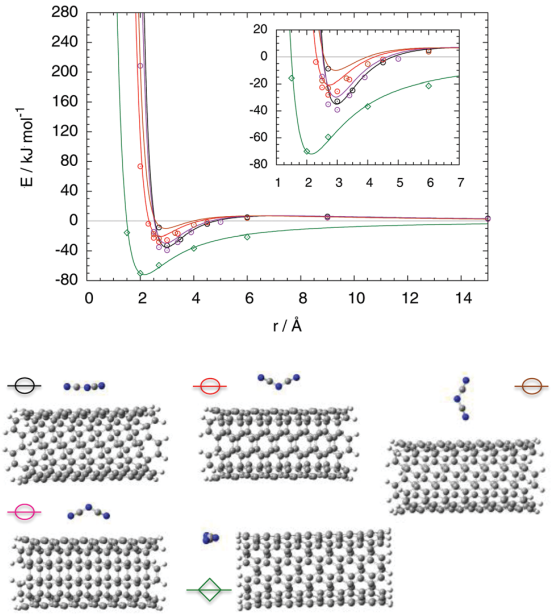

Fig. 3 Potential energy of interaction between the dicyanamide fragment and a 168 C atoms nanotube. Symbols are quantum calculations of the interaction energy at the M06-2X/cc-pVTZ level. Lines result from the *n*–*m* potential function with parameters obtained from the fitting on graphene. The color and the symbol below the plot indicate the mutual orientation of the ionic liquid fragment and the nanotube.

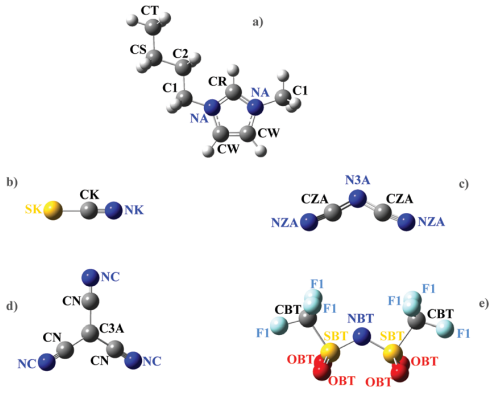

Fig. 4 Molecular structures of the ionic liquids: (a) $C_4C_1im^+$ (cation), (b) SCN^-, (c) $N(CN)_2^-$, and (d) $C(CN)_3^-$, tf_2N^-. The labels identify the atoms according to the force field used. The hydrogen atoms in the cation are not labeled since they are lumped into the heavier atoms.

5 parallel graphene sheets using the VESTA software in the ABABA form. The sheets are approximately square, with L_x = 51.7 Å and L_y = 51.3 Å, separated by 3.36 Å.

The structures of the ionic liquids studied are presented in Fig. 4. The amount of ionic liquid in the simulation boxes necessary to reach the bulk phase structure (about 20 Å to the edge of the periodic simulation boxes) was defined based on the solvent densities and ranged from 388 to 960 ions pairs (details in Table S2, ESI†). The simulation box for the SWCNTs is a rectangular parallelepiped of dimensions $L_xL_yL_z$ (L_x = L_y = 50 Å, L_z = 118–129 Å), depending on the ionic liquid. For graphene, the box was fitted to the graphene sheets in the *x* and *y* dimensions in order to respect the periodic boundaries and obtain virtually infinite sheets, whereas L_z was set at around 65 Å depending on the IL. The initial configurations were prepared using the Packmol[44] tool.

The LAMMPS[45] molecular dynamics package was used to perform all the simulations. A cutoff of 12 Å was used for the *n*–*m* potential and Coulomb interactions were computed using a particle–particle particle-mesh solver with a relative accuracy of 10^{-4} in energy. The simulations were performed above room temperature, namely at 363 K, in order to ensure lower viscosities of the ionic liquids allowing shorter simulation times. The initial configurations were equilibrated in constant *NpT* simulations using Nosé–Hoover integrators. For the SWCNTs, high pressure was used initially in order to force the ions into the nanotube, followed by equilibration. Afterwards, constant *NVT* trajectories of 5 ns were executed with a time step of 1 fs. Snapshots were saved every 1000 steps for post-treatment.

In order to evaluate if the systems were indeed equilibrated up to a diffusive regime, an exponent β of the mean-square displacement (MSD) as a function of time[46,47] was computed for the pure ionic liquids. When a system reaches the diffusive regime, β = 1, therefore we used this as a criterion for equilibration and to defined the length of our trajectories (see Fig. S11–S14, ESI†).

The thermal conductivity of pure ionic liquids and the composite systems containing a SWCNT or a stack of graphene sheets was calculated using the reverse non-equilibrium scheme of Müller-Plathe[48] (MP) to relate a temperature gradient to the heat flux across the simulation box. Starting from the final configurations of the previously mentioned MD trajectories, the same boxes were used for subsequent RNEMD *NVT* runs of 8 ns (partitioned into two 4 ns runs) executed with a time step of 0.5 and without the SHAKE method. The simulation box was divided into 20 slabs along the *z* direction and exchange of kinetic energy between particles in the central and top slabs defined in the simulation box took place every 350 time steps or every 500 time steps, in order to attain a straight temperature profile, as shown in Fig. S22–S25 (ESI†) for pure ionic liquids. H atoms were excluded from the energy swaps to avoid velocity jumps in exchanges due to the difference in mass between H atoms and the remainder atoms in the system. The partition of the 8 ns into two panels was done in order to reduce the influence of the temperature inhomogeneity into the final value of thermal conductivity (see Fig. S18 in the ESI†).

The thermal conductivity of the systems containing the SWCNT was calculated from the ratio between the slope obtained from linear regression of the local temperatures and the heat flux data computed during the last nanosecond of the simulation, in the direction aligned with the longitudinal axis of the nanotubes, including the areas where the nanotube is found, its edges and also the surrounding IL. In the systems containing a stack of graphene sheets, a temperature gradient

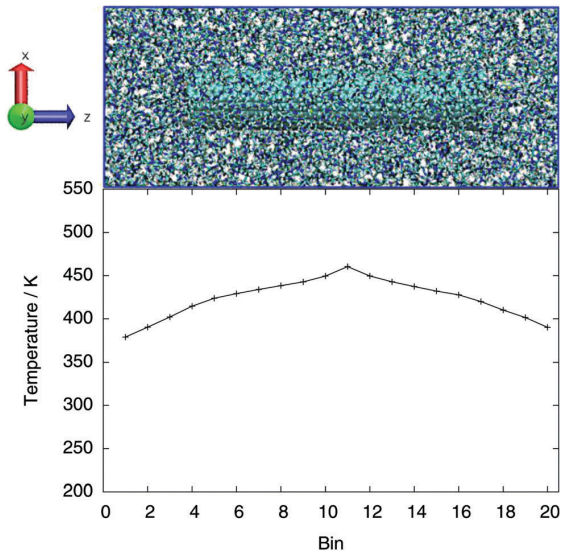

Fig. 5 Snapshot of the simulation box with $[C_4C_1im][SCN]$ + SWCNT (top) and temperature profile (bottom). NEMD simulation at 423 K with exchange of kinetic energy every 500 time steps.

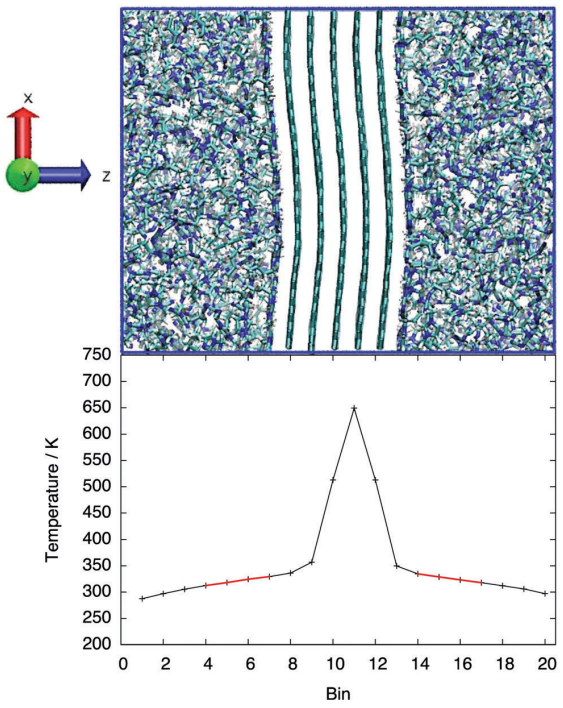

Fig. 6 Snapshot of the equilibrated simulation box with $[C_4C_1im][N(CN)_2]$ + graphene (top) and temperature profile (bottom) with the interfacial zone shown in red. NEMD simulation at 363 K with exchange of kinetic energy every 350 time steps.

is created perpendicular to the planes, from the stack in the center of the box going into the ionic liquid. As such, the simulations with the nanotube will contain a contribution due to longitudinal heat transport, whereas those with the graphene sheet will contain contributions perpendicular to the basal planes. Fig. 5 and 6 show equilibrated simulation boxes and examples of temperature profiles for the IL + SWCNT and IL + graphene systems, respectively.

Interfacial ordering of the ionic liquids

The importance of parameterizing a specific interaction model can be seen by comparing the interfacial ordering of the $[C_4C_1im][N(CN)_2]$ ionic liquid near carbon nanomaterials at 343 K both using our model and Lennard-Jones parameters from the literature (assuming simple Lorentz–Berthelot combining rules). Cylindrical density distribution functions were computed with respect to the axis of the nanotubes and are shown in Fig. 7 for the (7,7) SWCNT.

The present interaction potential leads to higher-intensity first peaks, corresponding to the increased ordering, especially of the charged moieties of the cation and the anion, whereas the literature LJ model produces a structure in which the alkyl tails (atom type CT) are more likely present at the interface. With the present interaction model, alkyl side chains are pointing away from the nanotube. After the first layer of ions outside the SWCNT, there is a depletion of anions at distances of *ca.* 9 Å, where imidazolium head-groups are found. In the pore inside the nanotube, the present model gives a higher density of ions, which again is a result of the more favorable interactions when compared to the assumption of LJ parameters from combining rules.

Several studies on the interaction between ionic liquids and carbon nanomaterials have been performed in recent years, from which the same interpretations of the use a parameterized interaction model can be inferred. When devising the IL–carbon potential from mixing rules of LJ force fields,[49–52] the ionic liquids appear less structured in the solvation layers with several atoms from both anions and cations appearing at the same distances from the carbon surface. However, specifically parameterized models based on quantum calculations, such as those reported here and in the work of Pensado *et al.*[42] for $[C_2C_1im][SCN]$, show that interfacial ordering is more pronounced.

In Fig. 8, we show the structural information (CDFs) for $[C_4C_1im][N(CN)_2]$ around the (10,10) and (7,7) nanotubes and also density profiles near flat graphene sheets. Equivalent results concerning SCN^- and $C(CN)_3^-$ ionic liquids can be found in the ESI† (Fig. S15 and S16).

In the local atomic densities of the ionic liquid $[C_4C_1im][N(CN)_2]$ with the SWCNT (10,10) (Fig. 8a), we can observe one layer of both cation head-groups (NA and CR atoms) and anions (N3A and NZA atoms) closer to the inner wall of the nanotube. A strong peak of the terminal C atom of the alkyl chain of the cation (CT) is found near the center of the nanotube. This arrangement is due to strong interactions between the imidazolium ring and the nanotube. Outside the nanotube, we can observe a symmetric organization by comparison with the inner structure. The interfacial layer is composed by anions and cation head-groups, separated

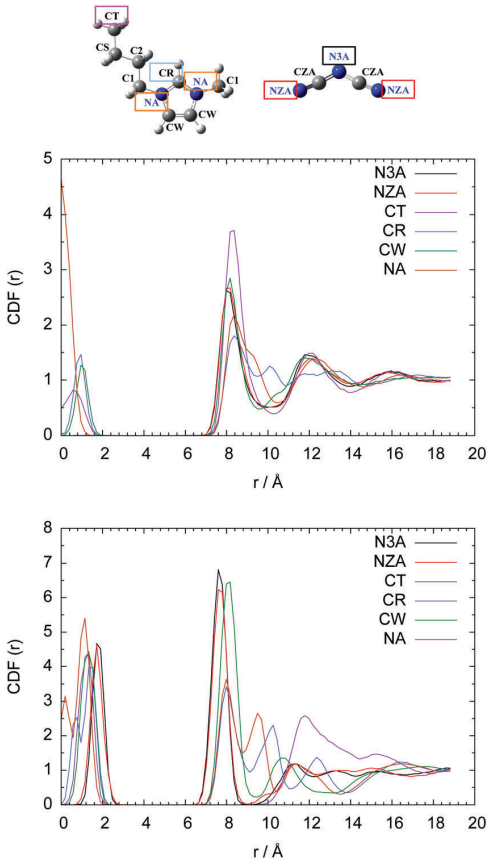

Fig. 7 Cylindrical distribution function (CDF) of atoms of $[C_4C_1im][N(CN)_2]$ with respect to the axis of the (7,7) SWNCT at 343 K. LJ force field (top); present n–m potential (bottom). The central 50 Å of the nanotube were considered. The region between 3 and 7 Å approximately is where the atoms of the nanotube are located.

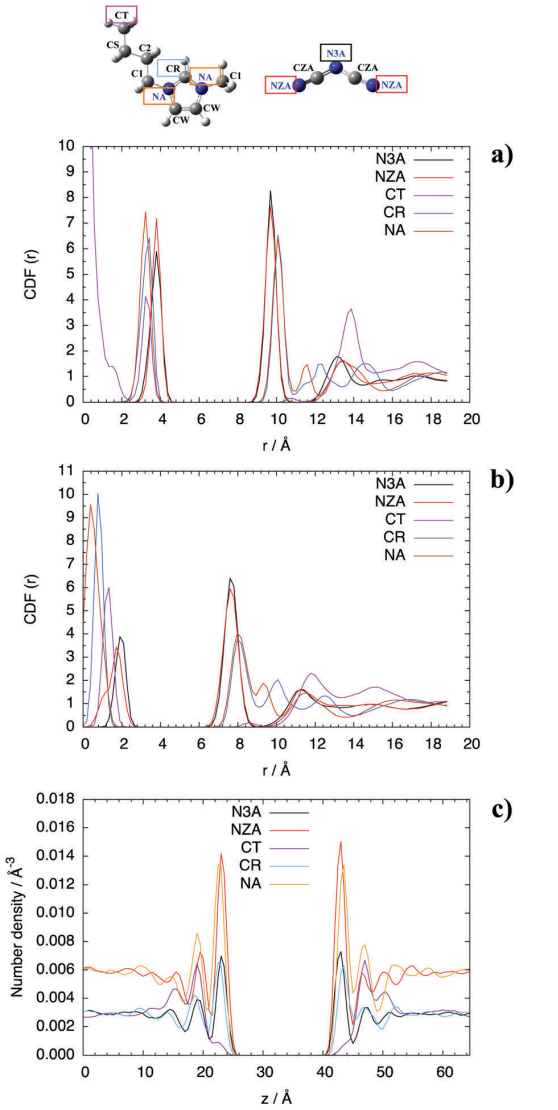

Fig. 8 Cylindrical distribution function (CDF) of (a) $[C_4C_1im][N(CN)_2]$ with the (10,10) SWNCT (10,10) and (b) $[C_4C_1im][N(CN)_2]$ with the (7,7) SWNCT and (c) number density of $[C_4C_1im][N(CN)_2]$ near the graphene stack. T = 363 K.

by approximately 0.37 Å (distance between peaks of N3A and NA outside the tube), while the alkyl chains are preferentially directed to the bulk liquid.

Confinement of the IL leads to a different structure inside the (7,7) SWCNT (Fig. 8b). While the anions are also found closer to the inner wall, the imidazolium rings are now found near the center and not the alkyl chains. Therefore, the (10,10) nanotube is sufficiently wide to allow the formation of a nonpolar domain near its axis, and this is not observed in the narrower one. The stronger curvature of the (7,7) nanotube only marginally affects the ordering of ions outside, when compared to the (10,10) SWCNT.

At the interfacial layers with graphene sheets, the ions of $[C_4C_1im][N(CN)_2]$ are organized in two distinct layers of both cations and anions, with a third, outer, less organized layer (Fig. 8c). As seen from the CT peak, the alkyl chains are directed towards the bulk liquid, in the same way as they were the outside the SWCNTs.

The interfacial layering of the other ILs based on anions with cyano groups, $[C_4C_1im][SCN]$, $[C_4C_1im][C(CN)_3]$, are shown in Fig. S15 and S16 in the ESI†. The ordering of these cyano ILs shares many similarities with those of $[C_4C_1im][N(CN)_2]$, with respect to each carbon nanomaterial. The composition of the first interfacial layers outside the SWCNTs is similar concerning the positions of anions and cation head-groups. The ordering inside the (10,10) and (7,7) nanotubes is also analogous for the three cyano-based ionic liquids, with the cation head-group present near the axis of the narrower tube and the alkyl side chains in the central region of the wider one. Another common feature is that the alkyl side chain of the cation is found in the axis of the (10,10) nanotube, with decreasing local density of CT

atoms near the nanotube axis in the order SCN^- > $N(CN)_2^-$ > $C(CN)_3^-$. Therefore, larger cyano anions lead to a less ordered non-polar domain in the center of the (10,10) tube.

Some information on the orientational ordering of the anions with respect to the surface of the graphene stack can be extracted from the density profiles (lower plots in Fig. 8 and Fig. S15, S16, ESI†), namely that the anions tend to be oriented planar to the surface, as inferred from the in-phase peaks for different atoms of each anion.

The patterns found with $[C_4C_1im][tf_2N]$, shown in Fig. 9, also present similarities to the overall structure picture for cyano ILs, namely in the ordering of the cations with the side chain directed towards the bulk liquid. Also, the CF_3 groups of the anions (represented by the F1 atoms in Fig. 9), which correspond to the least charged moieties of the anions, are also found near the center of the wider (10,10) tube and near the inner wall of the (7,7) tube. It is interesting to note that in the interfacial layers with planar graphene surfaces, the cation side chains are found near the interface with a higher probability than in the other ILs. Therefore, we conclude that the tf_2N^- IL has a "softer" structure compared to the cyano ILs studied, forming solvation layers that are less defined by electrostatic charge ordering, a behavior related to the larger, more flexible anion that contains lower charge-density groups (such as CF_3).

We calculated the charge density profiles along the simulation boxes containing the graphene stack (Fig. 10 for $[C_4C_1im][C(CN)_3]$ and the remaining ILs in Fig. S17, ESI†). The $[C_4C_1im][C(CN)_3]$ IL is the one showing longer-range charge ordering into the bulk liquid, which corresponds to the more defined layering also observed in the density profiles (Fig. S16, ESI†). Therefore, the flat and symmetric $C(CN)_3^-$ anion leads to a stronger layering seen in both the number density and electrostatic charge profiles.

Thermal conductivity

The thermal conductivity of pure ILs, IL + SWCNT and IL + graphene was calculated using the NEMD method described above. Fig. 11 shows the results for the systems based on the $N(CN)_2^-$ anion. An example of the convergence of the heat flux and temperature profile is shown in Fig. S18 in the ESI†, along with the temperature profiles and heat fluxes of the remaining systems (Fig. S22–S33, ESI†), and also thermal conductivity values and plots (Table S3 and Fig. S19–S21, ESI†). Experimental values were obtained from the literature.[9–11]

The thermal conductivity of the IL + SWCNT and IL + graphene systems obtained using the *n*–*m* interaction potential between the ionic liquid and the carbon materials developed here was compared with the values obtained assuming combining rules for the unlike interactions and Lennard-Jones parameters from the literature. The comparison is presented in Table S5 and Fig. S34, S35 in the ESI† for $[C_4C_1im][N(CN)_2]$ at 363K. The results differ significantly for the IL + SWCNT system. Our specific interaction model leads to a higher thermal conductivity enhancement when compared to the pure IL (23% against 2%), suggesting that an increased order of the IL in the vicinity of the SWCNT surface improves heat conduction. The results are not as different for the IL + graphene system.

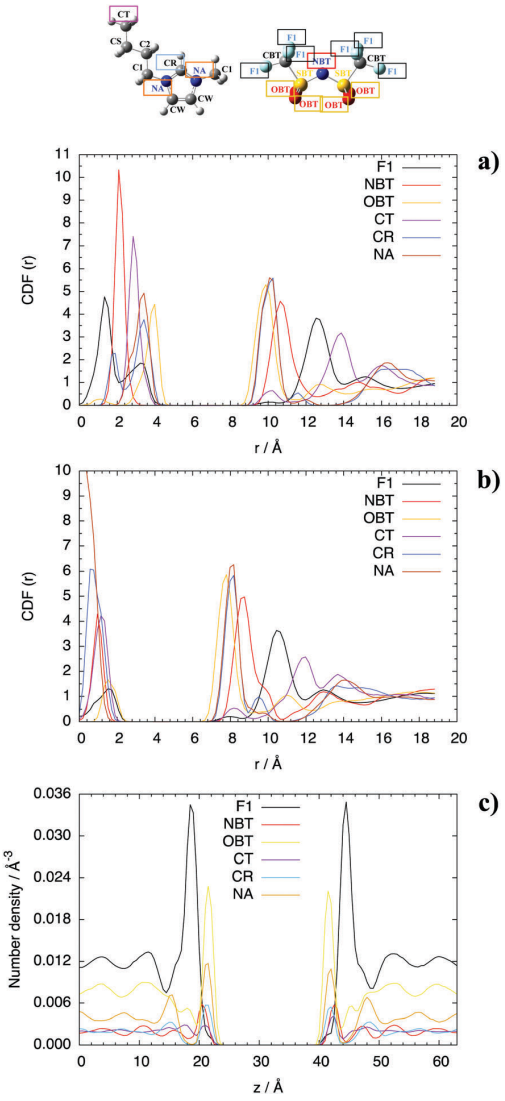

Fig. 9 Cylindrical distribution function (CDF) of (a) $[C_4C_1im][tf_2N]$ with the (10,10) SWNCT and (b) $[C_4C_1im][tf_2N]$ with the (7,7) SWNCT and (c) number density of $[C_4C_1im][tf_2N]$ near the graphene stack. T = 363 K.

When the thermal conductivity of the pure ILs obtained from simulation (Table S3, ESI†) is compared with experimental values from the literature, it is seen that simulation overestimates the experimental results by a factor of 1.5 approximately in most cases, with the exception of ILs with the $C(CN)_3^-$ anion where discrepancy is slightly higher, up to a factor of 1.8. The calculated thermal conductivity generally decreases with increasing temperature, as expected. The order obtained by the NEMD method between the different ILs is $[C_4C_1im][C(CN)_3]$ > $[C_4C_1im][N(CN)_2]$ > $[C_4C_1im][SCN]$ > $[C_4C_1im][tf_2N]$, while that

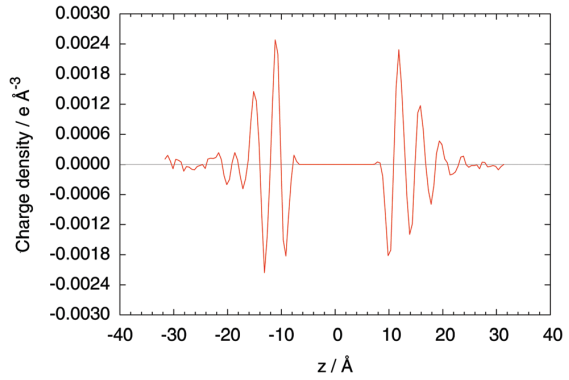

Fig. 10 Electrostatic charge density profile $[C_4C_1im][C(CN)_3]$ with graphene at T = 423 K. The higher temperature was chosen in order to obtain better-converged profiles.

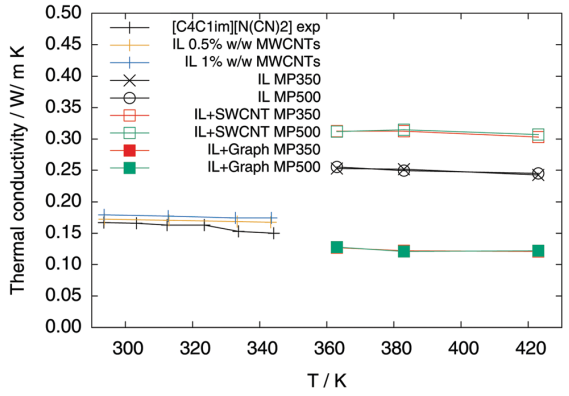

Fig. 11 Thermal conductivity of $N(CN)_2^-$ ILs, pure and with carbon nanomaterials. Experimental results[10] (pure and with MWCNTs) at lower temperatures and NEMD values (pure, with SWCNTs and with graphene) at higher temperatures. "MP 350" denotes the Müller-Plathe method with a kinetic energy exchange every 350 time steps, while "MP 500" denotes a kinetic energy exchange every 500 time steps.

of the experimental data is $[C_4C_1im][C(CN)_3] > [C_4C_1im][SCN] > [C_4C_1im][N(CN)_2] > [C_4C_1im][tf_2N]$, *i.e.*, there is a swap in the order of the two intermediate ILs. However, the difference within ± 3 mW m^{-1} K^{-1} of the thermal conductivity of the dicyanamide and thiocyanate ILs is commensurate with the experimental uncertainty. Other authors[53,54] have computed the thermal conductivity of pure ionic liquids through NEMD, particularly for $[C_4C_1im][tf_2N]$, where the results tend to show lower thermal conductivities when compared with the experimental values, although the experimental references presented in our plots have a better agreement with their NEMD results. However, the lack of information on the kinetic energy exchange rate and the use of partial ionic charges ($\pm qe < 1$) prevent a direct comparison.

In the composite systems with the SWCNT, we compute systematically an increased thermal conductivity with respect to the pure ILs, as seen in Fig. 11 and Fig. S19–S21 (ESI†).

This enhancement of the thermal conductivity is calculated from two separate NEMD simulations: nanotube + IL systems and in the pure ILs. The heat flux is generated across the simulation box (z axis) for both cases. In the IL + SWCNT systems, the heat flows through the SWCNT as shown in Fig. 5, which is favourable for heat transport and increases the overall thermal conductivity of the system. There is a noticeable presence of two linear regimes in the temperature profiles when compared to the ones obtained for the pure ILs, which is to be expected in inhomogeneous systems.[55] The increase in thermal conductivity is distinct between systems with different ILs, which is a result of the specific interaction models and is in agreement with the experimental observations. The values of thermal conductivity enhancement for the IL + SWCNT systems can be found in Table 2.

The ionic liquid presenting a greater thermal conductivity enhancement in the IL + SWCNT systems is $[C_4C_1im][tf_2N]$, likely due to the longer range of the interfacial region. In the cyano family, the ionic liquid presenting a smaller interfacial thickness and also a smaller enhancement is $[C_4C_1im][C(CN)_3]$.

When comparing the results between both kinetic energy exchange rates, the heat flux is always higher when the velocity is exchanged every 350 time steps, as expected, but the thermal conductivity is not always higher for this perturbation when comparing the same system at one exchange every 500 time steps, except for $[C_4C_1im][SCN]$ + SWCNT.

Similarly to the pure ILs, the simulation overestimates the experimental thermal conductivity by an approximate factor of 1.7 (2.0 for $C(CN)_3^-$ IL). The experimental results of thermal conductivity in MWCNT suspensions[9–11] of 0.5% and 1% w/w contents in multi-walled CNTs also show an enhancement, although smaller which is likely linked to the lower concentration than in our simulations.

The interactions between CNTs and organic liquids[56] are due to weak dispersion forces. The thermal conductivity of CNTs and CNT composite systems depends on several factors. For example, an armchair (10,10) nanotube has an approximate null band gap (metallic behaviour), which generates an electronic contribution to thermal conductivity.[23] However, the electronic contribution to the thermal conductivity is negligible in MWCNTs and SWCNTs[25,57] and the main scattering process is covered by

Table 2 Enhancement obtained for the IL + SWCNT systems. "MP 350" denotes the Müller-Plathe method with a kinetic energy exchange rate of 350 time steps, while "MP 500" denotes a kinetic energy exchange rate of 500 time steps

T/K	$[C_4C_1im]$ $[tf_2N]$	$[C_4C_1im]$ $[SCN]$	$[C_4C_1im]$ $[N(CN)_2]$	$[C_4C_1im]$ $[C(CN)_3]$
$((\lambda_{IL+SWCNT} - \lambda_{IL})/\lambda_{IL}) \times 100$/% IL + SWCNT MP 350				
363	26.62	23.47	23.32	14.73
383	28.96	23.36	23.81	18.33
423	34.31	24.15	24.69	19.61
$((\lambda_{IL+SWCNT} - \lambda_{IL})/\lambda_{IL}) \times 100$/% IL + SWCNT MP 500				
363	25.81	19.20	22.35	20.39
383	30.35	23.75	26.51	14.55
423	31.61	21.39	25.82	23.23

acoustic phonon–phonon scattering due to the acoustic mismatch between the solid and liquid phases in our systems,[22] leading to a smaller thermal conductivity when compared with a single CNT.

The relationship between the computed and experimental results while studying a liquid–carbon material interface has been reported, although with different systems and methodologies.[56] The presence of nanotube bundles in the experimental results is invoked to explain the lower values of thermal conductivity. While the experimental suspensions for which the present NEMD results are being compared are stable, aggregates cannot be excluded. On the other hand, in the simulated systems the SWCNT is isolated in the ionic liquid phases. Another mechanism to account for the difference between systems is based on the Kapitza resistance,[58] a barrier to heat transfer associated with weak dispersion forces between the liquid and the carbon nanomaterials.[26,55]

In the systems with graphene stacks, the temperature profiles have two well-defined zones corresponding to a lower thermal conductivity across the graphene planes and a higher one in the IL bulk phase, which lead to a weighed average (considering the number of slices associated with each slope) when computing the values of thermal conductivity throughout the simulation box. Overall, the thermal conductivity is considerably lower than in the longitudinal SWCNT systems (and lower than in pure ILs) but the different ILs show the same order of thermal conductivity as the IL + SWCNT systems. As mentioned in the Introduction, the thermal conductivity of IL + graphene systems is expected to be considerably lower when heat flows across the graphene stack. There is, however, an enhancement in conductivity in the interfacial region of the IL near the graphene planes. This is calculated considering the thermal conductivity of the bulk liquid in the same simulation box (far from the nanomaterial, see Table S3, ESI†) and the interfacial region in the IL + graphene systems. Based on the structural information described in the previous section, we know the thickness of the interface, and can calculate the local thermal conductivity, as depicted in Fig. 6 for the IL + graphene systems. The local enhancement verified in this region is not to be compared with the above-mentioned enhancement for the IL + SWCNT systems, since the latter is pertinent to the overall thermal conductivity of the system due to the presence of the SWCNT in the IL phase.

In our NEMD simulations (see Fig. 6), the temperature variation from the liquid to the carbon surface appears continuous, suggesting a small Kapitza resistance between ionic liquids and carbon surfaces. The models[13,15,59] used to calculate the interfacial thermal conductivity of suspensions with cylindrical or spherical nanoparticles are based on two assumptions: the interfacial thickness is 1–2 nm and the thermal conductivity of the interface has a value between that of the pure ionic liquid and that of the material. With regard to the width of the interface, our structural results show that the interfacial region has different widths depending on the liquid, being around 1 nm in $[C_4C_1im][tf_2N]$ and between 0.84 and 0.89 in cyano ILs. Concerning the second assumption, our results in Table S4, ESI† and Table 3 show that the local thermal conductivity at the interface between the IL and the graphene stack is higher than that of the pure ionic liquid, with an enhancement between 15 and 30% depending on the ionic liquid. These values of enhancement are lower than the value of 60% verified for the Au–Ar interface, considering a similar representation regarding the presence of the bulk liquid near the interface.[60] Although different methodologies and materials are being considered, the main difference in our work lies in the direction of the heat flux, being parallel to Au walls in the literature reference, while it is perpendicular to the graphene stack in this work. Given the considerable anisotropy of thermal conductivity in systems with graphene regarding the direction of the heat flux,[29] it is likely that the local thermal conductivity at the interface also depends on the direction of the heat flow. Consequently, a perpendicular heat flow relative to the nanomaterial yields a lower enhancement.

Table 3 Interfacial enhancement obtained for the IL + graphene systems. "MP 350" denotes the Müller-Plathe method with a kinetic energy exchange rate of 350 time steps, while "MP 500" denotes a kinetic energy exchange rate of 500 time steps

T/K	$[C_4C_1im]$ $[tf_2N]$	$[C_4C_1im]$ $[SCN]$	$[C_4C_1im]$ $[N(CN)_2]$	$[C_4C_1im]$ $[C(CN)_3]$
$((\lambda_{IL+graphene} - \lambda_{IL})/\lambda_{IL}) \times 100$/% IL + graphene MP 350				
363	18.70	20.96	31.55	12.40
383	15.83	36.22	22.99	24.11
423	15.63	17.63	22.81	8.21
$((\lambda_{IL+graphene} - \lambda_{IL})/\lambda_{IL}) \times 100$/% IL + graphene MP 500				
363	17.24	31.02	24.51	23.86
383	15.81	36.10	24.00	17.51
423	16.55	23.78	24.48	23.14

Conclusions

Our aim in this work was to study the interactions between ionic liquids and carbon nanomaterials, and more specifically how these interactions and the ordering of ions in the interfacial layers affect the thermal conductivity of the composite systems. We opted to develop specific interatomic interaction models, by parameterization against electronic structure calculations, because we thought that assuming simple mixing rules for unlike interactions and existing force fields for small organic molecules would not render the interactions between ions and highly polarizable materials, such as carbon nanotubes or graphene planes. Recent density functionals, suitable for non-covalent interactions, were used as a basis for our parameterization. Interactions between the ions of the liquid were described by existing force fields. We had followed similar strategies in previous works on the interactions of ionic liquids with metal nanoparticles,[61] surfaces[41] and nanomaterials.[42] As we had found before, the Lennard-Jones 12-6 potential does not describe the interaction energies from quantum mechanics correctly. Instead, we fit n–m potential functions with n values of 9 or 10 and m values between 5 and 8. By inspecting the potential energy surfaces (Fig. 2 and Fig. S3–S7, ESI†), we see that cations show a stronger attraction when placed above the π-system of the nanomaterials, whereas anions are more

attracted to the hydrogenated edges, as expected from the electrostatic charge distributions.

We studied using molecular simulation SWCNTs in various imidazolium ionic liquids: $[C_4C_1im][SCN]$, $[C_4C_1im][N(CN)_2]$, $[C_4C_1im][C(CN)_3]$, $[C_4C_1im][tf_2N]$, which are stable salts with relatively low viscosities. Structural information concerning the ordering of ions in the interfacial layer showed similarities in the cyano ILs, with the anion often found close to the carbon surface, which was unexpected given the relative intensity of attraction of isolated ions. With the $tf2N^-$ anion the non-polar alkyl side chains are found closer to the carbon surface than with the other ionic liquids. In the (7,7) and (10,10) nanotubes, cations are found most likely near the centre of the nanotubes, with their positions and orientations depending on the diameter of the tube. The alkyl side chains of the cations aggregate in the centre of the (10,10) nanotube creating a non-polar domain.

The thermal conductivity of the ionic liquids and composite systems with one nanotube or a stack of graphene sheets was calculated by non-equilibrium molecular dynamics. We found a reasonable agreement between the experimental data and the NEMD values of thermal conductivity in the pure ionic liquids, with a good prediction of the relative order between the different ILs. We calculated the thermal conductivity of the composite systems along the direction of the axis of the nanotube, but across the graphene planes. In the former, the thermal conductivity is enhanced due to conduction through the material. In the latter, a perpendicular orientation to heat flow reduces the thermal conductivity. The enhancement is system-dependent, with different rates obtained for different ILs with a SWCNT in the IL phase, as verified by the experimental data. We observed an enhancement of thermal conductivity in the interfacial layers of the ionic liquid near a graphene stack, of the order of 15–30% with respect to the value in the bulk fluid. The temperature gradients are continuous from the bulk ionic liquid to the interface in all the systems we studied, showing no remarkable interfacial discontinuity (Kapitza length). This result regarding the interfacial thermal conductivity is useful for establishing predictive models for heat transport.

Acknowledgements

J. M. P. França would like to thank FCT – Fundação para a Ciência e Tecnologia, Portugal, for the PhD Grant SFRH/BD/79378/2011. A. P. thanks the Agence Nationale de la Recherche project CLINT ANR-12-IS10-003.

References

1 T. Fukushima, A. Kosaka, Y. Ishimura, T. Yamamoto, T. Takigawa, N. Ishii and T. Aida, *Science*, 2003, **300**, 2072–2074.
2 J. Le Bideau, L. Viau and A. Vioux, *Chem. Soc. Rev.*, 2011, **40**, 907–925.
3 S. Ravula, S. N. Baker, G. Kamath and G. A. Baker, *Nanoscale*, 2015, **7**, 4338–4353.
4 M. Matsumoto, Y. Saito, C. Park, T. Fukushima and T. Aida, *Nat. Chem.*, 2015, **7**, 730–736.
5 M. Armand, F. Endres, D. R. MacFarlane, H. Ohno and B. Scrosati, *Nat. Mater.*, 2009, **8**, 621–629.
6 C. Merlet, B. Rotenberg, P. A. Madden, P.-L. Taberna, P. Simon, Y. Gogotsi and M. Salanne, *Nat. Mater.*, 2012, **11**, 306–310.
7 M. Ruta, I. Yuranov, P. J. Dyson, G. Laurenczy and L. Kiwi-Minsker, *J. Catal.*, 2007, **247**, 269–276.
8 H. Xiong, X. Zhang, B. Dong, H. Lu, L. Zhao, L. Wan, G. Dai and S. Wang, *Electrochim. Acta*, 2013, **88**, 100–106.
9 J. M. P. França, S. I. C. Vieira, M. J. V. Lourenço, S. M. S. Murshed and C. A. Nieto de Castro, *J. Chem. Eng. Data*, 2013, **58**, 467–476.
10 J. M. P. França, F. Reis, S. I. C. Vieira, M. J. V. Lourenço, F. J. V. Santos, C. A. Nieto de Castro and A. A. H. Pádua, *J. Chem. Thermodyn.*, 2014, **79**, 248–257.
11 J. M. P. França, S. M. S. Murshed, A. A. H. Pádua and C. A. Nieto de Castro, *Ind. Eng. Chem. Res.*, to be submmited.
12 J. M. P. França, C. A. Nieto de Castro, M. M. Lopes and V. M. B. Nunes, *J. Chem. Eng. Data*, 2009, **54**, 2569–2575.
13 S. M. S. Murshed and C. A. Nieto de Castro, *Proceedings of The World Congress on Engineering 2011 Vol III*, 2011, 1905–1909.
14 R. Pal, *Nanomaterials*, 2014, **4**, 844–855.
15 C. A. Nieto de Castro, M. J. V. Lourenço, A. P. C. Ribeiro, E. Langa, S. I. C. Vieira, P. Goodrich and C. Hardacre, *J. Chem. Eng. Data*, 2010, **55**, 653–661.
16 M. Atilhan and S. Aparicio, *J. Phys. Chem. C*, 2014, **118**, 21081–21091.
17 P. Wasserscheid and T. Welton, in *Ionic Liquids in Synthesis*, ed. P. Wasserscheid and T. Welton, Wiley-VCH, 2nd edn, 2008, pp. 1–740.
18 G. R. Jenness, O. Karalti and K. D. Jordan, *Phys. Chem. Chem. Phys.*, 2010, **12**, 6375–6381.
19 Y. Wu and N. R. Aluru, *J. Phys. Chem. B*, 2013, **117**, 8802–8813.
20 P. Schyman and W. L. Jorgensen, *J. Phys. Chem. Lett.*, 2013, **4**, 468–474.
21 A. Striolo, A. Michaelides and L. Joly, *Annu. Rev. Chem. Biomol. Eng.*, 2016, **7**, 533–556.
22 Z. Han and A. Fina, *Prog. Polym. Sci.*, 2011, **36**, 914–944.
23 M. Grujicic, G. Cao and B. Gersten, *Mater. Sci. Eng., B*, 2004, **107**, 204–216.
24 S. Berber, Y.-K. Kwon and D. Tománek, *Phys. Rev. Lett.*, 2000, **84**, 4613–4616.
25 J. R. Lukes and H. Zhong, *J. Heat Transfer*, 2007, **129**, 705–716.
26 J. Jin-Wu, W. Bing-Shen, W. Jian-Sheng and S. P. Harold, *J. Phys.: Condens. Matter*, 2015, **27**, 083001.
27 E. Pop, V. Varshney and A. Roy, *MRS Bull.*, 2012, **37**, 1273–1281.
28 Z. G. Fthenakis, Z. Zhu and D. Tománek, *Phys. Rev. B: Condens. Matter Mater. Phys.*, 2014, **89**, 125421.
29 D. Konatham, K. N. D. Bui, D. V. Papavassiliou and A. Striolo, *Mol. Phys.*, 2011, **109**, 97–111.

30 J. N. Canongia Lopes, J. Deschamps and A. A. H. Pádua, *J. Phys. Chem. B*, 2004, **108**, 2038–2047.
31 J. N. Canongia Lopes and A. A. H. Pádua, *Theor. Chem. Acc.*, 2012, **131**, 1129.
32 W. L. Jorgensen, D. S. Maxwell and J. Tirado-Rives, *J. Am. Chem. Soc.*, 1996, **118**, 11225–11236.
33 C. A. Silvera Batista, R. G. Larson and N. A. Kotov, *Science*, 2015, **350**, 1242477.
34 M. J. Frisch, G. W. Trucks, H. B. Schlegel, G. E. Scuseria, M. A. Robb, J. R. Cheeseman, G. Scalmani, V. Barone, G. A. Petersson, H. Nakatsuji, X. Li, M. Caricato, A. V. Marenich, J. Bloino, B. G. Janesko, R. Gomperts, B. Mennucci, H. P. Hratchian, J. V. Ortiz, A. F. Izmaylov, J. L. Sonnenberg, D. Williams-Young, F. Ding, F. Lipparini, F. Egidi, J. Goings, B. Peng, A. Petrone, T. Henderson, D. Ranasinghe, V. G. Zakrzewski, J. Gao, N. Rega, G. Zheng, W. Liang, M. Hada, M. Ehara, K. Toyota, R. Fukuda, J. Hasegawa, M. Ishida, T. Nakajima, Y. Honda, O. Kitao, H. Nakai, T. Vreven, K. Throssell, J. A. Montgomery, Jr., J. E. Peralta, F. Ogliaro, M. J. Bearpark, J. J. Heyd, E. N. Brothers, K. N. Kudin, V. N. Staroverov, T. A. Keith, R. Kobayashi, J. Normand, K. Raghavachari, A. P. Rendell, J. C. Burant, S. S. Iyengar, J. Tomasi, M. Cossi, J. M. Millam, M. Klene, C. Adamo, R. Cammi, J. W. Ochterski, R. L. Martin, K. Morokuma, O. Farkas, J. B. Foresman and D. J. Fox, *Gaussian 09 Revision C.01*, 2009.
35 Y. Zhao and D. G. Truhlar, *Theor. Chem. Acc.*, 2008, **120**, 215–241.
36 R. A. Friesner, R. B. Murphy, M. D. Beachy, M. N. Ringnalda, W. T. Pollard, B. D. Dunietz and Y. Cao, *J. Phys. Chem. A*, 1999, **103**, 1913–1928.
37 C. M. Breneman and K. B. Wiberg, *J. Comput. Chem.*, 1990, **11**, 361–373.
38 W. L. Jorgensen and D. L. Severance, *J. Am. Chem. Soc.*, 1990, **112**, 4768–4774.
39 H. J. C. Berendsen, J. R. Grigera and T. P. Straatsma, *J. Phys. Chem.*, 1987, **91**, 6269–6271.
40 C. Coletti and N. Re, *Chem. Phys.*, 2012, **398**, 168–175.
41 A. C. F. Mendonça, P. Malfreyt and A. A. H. Pádua, *J. Chem. Theory Comput.*, 2012, **8**, 3348–3355.
42 A. S. Pensado, F. Malberg, M. F. C. Gomes, A. A. H. Padua, J. Fernandez and B. Kirchner, *RSC Adv.*, 2014, **4**, 18017–18024.
43 J. N. Canongia Lopes and A. A. H. Pádua, *J. Phys. Chem. B*, 2006, **110**, 19586–19592.
44 L. Martínez, R. Andrade, E. G. Birgin and J. M. Martínez, *J. Comput. Chem.*, 2009, **30**, 2157–2164.
45 S. Plimpton, *J. Comput. Phys.*, 1995, **117**, 1–19.
46 M. G. Del Pópolo and G. A. Voth, *J. Phys. Chem. B*, 2004, **108**, 1744–1752.
47 C. Cadena and E. J. Maginn, *J. Phys. Chem. B*, 2006, **110**, 18026–18039.
48 F. Müller-Plathe, *J. Chem. Phys.*, 1997, **106**, 6082–6085.
49 Y. Shim and H. J. Kim, *ACS Nano*, 2009, **3**, 1693–1702.
50 M. Mohammadi and M. Foroutan, *Phys. Chem. Chem. Phys.*, 2013, **15**, 2482–2494.
51 G. García, M. Atilhan and S. Aparicio, *J. Phys. Chem. B*, 2015, **119**, 12224–12237.
52 A. I. Frolov, K. Kirchner, T. Kirchner and M. V. Fedorov, *Faraday Discuss.*, 2012, **154**, 235–247.
53 H. Liu, E. Maginn, A. E. Visser, N. J. Bridges and E. B. Fox, *Ind. Eng. Chem. Res.*, 2012, **51**, 7242–7254.
54 H. Liu and E. Maginn, *J. Chem. Phys.*, 2011, **135**, 124507.
55 M. Alaghemandi, E. Algaer, M. C. Böhm and F. Müller-Plathe, *Nanotechnology*, 2009, **20**, 115704.
56 S. Shenogin, L. Xue, R. Ozisik and P. Keblinski, *J. Appl. Phys.*, 2004, **95**, 8136–8144.
57 M. S. Dresselhaus and P. C. Eklund, *Adv. Phys.*, 2000, **49**, 705–814.
58 P. L. Kapitza, *Zh. Eksp. Teor. Fiz.*, 1941, **11**, 1.
59 S. M. S. Murshed, K. C. Leong and C. Yang, *Appl. Therm. Eng.*, 2009, **29**, 2477–2483.
60 Z. Liang and H.-L. Tsai, *Phys. Rev. E: Stat., Nonlinear, Soft Matter Phys.*, 2011, **83**, 041602.
61 A. S. Pensado and A. A. H. Pádua, *Angew. Chem., Int. Ed.*, 2011, **50**, 8683–8687.

Chapter 5

Thermal Conductivity of Ionic Liquids and IoNanofluids and their Feasibility as Heat Transfer Fluids

In this chapter, the last sets of experimental data on the topic at hand are presented. As it was mentioned in the introductory section of Chapter 3, the suspension of a nanomaterial leads to an increase in viscosity of the base fluid and, consequently, if the starting point were to be an ionic liquid of low viscosity, the end product would have an acceptable value of this property when envisioning the flow of the fluid in a tube. In this sense, cyano alkylimidazolium ionic liquids, such as the ones based on thiocyanate (SCN^-) and tricyanomethanide ($C(CN)_3^-$) anions, should have close values of viscosity, a fact confirmed in the literature [36]. Additionally, these anions tend to have a lower ecotoxicity than anions such as $(CF_3SO_2)_2N^-$ and tris(perfluoroalkyl)trifluorophosphate) [13, 37], which is an advantage from an environmental point of view. Unfortunately, the same cannot be said of the alkylimidazolium cations in general. However, the selection of smaller side chains reduces the biological effects and, in this sense, an acceptable cost-benefit ratio can be attained from the use of these fluids.

In line with Chapters 2 and 3, the data obtained in this work showed a considerable enhancement of the thermal conductivity of the ionic liquid when 0.5 and 1% w/w MWCNTs are dispersed in the fluids. Similarly, the data also shows the diverse variations of the enhancement with varying base fluid. This was supported by what was shown in chapter 4. It was seen there that the interactions of similar ionic liquids with the same material are specific (although similarities exist), leading to different values of enhancement of the thermal conductivity among them. At this time, the idea of creating a unified model to predict the enhancement of the thermal conductivity

by adding MWCNTs to an ionic liquid, or modifying an existing one, was discarded. The time necessary to attain such a goal was not feasible in the allowed time frame for this project.

As such, an alternative was provided. Consider the application discussed throughout this work: the use of ionanofluids as heat transfer fluids. In this sense, a specific heat transfer process was selected and the heat transfer area necessary was calculated, using currently commercialized heat transfer fluids, pure ionic liquids and ionanofluids. Although the addition of nanomaterial to the ionic liquids leads to an increase in the heat transfer area when comparing ionic liquids and ionanofluids, the latter exhibit a smaller variation of the area with temperature. While the area calculated for the considered process for heat transfer fluids and ionic liquids decrease in a range from -10 to -43%, ionanofluids show a decrease in area that ranges from -7 to -26%. This feature is important when considering heat transfer fluids for multiple processes and/or considering different temperature values.

Depending on the base ionic liquid, some of the ionanofluids studied are head-to-head with a significant number of currently used heat transfer fluids, considering the area necessary to transfer the same amount of heat. It all comes down to the requirements of the process in question, in terms of heat transfer capabilities (area, unit cost, fluid cost) when choosing a heat transfer fluid for the task.

The supporting information for the work presented in this chapter can be found in Annex 2.

In the coming article, the author of the present dissertation designed the experiments regarding the cyano ionic liquids/ionanofluids, prepared the suspensions, performed the measurements, processed the data, performed the heat transfer area calculations and wrote the manuscript draft.

Submitted to I&EC Research (ACS)

Thermal Conductivity of Ionic Liquids and IoNanofluids and their Feasibility as Heat Transfer Fluids

João M.P. França[†,‡,#], Maria José V. Lourenço[†], S.M. Sohel Murshed[†], Agílio A.H. Pádua[‡], Carlos A. Nieto de Castro [†,*]

[†]Centro de Química Estrutural, Faculdade de Ciências, Universidade de Lisboa, Campo Grande, 1749-016, Lisboa, Portugal.
[‡]Institut de Chimie de Clermont-Ferrand, Université Clermont Auvergne & CNRS, 63178 Aubière, France.

KEYWORDS ionic liquids, IoNanofluids, thermal conductivity, heat transfer area.

ABSTRACT: Over the past few years, ionic liquids and IoNanofluids have been studied as a possible alternative to current engineering fluids. Considering heat transfer, ionic liquids have been studied as possible heat transfer fluids due to their high volumetric heat capacity and good thermal conductivity and the combination of nanomaterials with these fluids creates great expectation considering the enhancement of their thermophysical properties. In the present paper we report new data on the thermal conductivity of $[P_{66614}][N(CN)_2]$, $[P_{66614}][Br]$, $[C_2mim][SCN]$, $[C_4mim][SCN]$, $[C_2mim][C(CN)_3]$ and $[C_4mim][C(CN)_3]$ at temperatures between 293 and 343 K at 0.1 MPa and IoNanofluids based on them with MWCNTs. While we could not obtain stable suspensions with phosphonium based ionic liquids, the enhancement of the thermal conductivity of cyano based ionic liquids was compared with previous work using dicyanamide ionic liquids. The thermal conductivity of C_2mim^+ based ionic liquids and IoNanofluids is generally higher than the corresponding C_4mim^+ based fluids. The variation of enhancement with temperature hinders the conception of a unified model that can predict the enhancement of the thermal conductivity of the presented IoNanofluids and current theories under predict the enhancement of the thermal conductivity of these suspensions. Finally, we selected a specific heat transfer process and calculated the heat transfer area necessary using currently commercialized heat transfer fluids, ionic liquids and IoNanofluids. While the addition of nanomaterial to the ionic liquids leads to an increase in the heat transfer area, the enhancement of the thermophysical properties leads to a smaller variation of the area with temperature. Depending on the ionic liquid, some of the IoNanofluids studied are head-to-head with a significant number of currently used heat transfer fluids concerning the heat transfer area necessary to transfer the same amount of heat.

INTRODUCTION

The past few decades have brought to light a great concern regarding environmental awareness and the pursuit for optimal energy technologies, either from an efficiency and/or economical perspective. In this sense, the unique characteristics of ionic liquids have drawn the attention of chemical companies and scientific community over recent years. The potential displayed by these fluids reveals applicability in several areas of modern chemistry, from analytical chemistry to catalysis and from petrochemical industry to nuclear industry. Furthermore, these substances promise some benefits regarding the preservation of the environment, stimulating the practice of the philosophy of green chemistry.[1-2] In the field of heat transfer, there is a need for new heat transfer fluids, capable of replacing environmentally harmful existing ones with properties that can result in maximum possible energy efficiency, in order to support healthy and sustainable applications, either domestic and/or industrial.

Nanomaterials and nanotechnology have become a natural topic in our society, where almost on a daily basis new ideas and applications are being developed and revolutionizing modern life within various fields, from engineering to medicine. The main objective of current research consists on minimizing the volume of any material used, maintaining or upgrading the efficiency of the latter. Nanomaterials vary from metallic or non-metallic particles with distinct mechanical, optical, magnetic, electrical, chemical and thermal properties.[3] Once stably suspended in a fluid, these particles can greatly enhance the properties of the host fluid, becoming a nanofluid.[4] However, care must be taken when using nanomaterials, as their effect toxicological effect on humans and environment is not yet completely studied.[5] A wide range of physicochemical properties are relevant to toxicology, like particle size distribution, morphology, chemical composition, solubility and surface chemistry and reactivity.[6] The amount of nanomaterial used in our work (nanocarbons) is small and was handled without contact to skin or breathing.

If we consider an ionic liquid as the base fluid, the use of nanoparticles as enhancing agents of the fluids' properties enables the association of small quantities of different nanoparticles with different ionic liquids, thus obtaining flexible and designable (on a molecular level) substances that can be

conceived according to the properties needed for a certain application. Considering an application such as heat transfer, ionic liquids have been studied as possible heat transfer fluids due to their high volumetric heat capacity and good thermal conductivity[7] and the combination of nanomaterials with these fluids creates great expectation considering the enhancement of their thermophysical properties. Over the past eight years, work on this area has been accomplished by Nieto de Castro *et al*.[8-14] successfully measuring the thermal conductivity, heat capacity, viscosity and density of mainly imidazolium based ionic liquids with suspended multi-walled carbon nanotubes (MWCNTs) as a function of temperature, giving rise to the term IoNanofluids (INFs), a stable suspension of nanoparticles in ionic liquids.[8]

In what concerns heat transfer, the fluid chosen for such a task should possess fluidity in order to be able to flow through the tubes of, for example, a shell and tube heat exchanger, or any other heat transfer unit. On the other hand, the fluidity of the suspension of nanoparticles will depend on the method used to attain the suspension itself.

The preparation of nanofluids has been discussed in a previous publication of the Lisbon group.[15] It is a fundamental step concerning stability, characterization and use. A recent analysis of the possible steps for nanofluid preparation and characterization, including recommended stability tests, showed that is possible, to prepare stable nanofluids (over a period of several months to years).[16]

In our latest work on this topic,[13] we discussed the use of dicyanamide (alkylimidazolium and alkylpyrrolidinium) based IoNanofluids in heat transfer since ionic liquids based on the dicyanamide anion are considered to be of "low-viscosity". The argument rested on the fact that the suspension of a nanomaterial should lead to an increase in viscosity and, consequently, if the starting point were to be an ionic liquid of low viscosity, the end product would have a more acceptable value of this property when envisioning the flow of the fluid in a tube. In this sense, cyano alkylimidazolium ionic liquids, such as the ones based on thiocyanate (SCN^-) and tricyanomethanide ($C(CN)_3^-$) anions, should have an approximate value of viscosity, a fact that we confirmed in the literature.[17] Additionally, these anions tend to have a lower ecotoxicity than anions such as $(CF_3SO_2)_2N^-$ and tris(perfluoroalkyl)trifluorophosphate),[18-19] which is an advantage from an environmental point of view. Unfortunately, the same cannot be said from the alkylimidazolium cations. However, the selection of smaller side chains reduces the biological effects and, in this sense, an acceptable cost-benefit ratio can be attained from the use of these fluids.

Considering another approach, besides viscosity, the heat capacity of a fluid can have a significant effect on its viability as a heat transfer fluid. As it has been mentioned in previous work,[7] heat transfer area is one of the main design parameters of heat exchangers, which can be estimated from the thermophysical properties of the heat transfer fluid. Related to the heat transfer area, the inner heat transfer coefficient (h_i) of a shell and tube heat exchanger is directly proportional to the thermophysical properties of a fluid by

$$h_i \propto \lambda^{0.67} \rho^{0.8} \eta^{-0.47} C_P^{0.33} \quad (1)$$

Although the heat capacity has the smallest influence in this relation, a viable heat transfer fluid could be obtained if the latter were to be great enough to account for any variations of the remaining properties. Such is the case for phosphonium cation based ionic liquids, with greater C_P values when compared with their alkylimidazolium counterparts.[20-22] Even though the values of viscosity are much greater in the case of ionic liquids with the $[P_{66614}]$ cation, we found to be valuable to explore these ionic liquids and IoNanofluids based on them as potential heat transfer fluids.

This work reports thermal conductivity measurements of trihexyltetradecylphosphonium dicyanamide ($[P_{66614}][N(CN)_2]$), trihexyltetradecylphosphonium bromide ($[P_{66614}][Br]$), 1-ethyl-3-methyl-imidazolium thiocyanate ($[C_2mim][SCN]$), 1-n-butyl-3-methyl-imidazolium thiocyanate ($[C_4mim][SCN]$), 1-ethyl-3-methyl-imidazolium tricyanomethanide ($[C_2mim][C(CN)_3]$) and 1-n-butyl-3-methyl-imidazolium tricyanomethanide ($[C_4mim][C(CN)_3]$) at temperatures between 293 and 343 K at 0.1 MPa and IoNanofluids based on them with MWCNTs. It also compares the obtained results with current theories of thermal enhancement in nanofluids, evaluate the heat transfer area necessary for a given process using currently commercialized heat transfer fluids (HTFs), ionic liquids or IoNanofluids and ponder the pros and cons of using these substances as new heat transfer fluids.

MATERIALS AND METHODS

Materials

All six ionic liquids were purchased from IoLiTec, Ionic Liquids Technologies, Germany, and the product specifications of the certificate analysis can be found in Table S1 in the Supporting Information. The estimated mass fraction purity is 0.98 or better. As it is customary in the ionic liquids supplied by this company, the unusual colour of the liquids is due to the presence (below 2%) of the corresponding bromide precursor since it is common for these liquids to be synthesized with a chloride precursor and therefore, usually, remain colourless.

Several minor impurities at low concentrations, such as halides, will not play a significant role on the thermal conductivity values.[23] However, the water content of the ionic liquids is relevant since it may change considerably the properties of the liquid, in particular for the thermal conductivity[12] when above 1000 ppm. Further purification was performed through drying the ionic liquids at T = 333K, under vacuum, for a minimum period of 72 h. However, some equipment problems did not allow the confirmation of the water content of every sample, and we were only able to perform this confirmation on the phosphonium based ionic liquids. Nonetheless, given our experience with these substances and methods from our previous work, we can confidently assume the water content was minimized to a point were its presence did not affect the presented results. Another factor in favor of this statement lies in the extra 24 h of drying under vacuum instead of the typically used 48 h.

The carbon nanotubes used were multi-walled carbon nanotubes Baytubes C150 HP (MWCNTs) form Bayer Material Science, a development product that has been previously used

by our group,[8] and whose characteristics are displayed in Table S2 in the Supporting Information.

Equipment and methodology

Thermal conductivity was measured using the KD2 Pro™ Thermal Properties Analyzer (Decagon Devices, Inc.). The principle of measurement is based on the transient hot-wire method (THW) using a single-needle sensor (1.3 mm diameter and 60 mm long). This sensor contains a heating element and a thermal resistor, which should be inserted vertically in the sample to assure that free convection is minimized. The measurement is accomplished through the heating of the sensor (inserted in the sample) at a certain rate while simultaneously monitoring the temperature variation. All this is controlled by a microprocessor connected to the sensor that also calculates the thermal conductivity of the sample based on a parameter-based corrected version of the temperature model given by Carslaw and Jaeger for an infinite line heat source with constant heat output and zero mass in an infinite medium.[24] Further information on these calculations can be found elsewhere.[8, 25] Each measured sample had an approximate volume of 85 cm^3 to ensure that the dimensional requirements of the sensor were matched, since it was specified in the device's manual that a minimum amount of material should be present in all directions. With the sensor inserted vertically, the glass vial was then suspended (not inserted, in order to avoid the vibrations of the bath that could induce convection) in a temperature-controlled oil bath (Haake C25; oil – Galp Electric 2) and allowed to stabilize the temperature for each sample measured. The time to reach the desired temperature fluctuated with the sample being measured, as for the IoNanofluids it took longer because these fluids are more viscous and thick, therefore with smaller thermal diffusivity. Once attained the desired temperature, 8 to 10 measurements were taken with an interval of 15 min between each one to ensure reproducibility. Temperature was measured by a platinum resistance probe, part of the thermal conductivity probe, with an uncertainty $u(T) = 0.1$ K.

The procedure of the calibration for the thermal conductivity measurements presented on this work has been extensively described elsewhere.[12] Since our last publication on this matter, the software of the KD2 Pro™ was updated and a new calibration was performed exactly in the same way as before. In summary, the experimental thermal conductivity of substances such as water, toluene, glycerin, a mixture of glycerin and water (50/50 w/w) and an aqueous solution of NaCl was used to obtain a calibration constant, K, given by equation 2:

$$K = \frac{\lambda_{meas}}{\lambda_{ref}} \quad (2)$$

based on the ratio between the experimental thermal conductivity (λ_{meas}) and a bibliographic reference (λ_{ref}) of the same property at the same temperature and pressure. This constant, liquid and temperature-independent, was found to have the value of (1.028 ± 0.012), illustrating an overestimate (+2.8% relatively to the reference values) by the device and leading to a necessary correction of the experimental data. The reference values of the calibrating fluids can be found in reference 13.

Preparation of IoNanofluids

Based on previous work, IoNanofluids were prepared using a sonication probe (Sonicator Sonics & Materials, VC50) to disperse 0.5 and 1% mass fraction of MWCNTs in the ionic liquids. Following the above-cited work,[12-13] the present goal was to obtain a fluid and not a gel, in order to acknowledge the possible use of these IoNanofluids as a heat transfer fluids and, hence, possess some fluidity.

It is worth mentioning that no surfactant was added to the dispersion since any thermal conductivity values would be masked due to the presence of such substances and it was our intention to acquire the most truthful data possible. In fact, Murshed *et al*.[26] demonstrated that all surfactant-added nanofluids have a larger enhancement of the thermal conductivity compared to the same nanofluids without any surfactant, for nanofluids based on water. Moreover, while addition of surfactant contributes in enhancing the effective thermal conductivity, the nanoparticle clustering showed negative impact on both the stability and the effective thermal conductivity of nanofluids. The uncertainty in the IoNanofluids mass fraction was found to be $u(w) = 0.0004$. The sonication time used for each mass fraction was around 1h30, divided into several periods to allow the cooling of the sample.

The demonstration that aggregates are not present in the IoNanofluids can be made by dynamical light scattering (DLS) studies, a procedure used for nanofluids before, and by TEM imaging and subsequent counting of number of particles with average sizes. Both these methods, important for the nanomaterials and nanofluids are well understood but have many limitations for nanofluids, namely for those that are non-light transparent like the carbon nanofluids in DLS, and because TEM imaging can characterise solids and even solid-liquid interfaces, but never the liquid itself.[27] Our previous experience with other IoNanofluids suggest that no aggregation is present at a microscopic scale, as the suspension could sediment with the presence of surfactants, which was not observed for several months in the case of the SCN^-, $N(CN)_2)^-$ and $C(CN)_3^-$ based IoNanofluids. The same could not be said for the phosphonium based IoNanofluids, as we will discuss in the results section.

Theoretical Interpretation

Depending on nanoparticles (concentration, type, and morphology) and liquid type, the enhancements of the effective thermal conductivity of nanofluids relative to their base liquids vary considerably from moderate to large percentage.[28-30] In addition to aforementioned factors related to nanoparticles and base liquids there are other mechanisms, which also contribute to the enhancement of the effective thermal conductivity of ionanofluids. Therefore like nanofluids, the effective thermal conductivity of these ionanofluids cannot be predicted by the classical effective medium theory-based models such as those

attributed by Maxwell[31] and Hamilton and Crosser.[32] It is noted that Hamilton and Crosser modified Maxwell's model (applicable for spherical particles only) and applied particle shape factor for suspensions of non-spherical particles as well. Although such classical models have been widely applied to determine the effective thermal conductivity of nanofluids, they were found unable to predict and explain the experimental thermal conductivity.[28-29, 33] Despite large number of research efforts devoted in the last decade to identify the mechanisms and to develop theoretical models for nanofluids,[29-30, 34] our current knowledge on the real heat transfer mechanisms is scarce and sometimes controversial.[28, 35] Nonetheless, apart from those aforementioned nanoparticle and base fluid related common factors, there are a few main mechanisms which researchers considered to explain significantly enhanced thermal conductivity of nanofluids. These include Brownian motion of nanoparticles (for spherical shape), interfacial nanolayer at the surface of nanoparticle/base fluid interface, and nanoparticle clustering or aggregation. Regarding the interfacial nanolayer, the liquid molecules near the particle surface interact and/or are absorbed at the nanoparticle surface creating a layered structure, which shows characteristics of an organized "solid" like system.[34, 36-37] These mechanisms are well discussed in the literature[29, 34, 36] and are not elaborated further here. Among these mechanisms, interfacial nanolayer was found to be major the factor behind such increase in thermal conductivity of nanofluids.[34, 37-38] Unlike nanofluids, no attempt has so far been made on the theoretical development for the prediction of the thermal conductivity of IoNanofluids. Since the latter are a new class of nanofluids, these mechanisms are also presumed to be applicable for their thermal conductivity.

The Hamilton and Crosser (HC) model[32] for the effective thermal conductivity of suspensions (λ_{eff}) is the function of the thermal conductivities of both particles (λ_p) and liquid (λ_f), volume fraction of particles (ϕ_p), and the shape of the particles. The model is expressed as:

$$\lambda_{\text{eff}} = \lambda_{\text{f}}\left[\frac{\lambda_p + (n-1)\lambda_{\text{f}} - (n-1)\phi_p(\lambda_{\text{f}} - \lambda_{\text{p}})}{\lambda_p + (n-1)\lambda_{\text{f}} + \phi_p(\lambda_{\text{f}} - \lambda_p)}\right] \qquad \textbf{(3)}$$

where the shape factor $n = 3$ for spherical particles and $n = 6$ for cylindrical particles (e.g., nanotubes)

Among a handful of efforts, Murshed *et al*. [38] developed two models by taking into account the effects of particle size, concentration, and interfacial nanolayer for nanofluids ($\lambda_{eff\text{-}nf}$) containing spherical and cylindrical nanoparticles. Their model (MLY) for nanofluids containing cylindrical/tube nanoparticles has the form:

$$\lambda_{\text{eff-nf}} = \lambda_{\text{f}}\frac{\begin{array}{c}\phi_p\omega(\lambda_p - \omega\lambda_f)[\gamma_1^2 - \gamma^2 + 1] + \\ (\lambda_p + \omega\lambda_f)\gamma_1^2[\phi_p\gamma^2(\omega - 1)] + 1\end{array}}{\begin{array}{c}\gamma_1^2(\lambda_p + \omega\lambda_f) - \\ (\lambda_p - \omega\lambda_f)\phi_p[\gamma_1^2 + \gamma^3 + 1]\end{array}} \qquad \textbf{(4)}$$

where $\omega=\lambda_{lr}/\lambda_f$, $\gamma=1+h/r_p$, $\gamma_1=1+h/(2r_p)$, r_p is the radius of the nanoparticle, h and λ_{lr} are the thickness and the thermal conductivity of interfacial nanolayer, respectively.

Although the thickness of nanolayer can be considered to be 2 nm,[30, 38] recent molecular dynamics studies have shown that the interfacial layer is around 0.9 nm for cyano based IoNanofluids.[39] However, the order and orientation of fluid molecules absorbed on a nanoparticle surface result in an intermediate value (between solid and base fluid) of thermal conductivity of nanolayer i.e., $\lambda_f < \lambda_{lr} < \lambda_p$. Hence, the thermal conductivity nanolayer is given by $\lambda_{lr} = \omega\lambda_f$, where $\omega > 1$ is an empirical parameter which depends on the order of fluid molecules in the interface as well as the nature and surface chemistry of nanoparticle. According to the model, the thermal conductivity value of such a nanolayer is up to several times of thermal conductivity of base liquid.

Heat transfer area calculation

The methods used to calculate the heat transfer area have been described extensively in previous publications,[7, 40] where the changes in design parameters of shell and tube heat exchanger arise solely from the variation of the heat transfer fluids' thermophysical properties, namely thermal conductivity, viscosity, heat capacity and density.

The degrees of freedom of a heat exchanger can be reduced to two by selecting a specific type of device and by specifying its duty to satisfy the external constraints of a particular process: the heat transfer area and the pressure drop across the fluid ducts. Since the latter is not usually considered a major factor in the design, the heat transfer area has been considered as the sole factor reflecting the variation of the thermophysical properties of heat transfer fluid considered, as before. The equipment chosen, also described in references 7 and 41 consists on a modern solar power equipment using a molten salt receiver as the thermal energy storage system. The latter captures solar energy and stores it in hot molten sodium nitrate or molten nitrate mixtures in order to generate power, independently of the daytime period. Using a set of reference conditions and the thermophysical properties of each fluid we calculated the heat transfer area from the general principles,[41-42] which is given by

$$Q = U_0 A_0 (\Delta T)_{lm} \qquad (5)$$

where Q is the rate of heat transfer, U_0 is the overall heat transfer coefficient, A_0 is the area across which the heat is being transferred and $(\Delta T)_{lm}$ is the logarithm mean temperature difference between the inlet and outlet stream temperatures of the two fluids. For a particular duty, the only design parameter allowed to depend on thermophysical properties is the area for heat transfer or, in a shell and tube heat exchanger, the number of tubes and passages of fluid. The overall heat transfer coefficient measures the "barrier resistance" to heat transfer and includes all the resistances to the latter. In this case it includes the contribution due to convection at the tubes' inner and outer surfaces and across the tube walls. Convection transfer is determined by the boundary layers developed at the surfaces, depending on the abovementioned thermophysical properties.

For circular tubes, the overall heat transfer coefficient is calculated by

$$\frac{1}{U_0} = \frac{1}{h_0} + \frac{1}{h_i}\frac{D_0}{D_i} + r_w + r_0 + r_i\frac{D_0}{D_i} \quad (6)$$

where D_0 is the outside tube diameter, D_i is the inside tube diameter, r_w is the thermal resistance of the tube wall, r_i and r_0 are the fouling resistance, and h_i and h_0 are the heat transfer coefficients for the inside and outside film of fluids. For our purposes, this can be simplified to

$$\frac{1}{U_0} = \frac{1}{h_0} + \frac{1}{h_i}\frac{D_0}{D_i} + R \quad (7)$$

where R represents the combined resistance of the tube wall and other factors are considered constant. To obtain optimal heat transfer, the flow must be turbulent, which can be achieved by placing baffles in the shell part of the exchanger and controlling fluid velocity in the tubes.

For the turbulent flow in a smooth circular tube, the Sieder and Tate correlation[43] is

$$Nu = \frac{h_i D_i}{\lambda} = 0.027 Re^{0.8} Pr^{1/3} \left(\frac{\eta}{\eta_s}\right)^{0.14} \quad (8)$$

where Re is the Reynolds number, Pr is the Prandtl number, λ and η are the thermal conductivity and viscosity of the fluid, respectively, being evaluated at mean bulk temperature of the fluid. η_s is the fluid viscosity at wall temperature. The ratio at the left-side of the equation is known as the Nusselt number. The Prandtl and Reynolds numbers are given by

$$Pr = \frac{C_P \eta}{\lambda} \quad (9)$$

$$Re = \frac{\rho u D}{\eta} \quad (10)$$

where C_P is the heat capacity, ρ is the fluid density and u is the mean fluid velocity over the tube cross section. Since the thermophysical properties are functions of the fluid, only the fluid velocity must be fixed, being considered the same for the calculations of total area of tubes. For the heat transfer coefficients on the shell side of the heat exchanger, referred as to the outside area, h_o is given by

$$\frac{h_o D_e}{\lambda} = 0.36 Re^{0.55} Pr^{1/3} \left(\frac{\eta}{\eta_s}\right)^{0.14} \quad (11)$$

where D_e is the equivalent diameter between the tubes.

The values for the operation of the heat exchanger were the same as used before,[7, 40] being u = 0.5 m s^{-1}, D_i = 0.018 m, D_o = 0.020 m, D_e = 0.020 m, R = 0 (ideal flow), $(\Delta T)_{lm}$ = 20 K, Q = 1 MW and h_o = 2000 W m^{-2} K^{-1}. These values were used for the calculation of the heat transfer area values of every fluid described in this work in order to have a viable comparison between fluids.

RESULTS

Ionic liquids – Phosphonium cation

The thermal conductivity of ionic liquids was measured at temperatures between 293 and 343 K at 0.1 MPa. The water content was confirmed using Coulometric Karl Fischer titration after the thermal conductivity measurements, values that are presented in Table 1. Increase in the water content was to be expected but was small and did not affect the measurements within their mutual uncertainty.[12] In this sense, we can consider these values as "water-free" ionic liquids, preferably to "pure" ionic liquids.

Table 1. Water content of phosphonium ionic liquids (Karl-Fischer coulometer)

Ionic liquid	$[P_{66614}][N(CN)_2)]$	$[P_{66614}][Br]$
Before drying $H_2O/10^{-6}$	1405.3 ±81.7	3152.2 ± 120.6
After drying $H_2O/10^{-6}$	83.4 ± 21.6	10.5 ± 5.3
After measuring λ $H_2O/10^{-6}$	258.9 ± 87.7	---[a]

[a] Not possible to obtain,

Table 2 displays the values obtained for the ionic liquids, which tend to softly decrease with temperature. The results obtained were fitted to a straight line, according to equation 12

$$\lambda\ (\mathrm{W\ m^{-1}\ K^{-1}}) = a_1 + a_2(T/\mathrm{K}) \quad (12)$$

and Table S3 in the Supporting Information shows the resulting coefficients as well as the root mean square deviations of the fits.

Figure 1 shows the variation of the thermal conductivity of the ionic liquids with temperature, for the range between 293 and 343 K at 0.1 MPa. It can be seen that the variation is linear for both ionic liquids. For $[P_{66614}][N(CN)_2]$ no data point departs from linearity by more than ± 0.44 %. The root mean square deviation of the fits did not exceed 0.52 mW m^{-1} K^{-1}, around 0.32 %. In the case of $[P_{66614}][Br]$, also no data point departs from linearity by more than ± 0.44 %. The root mean square deviation of the fits did not exceed 0.46 mW m^{-1} K^{-1}, around 0.30 %. For both ionic liquids, the variation of the values is virtually independent of temperature.

The uncertainties of the experimental data were estimated to obtain the expanded uncertainty, U_G, using the normal procedure. This parameter is obtained multiplying the combined standard uncertainty, u_G, by an expansion factor, k, that depends of the confidence limit of the interval, usually 95%, and

therefore $k = 2$. The expression to calculate the standard uncertainty is the following:

$$u_G^2 = u_{cal}^2 + u_{exp}^2 \quad (13)$$

Table 2. Thermal conductivities of phosphonium ionic liquids based on the phosphonium cation as a function of temperature at p = 0.1 MPa[a]

Ionic liquid	T / K	λ / W m^{-1} K^{-1}
[P_{66614}][$N(CN)_2$)]	293.6	0.163 ± 0.004
	303.9	0.163 ± 0.004
	314.9	0.161 ± 0.004
	324.5	0.161 ± 0.005
	333.4	0.161 ± 0.004
	343.4	0.161 ± 0.005
[P_{66614}][Br]	293.4	0.156 ± 0.004
	303.2	0.156 ± 0.004
	313.3	0.155 ± 0.004
	323.7	0.155 ± 0.004
	333.8	0.154 ± 0.004
	343.4	0.153 ± 0.004

a With expanded uncertainty at 0.95 level of confidence (k =2).

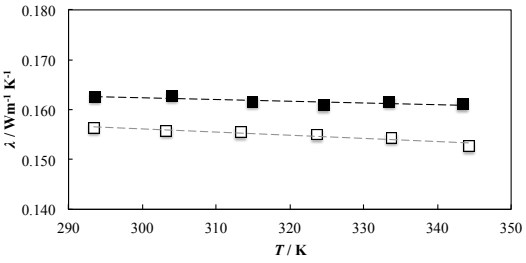

Figure 1. Plot of the thermal conductivity of phosphonium based ionic liquids as a function of temperature. ■ – [P_{66614}][$N(CN)_2$)]; □ – [P_{66614}][Br]; Lines are given by equation 12 with coefficients shown in Table S3.

where u_{cal} represents the uncertainty of the calibration (the standard deviation of the calibration constant, 0.012) and u_{exp} the uncertainty of each experimental measurement (the standard deviation of the average thermal conductivity at each temperature, taken from 8 to 10 measurements). The value of U_G is therefore given by:

$$U_G = k u_G \quad (14)$$

In the phosphonium based ionic liquids, the major contribution for the uncertainty results from the uncertainty of the calibration constant, due to the high viscosity of the liquid. The uncertainty obtained fluctuated between 0.004 and 0.005 W m^{-1} K^{-1} (2.3 to 3.1%) for [P_{66614}][$N(CN)_2$)] and around 0.004 W m^{-1} K^{-1} (2.3 to 2.6%) for [P_{66614}][Br].

No data was available to compare our results regarding the phosphonium based ionic liquids. In its place, we offer a different analysis based on data found in the literature. Figure 2 illustrates thermal conductivity data of several ionic liquids based on the phosphonium cation.

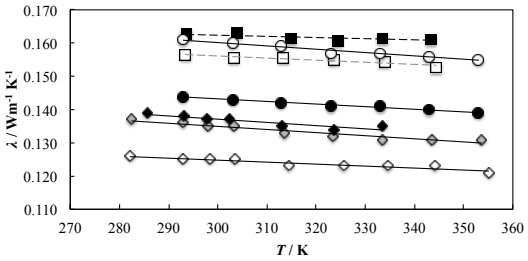

Figure 2. Comparison between the data obtained and those existing in the literature of the thermal conductivity of phosphonium based ionic liquids as a function of temperature. Our work: ■ – [P_{66614}][$N(CN)_2$)]; □ – [P_{66614}][Br]; Ferreira *et al.*[44]: ◇ - [P_{66614}][FAP]; ◈ (grey) - [P_{66614}][Phosph]; ◆ - [P_{66614}][$(CF_3SO_2)_2N$]; Ge *et al.* [23]: ○ - [P_{66614}][Cl]; ● - [P_{66614}][$(CF_3SO_2)_2N$].

From Figure 2 we can state that there are two distinct ranges of thermal conductivity: one where the anion is small (top of the plot) where the order is $N(CN)_2^-$ > Cl^- > Br^- and one where the anion is bulky (lower part of the plot) with the order $(CF_3SO_2)_2N^-$ > $Phosph^-$ > FAP^-. Given that the cation is the same in every ionic liquid presented, if we compare these results with the ones we obtained in our previous work,[12-13] namely with the C_4mim^+ cation combined with the $N(CN)_2^-$ and $(CF_3SO_2)_2N^-$ anions, we can state that the same order is confirmed, where an ionic liquid with the $N(CN)_2^-$ anion will always have a larger thermal conductivity than one with $(CF_3SO_2)_2N^-$ anion. Ultimately, such fact is important regarding the application of these liquids as heat transfer fluids, where the best combination between the thermophysical properties (λ, η, ρ, C_P), that dictates the operation of a heat transfer unit, is necessary. Low viscosity and high thermal conductivity implicate better heat transfer coefficients, a scenario more likely to be obtained if using $N(CN)_2^-$ anion based ionic liquids rather than $(CF_3SO_2)_2N^-$ based ones.

Ionic liquids – Cyano anions

The thermal conductivity of cyano-based ionic liquids was measured at temperatures between 293 and 343 K at 0.1 MPa. The malfunction of the our Coulometric Karl Fischer titration apparatus at that time did not allow us to measure the water content after the measurement of the thermal conductivity but, as we know from our previous work, the increase that may arise from this experimental procedure is of little significance, being around 250 and 350 ppm.[12-13]

Table 3 displays the values obtained for ionic liquids, which generally tend to softly decrease with temperature, although the overall result was a more accentuated decrease in this study. The most relevant case is the thermal conductivity of [C_2mim][SCN] where a considerable oscillation can be observed. Such a fact can be attributed to the sensitivity of the KD2 Pro™ to the variation of viscosity of the fluid being measured,[12-13, 45] given that the viscosity of ionic liquids decreases with the increase of temperature.

Table 3. Thermal conductivities of the ionic liquids as a function of temperature at p = 0.1 MPa[a]

Ionic liquid	T / K	λ / W m^{-1} K^{-1}
[C_2mim][SCN]	293.6	0.185 ± 0.004
	303.4	0.182 ± 0.005
	313.6	0.182 ± 0.006
	323.7	0.178 ± 0.009
	333.9	0.163 ± 0.017
	343.6	0.145 ± 0.010
[C_4mim][SCN]	293.8	0.169 ± 0.004
	303.2	0.169 ± 0.004
	313.4	0.169 ± 0.005
	323.6	0.167 ± 0.005
	333.9	0.160 ± 0.008
	343.4	0.152 ± 0.017
[C_2mim][$C(CN)_3$]	294.0	0.188 ± 0.005
	303.3	0.190 ± 0.005
	313.2	0.176 ± 0.008
	323.8	0.167 ± 0.019
	333.5	0.156 ± 0.018
	343.2	0.166 ± 0.026
[C_4mim][$C(CN)_3$]	293.7	0.171 ± 0.004
	303.4	0.170 ± 0.004
	313.5	0.171 ± 0.006
	323.5	0.168 ± 0.008
	332.9	0.154 ± 0.014
	343.9	0.160 ± 0.020

a Standard uncertainties are $u(T)$ = 0.1 K, $u(p)$ = 1 kPa and the experimental expanded uncertainty $U_c = U_c(\lambda)$ = 0.004 to 0.02 W m-1 K-1 with 0.95 level of confidence (k = 2).

The results obtained for each liquid were fitted to a straight line, according to equation 12 and Table S3 in the Supporting Information shows the coefficients obtained, as well as the root mean square deviations of the fits.

Figure 3 shows the variation of the thermal conductivity of the ionic liquids with temperature, for the range between 293 and 343 K at 0.1 MPa. In the case of [C_2mim][SCN] the variation of the thermal conductivity is linear from the lowest temperature up to 323 K but from that point onwards there is a departure from linearity as the thermal conductivity decreases abruptly with the increase of temperature. Hence, the fit parameters presented in Table S3 illustrate a poor global linearity in the studied temperature range, departing from linearity by up to 6% and with a maximum root mean square deviation of 7.81 mW m^{-1} K^{-1}, between 4 and 5%. For [C_4mim][SCN] no data point departs from linearity by more than ±2.9%, with the decrease of the thermal conductivity being more accentuated at the highest temperatures. The root mean square deviation did not exceed 4.02 mW m^{-1} K^{-1}, about 2.5%. For [C_2mim][$C(CN)_3$], the linear fit is not the best option, since the thermal conductivity is generally decreasing up to 333 K and then increases at 343 K. The last two points depart from linearity in about 4.9%, while before no point departs from linearity by more than 3%. The root mean square deviation did not exceed 6.72 mW m^{-1} K^{-1}, between 3.5 and 4%. Lastly, in the case of [C_4mim][$C(CN)_3$], no data point departs from linearity by more than 2.4%, with the exception of the data point at 333 K, with a divergence of about 4%. The root mean square deviation did not exceed 4.56 mW m^{-1} K^{-1}, about 2.7%. In general, the thermal conductivity of the four ionic liquids tends to decrease with temperature, being more noticeable in the case of [C_2mim][SCN] and less with [C_4mim][$C(CN)_3$].

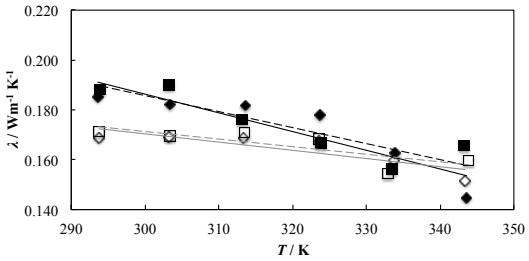

Figure 3. Plot of the thermal conductivity of ionic liquids as a function of temperature. ◆ – [C_2mim][SCN]; ◇ – [C_4mim][SCN]; ■ – [C_2mim][$C(CN)_3$]; □ – [C_4mim][$C(CN)_3$]; — — - trendline for SCN^- based ionic liquids, black C_2mim^+, grey C_4mim^+; -- -- -- - trendline for $C(CN)_3^-$ based ionic liquids, black C_2mim^+, grey C_4mim^+.

The uncertainties of the experimental data were estimated in the same fashion as described in the previous section. The major contribution for the uncertainty originates from the uncertainty of each experimental measurement. The uncertainty obtained fluctuated between 0.004 and 0.017 Wm^{-1}K^{-1} (2.4 to 10.3%) for [C_2mim][SCN], between 0.004 and 0.017 Wm^{-1}K^{-1} (2.4 to 10.9%) for [C_4mim][SCN], between 0.005 and 0.026 Wm^{-1}K^{-1} (2.7 to 15.4%) for [C_2mim][$C(CN)_3$] and

between 0.004 and 0.020 W m^{-1} K^{-1} (2.4 to 12.3%) for $[C_4mim][C(CN)_3]$. The poorest case is represented by $[C_2mim][C(CN)_3]$, which exhibits only three values of thermal conductivity below 11% uncertainty.

In our previous work[13] we observed a similar problem with $[C_2mim][N(CN)_2]$, where the low viscosity of the ionic liquid and the continued decrease of the latter with temperature had a considerable influence on the results. This is an intrinsic feature of the KD2 Pro™, which in turn led to an oscillation of the thermal conductivity value. As it was then, more than 10 measurements were acquired in order to minimize the fluctuation of the value obtained, specifically at the temperatures were this oscillation was observed. However, the results kept on fluctuating in the same fashion, which resulted in an increased uncertainty of the value. The viscosity values of $[C_2mim][N(CN)_2]$ and $[C_2mim][C(CN)_3]$ are similar (the latter being slightly lower) [14, 17] in the considered temperature range. Therefore, this uncertainty was expected. All of the remainder ionic liquids in this study (and the previous one) have higher values of viscosity. With highly viscous ionic liquids, such as $[C_4mim][(CF_3SO_2)_2N]$ and $[C_2mim][C_2H_5SO_4]$,[12] this situation did not occur, where the uncertainty of the thermal conductivity fluctuated between 6 and 7% at a 95% confidence level, greatly influenced by the value of the calibration at the time.

Figure 4 presents a comparison between our results and ones found in the literature to date. From all four ionic liquids, we were not able to find data to compare to only in the case of $[C_4mim][SCN]$. In the case of $[C_2mim][SCN]$ (Figure 4a), the values of Tenney *et al.*[46] were obtained through measurement of the thermal conductivity using a stationary guarded parallel-plate instrument with a relative standard uncertainty of 0.08. Their value at 300 K differs from ours at 303 K by 15%, which may seem considerable but it has an uncertainty of ±9.5%, within the mutual uncertainty of the two data sets. In the case of $[C_2mim][C(CN)_3]$ (Figure 4b), the values of Fröba *et al.* [47] and Koller *et al.*[48] were obtained both by using a stationary guarded parallel-plate instrument, with 3% and 5% of total measurement uncertainty, respectively. While between 293 and 313 K there is an acceptable agreement between authors, our measurements reveal a considerably faster decrease of the thermal conductivity as the temperature increases. In the case of $[C_4mim][C(CN)_3]$ (Figure 4c), the values of Koller *et al.*[48] were obtained in the same conditions as they were for the previously mentioned ionic liquid. There is a satisfactory agreement between values since every data point is within the mutual uncertainty of the data sets. In every case our data has a slightly more accentuated decrease with temperature.

IoNanofluids – Phosphonium cation

In this section, we report and analyze for the first time thermal conductivity data when we could not obtain a stable suspension in the referred conditions. We have had similar situations with other nanomaterials, such as TiO_2 and nano-Ag. However, while in the latter cases the material would deposit almost immediately after the experimental procedure to create the suspension, in the present case it took several hours, having an apparent stability. We started with an IoNanofluid based on $[P_{66614}][N(CN)_2]$ and 0.5 % mass fraction of MWCTNs. The thermal conductivity of the IoNanofluid was measured at temperatures between 293 and 333 K at 0.1 MPa. Table 4 and Figure 5 show the results obtained as well as the percentage of enhancement of the thermal conductivity. This enhancement is estimated based on the thermal conductivity at the correspondent temperature of the base fluid.

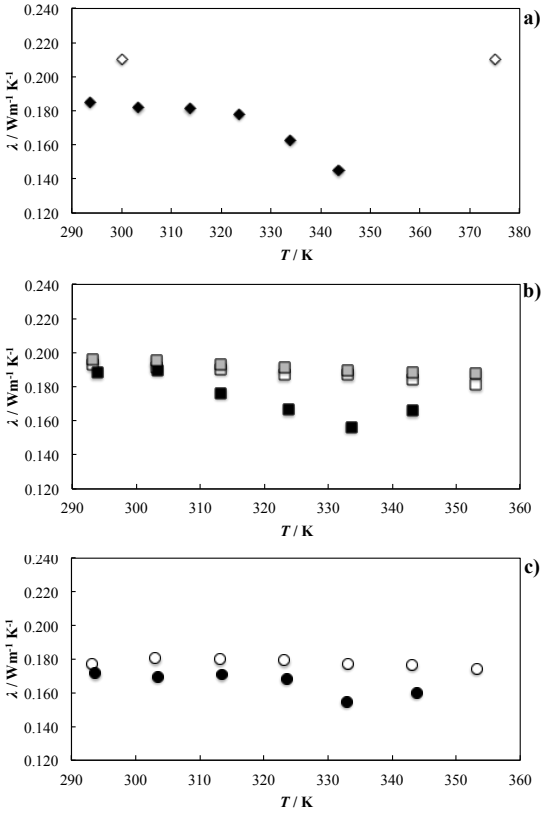

Figure 4. Comparison between the data obtained and those existing in the literature; a) $[C_2mim][SCN]$: ◆ – our work, ◇ - Tenney *et al.*[46]; b) $[C_2mim][C(CN)_3]$: ■ – Our work, □ – Fröba *et al.*[47], ▩ (grey) – Koller *et al.*[48]; c) $[C_4mim][C(CN)_3]$: ● – Our work, ○ - Koller *et al.*[48].

Table 4. Thermal conductivities of IoNanofluids based on the $[P_{66614}]$ cation as a function of temperature at p = 0.1 MPa[a]

Substance	T / K	λ / W m^{-1} K^{-1}	Enhancement / %
$[P_{66614}][N(CN)_2]$ 0.5% w/w MWCNTs	293.7	0.161	-0.66
	313.5	0.161	-0.09
	335.3	0.158	-1.82

a Standard uncertainties are $u(T)$ = 0.1 K, $u(p)$ = 1 kPa, $u(w)$ = 0.0004 and the experimental expanded uncertainty, $U_c = U_c(\lambda)$ = 0.004 – 0.005 W m-1 K-1 with 0.95 level of confidence (k =2).

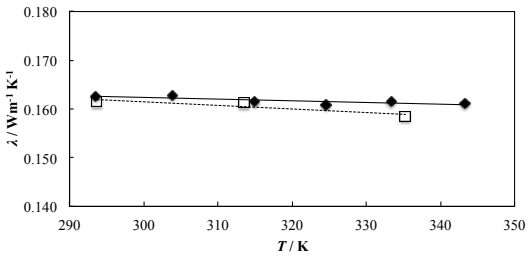

Figure 5. Plot of the thermal conductivity of $[P_{66614}][N(CN)_2]$ and its IoNanofluid (INF) as a function of temperature. ◆ – $[P_{66614}][N(CN)_2]$; □ – INF 0.5% w/w MWCNTs. Lines are given by equation 12 with coefficients shown in Table S3.

Typically, the thermal conductivity of the IoNanofluid is measured at four different temperatures, as it will be seen in the next section. In this case, only three temperatures were measured since deposits of the nanomaterial were observed at the bottom of the vessel during the monitoring of the stability of the suspension. While the enhancement of the thermal conductivity is within the uncertainty of the value, a clear augmentation of the thermal property was to be expected as it was seen with every other stable suspension. There was visual confirmation that some nanomaterial was suspended in the ionic liquid as the KD2 Pro™'s probe was cleaned and the residue had a great amount of black particles and a darker coloration than the ionic liquid itself. The deposits at the bottom of the vessel were too great in number and size to ignore. A few days later, practically all the nanomaterial had been deposited at the bottom of the vessel. Further sonication of the sample was performed, with no success. Taking a different approach, we reduced the starting volume of ionic liquid to make a suspension of the same mass fraction and performed a stability study, in order to confirm how long would the nanomaterial take to deposit at the bottom of the vial. Both phosphonium ionic liquids were used in this study. By the end of the sonication procedure, a great amount of nanomaterial was suspended but the deposits at the bottom were easily visible in both ionic liquids. After a 45 day period, both ionic liquids visually appeared to be "pure" at the top of the vial, more so in the case of $[P_{66614}][N(CN)_2]$ with practically all the MWCNTs deposited at the bottom. Different sonication times, even cooling the vials with ice to cancel the temperature increase originated by the sonication did not provide stable IoNanofluids. Further information on this matter can be found in references 15 and 16. Given this outcome, we did not attempt to measure the thermal conductivity of any other IoNanofluid based on either of these two phosphonium ionic liquids.

There are some ways to analyze this unfeasibility of suspending MWCNTs in phosphonium ionic liquids. From a structural point of view, the density of a liquid can be significant when suspending a nanomaterial. It will be that amount of matter in a certain volume that prevents a low-density nanomaterial such as the MWCNTs to sink to the bottom of the vessel when no surfactants are used, as it is in our case. Usually, ionic liquids present themselves as dense fluids at room temperature. If we consider the density of these ionic liquids, 898 kg m^{-3} for $[P_{66614}][N(CN)_2]$[49] and 955 kg m^{-3} for $[P_{66614}][Br]$[50] at 298 K, two statements can be made: firstly, these values of density are considerably lower than the one of the ionic liquids normally used by our group, being based on aromatic cations with small alkyl chains; secondly, the values of density of these ionic liquids are lower than the density of water, on which is extremely difficult to suspend similar mass fractions of MWCNTs without the use of a surfactant.[51-52] Consequently, although we should expect some affinity between the alkyl chains of the phosphonium cations and the walls of the MWCNTs, it is ultimately proved that density of the base fluid plays a relevant role when it comes to the stability of the nanofluid.[16] As it was mentioned in the introductory section, we believe that the use of surfactants masks the value of the thermal property. Not only would we obtain an increased and inaccurate value of the enhancement gained by the addition of the MWCNTs, the foam originated by the surfactant in a turbulent regime is undesirable for any flowing application.

IoNanofluids – Cyano anions

The thermal conductivities of the IoNanofluids based on $[C_2mim][SCN]$, $[C_4mim][SCN]$, $[C_2mim][C(CN)_3]$ and $[C_4mim][C(CN)_3]$, with 0.5 and 1% mass fraction were measured at temperatures between 293 and 343 K at 0.1 MPa. Tables 5–6 show the results obtained as well as the percentage of enhancement of the thermal conductivity. This enhancement is estimated based on the thermal conductivity at the correspondent temperature of the base fluid for each case.

Figure 6 shows a plot of the thermal conductivity of the IoNanofluids based on $[C_4mim][SCN]$ as a function of temperature. These figures also display the thermal conductivity of the base ionic liquid. Similar plots for the remainder IoNanofluids can be found in Supporting Information in Figures S1-S3.

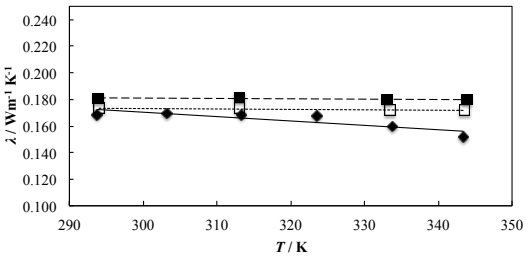

Figure 6. Plot of the thermal conductivity of $[C_4mim][SCN]$ and its IoNanofluids (INF) as a function of temperature. ◆ – $[C_4mim][SCN]$; □ – INF 0.5% w/w MWCNTs; ■ – INF 1% w/w MWCNTs; lines are given by equation 12 with coefficients shown in Table S3.

Table 5. Thermal conductivities of IoNanofluids based on the SCN^- anion as a function of temperature at p = 0.1 MPa[a]

Substance	T / K	λ / W m^{-1} K^{-1}	Enhancement / %
[C_2mim][SCN] 0.5% w/w MWCNTs	293.9	0.188	1.49
	313.2	0.187	2.86
	333.4	0.186	14.2
	343.6	0.185	27.9
[C_2mim][SCN] 1% w/w MWCNTs	293.8	0.194	5.00
	313.3	0.193	6.52
	333.6	0.192	18.0
	343.7	0.191	32.3
[C_4mim][SCN] 0.5% w/w MWCNTs	294.0	0.173	2.52
	313.0	0.173	2.52
	333.5	0.171	7.38
	343.6	0.172	13.4
[C_4mim][SCN] 1% w/w MWCNTs	293.8	0.181	7.13
	313.1	0.181	7.32
	333.1	0.179	12.4
	343.8	0.180	18.7

a Standard uncertainties are $u(T)$ = 0.1 K, $u(p)$ = 1 kPa, $u(w)$ = 0.0004 and the experimental expanded uncertainty, $U_c = U_c(\lambda)$ = 0.004 – 0.005 W m-1 K-1 with 0.95 level of confidence (k =2).

Table 6. Thermal conductivities of IoNanofluids based on the $C(CN)_3^-$ anion as a function of temperature at p = 0.1 MPa[a]

Substance	T / K	λ / W m^{-1} K^{-1}	Enhancement / %
[C_2mim][$C(CN)_3$] 0.5% w/w MWCNTs	293.2	0.187	-0.73
	313.2	0.186	5.77
	333.3	0.181	15.8
	343.1	0.183	10.6
[C_2mim][$C(CN)_3$] 1% w/w MWCNTs	293.5	0.193	2.25
	313.3	0.192	8.86
	333.8	0.189	20.9
	343.8	0.189	13.7
[C_4mim][$C(CN)_3$] 0.5% w/w MWCNTs	293.7	0.176	2.83
	312.9	0.174	2.16
	333.7	0.173	12.1
	343.9	0.173	8.38
[C_4mim][$C(CN)_3$] 1% w/w MWCNTs	293.8	0.181	5.60
	313.3	0.180	5.31
	334.0	0.178	15.3
	343.7	0.178	11.2

a Standard uncertainties are $u(T)$ = 0.1 K, $u(p)$ = 1 kPa, $u(w)$ = 0.0004 and the experimental expanded uncertainty, $U_c = U_c(\lambda)$ = 0.004 – 0.005 W m-1 K-1 with 0.95 level of confidence (k =2).

The uncertainty of the values of thermal conductivity of the IoNanofluids fluctuated between 2.3 and 2.5%. The situation of these suspensions is clearly different than the one stated for ionic liquids since the viscosity is considerably greater due to the addition of MWCNTs. As expected, the dispersion of data obtained at each temperature was almost negligible and the uncertainty values are almost entirely dictated by the calibration.

The increase in the thermal conductivity of the base ionic liquid is easily observed, as is the stabilization of the thermal property, i.e., the decrease in thermal conductivity as a function of temperature is distinctively smaller due to the addition of MWCNTs. As it was mentioned before,[13] from an application perspective, such feature could be significant if the process in question would require a heat transfer fluid that can be used in a range of temperature without compromising its efficiency. Additionally, and as expected, the enhancement of the thermal conductivity is directly proportional to the mass fraction of the nanomaterial. Although the largest enhancement was verified for the IoNanofluids based on [C_2mim][SCN], with percentages of enhancement that go over 32 %, the lack of data in the literature to compare our ionic liquid results (essential to estimate the enhancement) and the unusual slope relative to the decrease of the thermal property at higher temperatures suggests some caution on the magnitude of this enhancement. This particular subject requires further investigation.

If we consider the IoNanofluids based on the ionic liquids that were closer in agreement with literature, namely [C_2mim][$C(CN)_3$] and [C_4mim][$C(CN)_3$], the enhancement of the thermal conductivity reached values such as 20.92 % and 15.32 % with 1% w/w MWCNTs, respectively. In the case of [C_4mim][SCN], which no data was found to compare our results with, the enhancement went as high as 18.74% with 1% MWCNTs.

Figures 7 and 8 show the plot of the enhancement, ($\lambda_{INF}/\lambda_{IL}$-1), where λ_{INF} is the thermal conductivity of the IoNanofluid and λ_{IL} the thermal conductivity of the base ionic liquid, as a function of temperature. Figure 9 illustrates a comparison of the enhancement between INFs based on the cyano-based anions studied by our group so far. While the thermal conductivity of C_2mim^+ based ionic liquids and IoNanofluids is generally higher than the corresponding C_4mim^+ based fluids (considering the same nanomaterial, mass fraction and T), only $N(CN)_2^-$ nanofluids have a reverse order in enhancement, with SCN^- and $C(CN)_3^-$ IoNanofluids's enhancement having the same order regarding the cation. Particularly for the C_2mim^+ based IoNanofluids, the thermal conductivity has always the order $N(CN)_2^- < C(CN)_3^- < SCN^-$, independently of the mass fraction of MWCNTs. Additionally, the enhancement is directly proportional to the number of cyano groups of the anion only in just 30% of the presented cases considering both mass fractions, and the enhancement variation with temperature is considerably different on each case. All of these factors might hinder the conception of a unified model that can predict the enhancement of the thermal conductivity of the presented IoNanofluids.

From molecular interaction information,[39] the ordering of the C_4mim^+ cyano ionic liquids is similar when near the surface of single-walled carbon nanotube or a stack of graphene, which allows to consider that the structure of the ionic liquids

will also be similar if near a MWCNT. In the present study there are several MWCNTs suspended in the ionic liquid, which may imply a structural perturbation in the vicinity of each MWCNT. However, the anion is closer to the outer wall of the nanotube and the cations' alkyl chains directed to the bulk liquid in all cyano ionic liquids studied, independently of the diameter of the nanotube and number of stacked carbon surfaces. In this way, the structure of cyano IoNanofluids with MWCNTs ought to be composed by nonpolar domains preferentially formed by the ionic liquids' side chain ($C_n$mim with $n \geq 4$)[53] further from the nanotube wall, giving rise to a more organized structure when compared with the ionic liquid. The nonpolar domains are less noticeable in C_2mim^+ ionic liquids but the first structured layers near a carbon surface should be similar to C_4mim^+ based ionic liquids, given the greater interaction between the surface and the anion. The main difference should be the extent of that structure, due to the smaller alkyl chains. From another point of view, while C_4mim^+ ionic liquids have a more defined structure, they also exhibit lower values of thermal conductivity when compared to C_2mim^+ ionic liquids. As mentioned in reference 40, phonon scattering is responsible for the decrease in thermal conductivity values, where an acoustic mismatch between the nanotubes and the liquid phase originates that scattering. Therefore, an organized structure is not the only relevant factor and there is possibly a smaller discrepancy between vibrational frequencies concerning C_2mim^+ ionic liquids and MWCNTs, leading to an increase in phonon-phonon coupling. This fact requires further investigation.

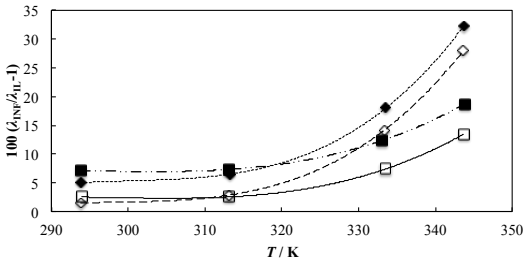

Figure 7. Plot of thermal conductivity enhancement of INFs based on the SCN^- anion as a function of temperature. Open symbols – 0.5% w/w INFs; Full symbols – 1% w/w INFs; ◇, ◆ – [C_2mim][SCN]; □, ■ – [C_4mim][SCN].

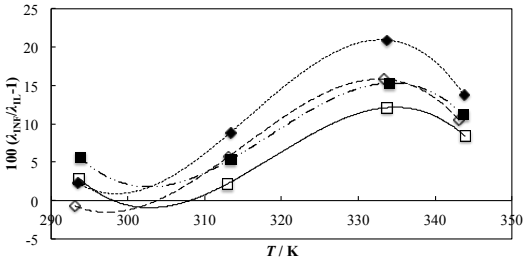

Figure 8. Plot of thermal conductivity enhancement of INFs based on the $C(CN)_3^-$ anion as a function of temperature. Open symbols – 0.5% w/w INFs; Full symbols – 1% w/w INFs; ◇, ◆ – [C_2mim][$C(CN)_3$]; □, ■ – [C_4mim][$C(CN)_3$].

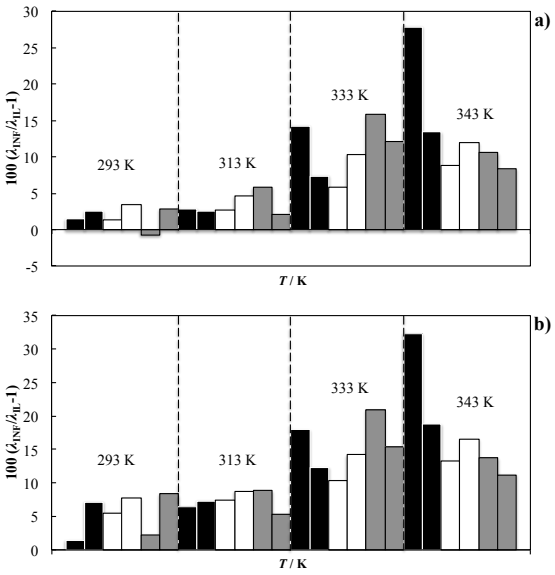

Figure 9. Plot of thermal conductivity enhancement of INFs as a function of temperature. The order at each temperature is as follows (crescent number of cyano groups): [C_2mim][SCN] and [C_4mim][SCN] - ■, [C_2mim][$N(CN)_2$][13] and [C_4mim][$N(CN)_2$][13] - □, [C_2mim][$C(CN)_3$] and [C_4mim][$C(CN)_3$] - ▩. a) 0.5 w/w MWCNTs INFs; b) 1% w/w MWCNTs INFs.

In order to evaluate the heat transfer mechanisms and feasibility of these existing models, the predictions by the classical HC model and recent MLY model are analyzed and compared with the experimental results of the reported IoNanofluids as presented in Figure 10. The calculations were performed using an interfacial layer value of 0.9 nm, according to the structural information recently obtained.[39] This demonstrates that although MLY model with fixed value of nanolayer thickness and adjusted values of nanolayer thermal conductivity (depending on the MWCNT concentration and ionic liquid type the values of ω were between 1.5 to 5) yields reasonable re-

sults,[12] the HC model severely under-predicts the thermal conductivity of these IoNanofluids. It is noted that the thermal conductivity of a single MWCNT was measured using a microfabricated suspended device and found to be 3000 $Wm^{-1}K^{-1}$ [54], and this value was assumed for the calculations. The measured thermal conductivity of base ionic liquids at room temperature was used to predict the thermal conductivity of these ionanofluids. Calculations performed for a higher layer thickness (~2nm) yield similar results. We consider that the interfacial nanolayer plays a key role in the thermal conductivity of IoNanofluids. The magnitude of influence of this factor, as well as any other mechanisms for these new fluids, cannot be fully explored by these existing models. Thus, it is of great importance to study and understand both interfacial layer and interaction of ionic liquids with the nanoparticles, particularly with further contribution of the interface ions/nanoparticles by molecular dynamic simulations.

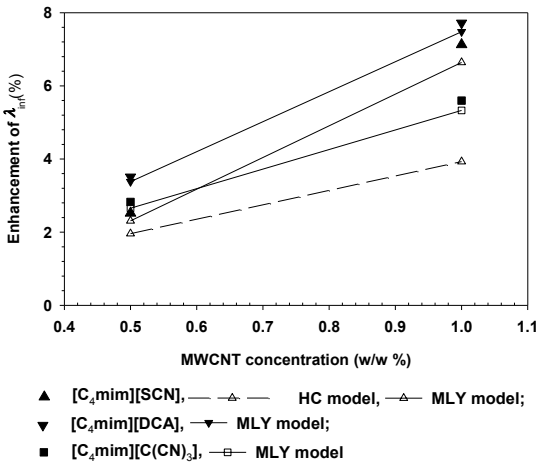

Figure 10. Comparison of measured and predicted thermal conductivity enhancement of ionanofluids as a function of MWCNT concentration.

Heat Transfer Area – HTFs & ILs

Data of the thermophysical properties for the heat transfer fluids were obtained from the product information brochure available online and/or requested to the supplier and are presented in Table S4 in the Supporting Information. The heat transfer area values were calculated according to the above-mentioned methodology and are depicted in Figure 11.

Figure 11 shows a considerable range in heat transfer area values for commercial fluids. If we consider the depiction of Globalterm Syntech as an outlier, heat transfer areas for the specific operational values used decrease between 14% (Dowtherm J) and 57% (Dowtherm RP) with temperature. A considerable decrease in area indicates that the heat transfer unit is limited to be used for a single temperature for most of the presented fluids. If used otherwise, its operation may not be as effective.[7]

To compare the commercial HTFs with ionic liquids we designated an interval between the commercial fluid with lowest and highest area values, Dowtherm J and Dowtherm T, respectively. Ionic liquids' thermophysical data was obtained from the literature. Table S5 in the Supporting Information shows the thermophysical properties and heat transfer area for ionic liquids, with the latter being represented in Figure 12 for the dicyanamide ($N(CN)_2^-$) ionic liquids.

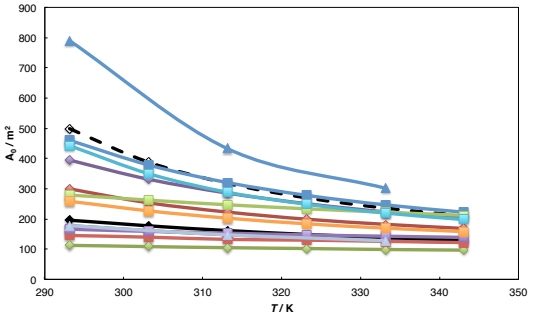

Figure 11 – Heat transfer area for commercial fluids as a function of temperature. ◆ (blue) – Dowtherm A; ◆ (red) – Dowtherm G; ◆ (green) – Dowtherm J; ◆ (purple) – Dowtherm MX; ◆ (black) – Dowtherm Q; ◇ – Dowtherm RP; ■ (blue) – Dowtherm T; ■ (red) – Sylthern XLT; ■ (green) – Sylthern 800; ■ (purple) – Sylthern HF; ■ (light blue) – Paratherm HR; ■ (orange) – Paratherm MR; ▲ (grey) – Globaltherm Omnitech; ▲ (blue) – Globaltherm Syntech.

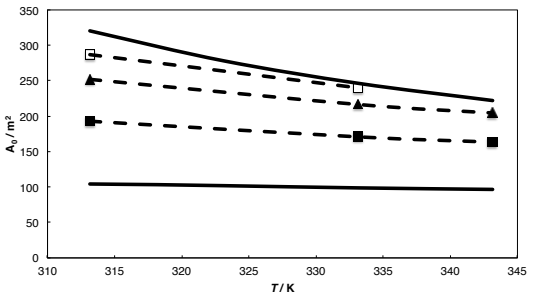

Figure 12 – Heat transfer area for $N(CN)_2^-$ based ionic liquids. Solid lines represent lowest (Dowtherm J) and highest (Dowtherm T) values obtained for commercial HTFs. ■ – $[C_2mim][N(CN)_2]$; ▲ – $[C_4mim][N(CN)_2]$; □ – $[C_4mpyr][N(CN)_2]$.

Heat transfer area for ionic liquids is only presented at 313, 333 and 343 K in order to simplify the comparison with IoNanofluids in the next sections. Plots for the remainder ionic

liquids are presented in Figure S4 and S5 in the Supplementary Information. Figure 12 shows that dicyanamide ionic liquids can offer heat transfer areas within the range of commercial fluids, with $[C_2mim][N(CN)_2]$ having the lowest area values. The decrease in area with temperature is around 7% for ionic liquids and Dowtherm J in the represented temperature range, while the area drops around 30% for Dowtherm T. Values for $[C_4mpyr][N(CN)_2]$ were not calculated at 343 K due to the lack of heat capacity data at that temperature.

Other ionic liquids such as $[C_2mim][SCN]$ and $[C_2mim][C(CN)_3]$ (Figures S4-S5) offer slightly higher heat transfer areas, decreasing with temperature around 14% and 20%, respectively. The areas calculated for $[C_4mim][SCN]$, $[C_2mim][C_2H_5SO_4]$ and $[C_4mim][(CF_3SO_2)_2N]$ are just above the upper limit of the considered interval, while the values of $[P_{66614}][N(CN)_2]$ are clearly apart far from the remainder fluids. This is due to the considerable values of viscosity of the latter, yielding a sluggish flow and, consequently, a need for a greater area to transfer the same amount of heat.

From the ionic liquids considered, we obtained favorable results with cyano ionic liquids based on the C_2mim^+ cation. The thermophysical properties of these ionic liquids are in favor of a lower heat transfer area when compared with their C_4mim^+ counterparts, with the former having higher thermal conductivity, density and heat capacity and lower viscosity. The only exception lies in $[C_4mim][N(CN)_2]$, with a heat transfer area lower than the upper limit of the area interval.

Heat Transfer Area –HTFs & INFs

The data available on IoNanofluids' thermophysical data is scarce. Apart from thermal conductivity, there is only density[13] and viscosity[14] data for dicyanamide-based IoNanofluids available on the literature. Nevertheless, we consider these to be sufficient to extrapolate for the remainder ionic liquids.

The impact of the addition of MWCNTs on the base fluid's density is minimal due to the large difference in density between ionic liquids and nanomaterial. The density increases around 0.25% for 0.5% w/w MWCNTs and around 0.5% for 1% w/w MWCNTs, with no particular distinction between ionic liquids. For viscosity, the enhancement is much greater and with a distinction between different cations. However, recent work in molecular dynamics showed that the structure of C_4mim^+ cyano-based anions, namely SCN^-, $N(CN)_2^-$ and $C(CN)_3^-$, is very similar when close to a carbon surface.[39] In this sense and assuming that similar mass fractions would have an analogous impact on the base fluid's viscosity, we calculated the viscosity and density of the remainder IoNanofluids based on the enhancement of the dicyanamide IoNanofluids. These calculations were performed considering the same cation. The enhancement values for viscosity and density are presented in Table 7.

Table 7 – Enhancement (%) of density and viscosity of dicyanamide IoNanofluids[13-14]

Fluid	T/K	ρ		η	
		0.5% w/w	1% w/w	0.5% w/w	1% w/w
$[C_2mim][N(CN)_2]$	313.15	0.26	0.45	77.5	137.4
	333.15	0.27	0.43	111.1	188.0
	343.15	0.23	0.40	143.4	221.6
$[C_4mim][N(CN)_2]$	313.15	0.32	0.65	80.7	159.5
	333.15	0.22	0.42	147.4	225.2
	343.15	0.20	0.33	180.9	245.3
$[C_4mpyr][N(CN)_2]$	313.15	0.23	0.60	27.8	101.4
	333.15	0.22	0.59	70.7	155.3
	343.15	0.23	0.61	94.8	182.7

Lastly, there was no available heat capacity data on the literature for the IoNanofluids considered. Other authors have studied the heat capacity of nanofluids based on ionic liquids and MWCNTs. Nanofluids based on $[C_4mim][BF_4]$[55] and $[hmim][BF_4]$[56] revealed lower heat capacities when compared to the ionic liquid (approximately -6.5% and -1%, respectively) while the heat capacity of $[C_4mim][PF_6]$[8] was enhanced up to 8% due to the addition of MWCNTs. The methodology and amount of nanomaterial differs significantly between these studies. We used the ionic liquids heat capacity value to calculate the heat transfer area, followed by a variation of the former up to +30% due to the presence of the MWCNTs in the suspension.

The heat transfer areas for the dicyanamide based IoNanofluids, using the C_P value of the ionic liquid, are presented in Figure 13.

Similar plots for IoNanofluids based on $[C_2mim][SCN]$, $[C_4mim][SCN]$ and $[C_2mim][C(CN)_3]$ can be found on Figures S6 and S7 in the Supplementary Information. As it would be expected due to the great increase in viscosity, the heat transfer area increases while the variation with temperature is softer in every case. Heat transfer areas of IoNanofluids based on $[C_2mim][C_2H_5SO_4]$ and $[C_4mim][(CF_3SO_2)_2N]$ are not represented in the plots since the areas calculated based on these ionic liquids were considerably outside the considered area interval.

In IoNanofluids with 0.5% w/w of MWCNTs, the increase in heat transfer area relatively to that of ionic liquid ranges from 25% to 44% in general, with the exception of $[C_4mpyr][N(CN)_2]$ (see Table S8 in Supporting Information). However, the area of the former is outside the considered area interval and only INFs based on $[C_2mim][N(CN)_2]$ and $[C_2mim][C(CN)_3]$ provide heat transfer areas fully within the interval. Heat transfer areas of INFs based on $[C_4mim][N(CN)_2]$, $[C_4mpyr][N(CN)_2]$ and $[C_4mim][SCN]$ are only below the upper limit at the 293K. A similar analysis can be made for INFs with 1% w/w MWCNTs, were the increase in heat transfer area is expectedly higher relatively to the corresponding ionic liquid. The heat transfer areas increase up to 54%. Heat transfer areas of INFs based on $[C_2mim][N(CN)_2]$

and $[C_2mim][C(CN)_3]$ are the closest to upper limit of the interval, only surpassing it at 343K.

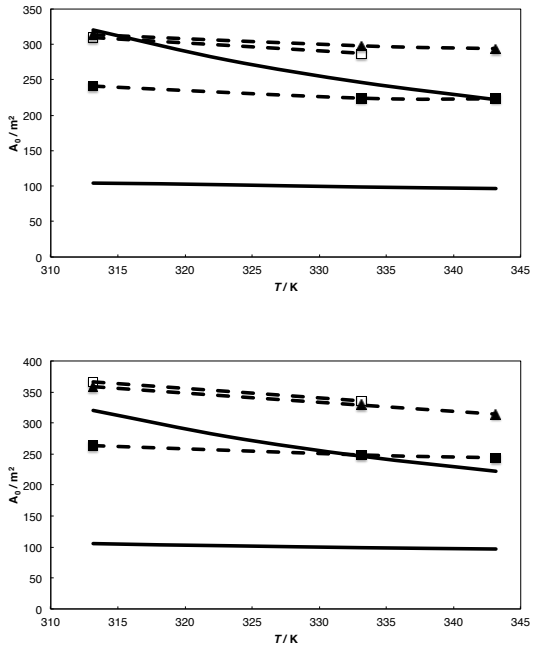

Figure 13 – Heat transfer area for $N(CN)_2^-$ based IoNanofluids considering C_P of the base ionic liquid. Top: 0.5% w/w MWCNTs; Bottom: 1% w/w MWCNTs. Solid lines represent lowest (Dowtherm J) and highest (Dowtherm T) values obtained for commercial HTFs. ■ – $[C_2mim][N(CN)_2]$; ▲ – $[C_4mim][N(CN)_2]$; □ – $[C_4mpyr][N(CN)_2]$.

Figure 14 presents a 3D plot of the heat transfer area obtained for IoNanofluids based on $[C_2mim][N(CN)_2]$ with a variation up to +30% of the heat capacity. Plots for INFs based on $[C_4mim][N(CN)_2]$, $[C_4mpyr][N(CN)_2]$, $[C_2mim][SCN]$, $[C_4mim][SCN]$ and $[C_2mim][C(CN)_3]$ can be found in Figures S8-S12 in the Supporting Information.

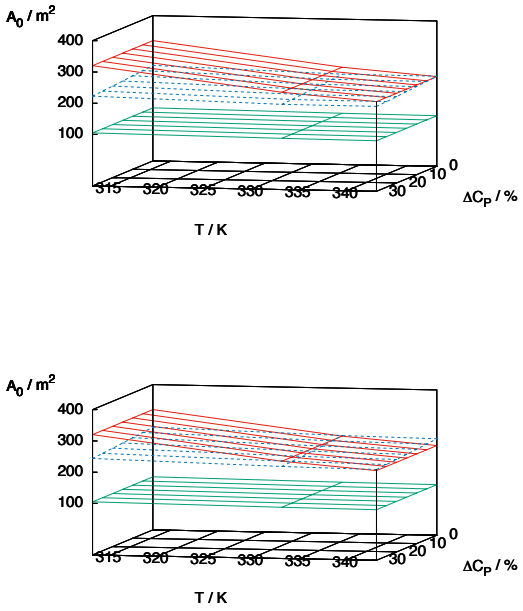

Figure 14 – Heat transfer area for $[C_2mim][N(CN)_2]$ based IoNanofluids considering a variation up to +30% of C_P of the base ionic liquid. Top: 0.5% w/w MWCNTs; Bottom: 1% w/w MWCNTs. Solid lines represent lowest (Dowtherm J) and highest (Dowtherm T) values obtained for commercial HTFs.

Given the methodology used, we know that a variation in C_P of the INF up to +30% translates into a maximum decrease of the area between -7 and -8%. For IoNanofluids with 0.5% w/w of MWCNTs, only $[C_2mim][N(CN)_2]$ and $[C_2mim][C(CN)_3]$ are always below the upper limit of the area interval in the considered temperature range, as expected. As C_P increases, the remainder IoNanofluids cross that threshold at a certain point, with exception of $[C_4mim][SCN]$. On the other hand, IoNanofluids with 1% w/w MWCNTs need a heat transfer area that surpasses in general the upper limit of the interval. $[C_2mim][N(CN)_2]$ and $[C_2mim][C(CN)_3]$ based IoNanofluids remain within the target area values except when the temperature is close to limit of the interval.

A straightforward benefit of adding MWCNTs to the studied ionic liquids consists on the smaller variation of the heat transfer area with temperature. While the areas calculated for HTFs and ionic liquids decrease from -10 to -43% in the considered temperature range, INFs show a decrease that ranges from -7 to -26%. This feature is important when considering heat transfer fluids for multiple processes and/or considering different temperature ranges. The enhancement of thermal conductivity is also an advantage but it can be limited by the corresponding increase in viscosity. The addition of small amounts of water could help to limit the latter given it decreases the viscosity of the base fluid.[57-61] However, it might

compromise the stability of the nanofluid and, if the amount of water is too high, it can weaken the enhancement of the thermal conductivity.[12] Further thermophysical data of different ionic liquids and INFs is necessary in order to allow the possibility of overcoming these limitations.

From an economic standpoint, a smaller area yields a lower cost in the design of the heat transfer unit.[7] Although the superior price of ionic liquids represents an obstacle, some of the ionic liquids and INFs here presented need smaller heat transfer areas than the commercial HTFs for the same purpose.

CONCLUSIONS

The thermal conductivity of $[P_{66614}][N(CN)_2]$, $[P_{66614}][Br]$, $[C_2mim][SCN]$, $[C_4mim][SCN]$, $[C_2mim][C(CN)_3]$ and $[C_4mim][C(CN)_3]$ ionic liquids and their IoNanofluids with multi-walled carbon nanotubes (Baytubes C150 HP were studied at temperatures between 293 and 343 K, at 0.1 MPa. The results obtained for cyano-based ionic liquids show that there are significant enhancements of the thermal conductivity caused by the suspension of this nanomaterial in the base liquid, as we observed in our previous work. The same was not verified for phosphonium based INFs, where the methodology used could not provide a stable suspension of the MWCNTs.

After comparison with our previous work, we concluded that the thermal conductivity of C_2mim^+ based ionic liquids and IoNanofluids is generally higher than the corresponding C_4mim^+ based fluids. However, there is no clear relation between base ionic liquids regarding the enhancement of the thermal conductivity and the latter is independent of the number of cyano groups in the anion. Current models cannot yet accurately predict the enhancement obtained by the addition of MWCNTs, although some information on the structure between ionic liquids and carbon materials is available. The variety of morphologies, length values and number of layers of this nanomaterial and their influence on the thermal conductivity of INFs require further investigation.

Heat transfer areas for a specific process were calculated for some of the ionic liquids and INFs studied so far by our group and then compared to the areas calculated for currently commercialized heat transfer fluids. The interval represented by the latter was considered as a target area. C_2mim^+ and cyano based ionic liquids/INFs yield smaller area values due to their lower viscosity. Although the addition of MWCNTs to the ionic liquids leads to an increase in the area necessary to transfer the same amount of heat, a 0.5% w/w MWCNTs suspension has the advantage of enhancing the thermophysical properties and provide a smaller variation of the area with temperature. A 1% w/w MWCNTs suspension leads to an even higher enhancement of the thermophysical properties but it also leads to heat transfer areas that surpass the target interval in a considerable range of temperature. It all comes down to the requirements of the process in question in terms of heat transfer capabilities (area, unit cost, fluid cost) when choosing a heat transfer fluid for the task.

ASSOCIATED CONTENT

Supporting Information

The Supporting Information is available free of charge on the ACS Publications website.

Supporting information includes Ionic liquids and MWCNTs specifications, coefficients of the fitting of the experimental data, plots of thermal conductivity, thermophysical data and heat transfer area values of heat transfer fluids, ionic liquids and IoNanofluids, as well as plots of heat transfer area for the above mentioned substances. (PDF)

AUTHOR INFORMATION

Corresponding Author

* Carlos Nieto de Castro, cacastro@ciencias.ulisboa.pt

Author Contributions

The manuscript was written through contributions of all authors. / All authors have given approval to the final version of the manuscript. / # This author contributed with 80% of the work related here. All the other authors contributed equally with 5%.

Funding Sources

This work was partially funded by Fundação para a Ciência e Tecnologia, Portugal, through projects SFRH/BPD/102518/2014, PTDC/EQU-FTT/104614/2008, PEST-OE/QUI/UI0536/2011-2014, and UID/QUI/00100/2013 and PhD research grant SFRH/BD/79378/2011.

Notes

Thermophysical data of Dow Chemical Company heat transfer fluids was retrieved from their product brochure available online. Thermophysical data of Paratherm™ heat transfer fluids was retrieved from their website (http://www.paratherm.com). Any additional relevant notes should be placed here.

ACKNOWLEDGMENT

The authors would like to thank Global Oil Company for providing thermophysical data of their heat transfer fluids (Globaltherm®). J.M.P. França would like to thank thank Fundação Para a Ciência e Tecnologia, Portugal, for his PhD Grant SFRH/BD/79378/2011. The authors would like to thank IoLiTec for providing the samples of cyano ionic liquids.

REFERENCES

1. Wasserscheid, P.; Welton, T., Ionic Liquids in Synthesis. In *Ionic Liquids in Synthesis*, 2nd ed.; Wasserscheid, P.; Welton, T., Eds. Wiley-VCH: **2008**; pp 1-740.
2. Pârvulescu, V. I.; Hardacre, C., Catalysis in Ionic Liquids. *Chemical Reviews* **2007,** *107* (6), 2615-2665.
3. Rao, C. N. R.; Müller, A.; Cheetham, A. K.; (Eds), *The Chemistry of Nanomaterials: Synthesis, Properties and Applications*. WILEY-VCH Verlag GmbH & Co. KGaA: Weinheim, **2004**.
4. Choi, S. U. S.; Zhang, Z. G.; Yu, W.; Lockwood, F. E.; Grulke, E. A., Anomalous thermal conductivity enhancement in nanotube suspensions. *Applied Physics Letters* **2001,** *79* (14), 2252-2254.
5. Nieto de Castro, C. A.; Ribeiro, A. P. C.; Vieira, S. I. C.; França, J. M. P.; Lourenço, M. J. V.; Santos, F. V.; Murshed, S. S. M.; Goodrich, P.; Hardacre, C., Synthesis, Properties and Physical Applications of IoNanofluids. In *Ionic Liquids - New Aspects for the Future*, Kadokawa, J.-i., Ed. Intech: **2013**; pp 165-193.
6. Sayes, C. M.; Warheit, D. B., Characterization of nanomaterials for toxicity assessment. *WIREs Nanomed. Nanobiotechnol* **2009,** *1* (6), 660-670.
7. França, J. M. P.; Nieto de Castro, C. A.; Lopes, M. M.; Nunes, V. M. B., Influence of Thermophysical Properties of Ionic Liquids in Chemical Process Design. *Journal of Chemical & Engineering Data* **2009,** *54* (9), 2569-2575.
8. Nieto de Castro, C. A.; Lourenço, M. J. V.; Ribeiro, A. P. C.; Langa, E.; Vieira, S. I. C.; Goodrich, P.; Hardacre, C., Thermal Properties of Ionic Liquids and IoNanofluids of Imidazolium and Pyrrolidinium Liquids. *Journal of Chemical & Engineering Data* **2010,** *55* (2), 653-661.
9. Ribeiro, A. P. C.; Vieira, S. I. C.; Goodrich, P.; Hardacre, C.; Lourenço, M. J. V.; Nieto de Castro, C. A., Thermal Conductivity of [Cnmim][(CF3SO2)2N] and [C4mim][BF4] IoNanofluids with Carbon Nanotubes—Measurement, Theory and Structural Characterization. *Journal of Nanofluids* **2013,** *2* (1), 55-62.
10. Nieto de Castro, C. A.; Murshed, S. M. S.; Lourenço, M. J. V.; Santos, F. J. V.; Lopes, M. L. M.; França, J. M. P., Ionanofluids: New Heat Transfer Fluids for Green Processes Development. In *Green Solvents I: Properties and Applications in Chemistry*, Mohammad, A.; Dr., I., Eds. Springer Netherlands: **2012**.
11. Nieto de Castro, C. A.; Murshed, S. M. S.; Lourenço, M. J. V.; Santos, F. J. V.; Lopes, M. L. M.; França, J. M. P., Enhanced thermal conductivity and specific heat capacity of carbon nanotubes ionanofluids. *International Journal of Thermal Sciences* **2012,** *62*, 34-39.
12. França, J. M. P.; Vieira, S. I. C.; Lourenço, M. J. V.; Murshed, S. M. S.; Nieto de Castro, C. A., Thermal Conductivity of [C4mim][(CF3SO2)2N] and [C2mim][EtSO4] and Their IoNanofluids with Carbon Nanotubes: Experiment and Theory. *Journal of Chemical & Engineering Data* **2013,** *58* (2), 467-476.
13. França, J. M. P.; Reis, F.; Vieira, S. I. C.; Lourenço, M. J. V.; Santos, F. J. V.; Nieto de Castro, C. A.; Pádua, A. A. H., Thermophysical properties of ionic liquid dicyanamide (DCA) nanosystems. *The Journal of Chemical Thermodynamics* **2014,** *79*, 248-257.
14. Reis, F.; França, J. M. P.; Santos, F. J. V.; Murshed, S. M. S.; Lourenço, M. J. V.; Castro, C. A. N. d., Thermophysical Properties of DCA Ionanofluids. In *COIL-5/3IMIL, Congress on Ionic Liquids*, Vilamoura, Portugal, **2013**.
15. Lourenço, M. J.; Vieira, S. I., Nanofluids Preparation Methodology. In *Nanofluids: Synthesis, Properties and Applications*, Sohel Murshed, S. M.; Nieto de Castro, C. A., Eds. NOVA Science Publishers, Inc.: New York, **2014**; pp 1-28.
16. Castro, C. N. d.; Paredes, X.; Vieira, S.; Murshed, S.; Lourenço, M. J.; Santos, F., IoNanofluids: Innovative Agents for Sustainable Development. In *Nanotechnology for Energy Sustainability*, Raj, B.; Voorde, M. V. d.; Mahajan, Y., Eds. WILEY-VCH Verlag GmbH & Co. KGaA: Weinheim, **2017**; Vol. 3.
17. Neves, C. M. S. S.; Kurnia, K. A.; Coutinho, J. A. P.; Marrucho, I. M.; Lopes, J. N. C.; Freire, M. G.; Rebelo, L. P. N., Systematic Study of the Thermophysical Properties of Imidazolium-Based Ionic Liquids with Cyano-Functionalized Anions. *The Journal of Physical Chemistry B* **2013,** *117* (35), 10271-10283.
18. Stolte, S.; Matzke, M.; Arning, J., (Eco)Toxicology and Biodegradation of Ionic Liquids. In *Ionic Liquids Completely UnCOILed: Critical Expert Overviews*, Plechkova, N. V.; Seddon, K. R., Eds. John Wiley & Sons, Inc: Hoboken, NJ., **2015**.
19. Viboud, S.; Papaiconomou, N.; Cortesi, A.; Chatel, G.; Draye, M.; Fontvieille, D., Correlating the structure and composition of ionic liquids with their toxicity on Vibrio fischeri: A systematic study. *Journal of Hazardous Materials* **2012,** *215-216*, 40-48.
20. Ferreira, A. F.; Simões, P. N.; Ferreira, A. G. M., Quaternary phosphonium-based ionic liquids: Thermal stability and heat capacity of the liquid phase. *The Journal of Chemical Thermodynamics* **2011,** *45* (1), 16-27.
21. Navarro, P.; Larriba, M.; Rojo, E.; García, J.; Rodríguez, F., Thermal Properties of Cyano-Based Ionic Liquids. *Journal of Chemical & Engineering Data* **2013,** *58* (8), 2187-2193.
22. Nieto de Castro, C. A.; Langa, E.; Morais, A. L.; Lopes, M. L. M.; Lourenço, M. J. V.; Santos, F. J. V.; Santos, M. S. C. S.; Lopes, J. N. C.; Veiga, H. I. M.; Macatrão, M.; Esperança, J. M. S. S.; Marques, C. S.; Rebelo, L. P. N.; Afonso, C. A. M., Studies on the density, heat capacity, surface tension and infinite dilution diffusion with the ionic liquids [C4mim][NTf2], [C4mim][dca], [C2mim][EtOSO3] and [Aliquat][dca]. *Fluid Phase Equilibria* **2010,** *294* (1–2), 157-179.
23. Ge, R.; Hardacre, C.; Nancarrow, P.; Rooney, D. W., Thermal Conductivities of Ionic Liquids over the Temperature Range from 293 K to 353 K. *Journal of Chemical & Engineering Data* **2007,** *52* (5), 1819-1823.
24. Carslaw, H. S.; Jaeger, J. C., *Conduction of Heat in Solids*. Oxford University Press: London, 1959.
25. Kluitenberg, G. J.; Ham, J. M.; Bristow, K. L., Error Analysis of the Heat Pulse Method for Measuring Soil Volumetric Heat Capacity. *Soil Science Society of America Journal* **1993,** *57*, 1444-1451.
26. Murshed, S. M. S.; Nieto de Castro, C. A.; Lourenço, M. J. V., Effect of Surfactant and Nanoparticle Clustering on Thermal Conductivity of Aqueous Nanofluids. *Journal of Nanofluids* **2012,** *1* (2), 175-179.
27. Castro, C. A. N. d.; Lourenço, M. J. V.; Murshed, S. M. S., Understanding Stability, Measurements, and Mechanisms of Thermal Conductivity of Nanofluids. *J. Nanofluids* **2017,** (6), 804-811.
28. Murshed, S. M. S.; Nieto de Castro, C. A., *Nanofluids: Synthesis, Properties and Applications*. NOVA Science Publishers, Inc.: New York, **2014**.
29. Murshed, S. M. S.; Leong, K. C.; Yang, C., Thermophysical and electrokinetic properties of nanofluids – A critical review. *Applied Thermal Engineering* **2008,** *28* (17–18), 2109-2125.
30. Angayarkanni, S. A.; Philip, J., Review on thermal properties of nanofluids: Recent developments. *Advances in Colloid and Interface Science* **2015,** *225*, 146-176.
31. Maxwell, J. C., *A Treatise on Electricity and Magnetism*. Clarendon Press: Oxford, UK, **1891**.

32. Hamilton, R. L.; Crosser, O. K., Thermal Conductivity of Heterogeneous Two-Component Systems. *Industrial & Engineering Chemistry Fundamentals* **1962,** *1* (3), 187-191.

33. Murshed, S. M. S.; Nieto de Castro, C. A., Superior thermal features of carbon nanotubes-based nanofluids – A review. *Renewable and Sustainable Energy Reviews* **2014,** *37*, 155-167.

34. Murshed, S. M. S.; Leong, K. C.; Yang, C., A combined model for the effective thermal conductivity of nanofluids. *Applied Thermal Engineering* **2009,** *29* (11–12), 2477-2483.

35. Murshed, S. M. S., Correction and comment on "thermal conductance of nanofluids: is the controversy over?". *Journal of Nanoparticle Research* **2009,** *11*, 511-512.

36. Keblinski, P.; Phillpot, S. R.; Choi, S. U. S.; Eastman, J. A., Mechanisms of heat flow in suspensions of nano-sized particles (nanofluids). *International Journal of Heat and Mass Transfer* **2002,** *45* (4), 855-863.

37. Xie, H.; Fujii, M.; Zhang, X., Effect of interfacial nanolayer on the effective thermal conductivity of nanoparticle-fluid mixture. *International Journal of Heat and Mass Transfer* **2005,** *48* (14), 2926-2932.

38. Murshed, S. M. S.; Leong, K. C.; Yang, C., Investigations of thermal conductivity and viscosity of nanofluids. *International Journal of Thermal Sciences* **2008,** *47* (5), 560-568.

39. França, J. M. P.; Nieto de Castro, C. A.; Pádua, A. A. H., Molecular Interactions and Thermal Transport in Ionic Liquids with Carbon Nanomaterials. *Physical Chemistry Chemical Physics* **2017,** *19*, 17075 - 17087.

40. Nunes, V. M. B.; Lourenço, M. J. V.; Santos, F. J. V.; Nieto de Castro, C. A., Importance of Accurate Data on Viscosity and Thermal Conductivity in Molten Salts Applications. *Journal of Chemical & Engineering Data* **2003,** *48* (3), 446-450.

41. Kou, S., *Transport Phenomena and Materials Processing*. John Wiley& Sons, Inc: New York, **1996**.

42. Smith, E. M., *Thermal Design of Heat Exchangers. A Numerical Approach: Direct Sizing and Stepwise Rating*. John Wiley & Sons, Inc.: New York, **1997**.

43. Sieder, E. N.; Tate, G. E., Heat Transfer and Pressure Drop of Liquids in Tubes. *Ind. Eng. Chem.* **1936,** (28), 1429–1435.

44. Ferreira, A. G. M.; Simões, P. N.; Ferreira, A. F.; Fonseca, M. A.; Oliveira, M. S. A.; Trino, A. S. M., Transport and thermal properties of quaternary phosphonium ionic liquids and IoNanofluids. *The Journal of Chemical Thermodynamics* **2013,** *64*, 80-92.

45. *KD2 Pro Thermal Properties Analyzer Operator's Manual (version 7)*. Decagon Devices Inc.: Pullman, WA, 2008-**2009**.

46. Tenney, C. M.; Massel, M.; Mayes, J. M.; Sen, M.; Brennecke, J. F.; Maginn, E. J., A Computational and Experimental Study of the Heat Transfer Properties of Nine Different Ionic Liquids. *Journal of Chemical & Engineering Data* **2014,** *59* (2), 391-399.

47. Fröba, A. P.; Rausch, M. H.; Krzeminski, K.; Assenbaum, D.; Wasserscheid, P.; Leipertz, A., Thermal Conductivity of Ionic Liquids: Measurement and Prediction. *International Journal of Thermophysics* **2010,** *31* (11), 2059-2077.

48. Koller, T. M.; Schmid, S. R.; Sachnov, S. J.; Rausch, M. H.; Wasserscheid, P.; Fröba, A. P., Measurement and Prediction of the Thermal Conductivity of Tricyanomethanide- and Tetracyanoborate-Based Imidazolium Ionic Liquids. *International Journal of Thermophysics* **2014,** *35* (2), 195-217.

49. Pereiro, A. B.; Veiga, H. I. M.; Esperança, J. M. S. S.; Rodríguez, A., Effect of temperature on the physical properties of two ionic liquids. *The Journal of Chemical Thermodynamics* **2009,** *41* (12), 1419-1423.

50. Fraser, K. J.; MacFarlane, D. R., Phosphonium-Based Ionic Liquids: An Overview. *Australian Journal of Chemistry* **2009,** *62* (4), 309-321.

51. Assael, M. J.; Chen, C. F.; Metaxa, I.; Wakeham, W. A., Thermal Conductivity of Suspensions of Carbon Nanotubes in Water. *International Journal of Thermophysics* **2004,** *25* (4), 971-985.

52. Assael, M. J.; Metaxa, I. N.; Arvanitidis, J.; Christofilos, D.; Lioutas, C., Thermal Conductivity Enhancement in Aqueous Suspensions of Carbon Multi-Walled and Double-Walled Nanotubes in the Presence of Two Different Dispersants. *International Journal of Thermophysics* **2005,** *26* (3), 647-664.

53. Canongia Lopes, J. N. A.; Pádua, A. A. H., Nanostructural Organization in Ionic Liquids. *The Journal of Physical Chemistry B* **2006,** *110* (7), 3330-3335.

54. Kim, P.; Shi, L.; Majumdar, A.; McEuen, P. L., Thermal Transport Measurements of Individual Multiwalled Nanotubes. *Physical Review Letters* **2001,** *87* (21), 215502.

55. Shevelyova, M. P.; Paulechka, Y. U.; Kabo, G. J.; Blokhin, A. V.; Kabo, A. G.; Gubarevich, T. M., Physicochemical Properties of Imidazolium-Based Ionic Nanofluids: Density, Heat Capacity, and Enthalpy of Formation. *The Journal of Physical Chemistry C* **2013,** *117* (9), 4782-4790.

56. Wang, F.; Han, L.; Zhang, Z.; Fang, X.; Shi, J.; Ma, W., Surfactant-free ionic liquid-based nanofluids with remarkable thermal conductivity enhancement at very low loading of graphene. *Nanoscale Research Letters* **2012,** *7* (1), 314-314.

57. Quijada-Maldonado, E.; van der Boogaart, S.; Lijbers, J. H.; Meindersma, G. W.; de Haan, A. B., Experimental densities, dynamic viscosities and surface tensions of the ionic liquids series 1-ethyl-3-methylimidazolium acetate and dicyanamide and their binary and ternary mixtures with water and ethanol at T = (298.15 to 343.15 K). *The Journal of Chemical Thermodynamics* **2012,** *51*, 51-58.

58. Carvalho, P. J.; Regueira, T.; Santos, L. M. N. B. F.; Fernandez, J.; Coutinho, J. A. P., Effect of Water on the Viscosities and Densities of 1-Butyl-3-methylimidazolium Dicyanamide and 1-Butyl-3-methylimidazolium Tricyanomethane at Atmospheric Pressure. *Journal of Chemical & Engineering Data* **2010,** *55* (2), 645-652.

59. Domańska, U.; Królikowska, M., Density and Viscosity of Binary Mixtures of Thiocyanate Ionic Liquids + Water as a Function of Temperature. *Journal of Solution Chemistry* **2012,** *41* (8), 1422-1445.

60. Vataščin, E.; Dohnal, V., Thermophysical properties of aqueous solutions of the 1-ethyl-3-methylimidazolium tricyanomethanide ionic liquid. *The Journal of Chemical Thermodynamics* **2015,** *89*, 169-176.

61. Canongia Lopes, J. N.; Costa Gomes, M. F.; Husson, P.; Pádua, A. A. H.; Rebelo, L. P. N.; Sarraute, S.; Tariq, M., Polarity, Viscosity, and Ionic Conductivity of Liquid Mixtures Containing [C4C1im][Ntf2] and a Molecular Component. *The Journal of Physical Chemistry B* **2011,** *115* (19), 6088-6099.

Chapter 6

Conclusions and future perspectives

The goal of the presented work has been to study ionanofluids, complex systems of ionic liquids and nanomaterials, both experimentally and using molecular dynamics. Previous work performed by the groups involved in this project had established, on one hand, that the enhanced properties of ionanofluids could be relevant for potential applications. On the other hand, the solvation and stabilization mechanisms of nanoparticles in ionic liquids needed to be studied to fully understand the structure of nanosystems such as these.

Several systems were studied in an effort to increase the database on thermophysical data of ionic liquids and ionanofluids with several mass fractions. The quantification of the enhancement of the thermophysical properties was also an aim. From the four properties mentioned throughout this dissertation (thermal conductivity, density, viscosity and heat capacity), only heat capacity was not measured due to technical issues with the calorimeter. However, a significant amount of data was collected on the remainder properties, with particular emphasis on thermal conductivity.

The suspension of 0.5% and 1% w/w of MWCNTs in ionic liquids showed that the thermal conductivity of the base fluid increases between 2% and 30%, when considering a temperature range between 293 K and 343 K. This range of enhancement shows a clear benefit from adding MWCNTs to the ionic liquids considered when considering them as potential heat transfer fluids. Furthermore, the variation of the thermal property with temperature is reduced, an important feature when considering the application of a fluid at different temperature values. Regarding density and viscosity,

although the data gathered is not as diverse system-wise, some transversal conclusions can be drawn from the dicyanamide systems. As expected, the increase in density when suspending MWCNTs in ionic liquids is considerably low, reaching an average maximum of 0.5% of enhancement when considering a 1% w/w ionanofluid. A similar impact can be anticipated in the remainder systems due to a significant difference in density between nanomaterial and ionic liquid. An analogous reasoning can be used to account for the variation of viscosity of systems other than the dicyanamide: the results presented in Chapter 4 showed an alike structure of [C_4mim][(*cyano*)] ionic liquids when close to a carbon surface, which lead to the consideration that a similar mass fraction of suspended MWCNTs would have an equivalent impact on the base fluid's viscosity.

Future work on this matter is required to assess the validity of the mentioned comparison regarding density and viscosity and to obtain more thermophysical data on these and other suspensions. As both ionic liquids and ionanofluids are fairly recent, a larger set of data will allow to fully understand the capabilities and limitations when considering these fluids for a potential application. As mentioned in Chapter 1, the economic and environmental restrictions demand a rigorous characterization of materials used. It is believed that the present work has contributed to that requirement to some extent. The use of properties/heat transport prediction models is also relevant to comply with current standards. However, if the models are based on the largest experimental and simulation data sets possible, it will help building solider predictions when considering potential substances as heat transfer fluids. The experimental work presented in Chapters 2, 3 and 5 show that the enhancement of the thermal conductivity varies considerably when using different ionic liquids as base fluids. Further work on studying different ionic liquids and other mass fraction values of nanomaterial, including different carbon nanomaterials, is necessary to strengthen the understanding of ionanofluids' properties

and their variation, which in turn will allow the conception of sturdier models.

Further to present cause, molecular dynamics provided a unique insight on the studied systems. The fitting of a site-site interaction potential between the atoms of the ionic liquid and graphene allowed a more realistic portrayal of the ordering of the ions when near a carbon surface. When devising the ionic liquid–carbon potential from mixing rules of LJ force fields [38 - 41], ionic liquids appear less structured in the solvation layers with several atoms, from both anions and cations, appearing at the same distance from the carbon surface. However, specifically parameterized models based on quantum calculations, such as those reported in Chapter 4 and in the work of Pensado *et al.* [42] for [C_2mim][SCN], show that interfacial ordering is more pronounced. Additionally, the interaction models are relatively transferable between families of ionic liquids for future work on this topic. Other families of ionic liquids should also be parameterized in order to create an accessible source of information that can realistically describe the interactions between ionic liquids and carbon nanomaterials.

The ordering of ions around and inside (7,7) and (10,10) single-walled nanotubes, and near a stack of graphene sheets, was analyzed in terms of density distribution functions. It was verified that both ionic species are found in the first interfacial layer interacting with the carbon nanomaterials, having an analogous ordering when near a (7,7) SWCNT, a (10,10) SWCNT and a stack of graphene sheets. The stronger curvature of the (7,7) nanotube only marginally affects the ordering of ions outside, when compared to the (10,10) SWCNT. As it was mentioned in the introductory section in Chapter 4, cations are found most likely near the centre of the (7,7) and (10,10) nanotubes, with their positions and orientations depending on the diameter of the tube. The alkyl side chains of the cations aggregate in the centre of the (10,10) nanotube, creating a non-polar domain.

Regarding the heat transport, although the NEMD thermal conductivity values are overestimated when compared with the experimental values, there is an acceptable prediction of the relative order between different ionic liquids and composite systems with a SWCNT. The distinctive enhancement in each system is a product of the specific interaction model, which is also in agreement with the experiment. The analysis of the results obtained with the systems composed by ionic liquid and SWCNT are straightforward, as the thermal conductivity is enhanced due to conduction through the material. The results of the systems composed by ionic liquid and graphene provide information concerning the role of the interface between the two components. The increase in organization at this specific region leads to an enhancement of thermal conductivity of the ionic liquid of the order of 15 – 30% with respect to the value in the bulk fluid. This result was obtained since the temperature gradient was created perpendicularly to the graphene planes, from the stack in the center of the box going into the ionic liquid. Future work on this topic could include the study of perpendicular heat flux relative to the SWCNT to confirm the enhancement of the thermal conductivity at the interface between SWCNT and ionic liquid, using the structural information obtained in Chapter 4.

The apparent lack of discontinuity of the temperature variation from the ionic liquids to the graphene surface suggests a small Kapitza resistance [35] at the interface. This is also an important result since a smaller discontinuity in temperature variation will lead to improved heat conduction [43]. The information obtained on the interfacial thermal conductivity is useful for predictive models for heat transport in systems composed with similar elements. The above-mentioned enhancement at the interface between 15 and 30% and the different widths of the interfacial region illustrate that thermal conductivity clearly depends on the ionic liquid being considered. Future work on this matter could include the calculation of the thermal conductivity

of several other ionic liquids in similar conditions, using NEMD, to obtain more data on the interfacial thermal conductivity.

The theme of heat transfer was a constant throughout this dissertation. In this sense, the author considered to be relevant to have a notion if ionanofluids are indeed feasible heat transfer fluids. Although this was a simplified analysis, the intention was to estimate the heat transfer area that ionanofluids require to transfer a designated amount of heat in a specific process. This was then to be compared (in the same conditions) to currently commercialized heat transfer fluids and ionic liquids.

The lack of thermophysical data of ionanofluids lead to some necessary approximations to perform the heat transfer area calculation, as was explained in Chapter 5. It was concluded that C_2mim^+ and cyano based ionic liquids/ionanofluids yield smaller area values due to their lower viscosity. Although the addition of MWCNTs to the ionic liquids leads to an increase in the area necessary to transfer the same amount of heat, a 0.5% w/w MWCNTs suspension has the advantage of enhancing the thermophysical properties and provide a smaller variation of the area with temperature. A 1% w/w MWCNTs suspension leads to an even higher enhancement of the thermophysical properties but it also leads to heat transfer areas that are substantially higher than the ones of the considered commercial fluids.

As ionic liquids are considered to be *designer solvents*, there are potentially multiple combinations of ions. Consequently, numerous fluids could have thermophysical properties that are adequate for heat transfer. Although a considerable amount of research is still to be performed, the properties' database of ionic liquids and ionanofluids is growing. As time goes forward, environmental and ecotoxicity tests will become more significant, particularly with long-term data. Furthermore, a fundamental understanding at the level of molecular interactions, structure and dynamics of the liquid phase to explain

the mentioned enhancement is also expanding. In this sense, there may come a time where, when considering an ionanofluid to be used as a heat transfer fluid, the process will consist on balancing the values of the properties according to requirements of a particular process. As an analogy, one could think of a sound equalizer. In order to attain the desired tone (for example, heat transfer area), the frequencies (thermophysical properties) “simply” have to be adjusted and balanced.

References

[1] Wakeham, W. A.; Nieto de Castro, C. A. Technological Importance In *The Transport Properties of Fluids - Their Correlation, Prediction and Estimation*; Millat, J., Dymond, J. H., Nieto de Castro, C. A., Eds.; Cambridge University Press: London, **1996**; Chapter 2.

[2] Mendonça, A. J. F.; Nieto de Castro, C. A.; Assael, M. J.; Wakeham, W. A. *Rev. Port. Quím.* **1981**, *23*, 7–11.

[3] Amstrong, J. B.; Li, S. F. Y.; Wakeham, W. A. The effect of the errors in the thermophysical properties of fluids upon plant design. *ASME Winter Annual Meeting*, **1982**; Paper 82-WHAT-84.

[4] Matos Lopes, M. L. S.; Nieto de Castro, C. A.; Wakeham, W. A. The effect of uncertainty in diffusion coefficients in the design of packed columns. *Proc. Int. Chem. Eng. Conf.*, CHEMPOR 85, Coimbra, Portugal, **1985**.

[5] J. M. P. França, C. A. Nieto de Castro, M. M. Lopes and V. M. B. Nunes, *J. Chem. Eng. Data*, **2009**, 54, 2569–2575.

[6] Nunes, V. M. B.; Lourenc ¸o, M. J. V.; Santos, F. J. V.; Nieto de Castro, C. A., *J. Chem. Eng. Data* **2003**, *48*, 446–450.

[7] Parvulescu, V.I., Hardacre, C., *Chem. Rev.*, **2007**, *107*, 2615.

[8] Scurto, A.M.; Aki, S.N.V.K.; Brennecke, J.F., *J. Am. Chem. Soc.*, **2002**, *124*, 10276-10277.

[9] Quinn, B.M; Ding, Z.; Moulton, R.; Bard. A.J. *Langmuir*, *18*, 1734-1742, **2002**.

[10] Hagiwara, R., Lee, J.S, *Electrochemistry 75*, 23-34, **2007**.

[11] Pernak, J., Sobaszkiewicz, K., Mirska, I., *Green Chem.*, **2003**, *5*, 52-56.

[12] Ha, S., Menchavez, R., Koo, Y., Korean *J. Chem. Eng.*, *27*(5), **2010**,1360- 1365.

[13] Stolte, S.; Matzke, M.; Arning, J., (Eco)Toxicology and Biodegradation of Ionic Liquids. In *Ionic Liquids Completely UnCOILed: Critical Expert Overviews*, Plechkova, N. V.; Seddon, K. R., Eds. John Wiley & Sons, Inc: Hoboken, NJ., **2015**.

[14] Nieto de Castro, C.A., Lourenço, M.J.V., Ribeiro, A.P.C., Langa, E., Vieira, S.I.C., Goodrich, P., and Hardacre, C., **2010** *J. Chem. Eng. Data*, *55* (2), 653–661.

[15] Ma L, et al, *Nano Lett.* **2014**, *15*, 127–33.

[16] Masuda H, Ebata A, Teramae K, Hishinuma N.. *Netsu Bussei,* **1993**, *7*, 227–33.

[17] Nanofluids: Science and Technology; Das, S. K., Choi, S. U. S., Yu, W., Pradeep, T., Eds.; John Wiley & Sons, Inc.: New York, **2008**; Chaps. 1–3.

[18] *A Treatise on Electricity and Magnetism*, 3rd ed.; Maxwell, J. C.; Clarendon Press: Oxford, U.K., 1891.

[19] Castro, C. N. d.; Paredes, X.; Vieira, S.; Murshed, S.; Lourenço, M. J.; Santos, F., IoNanofluids: Innovative Agents for Sustainable Development. In *Nanotechnology for Energy Sustainability*, Raj, B.;

Voorde, M. V . d.; Mahajan, Y ., Eds. WILEY-VCH Verlag GmbH & Co. KGaA: Weinheim, **2017**; Vol. 3.

[20] Fukushima, T.; Kosaka, A.; Ishimura, Y.; Yamamoto, T.; Takigawa, T.; Ishii, N.; Aida, T. *Science* **2003**, *300*, 2072–2075.

[21] Fukushima, T.; Aida, T., *Chem.-Eur. J.* **2007**, *13*, 5048– 5058.

[22] J. Le Bideau, L. Viau and A. Vioux, *Chem. Soc. Rev.*, **2011**, *40*, 907–925.

[23] S. Ravula, S. N. Baker, G. Kamath and G. A. Baker, *Nanoscale*, **2015**, *7*, 4338–4353.

[24] M. Matsumoto, Y. Saito, C. Park, T. Fukushima and T. Aida, *Nat. Chem.*, **2015**, *7*, 730–736.

[25] M. Armand, F. Endres, D. R. MacFarlane, H. Ohno and B. Scrosati, *Nat. Mater.*, **2009**, *8*, 621–629.

[26] C. Merlet, B. Rotenberg, P. A. Madden, P.-L. Taberna, P. Simon, Y. Gogotsi and M. Salanne, *Nat. Mater.*, **2012**, *11*, 306–310.

[27] M. Ruta, I. Yuranov, P. J. Dyson, G. Laurenczy and L. Kiwi-Minsker, *J. Catal.*, **2007**, *247*, 269–276

[28] H. Xiong, X. Zhang, B. Dong, H. Lu, L. Zhao, L. Wan, G. Dai and S. Wang, *Electrochim. Acta*, **2013**, *88*, 100–106.

[29] S. M. S. Murshed and C. A. Nieto de Castro, Proceedings of The World Congress on Engineering 2011 Vol III, **2011**, 1905–1909.

[30] R. Pal, *Nanomaterials*, **2014**, *4*, 844–855.

[31] M. Atilhan and S. Aparicio, *J. Phys. Chem. C*, **2014**, *118*, 21081–21091.

[32] F. Müller-Plathe, *J. Chem. Phys.*, **1997**, *106*, 6082–6085.

[33] M. Alaghemandi, E. Algaer, M. C. Böhm and F. Müller-Plathe, *Nanotechnology*, **2009**, *20*, 115704.

[34] H. Liu and E. Maginn, *J. Chem. Phys.*, **2011**, *135*, 124507.

[35] P. L. Kapitza, *Zh. Eksp. Teor. Fiz.*, **1941**, 11, 1.

[36] Neves, C. M. S. S.; Kurnia, K. A.; Coutinho, J. A. P.; Marrucho, I. M.; Lopes, J. N. C.; Freire, M. G.; Rebelo, L. P. N., *J. Phys. Chem. B,* **2013,** *117* (35), 10271-10283.

[37] Viboud, S.; Papaiconomou, N.; Cortesi, A.; Chatel, G.; Draye, M.; Fontvieille, D., *Journal of Hazardous Materials,* **2012,** *215-216*, 40-48.

[38] Y. Shim and H. J. Kim, *ACS Nano*, **2009**, *3*, 1693–1702.

[39] M. Mohammadi and M. Foroutan, *Phys. Chem. Chem. Phys.*, **2013**, *15*, 2482–2494.

[40] G. García, M. Atilhan and S. Aparicio, *J. Phys. Chem. B*, **2015**, *119*, 12224–12237.

[41] A. I. Frolov, K. Kirchner, T. Kirchner and M. V. Fedorov, *Faraday Discuss.*, **2012**, *154*, 235–247.

[42] A. S. Pensado, F. Malberg, M. F. C. Gomes, A. A. H. Padua, J. Fernandez and B. Kirchner, *RSC Adv.*, **2014**, *4*, 18017–18024.

[43] D. Konatham, K. N. D. Bui, D. V. Papavassiliou and A. Striolo, *Mol. Phys.*, **2011**, *109*, 97–111.

Annex 1

Molecular Interactions and Thermal Transport of Ionic Liquids with Carbon Nanomaterials – Supplementary Information

João M.P. França[a,b], Carlos A. Nieto de Castro[b], Agílio A.H. Pádua[a,*]

[a] Institut de Chimie de Clermont-Ferrand, Université Clermont Auvergne & CNRS, 63178 Aubière, France. *Email : agilio.padua@uca.fr

[b] Centro de Química Estrutural, Faculdade de Ciências, Universidade de Lisboa, Campo Grande, 1749-016, Lisboa, Portugal.

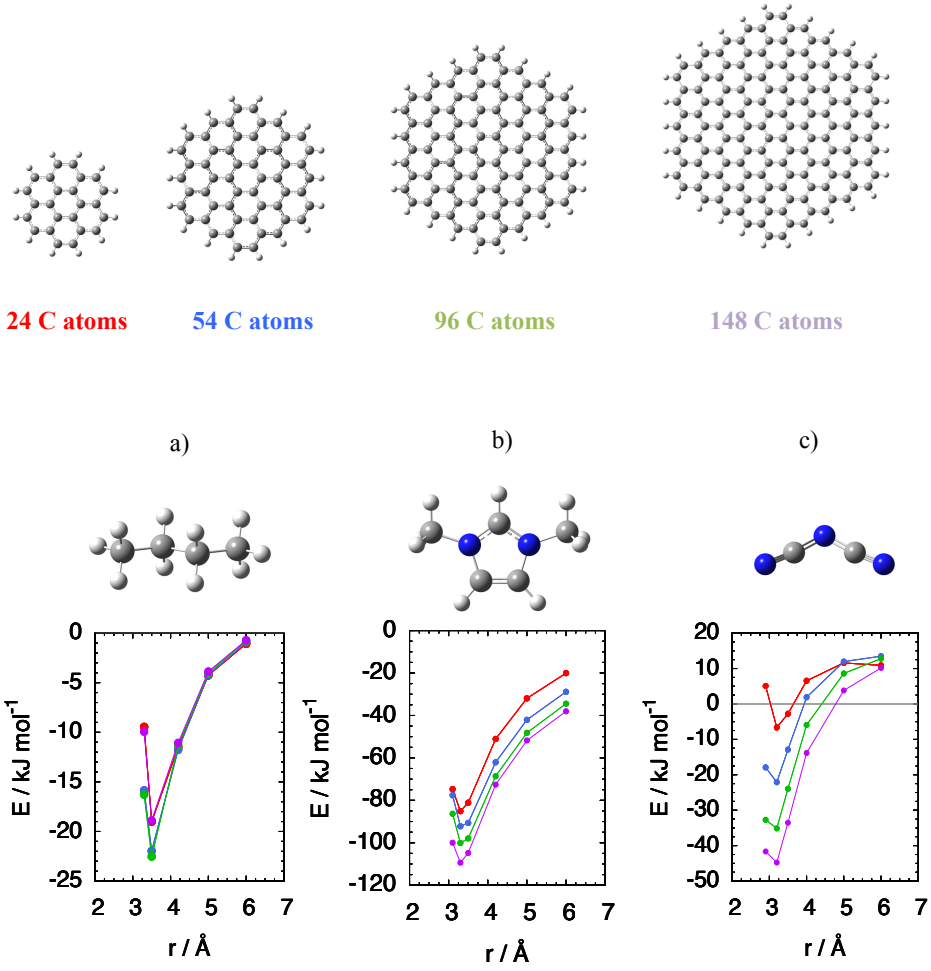

Figure S1. Evaluation of the effect of the size of the graphene flake on the potential energy of interaction with fragments of the ionic liquid, placed centered above the plane : a) butane, b) dimethylimidazolium cation, and c) dicyanamide anion.; red – 24 C atoms, blue – 54 C atoms, green – 96 C atoms; purple – 148 C atoms. Calculations performed using the density functional and basis set M06-2X/cc-pVTZ(-f), including corrections for basis set superposition error.

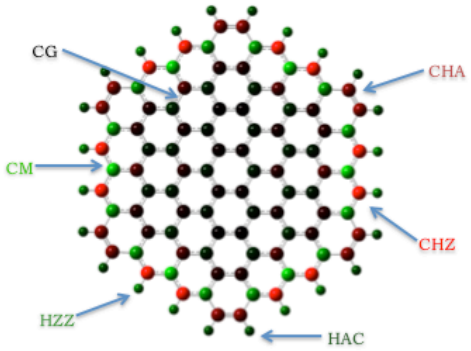

Figure S2. Partial charge scheme for a graphenic flake (δmax =0.05e).

Table S1. Values of the detailed partial charge scheme for graphene flakes.

Atom	HAC	HZZ	CHA	CHZ	CM	CG
q/e	+0.09	+0.16	-0.18	-0.34	+0.18	0.00

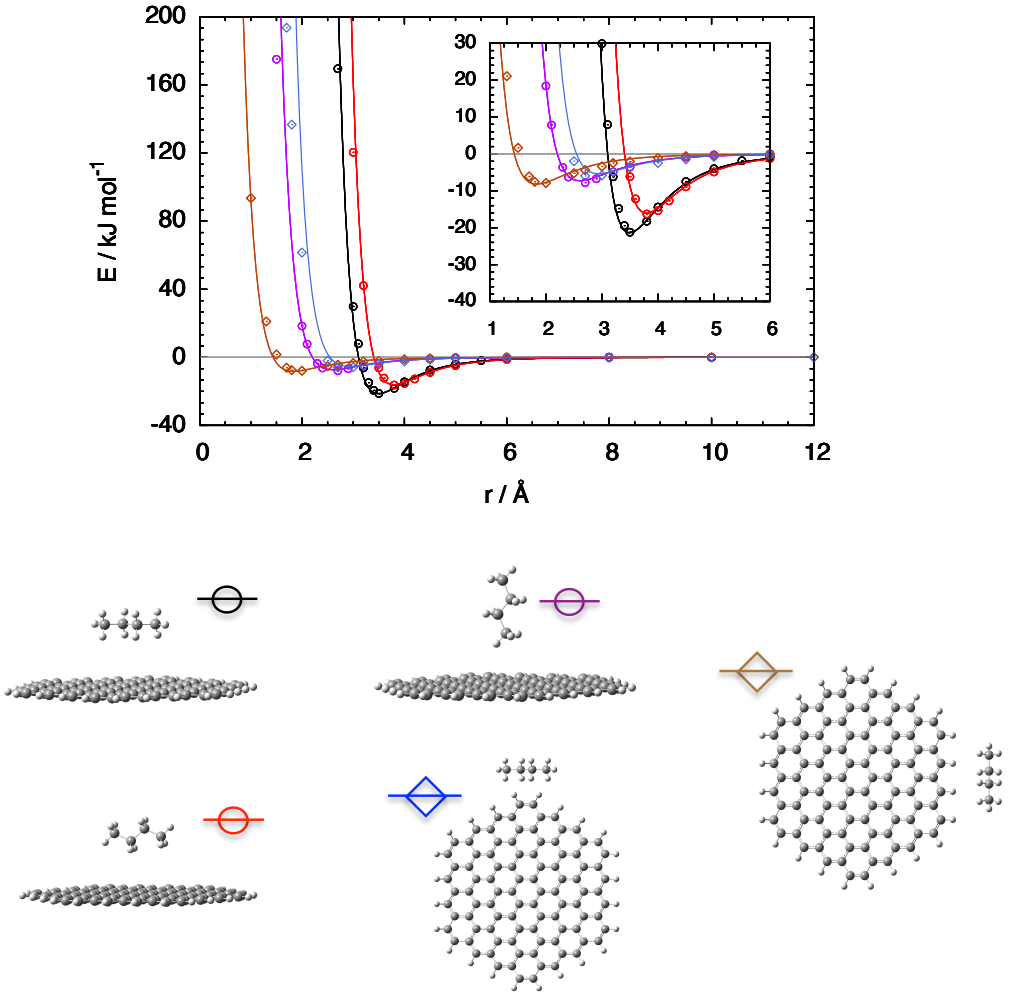

Figure S3. Potential energy of interaction between the **butane** fragment and a 96 C atom graphene flake. Symbols are quantum calculations at the M06-2X/cc-pVTZ level. Lines result from fitting the site-site *n-m* potential function. The color and the symbol below the plot indicate the orientation of the ionic liquid fragment regarding the graphene flake.

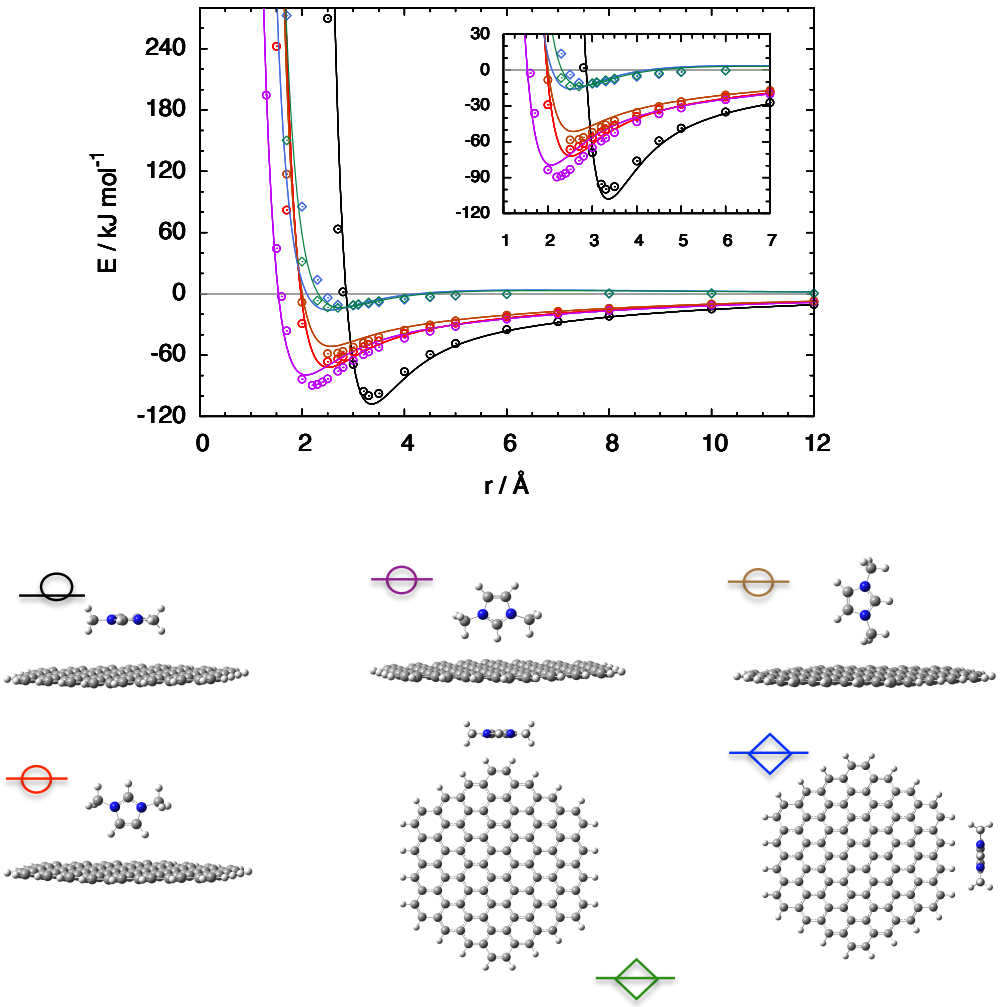

Figure S4. Potential energy of interaction between the **dimethylimidazolium** fragment and a 96 C atom graphene flake. Symbols are quantum calculations at the M06-2X/cc-pVTZ level. Lines result from fitting the site-site *n-m* potential function. The color and the symbol below the plot indicate the orientation of the ionic liquid fragment regarding the graphene flake.

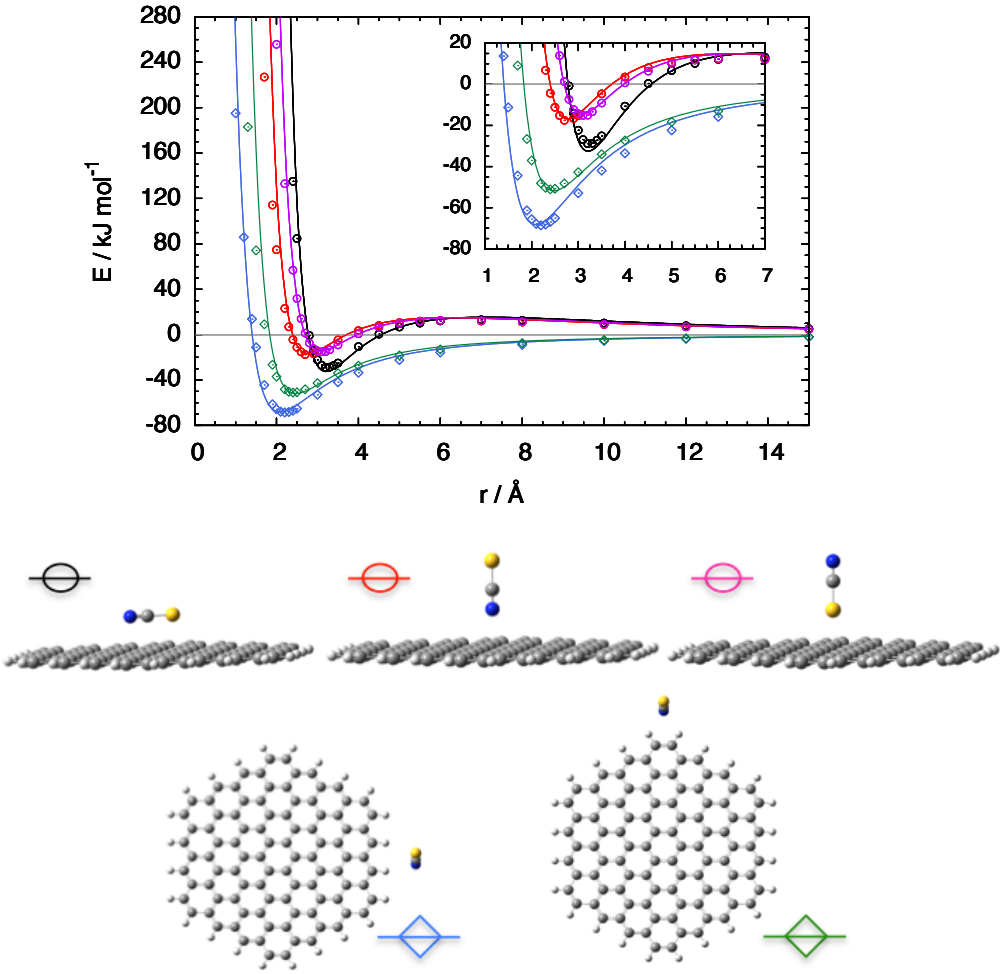

Figure S5. Potential energy of interaction between the **thiocyanate** fragment and a 96 C atom graphene flake. Symbols are quantum calculations at the M06-2X/cc-pVTZ level. Lines result from fitting the site-site *n-m* potential function. The color and the symbol below the plot indicate the orientation of the ionic liquid fragment regarding the graphene flake.

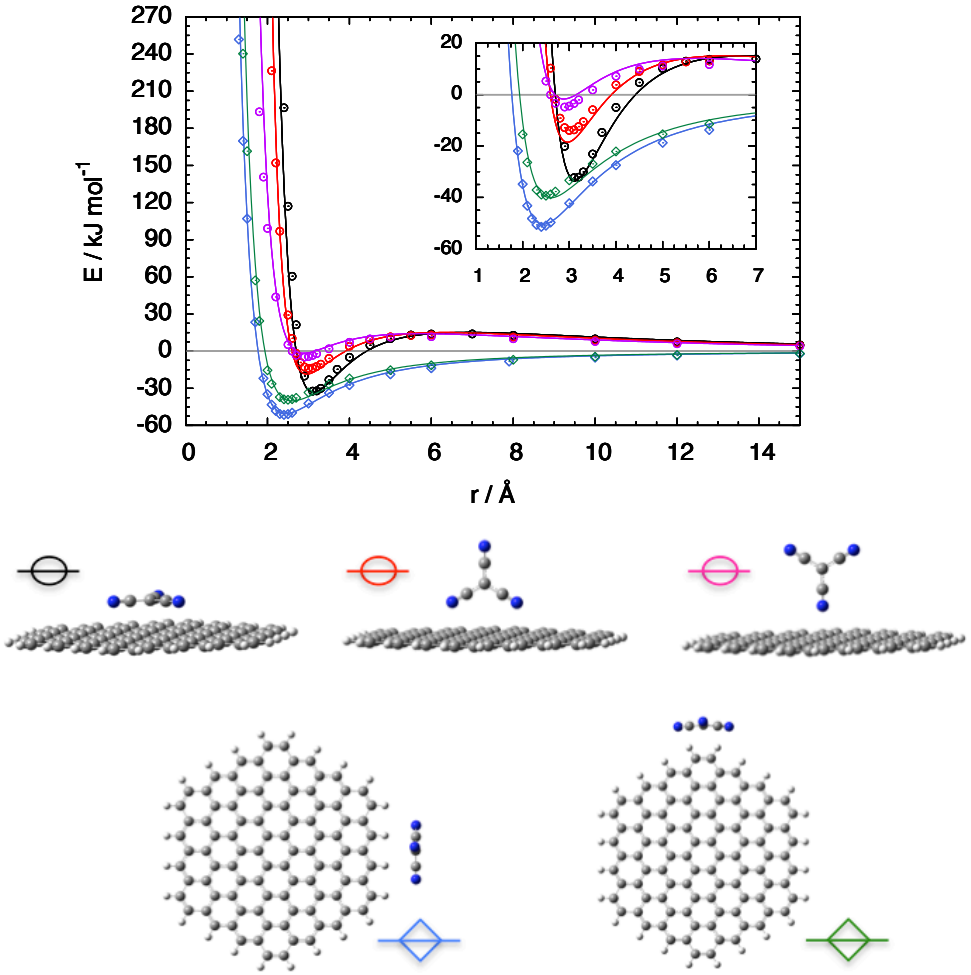

Figure S6. Potential energy of interaction between the **tricyanomethanide** fragment and a 96 C atom graphene flake. Symbols are quantum calculations at the M06-2X/cc-pVTZ level. Lines result from fitting the site-site *n-m* potential function. The color and the symbol below the plot indicate the orientation of the ionic liquid fragment regarding the graphene flake.

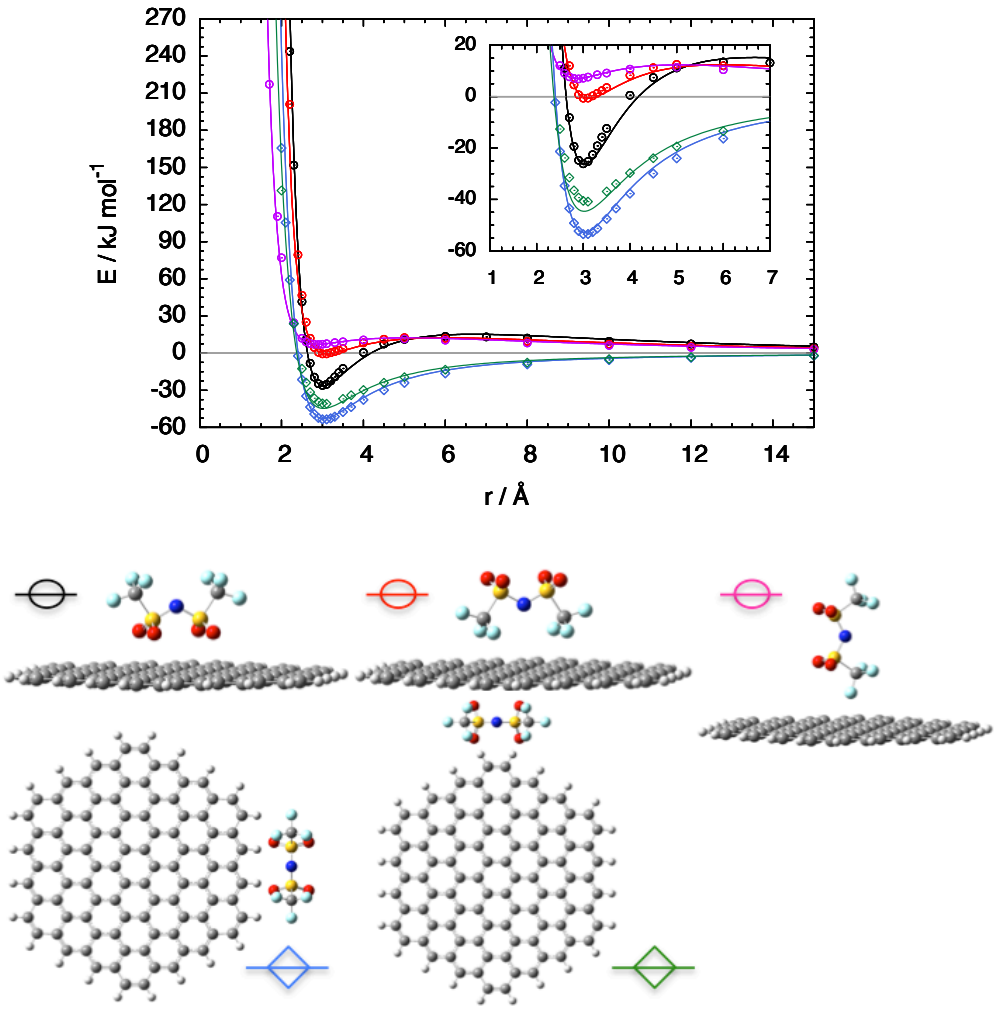

Figure S7. Potential energy of interaction between the **bis(trifluoromethylsulfonyl)imide** fragment and a 96 C atom graphene flake. Symbols are quantum calculations at the M06-2X/cc-pVTZ level. Lines result from fitting the site-site *n-m* potential function. The color and the symbol below the plot indicate the orientation of the ionic liquid fragment regarding the graphene flake.

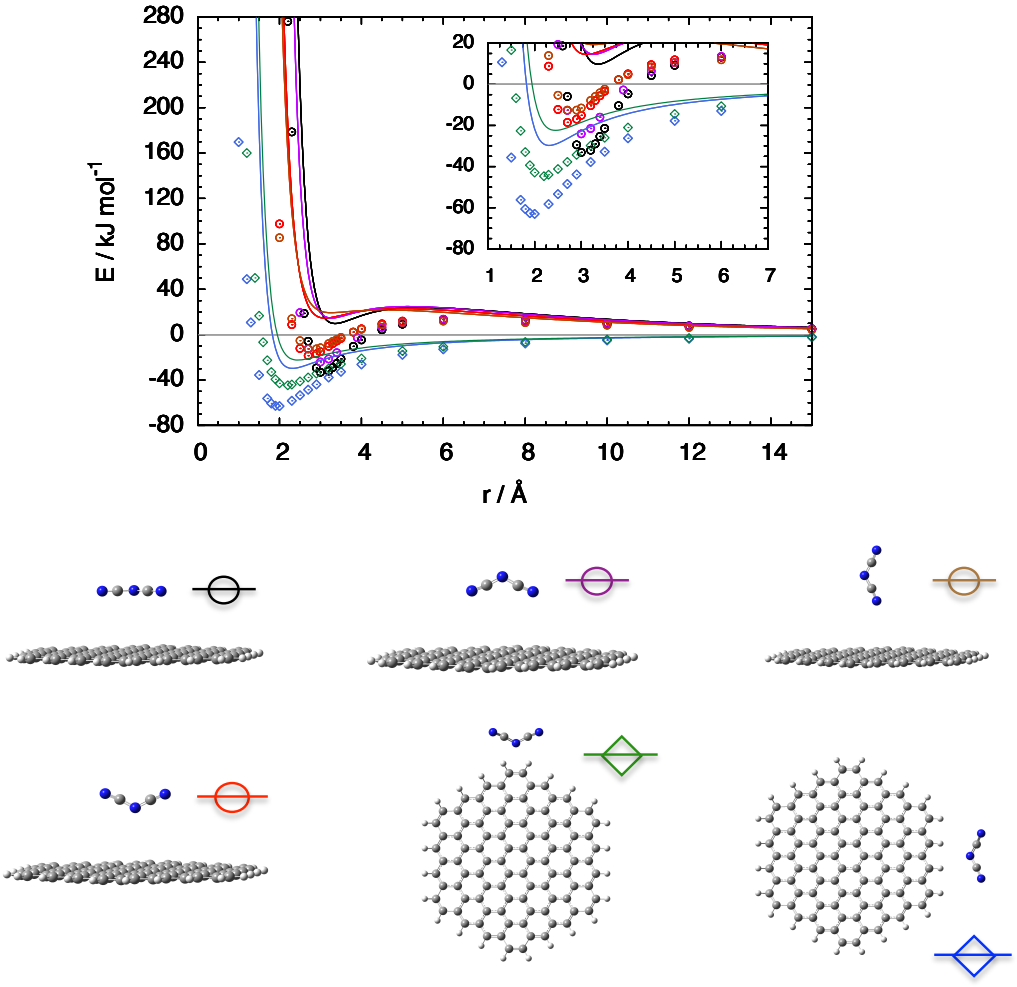

Figure S8. Potential energy of interaction between the **dicyanamide** fragment and a 96 C atom graphene flake. Symbols are quantum calculations at M06-2X/cc-pVTZ level. Lines are calculations using the **Lennard-Jones (12-6)** potential function with parameters from combining rules between LJ parameters of the dicyanamide anion and the force field for graphene.

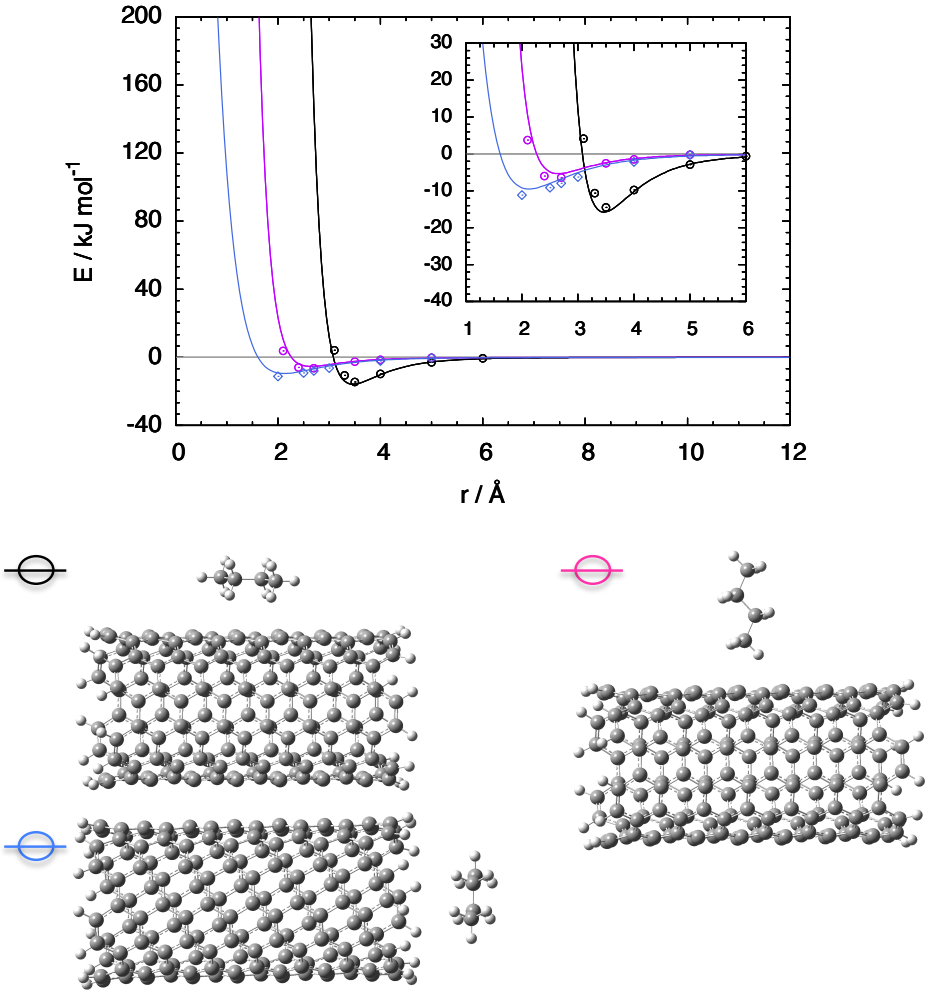

Figure S9. Potential energy of interaction between the **butane** fragment and a 168 C atom SWNT. Symbols are quantum calculations at the M06-2X/cc-pVTZ level. Lines are obtained from the *n-m* site-site potential functions using parameters derived from the fit to graphenic flakes.

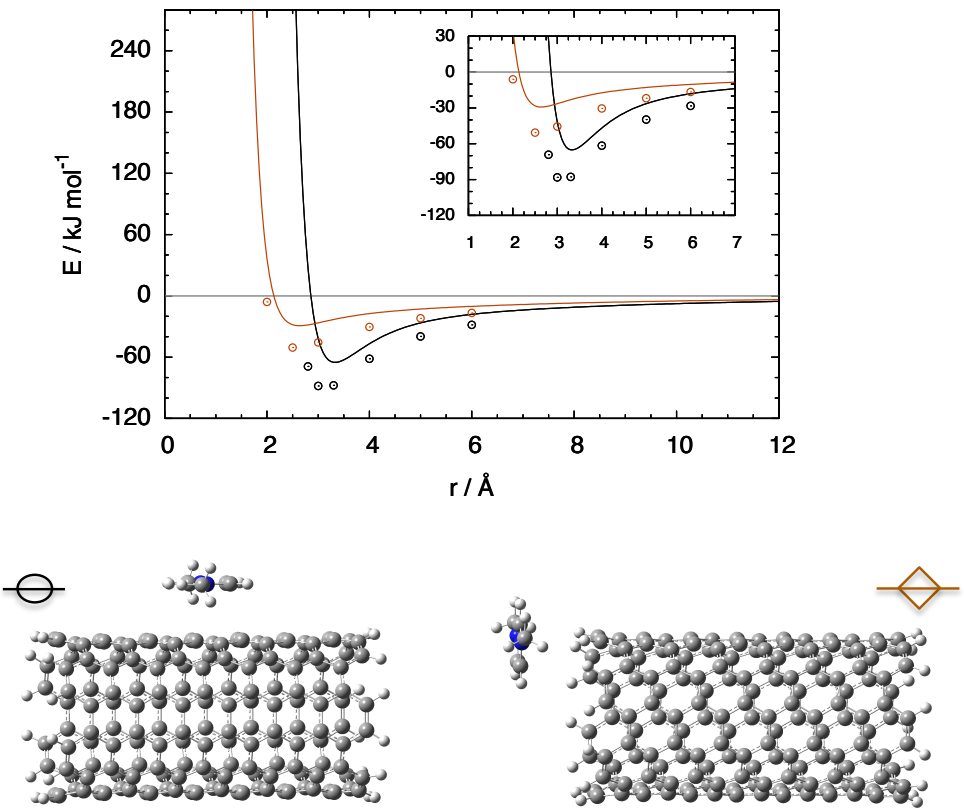

Figure S10. Potential energy of interaction between the **dimethylimidazolium** fragment and a 168 C atom SWNT. Symbols are quantum calculations at the M06-2X/cc-pVTZ level. Lines are obtained from the *n-m* site-site potential functions using parameters derived from the fit to graphenic flakes.

Table S2. Number of ion pairs used in molecular dynamics for each ionic liquid. Density values are at T = 363K.

Ionic liquid	ρ (kg m^{-3})	Ion pairs	
		graphene	(7,7) & (10,10)
$[C_4C_1im][N(CN)_2]$	1020.6[a]	388	950
$[C_4C_1im][SCN]$	1031.73[b]	401	960
$[C_4C_1im][C(CN)_3]$	1004.6[c]	336	800
$[C_4C_1im][tf_2N]$	1375.58[d]	252	600

a - J.M.P. França *et al., J. Chem. Thermodynamics* 79 (2014) 248–257
b- G. Vakili-Nezhaad *et al., J. Chem. Thermodynamics* 54 (2012) 148–154
c- P.J. Carvalho *et al., J. Chem. Eng. Data* **2010,** *55,* 645–652
d- C.A. Nieto de Castro, *et al., Fluid Phase Equilibria* 294 (2010) 157–179

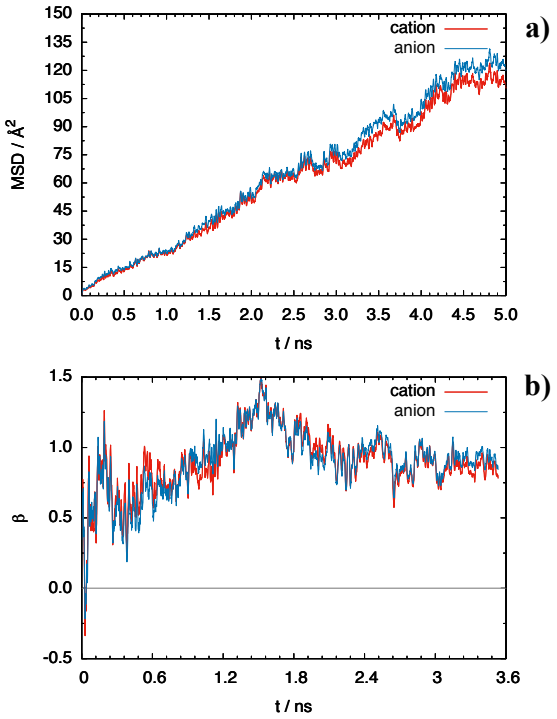

Figure S11. a) Global (xyz) mean-square displacement (MSD) and b) linearity parameter β for the ions in the pure ionic liquid $[C_4C_1im][SCN]$ at 363K.

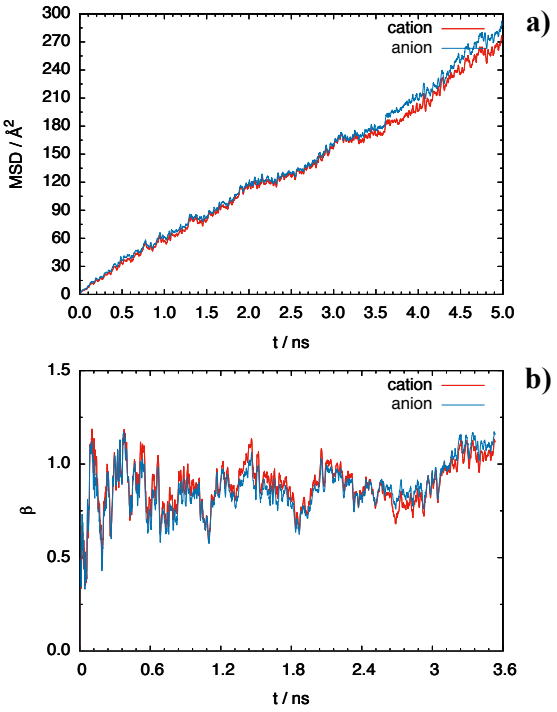

Figure S12. a) Global (xyz) mean-square displacement (MSD) and b) linearity parameter β for the ions in the pure ionic liquid $[C_4C_1im][N(CN)_2]$ at 363K.

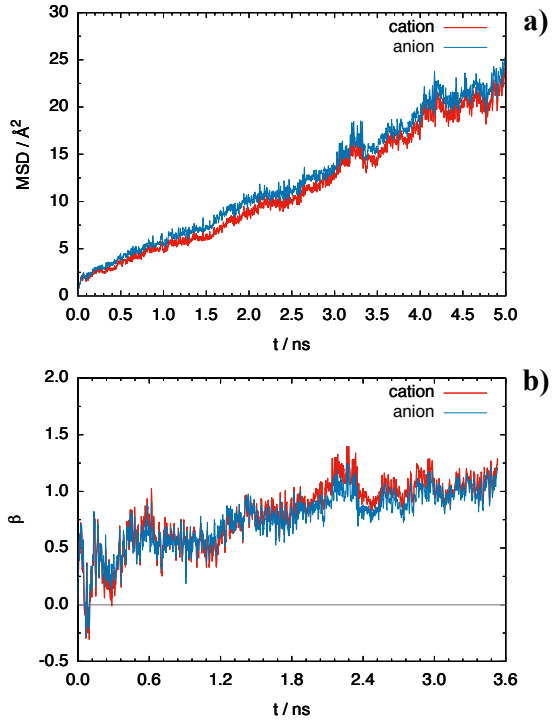

Figure S13. a) Global (xyz) mean-square displacement (MSD) and b) linearity parameter β for the ions in the pure ionic liquid $[C_4C_1im][C(CN)_3]$ at 363K.

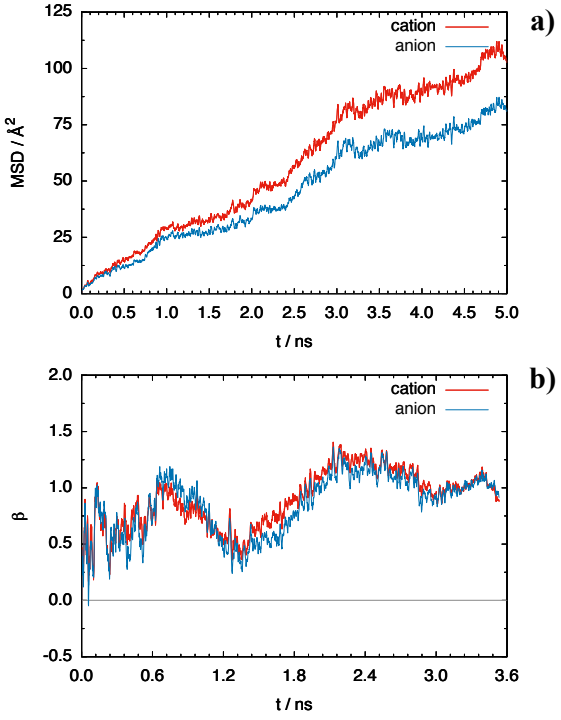

Figure S14. a) Global (xyz) mean-square displacement (MSD) and b) linearity parameter β for the ions in the pure ionic liquid $[C_4C_1im][tf_2N]$ at 363K.

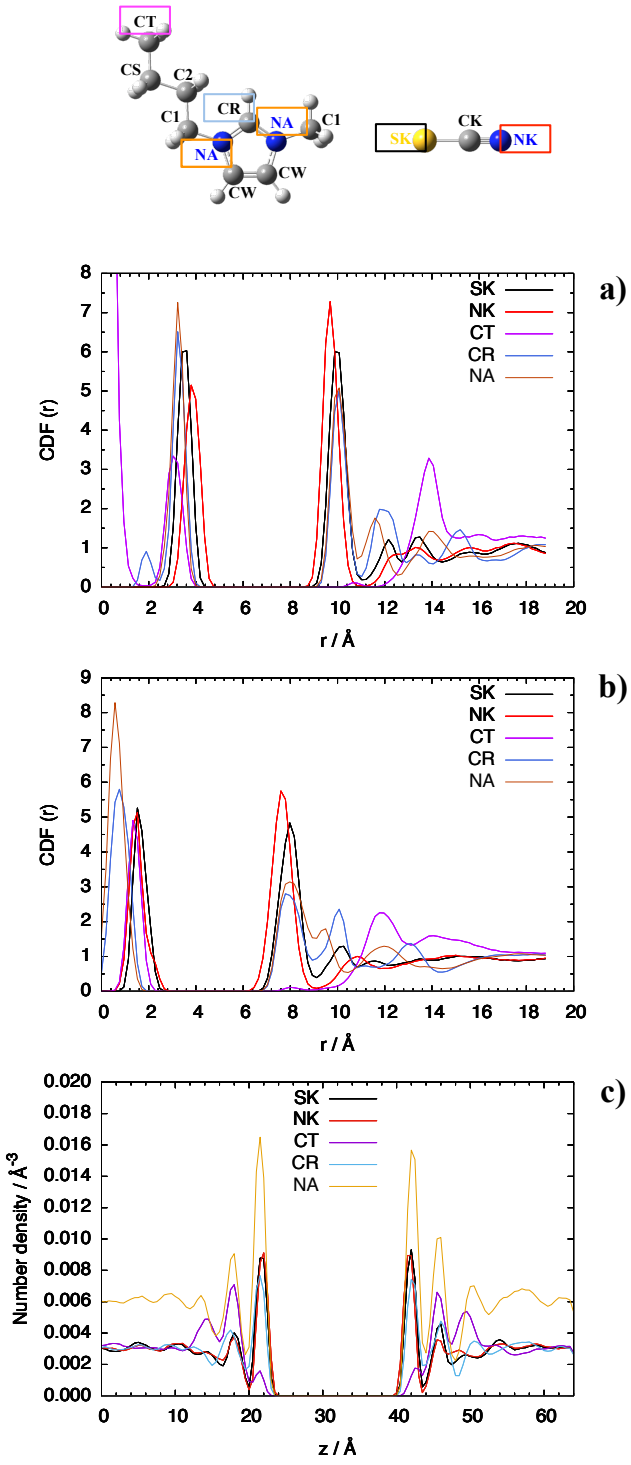

Figure S15. Cylindrical distribution function (CDF) of a) $[C_4C_1im][SCN]$ and SWNCT (10,10), b) $[C_4C_1im][SCN]$ and SWNCT (7,7) and c) Number density of $[C_4C_1im][SCN]$ and graphene. T = 363 K.

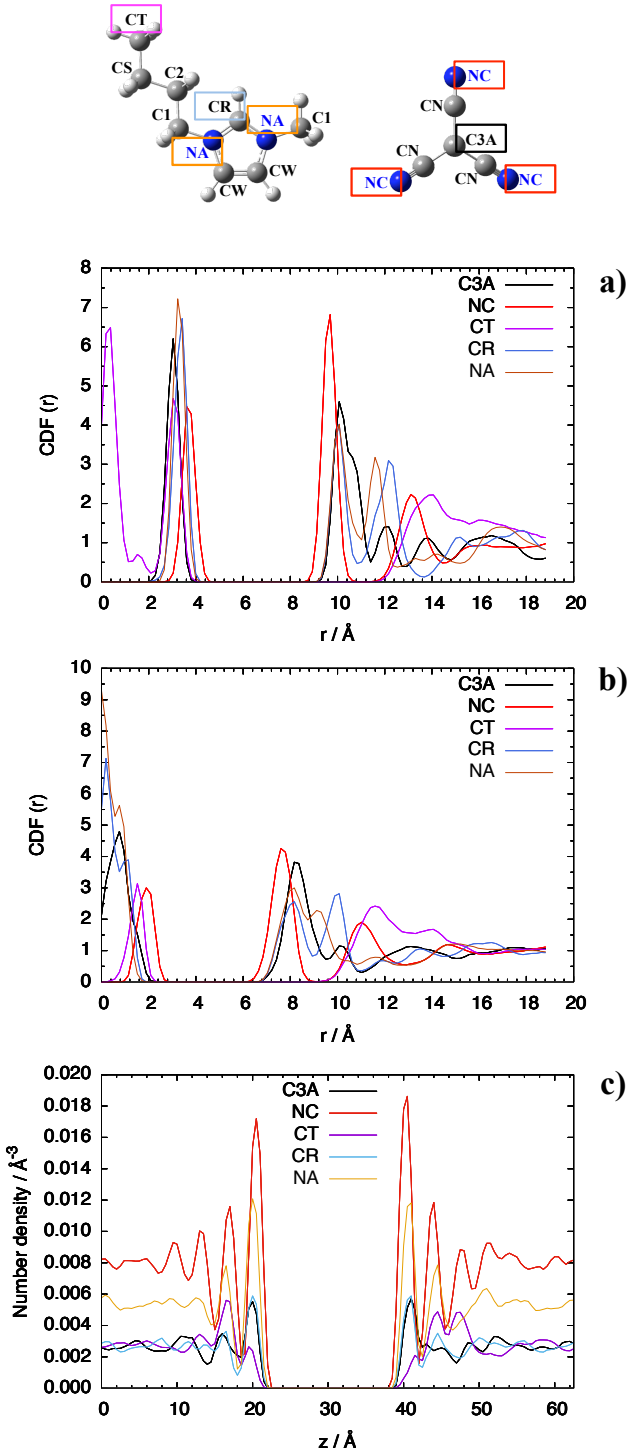

Figure S16. Cylindrical distribution function (CDF) of a) $[C_4C_1im][C(CN)_3]$ and SWNCT (10,10), b) $[C_4C_1im][C(CN)_3]$ and SWNCT (7,7) and c) Number density of $[C_4C_1im][C(CN)_3]$ and graphene. $T = 363$ K.

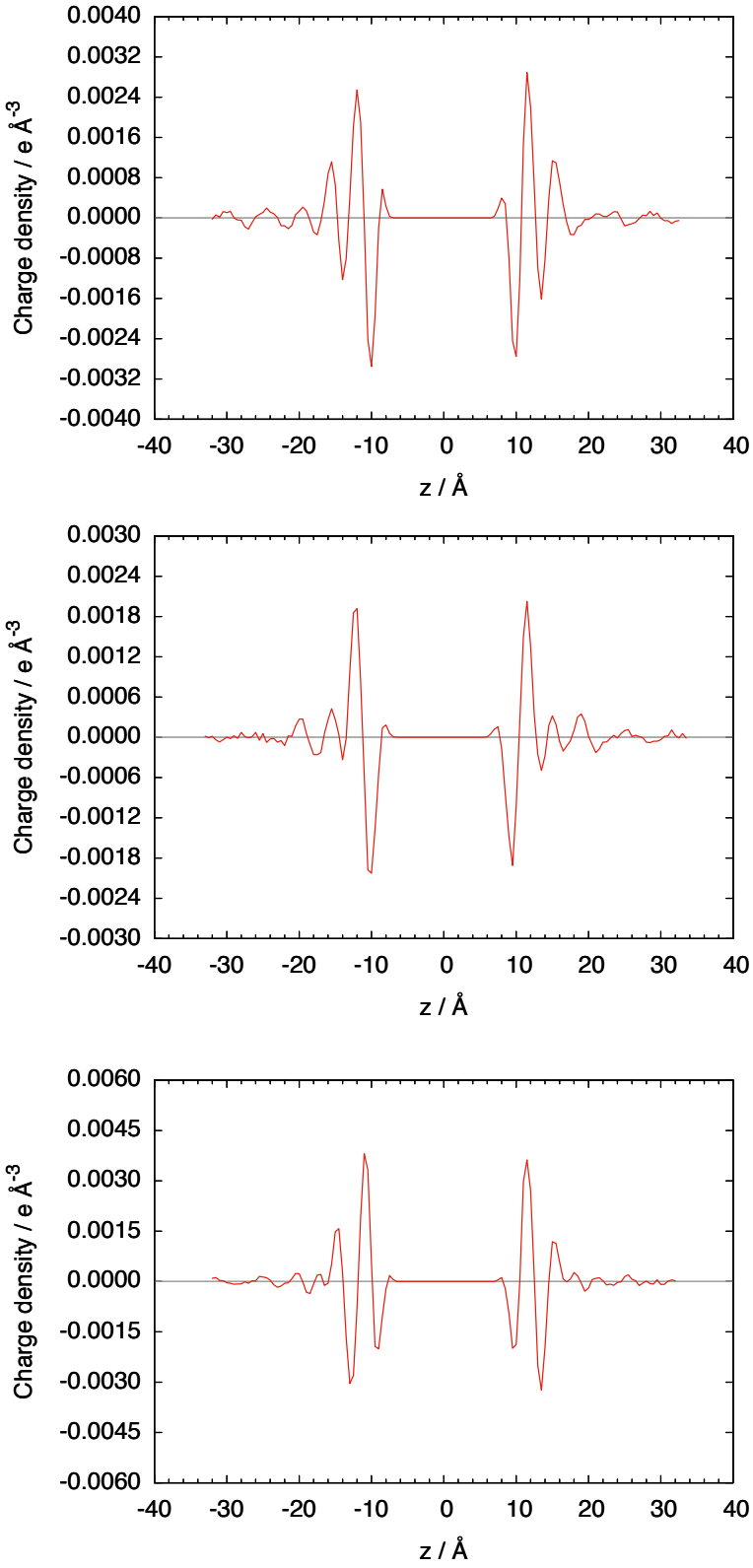

Figure S17. Electrostatic charge density profile of $[C_4C_1im][SCN]$ (top), $[C_4C_1im][N(CN)_2]$ (center) and $[C_4C_1im][tf_2N]$ (bottom) with graphene at T = 423 K. The higher temperature was chosen in order to obtain better-converged profiles.

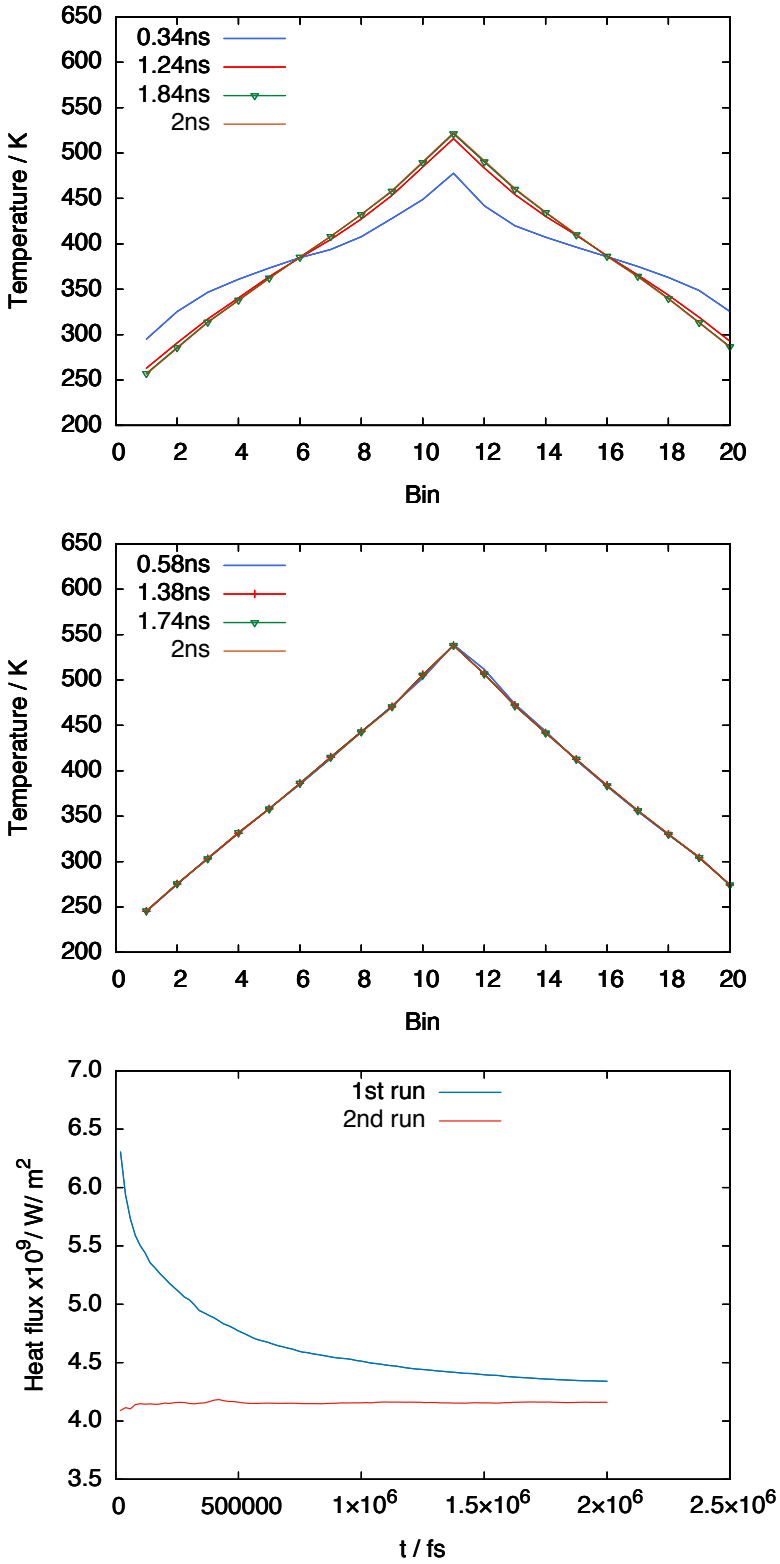

Figure S18 - Temperature profile along the simulation box (here represented in bins) during the first run (top), second run (middle) and heat flux (bottom) for pure $[C_4C_1im][tf_2N]$. These are referred to a 500 time steps exchange rate of kinetic energy at 383K.

Table S3. Thermal conductivities obtained from NEMD for pure IL, IL+SWCNT and IL+Graphene. "MP 350" stands for the Müller-Plathe method with a kinetic energy exchange rate of 350 time steps, while "MP 500" stands for a kinetic energy exchange rate of 500 time steps.

T / K	$[C_4C_1im][tf_2N]$	$[C_4C_1im][SCN]$	$[C_4C_1im][N(CN)_2]$	$[C_4C_1im][C(CN)_3]$
		λ / W $K^{-1}m^{-1}$ IL MP 350		
363	0.165	0.244	0.253	0.308
383	0.159	0.241	0.252	0.305
423	0.155	0.233	0.243	0.302
		λ / W $K^{-1}m^{-1}$ IL MP 500		
363	0.166	0.243	0.255	0.304
383	0.158	0.239	0.249	0.309
423	0.155	0.235	0.244	0.302
		λ / W $K^{-1}m^{-1}$ IL + SWCNT MP 350		
363	0.209	0.302	0.312	0.354
383	0.205	0.297	0.312	0.361
423	0.209	0.290	0.303	0.361
		λ / W $K^{-1}m^{-1}$ IL + SWCNT MP 500		
363	0.209	0.290	0.312	0.365
383	0.206	0.296	0.315	0.354
423	0.204	0.285	0.307	0.372
		λ / W $K^{-1}m^{-1}$ IL + Graphene MP 350		
363	0.066	0.109	0.127	0.130
383	0.068	0.117	0.122	0.135
423	0.069	0.116	0.121	0.138
		λ / W $K^{-1}m^{-1}$ IL + Graphene MP 500		
363	0.068	0.112	0.128	0.134
383	0.070	0.111	0.121	0.140
423	0.071	0.119	0.122	0.148
		λ / W $K^{-1}m^{-1}$ IL MP 350 (bulk liquid from IL+Graphene)		
363	0.075	0.131	0.143	0.164
383	0.079	0.133	0.145	0.157
423	0.080	0.141	0.143	0.178
		λ / W $K^{-1}m^{-1}$ IL MP 500 (bulk liquid from IL+Graphene)		
363	0.077	0.127	0.148	0.159
383	0.081	0.129	0.142	0.171
423	0.081	0.142	0.144	0.176

Table S4. Interfacial thermal conductivities obtained from NEMD for IL+Graphene. "MP 350" stands for the Müller-Plathe method with a kinetic energy exchange rate of 350 time steps, while "MP 500" stands for a kinetic energy exchange rate of 500 time steps.

T / K	$[C_4C_1im][tf_2N]$	$[C_4C_1im][SCN]$	$[C_4C_1im][N(CN)_2]$	$[C_4C_1im][C(CN)_3]$
	λ / W K^{-1}m^{-1} IL + Graphene MP 350			
363	0.089	0.158	0.188	0.184
383	0.091	0.181	0.179	0.195
423	0.092	0.166	0.176	0.193
	λ / W K^{-1}m^{-1} IL + Graphene MP 500			
363	0.090	0.166	0.184	0.197
383	0.094	0.176	0.176	0.201
423	0.094	0.176	0.179	0.217

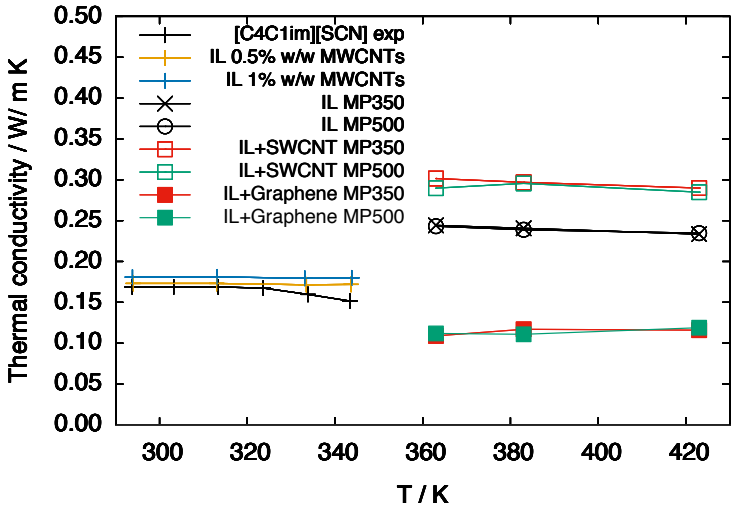

Figure S19. Thermal conductivity of $[C_4C_1im][SCN]$, pure and with carbon nanomaterials. Experimental results [J.M.P. França, S.M.S. Murshed, A.A.H Pádua, C.A. Nieto de Castro, "Thermal conductivity of Cyano and Phosphonium Ionic Liquids and their IoNanofluids", *J. Phys. Chem. B*, to be submitted] are on the left (pure and with MWCNTs) and NEMD values on the right (pure, with SWCNT and with Graphene). "MP 350" stands for the Müller-Plathe method with a kinetic energy exchange rate of 350 time steps, while "MP 500" stands for a kinetic energy exchange rate of 500 time steps.

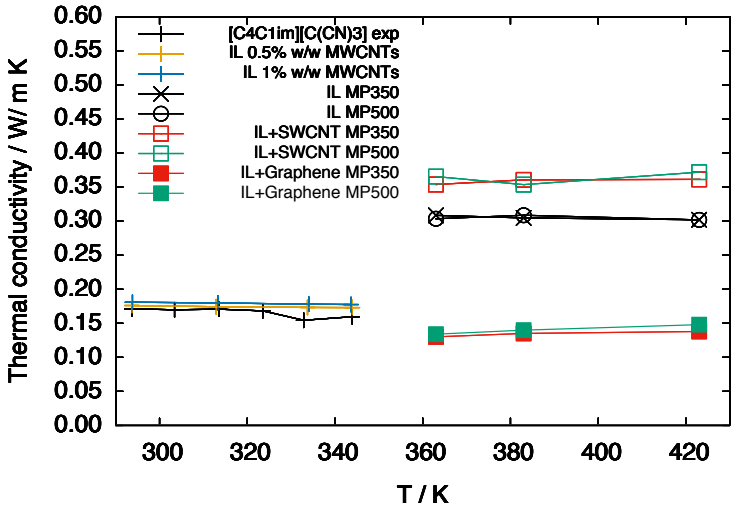

Figure S20. Thermal conductivity of $[C_4C_1im][C(CN)_3]$, pure and with carbon nanomaterials. Experimental results [J.M.P. França, S.M.S. Murshed, A.A.H Pádua, C.A. Nieto de Castro, "Thermal conductivity of Cyano and Phosphonium Ionic Liquids and their IoNanofluids", *J. Phys. Chem. B*, to be submitted] are on the left (pure and with MWCNTs) and NEMD values on the right (pure, with SWCNT and with Graphene). "MP 350" stands for the Müller-Plathe method with a kinetic energy exchange rate of 350 time steps, while "MP 500" stands for a kinetic energy exchange rate of 500 time steps.

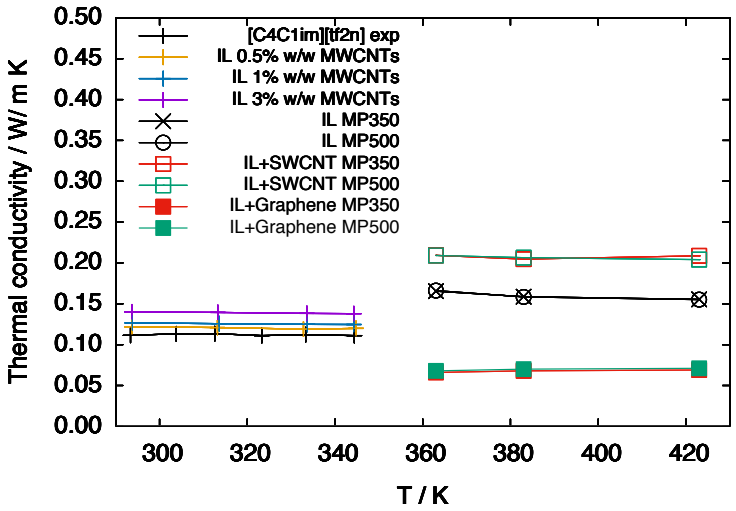

Figure S21. Thermal conductivity of $[C_4C_1im][tf_2N]$, pure and with carbon nanomaterials. Experimental results [J.M.P. França, *et al.*, *J. Chem. Eng. Data*, 2013, **58**, 467-476] are on the left (pure and with MWCNTs) and NEMD values on the right (pure, with SWCNT and with Graphene). "MP 350" stands for the Müller-Plathe method with a kinetic energy exchange rate of 350 time steps, while "MP 500" stands for a kinetic energy exchange rate of 500 time steps.

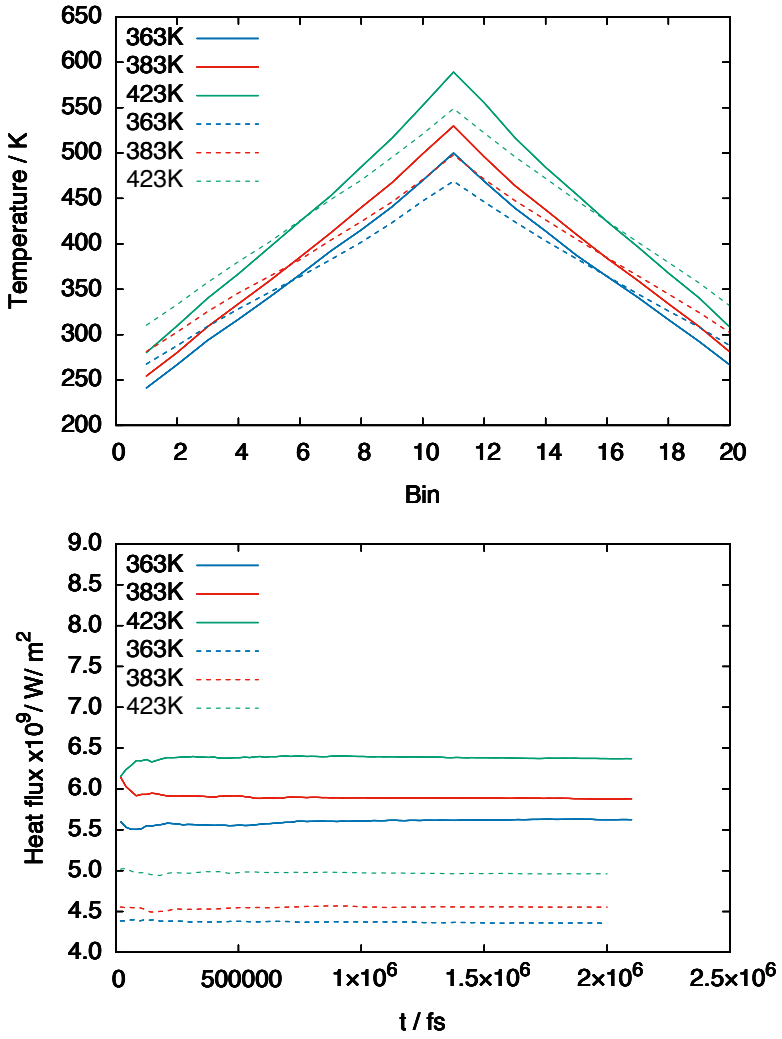

Figure S22. Temperature profile along the simulation box (here represented in bins) (top) and heat flux (bottom) for pure [C_4C_1im][SCN]. Solid lines represent a 350 time steps exchange rate of kinetic energy and the dashed lines represent 500 time steps exchange rate of kinetic energy.

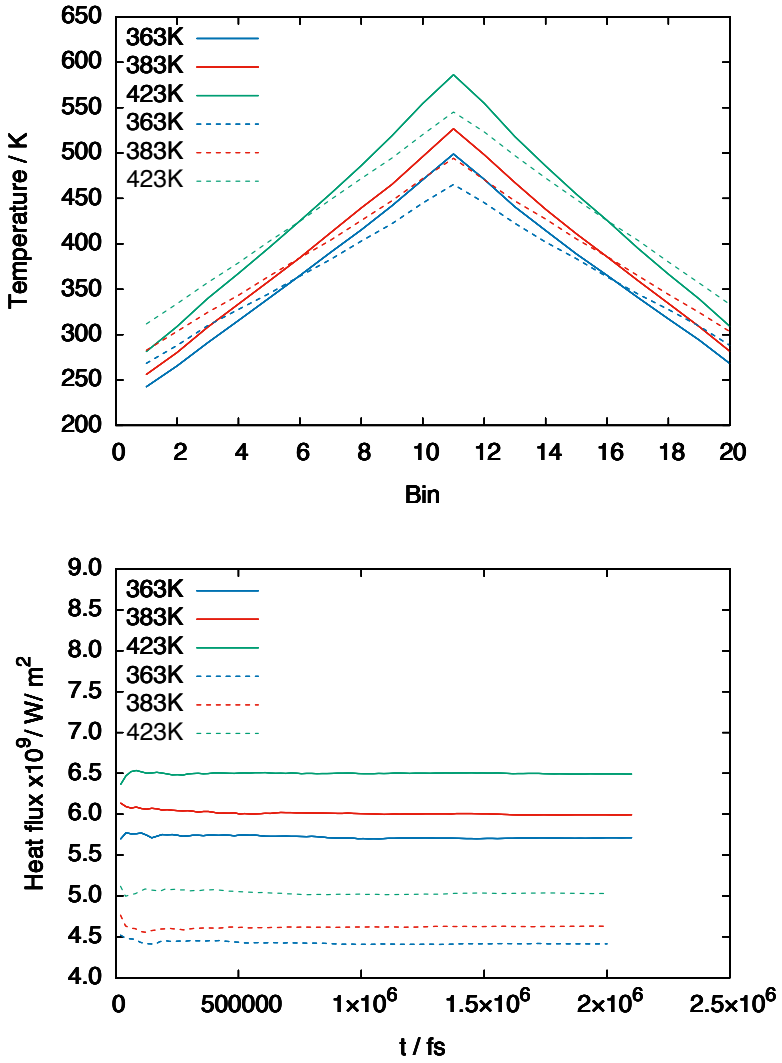

Figure S23. Temperature profile along the simulation box (here represented in bins) (top) and heat flux (bottom) for pure $[C_4C_1im][N(CN)_2]$. Solid lines represent a 350 time steps exchange rate of kinetic energy and the dashed lines represent 500 time steps exchange rate of kinetic energy.

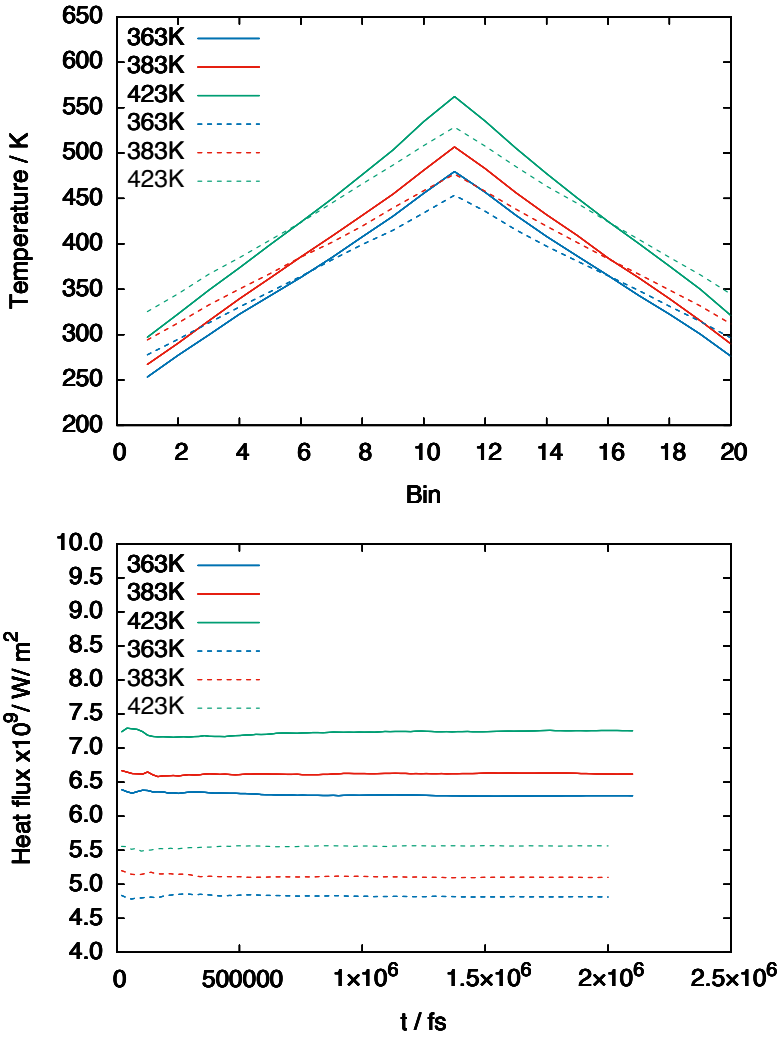

Figure S24. Temperature profile along the simulation box (here represented in bins) (top) and heat flux (bottom) for pure $[C_4C_1im][C(CN)_3]$. Solid lines represent a 350 time steps exchange rate of kinetic energy and the dashed lines represent 500 time steps exchange rate of kinetic energy.

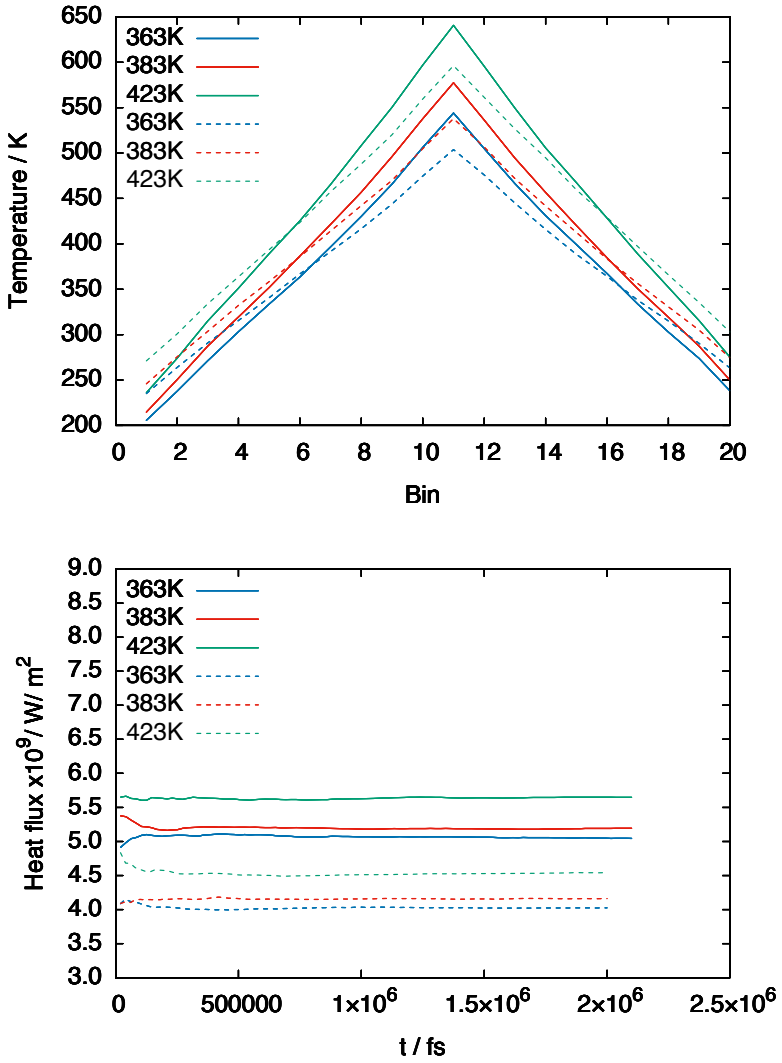

Figure S25. Temperature profile along the simulation box (here represented in bins) (top) and heat flux (bottom) for pure $[C_4C_1im][tf_2N]$. Solid lines represent a 350 time steps exchange rate of kinetic energy and the dashed lines represent 500 time steps exchange rate of kinetic energy.

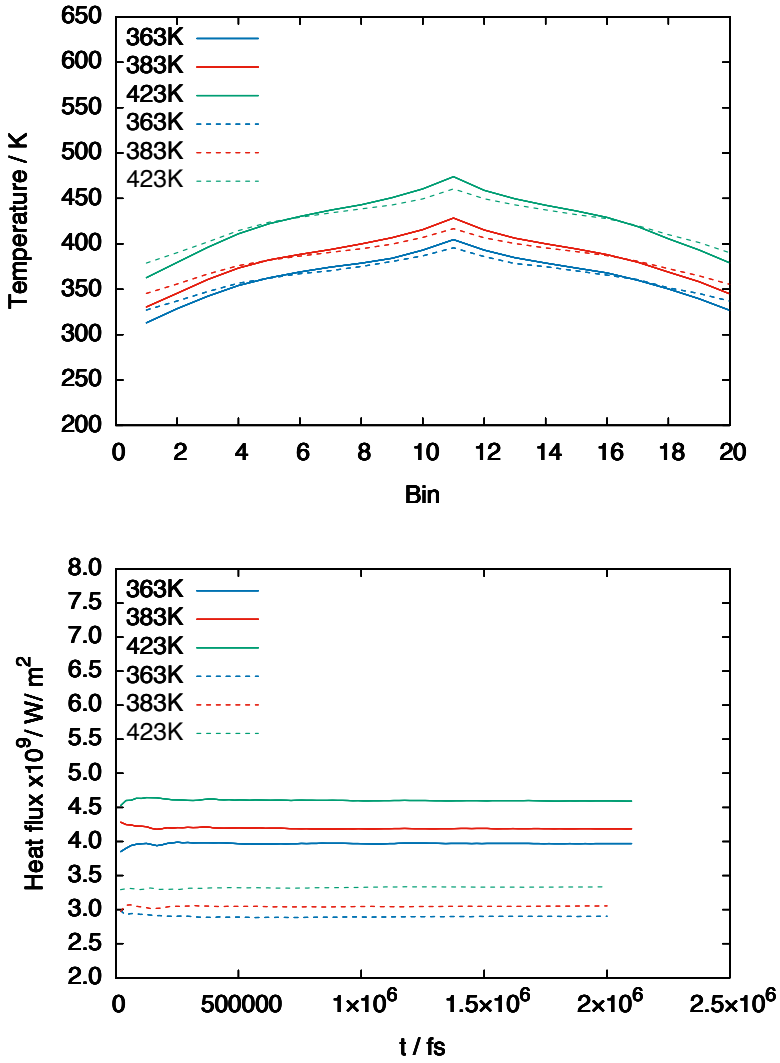

Figure S26. Temperature profile along the simulation box (here represented in bins) (top) and heat flux (bottom) for $[C_4C_1im][SCN]$ + SWCNT. Solid lines represent a 350 time steps exchange rate of kinetic energy and the dashed lines represent 500 time steps exchange rate of kinetic energy.

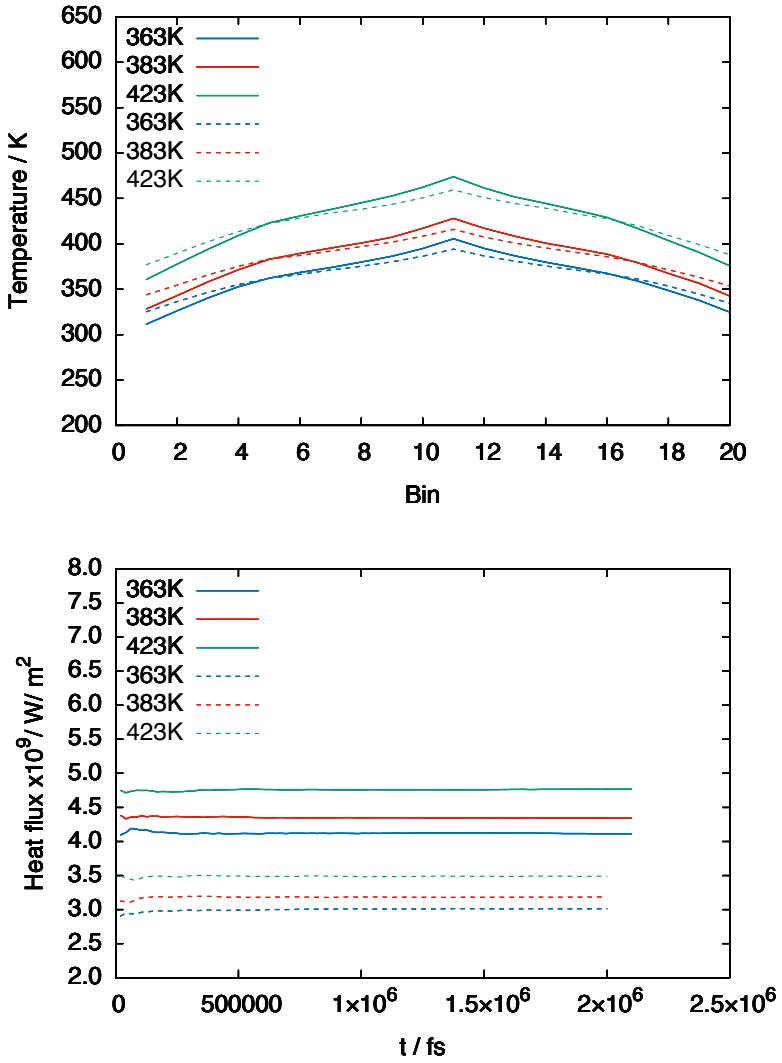

Figure S27. Temperature profile along the simulation box (here represented in bins) (top) and heat flux (bottom) for $[C_4C_1im][N(CN)_2]$ + SWCNT. Solid lines represent a 350 time steps exchange rate of kinetic energy and the dashed lines represent 500 time steps exchange rate of kinetic energy.

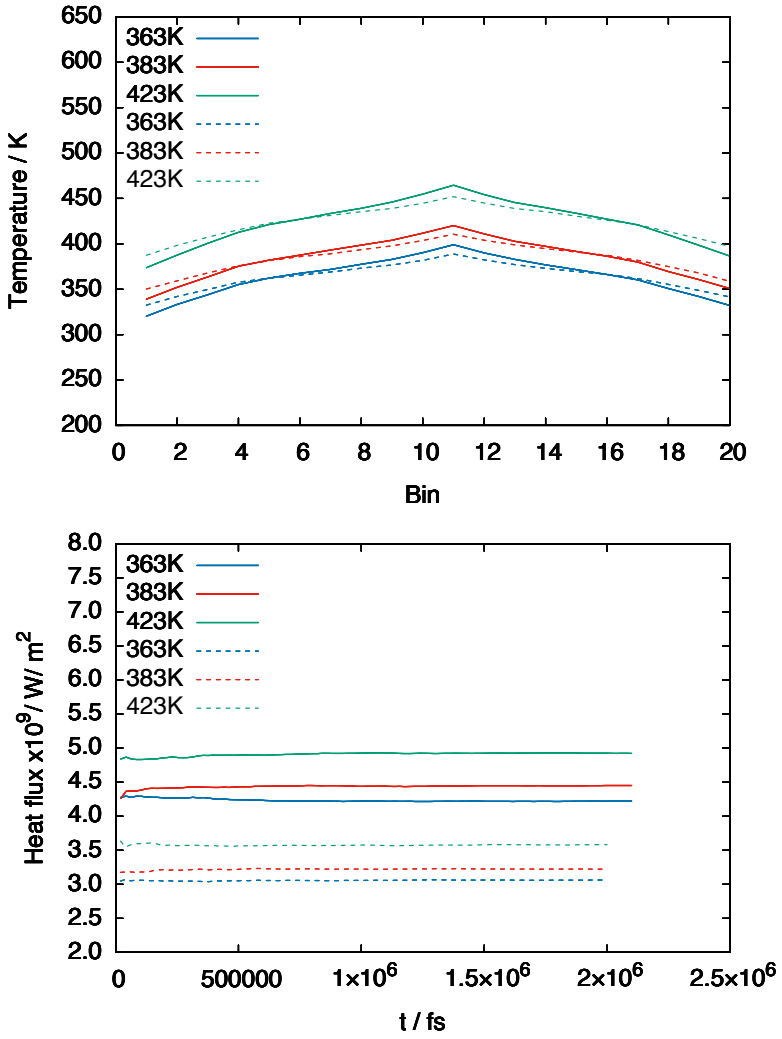

Figure S28. Temperature profile along the simulation box (here represented in bins) (top) and heat flux (bottom) for $[C_4C_1im][C(CN)_3]$ + SWCNT. Solid lines represent a 350 time steps exchange rate of kinetic energy and the dashed lines represent 500 time steps exchange rate of kinetic energy.

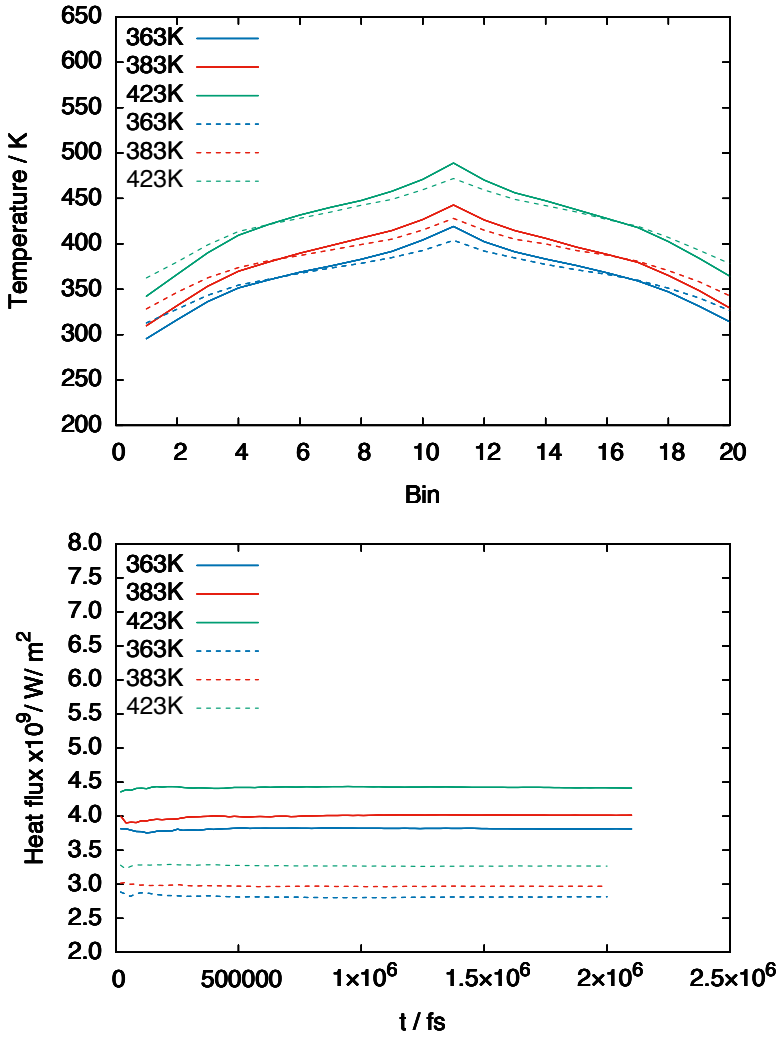

Figure S29. Temperature profile along the simulation box (here represented in bins) (top) and heat flux (bottom) for $[C_4C_1im][tf_2N]$ + SWCNT. Solid lines represent a 350 time steps exchange rate of kinetic energy and the dashed lines represent 500 time steps exchange rate of kinetic energy.

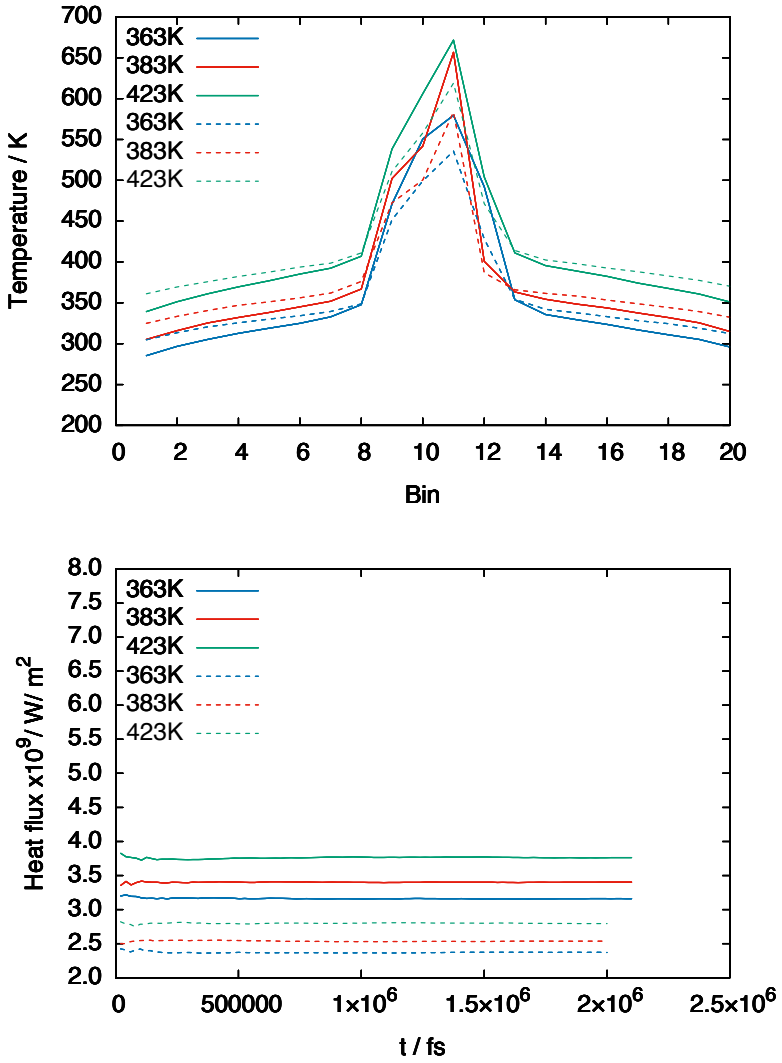

Figure S30. Temperature profile along the simulation box (here represented in bins) (top) and heat flux (bottom) for $[C_4C_1im][SCN]$ + Graphene. Solid lines represent a 350 time steps exchange rate of kinetic energy and the dashed lines represent 500 time steps exchange rate of kinetic energy.

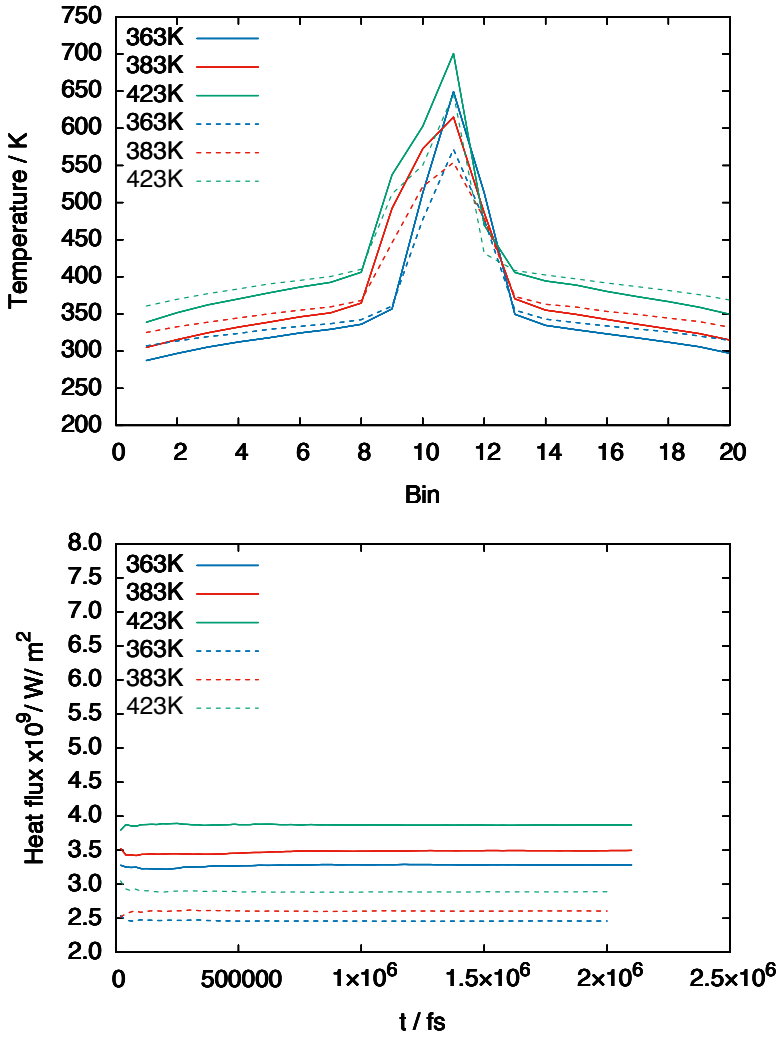

Figure S31. Temperature profile along the simulation box (here represented in bins) (top) and heat flux (bottom) for $[C_4C_1im][N(CN)_2]$ + Graphene. Solid lines represent a 350 time steps exchange rate of kinetic energy and the dashed lines represent 500 time steps exchange rate of kinetic energy.

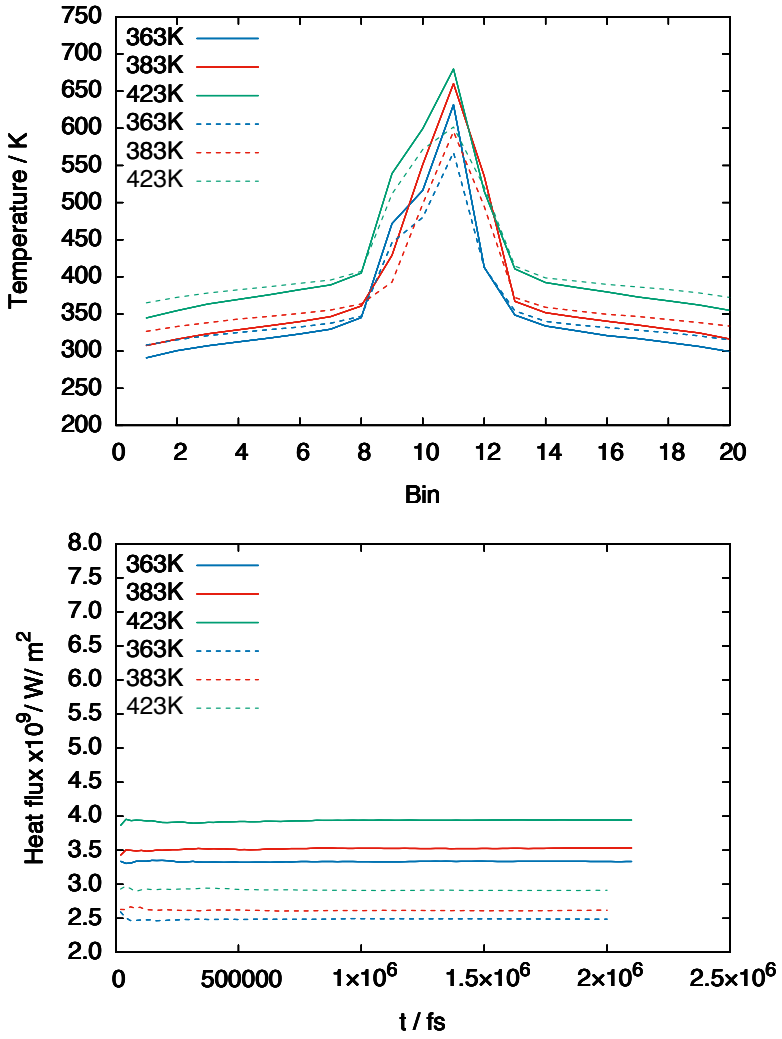

Figure S32. Temperature profile along the simulation box (here represented in bins) (top) and heat flux (bottom) for $[C_4C_1im][C(CN)_3]$ + Graphene. Solid lines represent a 350 time steps exchange rate of kinetic energy and the dashed lines represent 500 time steps exchange rate of kinetic energy.

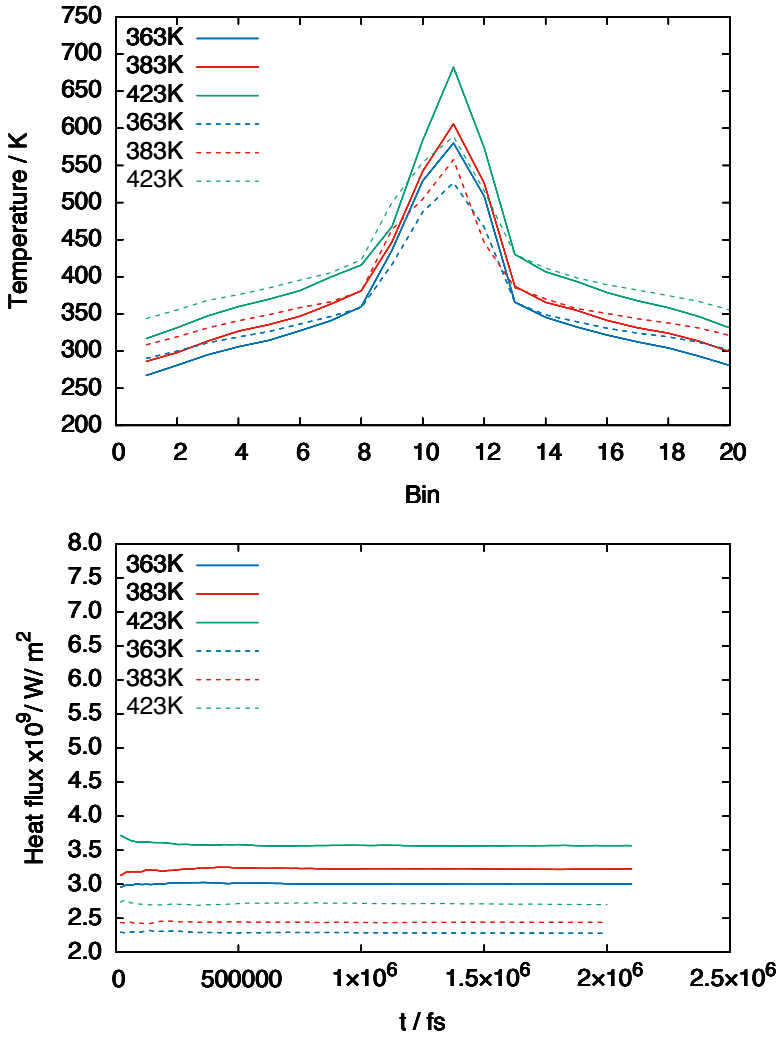

Figure S33. Temperature profile along the simulation box (here represented in bins) (top) and heat flux (bottom) for $[C_4C_1im][tf_2N]$ + Graphene. Solid lines represent a 350 time steps exchange rate of kinetic energy and the dashed lines represent 500 time steps exchange rate of kinetic energy.

Table S5. Comparison of thermal conductivity values obtained from NEMD for $[C_4C_1im][N(CN)_2]$ with SWCNT and graphene using different interaction potentials at 363 K. Kinetic energy exchanged once every 350 time steps.

Potential	*n-m*	LJ
SWCNT		
λ / (W m^{-1}K^{-1}) IL	0.253	
λ / (W m^{-1}K^{-1}) IL+SWCNT	0.312	0.259
Enhancement in λ / %	23.3	2.4
Graphene		
λ / (W m^{-1}K^{-1}) IL bulk	0.143	0.161
λ / (W m^{-1}K^{-1}) IL+Graphene	0.127	0.131
λ / (W m^{-1}K^{-1}) interface	0.188	0.184
Enhancement λ interface / %	31.5	14.8

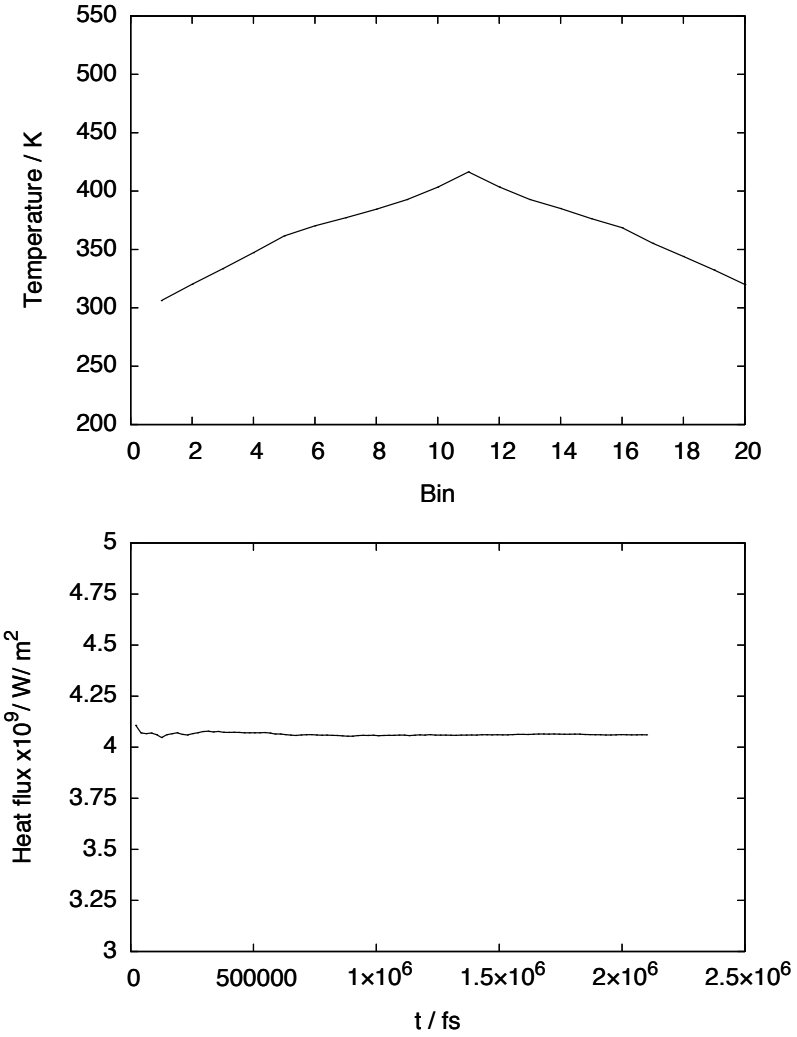

Figure S34. Temperature profile along the simulation box (here represented in bins) (top) and heat flux (bottom) for $[C_4C_1im][N(CN)_2]$ + SWCNT using a LJ potential with interaction parameters between ions and nanomaterial combination rules. Kinetic energy was exchanged once every 350 time steps.

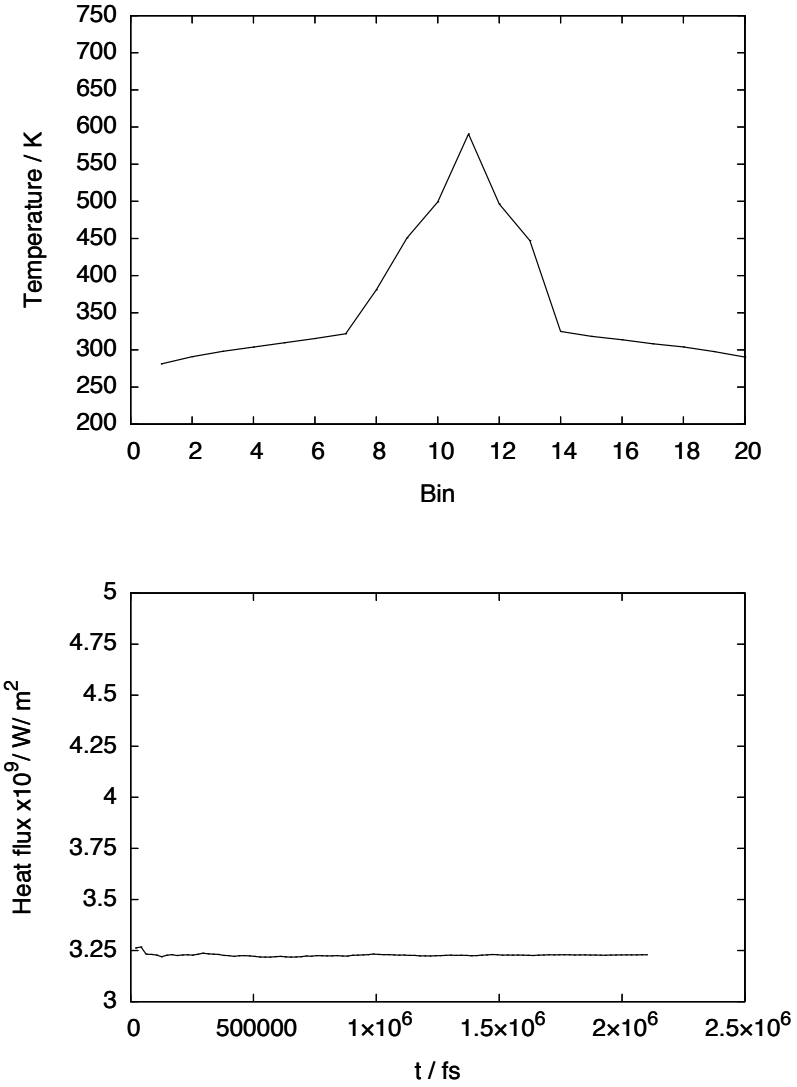

Figure S35. Temperature profile along the simulation box (here represented in bins) (top) and heat flux (bottom) for $[C_4C_1im][N(CN)_2]$ + Graphene using a LJ potential with interaction parameters between ions and nanomaterial combination rules. Kinetic energy was exchanged once every 350 time steps.

Annex 2

Thermal Conductivity of Ionic Liquids and IoNanofluids and their Feasibility as Heat Transfer Fluids – Supporting Information

João M.P. França[†,‡], Maria José V. Lourenço[†], Sohel M.S. Murshed[†], Agílio A.H. Pádua[‡], Carlos A. Nieto de Castro [†,*]

[†]Centro de Química Estrutural, Faculdade de Ciências, Universidade de Lisboa, Campo Grande, 1749-016, Lisboa, Portugal.

[‡]Institut de Chimie de Clermont-Ferrand, Clermont Auvergne & CNRS, 63178 Aubière, France.

Table S1 - Ionic liquids specifications, purity as mass fraction

Property	$[C_2mim][SCN]$	$[C_4mim][SCN]$	$[C_2mim][C(CN)_3]$	$[C_4mim][C(CN)_3]$	$[P_{66614}][dca]$	$[P_{66614}][Br]$
Identity (NMR, IR)	pass	pass	pass	pass	pass	Pass
Assay (NMR)	> 98%	> 98%	> 98%	> 98%	> 95%	> 95%
Cation (IC)	99.2%	98.5%	99.3%	99.8%	N/A	N/A
Anion (IC)	99.4%	99.9%	99.4%	99.6%	N/A	N/A
Halides (IC)	< 2%	< 2%	< 0.5%	< 0.5%	N/A	N/A
Water (KF)	1312 ppm	1725 ppm	87 ppm	590 ppm	N/A	N/A
Appearance	Yellow to brown liquid	Yellow to orange liquid	Yellow to brown liquid	Yellow to brown liquid	Yellow to orange liquid	Yellow to orange liquid
Date	01.12.2014	17.07.2014	31.10.2014	20.07.2012	11.01.2011	16.10.2012

Table S2 - Baytubes® C150 HP product specification.

Property	Value	Unit	Method
C-Purity	> 99	%	Elementary analysis
Free amorphous carbon	Not detectable	%	TEM
Number of walls	3-15	-	TEM
Outer mean diameter	13-16	nm	TEM
Outer diameter distribution	5-20	nm	TEM
Inner mean diameter	4	nm	TEM
Inner diameter distribution	2-6	nm	TEM
Length	1-10	µm	SEM
Bulk density	140-230	$kg \cdot m^{-3}$	EN ISO 60

Table S3 - Coefficients of equation 12 for ionic liquids and IoNanofluids[a]

Fluid	$a_1 \pm s_{a1}$ /W m^{-1} K^{-1}	10^5 ($a_2 \pm s_{a2}$) /W m^{-1} K^{-2}	$10^5 s$ W m^{-1} K^{-1}
$[P_{66614}][dca]$	0.17281 ± 0.0040	-3.477 ± 1.2	52
$[P_{66614}][Br]$	0.17515 ± 0.0034	-6.341 ± 1.1	46
$[P_{66614}][dca]$ 0.5% w/w MWCNTs	0.18345 ± 0.0112	-7.329 ± 3.6	105
$[C_2mim][SCN]$	0.41154 ± 0.059	-75.073 ± 18.6	781
$[C_4mim][SCN]$	0.26928 ± 0.031	-32.967 ± 9.6	402
$[C_2mim][C(CN)_3]$	0.37840 ± 0.052	-64.221 ± 16.2	672
$[C_4mim][C(CN)_3]$	0.26259 ± 0.035	-30.423 ± 10.9	456
$[C_2mim][SCN]$ 0.5% w/w MWCNTs	0.20417 ± 0.0010	-5.571 ± 0.32	12
$[C_2mim][SCN]$ 1% w/w MWCNTs	0.21206 ± 0.0018	-6.028 ± 0.55	21
$[C_4mim][SCN]$ 0.5% w/w MWCNTs	0.18254 ± 0.0048	-3.140 ± 1.5	57
$[C_4mim][SCN]$ 1% w/w MWCNTs	0.18913 ± 0.0056	-2.707 ± 1.8	67
$[C_2mim][C(CN)_3]$ 0.5% w/w MWCNTs	0.21667 ± 0.015	-10.074 ± 4.8	185
$[C_2mim][C(CN)_3]$ 1% w/w MWCNTs	0.21763 ± 0.0036	-8.471 ± 1.1	43
$[C_4mim][C(CN)_3]$ 0.5% w/w MWCNTs	0.19499 ± 0.0030	-6.475 ± 0.94	36
$[C_4mim][C(CN)_3]$ 1% w/w MWCNTs	0.20155 + 0.0013	-6.988 ± 0.39	15

[a] With expanded uncertainty at 0.95 level of confidence (k =2).

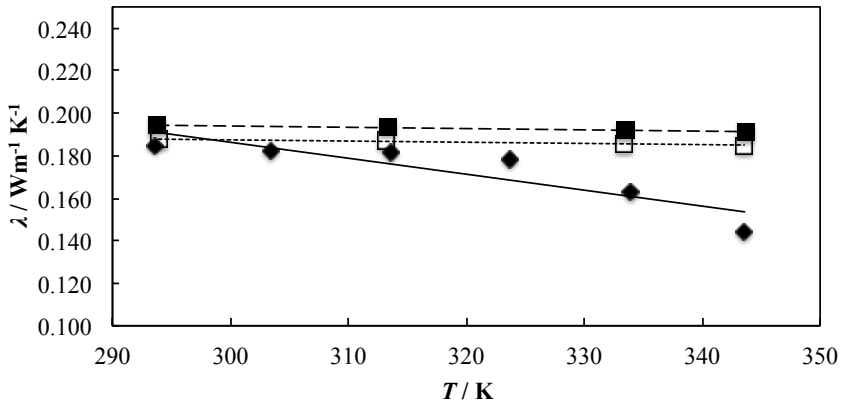

Figure S1. Plot of the thermal conductivity of $[C_2mim][SCN]$ and its IoNanofluids (INF) as a function of temperature. ◆ – $[C_2mim][SCN]$; □ – INF 0.5% w/w MWCNTs; ■ – INF 1% w/w MWCNTs; lines are given by equation 12 with coefficients shown in Table S3.

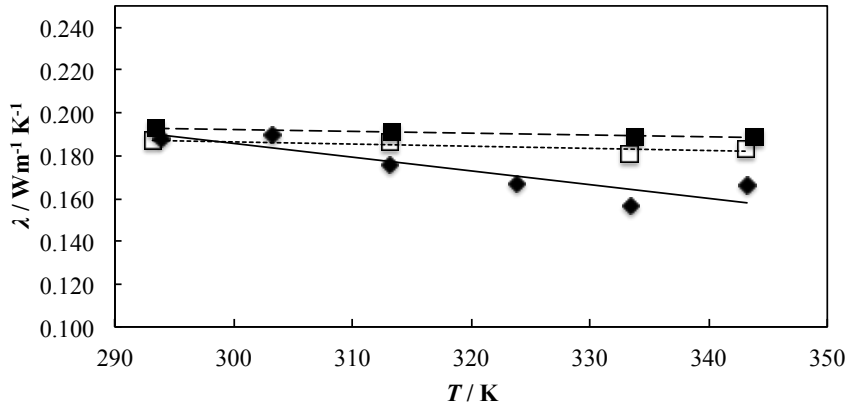

Figure S2. Plot of the thermal conductivity of $[C_2mim][C(CN)_3]$ and its IoNanofluids (INF) as a function of temperature. ◆ – $[C_2mim][C(CN)_3]$; □ – INF 0.5% w/w MWCNTs; ■ – INF 1% w/w MWCNTs; lines are given by equation 12 with coefficients shown in Table S3.

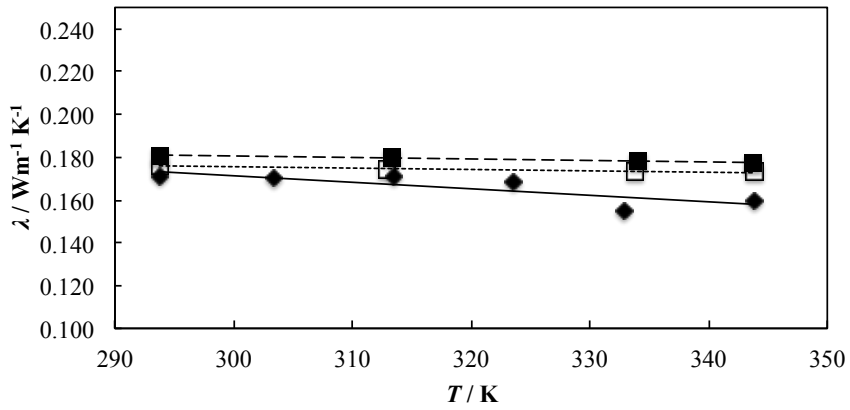

Figure S3. Plot of the thermal conductivity of $[C_4mim][C(CN)_3]$ and its IoNanofluids (INF) as a function of temperature. ◆ – $[C_4mim][C(CN)_3]$; □ – INF 0.5% w/w MWCNTs; ■ – INF 1% w/w MWCNTs; lines are given by equation 12 with coefficients shown in Table S3.

Table S4 – Thermophysical properties and heat transfer area (A_0) for commercial heat transfer fluids.

Fluid	T/ K	λ / W m^{-1} K^{-1}	η / mPa s	C_P / J kg^{-1} K^{-1}	ρ / kg m^{-3}	A_0 / m^2
Dowtherm A	293.15	0.139	4.29	1573	1059.6	178.69
	303.15	0.137	3.25	1601	1051.7	161.08
	313.15	0.136	2.56	1630	1043.8	**147.70**
	323.15	0.134	2.07	1658	1035.8	137.05
	333.15	0.132	1.72	1687	1027.8	**128.65**
	343.15	0.131	1.46	1715	1019.7	**121.88**
Dowtherm G	293.15	0.126	12.5	1546	1046.9	298.51
	303.15	0.125	8.40	1581	1039.1	253.19
	313.15	0.124	6.10	1616	1031.4	**222.54**
	323.15	0.123	4.60	1651	1023.6	199.01
	333.15	0.122	3.65	1686	1015.9	**182.08**
	343.15	0.121	2.96	1720	1008.1	**168.32**
Dowtherm J	293.15	0.128	0.91	1828	863.7	112.90
	303.15	0.126	0.79	1859	856.2	108.36
	313.15	0.124	0.70	1890	848.7	**104.79**
	323.15	0.122	0.63	1923	841.0	101.95
	333.15	0.120	0.56	1955	833.2	**98.82**
	343.15	0.118	0.51	1989	825.4	**96.68**
Dowtherm MX	293.15	0.123	20.3	1610	962.2	393.62
	303.15	0.122	13.5	1642	955.2	331.17
	313.15	0.121	9.44	1675	948.2	**285.32**
	323.15	0.120	6.86	1707	941.1	250.47
	333.15	0.119	5.15	1740	934.0	**223.27**
	343.15	0.118	3.98	1772	926.9	**201.80**
Dowtherm Q	293.15	0.122	4.00	1653	965.4	196.70
	303.15	0.121	3.04	1685	957.8	177.05
	313.15	0.120	2.37	1716	950.2	**161.39**
	323.15	0.118	1.89	1748	942.7	148.57
	333.15	0.117	1.54	1779	935.1	**138.21**
	343.15	0.116	1.28	1811	927.6	**129.74**
Dowtherm RP	293.15	0.131	42.82	1620	1029.2	497.54
	303.15	0.130	23.99	1650	1022.3	387.73
	313.15	0.129	14.92	1680	1015.3	**317.42**
	323.15	0.128	10.05	1710	1008.3	269.74
	333.15	0.126	7.19	1739	1001.3	**235.76**
	343.15	0.125	5.39	1769	994.2	**210.52**
Dowtherm T	293.15	0.130	30.55	1962	873.2	460.01
	303.15	0.128	19.09	1992	866.4	378.35
	313.15	0.127	12.80	2022	859.5	**320.18**
	323.15	0.126	9.07	2052	852.6	278.06
	333.15	0.125	6.71	2082	845.7	**246.40**
	343.15	0.124	5.15	2111	838.8	**222.11**
Syltherm XLT	293.15	0.111	1.40	1772	855.3	145.75
	303.15	0.109	1.20	1793	845.0	139.54
	313.15	0.106	1.00	1814	834.7	**132.28**
	323.15	0.104	0.91	1835	824.5	129.73
	333.15	0.102	0.80	1856	814.2	**125.72**
	343.15	0.100	0.70	1877	803.9	**121.71**
Syltherm 800	293.15	0.135	10.03	1608	934.99	280.20
	303.15	0.133	8.32	1625	926.0	262.11
	313.15	0.131	7.00	1643	917.07	**246.75**

	323.15	0.130	5.96	1660	908.18	233.53
	333.15	0.128	5.12	1677	899.32	**222.05**
	343.15	0.126	4.43	1694	890.49	**211.88**
Syltherm HF	293.15	0.107	1.84	1682	871.76	165.70
	303.15	0.105	1.58	1707	861.65	158.72
	313.15	0.102	1.37	1731	851.54	**152.76**
	323.15	0.100	1.19	1756	841.43	147.12
	333.15	0.097	1.05	1780	831.32	**142.77**
	343.15	0.095	0.93	1805	821.21	**138.82**
Paratherm HR	293.15	0.118	27.0	1900	943.0	442.50
	303.15	0.117	16.0	2000	937.0	349.63
	313.15	0.116	10.0	2000	931.0	**288.24**
	323.15	0.115	6.90	2000	925.0	248.56
	333.15	0.114	5.00	2000	919.0	**219.27**
	343.15	0.114	3.80	2000	913.0	**197.62**
Paratherm MR	293.15	0.132	8.20	2400	799.0	259.23
	303.15	0.131	5.80	2400	792.0	226.60
	313.15	0.130	4.30	2400	785.0	**202.48**
	323.15	0.129	3.30	2400	778.0	183.80
	333.15	0.128	2.70	2500	771.0	**169.44**
	343.15	0.127	2.20	2500	764.0	**157.93**
Globaltherm Omnitech	293.15	0.140	4.24	1580	1060.0	176.63
	313.15	0.138	2.61	1630	1044.0	**147.29**
	333.15	0.135	1.75	1690	1028.0	**127.94**
Globaltherm Syntec	293.15	0.120	100.8	1600	1008.0	789.30
	313.15	0.119	26.04	1670	994.0	**432.43**
	333.15	0.118	11.27	1740	980.0	**301.52**

Table S5 - Thermophysical properties and heat transfer area (A_0) for ionic liquids.

Fluid	T/ K	λ / W m^{-1} K^{-1}	η / mPa s	C_P / J kg^{-1} K^{-1}	ρ / kg m^{-3}	A_0 / m^2
[C_2mim][SCN]	313.15	0.182	15.5 [c]	2082.13 [h]	1112.9 [m]	**229.43**
	333.15	0.163	9.53 [c]	2157.16 [h]	1100.9 [m]	**199.86**
	343.15	0.145	7.77 [c]	2216.84 [h]	1094.9 [m]	**196.08**
[C_4mim][SCN]	313.15	0.169	30.5 [c]	2021.79 [h]	1066.6 [n]	**332.82**
	333.15	0.160	16.1 [c]	2098.83 [h]	1054.8 [n]	**260.86**
	343.15	0.152	12.3 [c]	2158.13 [h]	1048.9 [n]	**239.78**
[C_2mim][N(CN)$_2$]	313.15	0.178 [a]	8.87 [d]	1875.74 [h]	1093.5 [a]	**192.96**
	333.15	0.170 [a]	6.15 [d]	1934.99 [h]	1081.0 [a]	**170.81**
	343.15	0.165 [a]	5.32 [d]	1981.83 [h]	1076.1 [a]	**163.41**
[C_4mim][N(CN)$_2$]	313.15	0.163 [a]	13.9 [d]	1875.67 [i]	1051.0 [a]	**251.75**
	333.15	0.153 [a]	8.76 [d]	1895.16 [i]	1040.6 [a]	**216.52**
	343.15	0.150 [a]	7.40 [d]	1909.77 [i]	1035.7 [a]	**204.55**
[C_4mpyr][N(CN)$_2$]	313.15	0.153 [a]	19.96 [d]	2534.81 [j]	1006.1 [a]	**287.29**
	333.15	0.147 [a]	12.52 [d]	2659.63 [j]	995.60 [a]	**240.01**
[C_2mim][C(CN)$_3$]	313.15	0.176	9.50 [c]	1818.81 [k]	1070.6 [o]	**204.55**
	333.15	0.156	6.06 [c]	1858.57 [k]	1057.3 [o]	**183.18**
	343.15	0.166	5.03 [c]	1898.33 [k]	1050.5 [o]	**163.84**
[C_2mim][$C_2H_5SO_4$]	313.15	0.171 [b]	50.9 [e]	1680.14 [i]	1227.6 [i]	**393.71**
	333.15	0.165 [b]	25.2 [e]	1718.23 [i]	1214.2 [i]	**297.34**
	343.15	0.165 [b]	18.7 [e]	1739.39 [i]	1207.6 [i]	**262.01**
[C_4mim] [$(CF_3SO_2)_2$N]	313.15	0.114 [b]	28.3 [f]	1373.52 [i]	1422.0 [i]	**374.31**
	333.15	0.112 [b]	15.4 [f]	1402.14 [i]	1403.0 [i]	**291.95**
	343.15	0.111 [b]	11.9 [f]	1414.06 [i]	1394.0 [i]	**264.09**
[P_{66614}][N(CN)$_2$]	313.15	0.161	186.8 [g]	1927.62 [l]	890.3 [g]	**894.69**
	333.15	0.161	76.1 [g]	2000.36 [l]	879.0 [g]	**595.75**
	343.15	0.161	52.0 [g]	2036.73 [l]	873.4 [g]	**502.40**

a - França, J. M. P.; Reis, F.; Vieira, S. I. C.; Lourenço, M. J. V.; Santos, F. J. V.; Nieto de Castro, C. A.; Pádua, A. A. H., *The Journal of Chemical Thermodynamics* **2014,** *79*, 248-257.

b - França, J. M. P.; Vieira, S. I. C.; Lourenço, M. J. V.; Murshed, S. M. S.; Nieto de Castro, C. A., *Journal of Chemical & Engineering Data* **2013,** *58* (2), 467-476.

c - Neves, C. M. S. S.; Kurnia, K. A.; Coutinho, J. A. P.; Marrucho, I. M.; Lopes, J. N. C.; Freire, M. G.; Rebelo, L. P. N., *The Journal of Physical Chemistry B* **2013,** *117* (35), 10271-10283.

d - Reis, F.; França, J. M. P.; Santos, F. J. V.; Murshed, S. M. S.; Lourenço, M. J. V.; Castro, C. A. N. d., Thermophysical Properties of DCA Ionanofluids. In *COIL-5/3IMIL, Congress on Ionic Liquids*, Vilamoura, Portugal, 2013.

e - Schmidt, H.; Stephan, M.; Safarov, J.; Kul, I.; Nocke, J.; Abdulagatov, I. M.; Hassel, E., *The Journal of Chemical Thermodynamics* **2012,** *47*, 68-75.

f - Tariq, M.; Carvalho, P. J.; Coutinho, J. A. P.; Marrucho, I. M.; Lopes, J. N. C.; Rebelo, L. P. N., *Fluid Phase Equilibria* **2011,** *301* (1), 22-32.

g - Pereiro, A. B.; Veiga, H. I. M.; Esperança, J. M. S. S.; Rodríguez, A., *The Journal of Chemical Thermodynamics* **2009,** *41* (12), 1419-1423.

h - Navarro, P.; Larriba, M.; Rojo, E.; García, J.; Rodríguez, F., *Journal of Chemical & Engineering Data* **2013,** *58* (8), 2187-2193.

i - Nieto de Castro, C. A.; Langa, E.; Morais, A. L.; Lopes, M. L. M.; Lourenço, M. J. V.; Santos, F. J. V.; Santos, M. S. C. S.; Lopes, J. N. C.; Veiga, H. I. M.; Macatrão, M.; Esperança, J. M. S. S.; Marques, C. S.; Rebelo, L. P. N.; Afonso, C. A. M., *Fluid Phase Equilibria* **2010,** *294* (1–2), 157-179.

j - Gonzalez, E. J.; Gonzalez, B.; Macedo, E. A., *J. Chem. Eng. Data* **2013** *58* (6), 1440-1448.

k - Navarro, P.; Larriba, M.; Garcia, J.; Rodriguez, F., *Thermochim. Acta* **2014** *588*, 22-7.

l - Ferreira, A. F.; Simões, P. N.; Ferreira, A. G. M., *The Journal of Chemical Thermodynamics* **2011,** *45* (1), 16-27.

m - Ficke, L. E.; Novak, R.; Brennecke, J. F., *J. Chem. Eng. Data* **2010** *55* (11), 4946-4950.

n - Vakili-Nezhaad, G.; Vatani, M.; Asghari, M.; Ashour, I., *J. Chem. Thermodyn.* **2012** *54*, 148-154.

o - Souckova, M.; Klomfar, J.; Patek, J., *Fluid Phase Equilib.* **2015** *406*, 181-193.

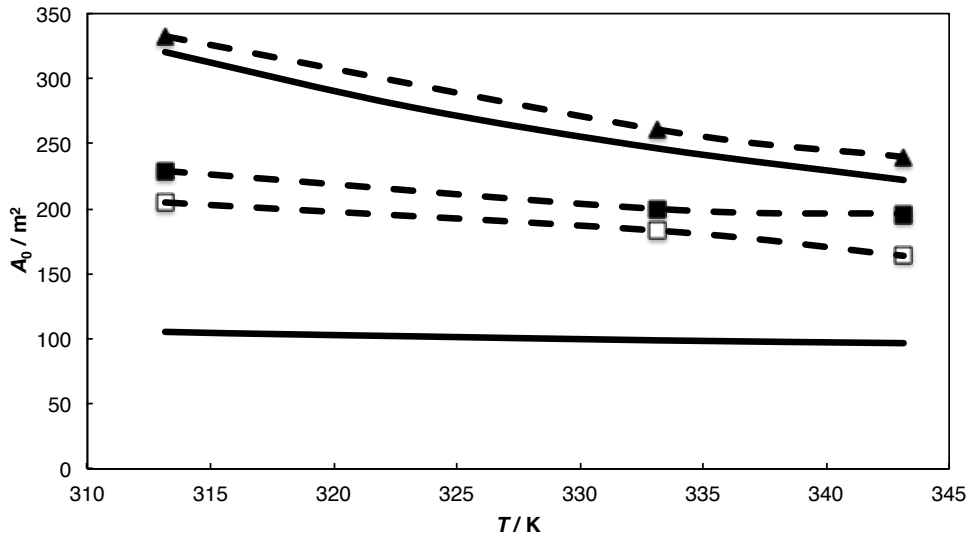

Figure S4 – Heat transfer area for ionic liquids. Solid lines represent lowest (Dowtherm J) and highest (Dowtherm T) values obtained for commercial HTFs. ■ – [C_2mim][SCN]; ▲ – [C_4mim][SCN]; □ – [C_2mim][$C(CN)_3$].

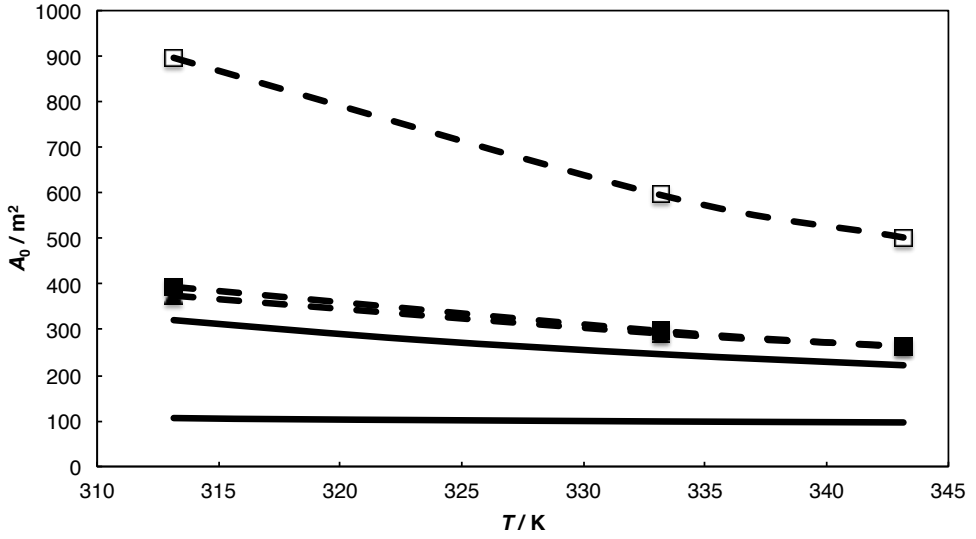

Figure S5 – Heat transfer area for ionic liquids. Solid lines represent lowest (Dowtherm J) and highest (Dowtherm T) values obtained for commercial HTFs. ■ – [C_2mim][$C_2H_5SO_4$]; ▲ – [C_4mim][$(CF_3SO_2)_2N$]; □ – [P_{66614}][$N(CN)_2$].

Table S6 - Thermophysical properties and heat transfer area (A_0) for INFs 0.5% w/w MWCNTs.

Base fluid	T/ K	λ / W m^{-1} K^{-1}	η / mPa s	C_P / J kg^{-1} K^{-1}	ρ / kg m^{-3}	A_0 / m^2
[C_2mim][SCN]	313.15	0.187	27.5	2082.13	1115.8	**286.85**
	333.15	0.186	20.1	2157.16	1103.8	**251.42**
	343.15	0.185	18.9	2216.84	1097.5	**244.86**
[C_4mim][SCN]	313.15	0.173	55.1	2021.79	1070.0	**423.39**
	333.15	0.171	39.7	2098.83	1057.1	**368.75**
	343.15	0.172	34.7	2158.13	1051.1	**344.77**
[C_2mim][N(CN)$_2$]	313.15	0.182 [a]	15.7	1875.74	1096.3 [a]	**240.84**
	333.15	0.179 [a]	13.0	1934.99	1083.9 [a]	**224.21**
	343.15	0.179 [a]	12.9	1981.83	1078.6 [a]	**223.19**
[C_4mim][N(CN)$_2$]	313.15	0.171 [a]	25.1 [c]	1875.67	1054.4 [a]	**313.71**
	333.15	0.169 [a]	21.7 [c]	1895.16	1042.9 [a]	**298.05**
	343.15	0.168 [a]	20.8 [c]	1909.77	1037.8 [a]	**294.16**
[C_4mpyr][N(CN)$_2$]	313.15	0.160 [a]	25.5 [c]	2534.81	1008.4 [a]	**309.92**
	333.15	0.158 [a]	21.4 [c]	2659.63	997.8 [a]	**287.56**
[C_2mim][C(CN)$_3$]	313.15	0.186	16.9	1818.81	1073.4	**250.71**
	333.15	0.181	12.8	1858.57	1060.1	**227.57**
	343.15	0.183	12.2	1898.33	1052.9	**221.68**
[C_2mim][$C_2H_5SO_4$]	313.15	0.178 [b]	90.3	1680.14	1230.7	**493.19**
	333.15	0.177 [b]	53.2	1718.23	1217.5	**392.49**
	343.15	0.177 [b]	45.5	1739.39	1210.4	**366.93**
[C_4mim][(CF_3SO_2)$_2$N]	313.15	0.121 [b]	51.1	1373.52	1426.6	**466.31**
	333.15	0.119 [b]	38.1	1402.14	1406.1	**415.58**
	343.15	0.120 [b]	33.5	1414.06	1396.8	**391.95**

a - França, J. M. P.; Reis, F.; Vieira, S. I. C.; Lourenço, M. J. V.; Santos, F. J. V.; Nieto de Castro, C. A.; Pádua, A. A. H., *The Journal of Chemical Thermodynamics* **2014,** *79*, 248-257.

b - França, J. M. P.; Vieira, S. I. C.; Lourenço, M. J. V.; Murshed, S. M. S.; Nieto de Castro, C. A., *Journal of Chemical & Engineering Data* **2013,** *58* (2), 467-476.

c - Reis, F.; França, J. M. P.; Santos, F. J. V.; Murshed, S. M. S.; Lourenço, M. J. V.; Castro, C. A. N. d., Thermophysical Properties of DCA Ionanofluids. In *COIL-5/3IMIL, Congress on Ionic Liquids*, Vilamoura, Portugal, 2013.

Table S7 - Thermophysical properties and heat transfer area (A_0) for INFs 1% w/w MWCNTs.

Base fluid	T/ K	λ / W m^{-1} K^{-1}	η / mPa s	C_P / J kg^{-1} K^{-1}	ρ / kg m^{-3}	A_0 / m^2
[C_2mim][SCN]	313.15	0.193	36.8	2082.13	1117.9	**318.24**
	333.15	0.192	27.4	2157.16	1105.5	**280.95**
	343.15	0.191	25.0	2216.84	1099.3	**269.79**
[C_4mim][SCN]	313.15	0.181	79.1	2021.79	1073.5	**481.55**
	333.15	0.179	52.2	2098.83	1059.2	**403.18**
	343.15	0.180	42.6	2158.13	1052.4	**366.25**
[C_2mim][N(CN)$_2$]	313.15	0.191 [a]	21.1 [c]	1875.74	1098.4 [a]	**264.04**
	333.15	0.187 [a]	17.7 [c]	1934.99	1085.6 [a]	**248.40**
	343.15	0.187 [a]	17.1 [c]	1981.83	1080.4 [a]	**243.93**
[C_4mim][N(CN)$_2$]	313.15	0.177 [a]	36.1 [c]	1875.67	1057.8 [a]	**358.23**
	333.15	0.174 [a]	28.5 [c]	1895.16	1045.0 [a]	**328.74**
	343.15	0.174 [a]	25.5 [c]	1909.77	1039.1 [a]	**314.23**
[C_4mpyr][N(CN)$_2$]	313.15	0.167 [a]	40.2 [c]	2534.81	1012.1 [a]	**366.42**
	333.15	0.162 [a]	31.9 [c]	2659.63	1001.5 [a]	**335.62**
[C_2mim][C(CN)$_3$]	313.15	0.192	22.6	1818.81	1075.4	**277.74**
	333.15	0.189	17.5	1858.57	1061.8	**252.24**
	343.15	0.189	16.2	1898.33	1054.7	**243.93**
[C_2mim][$C_2H_5SO_4$]	313.15	0.184 [b]	120.8	1680.14	1233.1	**548.77**
	333.15	0.183 [b]	72.6	1718.23	1219.4	**439.97**
	343.15	0.183 [b]	60.1	1739.39	1212.4	**405.34**
[C_4mim][(CF_3SO_2)$_2$N]	313.15	0.126 [b]	73.5	1373.52	1431.2	**532.32**
	333.15	0.125 [b]	50.0	1402.14	1408.9	**453.72**
	343.15	0.125 [b]	41.2	1414.06	1398.6	**417.81**

a - França, J. M. P.; Reis, F.; Vieira, S. I. C.; Lourenço, M. J. V.; Santos, F. J. V.; Nieto de Castro, C. A.; Pádua, A. A. H., *The Journal of Chemical Thermodynamics* **2014,** *79*, 248-257.

b - França, J. M. P.; Vieira, S. I. C.; Lourenço, M. J. V.; Murshed, S. M. S.; Nieto de Castro, C. A., *Journal of Chemical & Engineering Data* **2013,** *58* (2), 467-476.

c - Reis, F.; França, J. M. P.; Santos, F. J. V.; Murshed, S. M. S.; Lourenço, M. J. V.; Castro, C. A. N. d., Thermophysical Properties of DCA Ionanofluids. In *COIL-5/3IMIL, Congress on Ionic Liquids*, Vilamoura, Portugal, 2013.

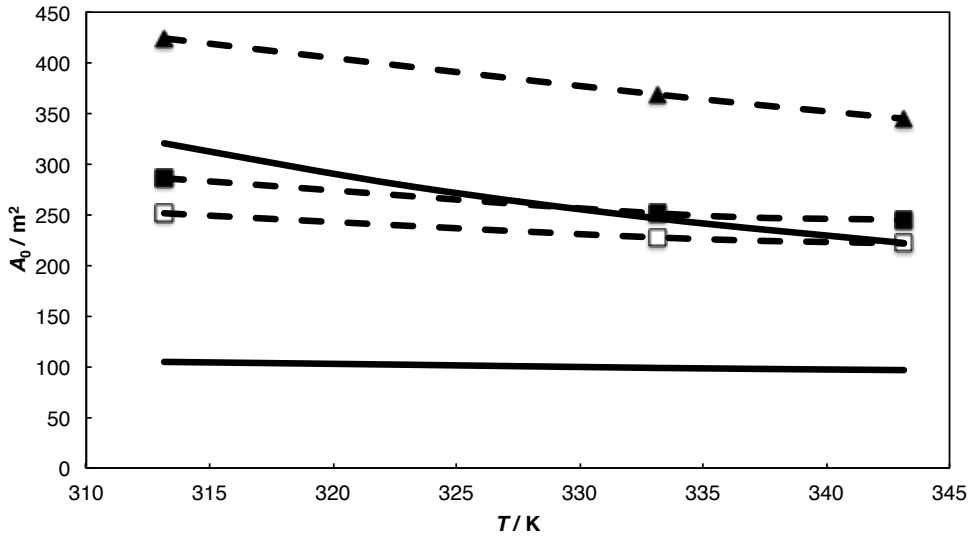

Figure S6 – Heat transfer area for IoNanofluids 0.5% w/w MWCNTs considering C_P of base ionic liquid. Solid lines represent lowest (Dowtherm J) and highest

(Dowtherm T) values obtained for commercial HTFs. ■ – [C_2mim][SCN]; ▲ – [C_4mim][SCN]; □ – [C_2mim][$C(CN)_3$].

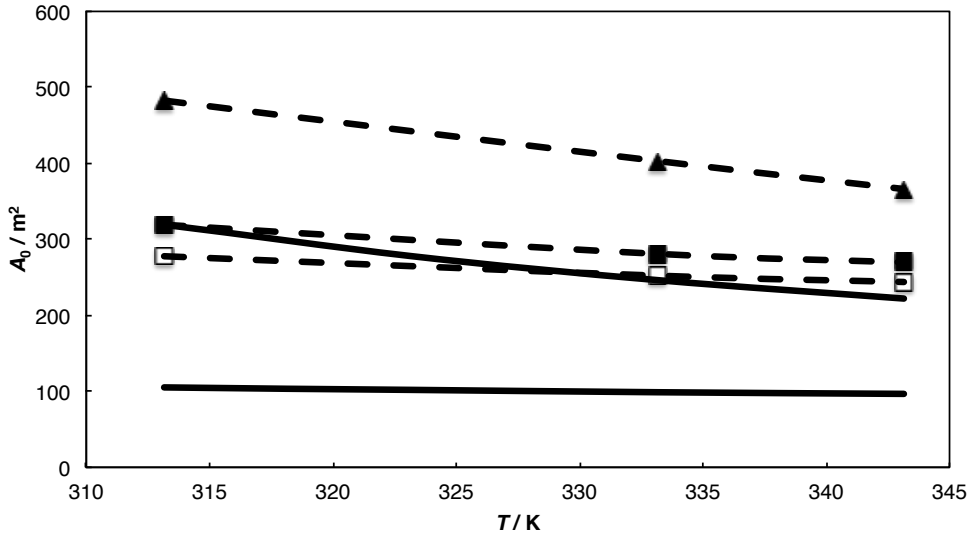

Figure S7 – Heat transfer area for IoNanofluids 1% w/w MWCNTs considering C_P of base ionic liquid. Solid lines represent lowest (Dowtherm J) and highest (Dowtherm T) values obtained for commercial HTFs. ■ – [C_2mim][SCN]; ▲ – [C_4mim][SCN]; □ – [C_2mim][$C(CN)_3$].

Table S8 – Increase in heat transfer area (%) of the IoNanofluids regarding base ionic liquids.

Base fluid	T / K	ΔA_0 0.5% w/w	ΔA_0 1% w/w
[C_2mim][SCN]	313.15	25.03	38.71
	333.15	25.80	40.58
	343.15	24.88	37.59
[C_4mim][SCN]	313.15	27.21	44.69
	333.15	41.36	54.56
	343.15	43.78	52.74
[C_2mim][$N(CN)_2$]	313.15	24.81	36.84
	333.15	31.26	45.42
	343.15	36.58	49.27
[C_4mim][$N(CN)_2$]	313.15	24.61	42.30
	333.15	37.66	51.83
	343.15	43.80	53.62
[C_4mpyr][$N(CN)_2$]	313.15	7.88	27.54
	333.15	19.81	39.83
[C_2mim][$C(CN)_3$]	313.15	22.56	35.78
	333.15	24.23	37.70
	343.15	35.31	48.89

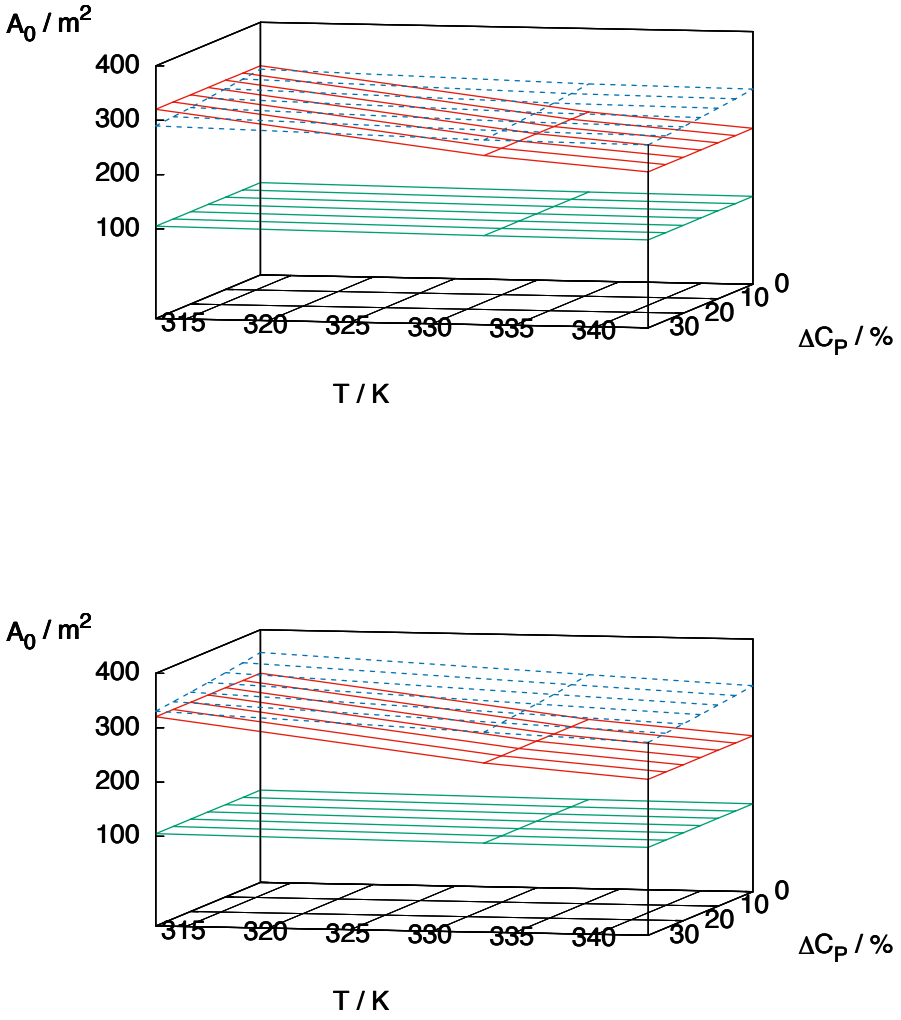

Figure S8 – Heat transfer area for $[C_4mim][N(CN)_2]$ based IoNanofluids considering a variation up to +30% of C_P of base ionic liquid. Top: 0.5% w/w MWCNTs; Bottom: 1% w/w MWCNTs. Solid lines represent lowest (Dowtherm J) and highest (Dowtherm T) values obtained for commercial HTFs.

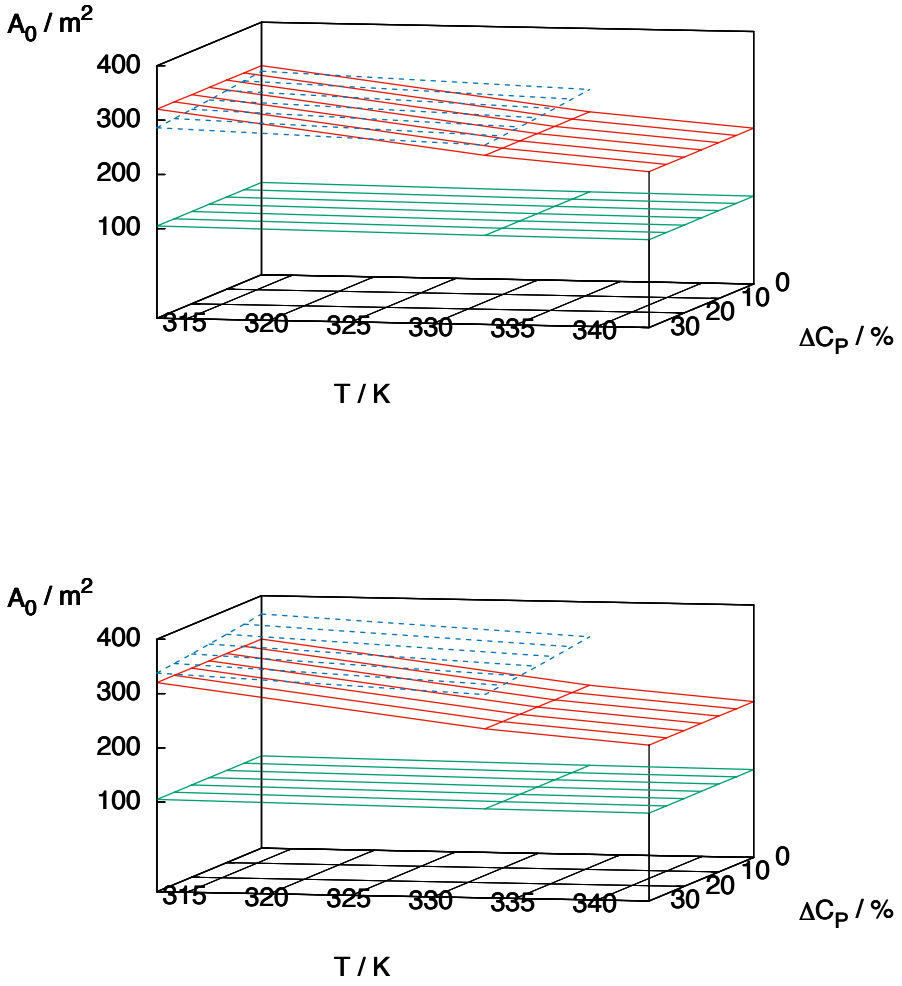

Figure S9 – Heat transfer area for $[C_4mpyr][N(CN)_2]$ based IoNanofluids considering a variation up to +30% of C_P of base ionic liquid. Top: 0.5% w/w MWCNTs; Bottom: 1% w/w MWCNTs. Solid lines represent lowest (Dowtherm J) and highest (Dowtherm T) values obtained for commercial HTFs.

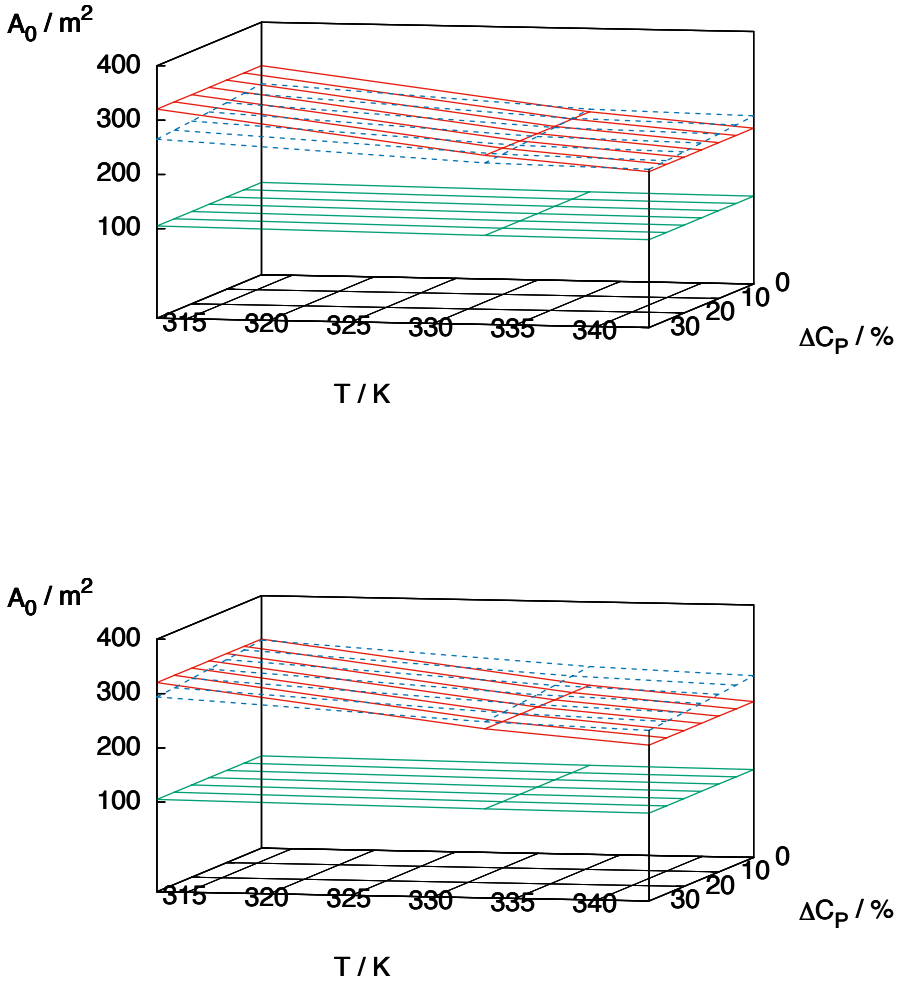

Figure S10 – Heat transfer area for [C_2mim][SCN] based IoNanofluids considering a variation up to +30% of C_P of base ionic liquid. Top: 0.5% w/w MWCNTs; Bottom: 1% w/w MWCNTs. Solid lines represent lowest (Dowtherm J) and highest (Dowtherm T) values obtained for commercial HTFs.

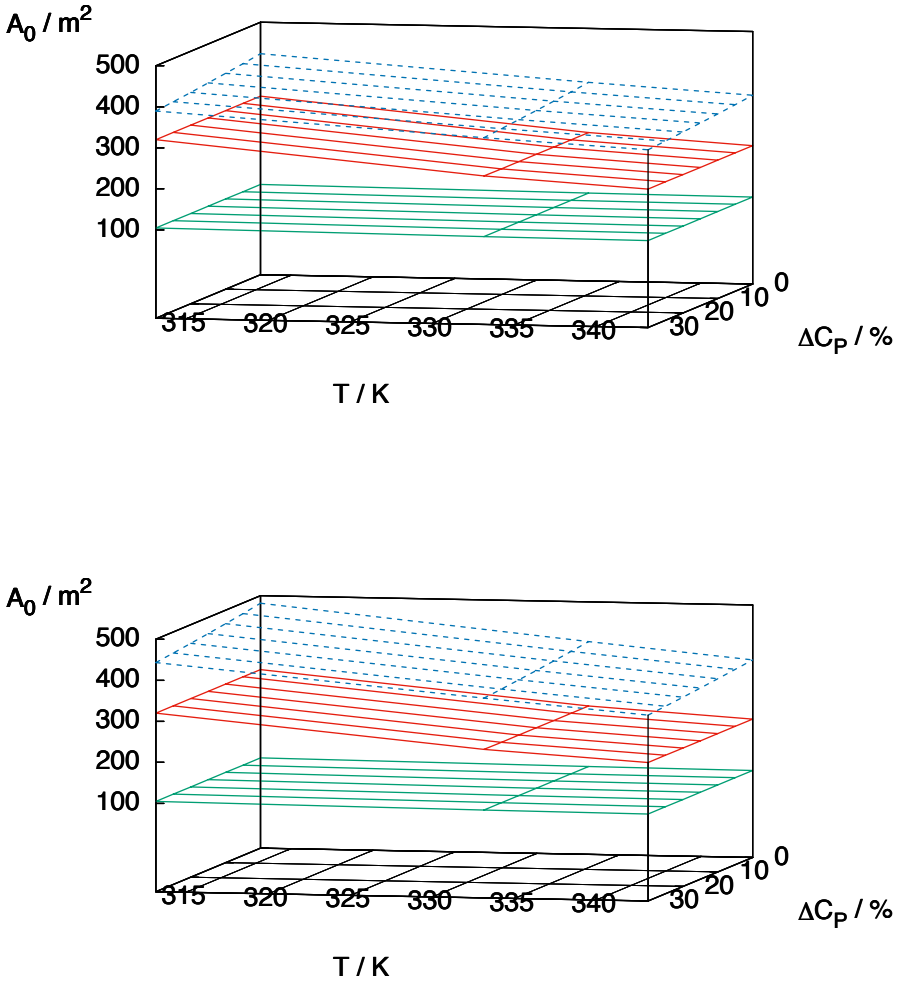

Figure S11 – Heat transfer area for [C_4mim][SCN] based IoNanofluids considering a variation up to +30% of C_P of base ionic liquid. Top: 0.5% w/w MWCNTs; Bottom: 1% w/w MWCNTs. Solid lines represent lowest (Dowtherm J) and highest (Dowtherm T) values obtained for commercial HTFs.

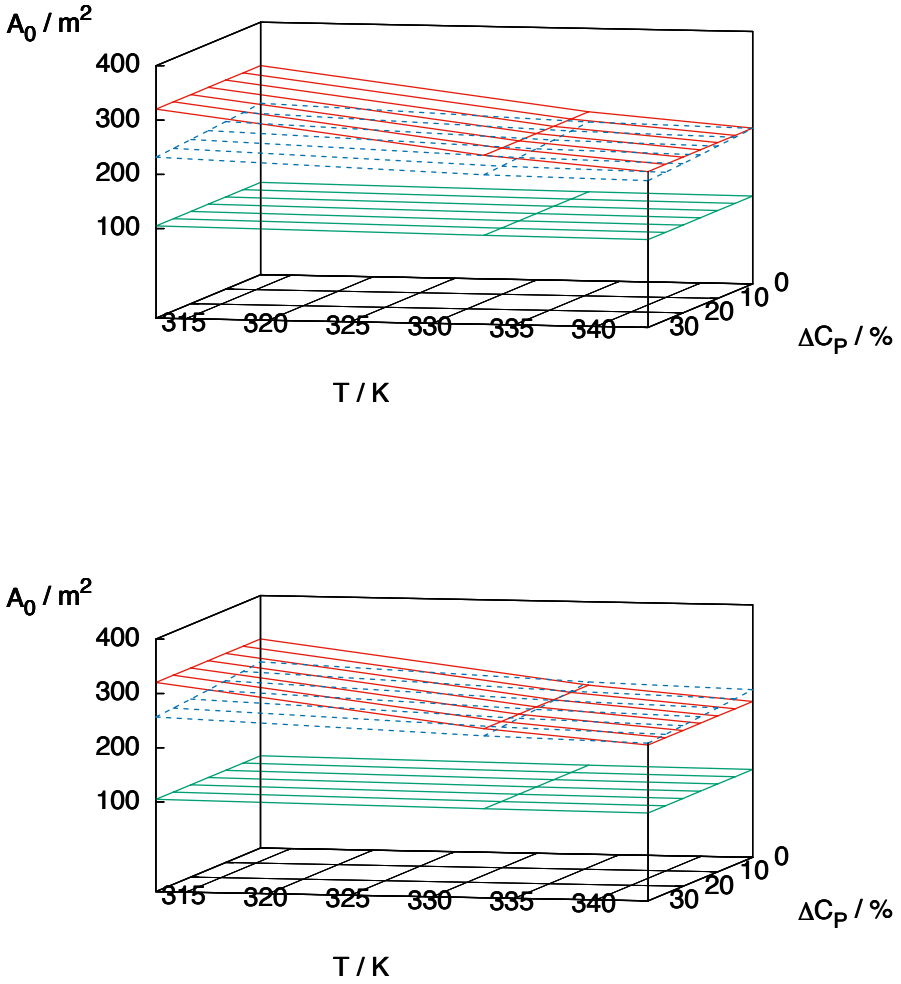

Figure S12 – Heat transfer area for $[C_2mim][C(CN)_3]$ based IoNanofluids considering a variation up to +30% of C_P of base ionic liquid. Top: 0.5% w/w MWCNTs; Bottom: 1% w/w MWCNTs. Solid lines represent lowest (Dowtherm J) and highest (Dowtherm T) values obtained for commercial HTFs.